Loughborough University

This item was submitted to Loughborough's Research Repository by the author.
Items in Figshare are protected by copyright, with all rights reserved, unless otherwise indicated.

Production and evaluation of electrospun polyaniline/biopolymer composite nanofibres for medical applications

PLEASE CITE THE PUBLISHED VERSION

PUBLISHER

© Panagiota Moutsatsou

PUBLISHER STATEMENT

This work is made available according to the conditions of the Creative Commons Attribution-NonCommercial-NoDerivatives 4.0 International (CC BY-NC-ND 4.0) licence. Full details of this licence are available at: https://creativecommons.org/licenses/by-nc-nd/4.0/

LICENCE

CC BY-NC-ND 4.0

REPOSITORY RECORD

Moutsatsou, Panagiota. 2017. “Production and Evaluation of Electrospun Polyaniline/biopolymer Composite Nanofibres for Medical Applications”. figshare. https://hdl.handle.net/2134/25673.

PRODUCTION AND EVALUATION OF ELECTROSPUN POLYANILINE/BIOPOLYMER COMPOSITE NANOFIBRES FOR MEDICAL APPLICATIONS

---

by

Panagiota Moutsatsou

A Doctoral Thesis

Submitted in partial fulfilment of the requirements

for the award of the degree of Doctor of Philosophy

Department of Chemical Engineering

Loughborough University

March, 2017

© Panagiota Moutsatsou, 2017

ABSTRACT

The aim of this study is the production of a nanofibrous electroactive mat and the investigation of its potential use in tissue engineering, and more specifically for wound dressing purposes. The limitations regarding electrospinnability of the conducting polymer will be identified and addressed and the factors related to its biological properties will be evaluated.

To this end, conducting polymer, polyaniline (PANI) was chosen as the electroactive component and blend electrospinning was identified as the most suitable method to produce continuous nanofibres containing PANI. Various biocompatible polymers and solvent systems were investigated for their suitability to assist in electrospinning and PEO (polyethylene oxide) and CH (chitosan) were chosen as carrier polymers for blend electrospinning of PANI.

Consequently, CSA (Camphor-10-sulfonic acid (β)) doped PANI/PEO and CSA doped PANI/CH conducting nanofibrous mats were produced by electrospinning. The electrospinning windows for both blends were determined by using full factorial experimental designs. The combined effects of the humidity, voltage and flow rate on the fibre morphology and diameter were examined for both blends, demonstrating that the ambient humidity is the critical factor affecting the electrospinning process and determining the electrospinning window for a conducting polymer. Low humidity favors the formation of defect free fibres while high humidity either hinders fibre formation or causes the formation of defects on the fibres. In the case of PANI/PEO blends, different levels of PANI doping were investigated, and high level of doping with CSA was found to lead to the formation of crystalline structures. Data fitting was used to explore the behavior of conducting polymers using the case of PANI/PEO electrospinning and very good agreement between experimental and theoretical predictions was obtained for only a limited range of experimental conditions, whereas deviation was observed for all other sets of conditions.

In the case of PANI/CH, the effect of different ratios of conducting polymer in the blend (0:1, 1:3, 3:5 and 1:1) was examined, as for the electrospinnability, resulting

nanofibrous morphology, mat contact angle, electrical conductivity, antibacterial activity and cellular biocompatibility. The incorporation of PANI in the electrospinning blend, affected the electrospinnability of the solution, making it more susceptible to RH deviations, and contributed to the decrease of nanofibre diameter. Higher PANI content was found to result in more hydrophobic and more conducting mats. The method that was used to stabilize the PANI/CH mats was also found to affect antibacterial activity and conductivity. The produced blend mats, exhibited antibacterial activity which was higher against Gram positive *B. subtilis* and lower against gram negative *E. coli*. The cellular biocompatibility was assessed with human osteoblasts and fibroblasts, in terms of cell proliferation rate as well as cell attachment and morphology. Cells of both cell lines adhered well and showed good growth rates on nanofibrous substrates of all blend ratios when compared to standard tissue culture plastic. Finally, amongst the PANI containing mats, the one of 1:3 PANI:CH ratio, was identified as the best to support osteoblast and fibroblast cell proliferation when compared to the pure chitosan.

Acknowledgements

I would like to express my gratitude to my supervisor Dr Stella Georgiadou, who trusted me with this project and gave me the opportunity to undertake a Phd in the UK. Thanks for the support during this whole time! I'd also like to deeply thank my other two supervisors Dr Karen Coopman and Dr Martin B Smith for their valuable feedback and academic advices.

I'd very much like to thank all the colleagues and friends that I made during my stay in Loughborough who helped me to also grow personally apart from professionally as well as all friends from Greece who stood by me.

I'd also like to acknowledge the support I received from the technical personnel in the materials and chemical engineering department, who offered technical advice and guaranteed a safe work environment, as well as the Loughborough University Graduate School who funded this project.

Lastly, and most importantly, a very special THANK YOU goes to my family, who have been inspiring me and helping me reach my goals not only during these four years, but throughout my life.

Cheers!

Table of Contents

ABSTRACT 2

Acknowledgements 4

Table of Contents 5

List of Tables 11

List of Figures 12

Nomenclature 16

Abbreviations 16

Symbols 18

Greek Letters 19

1 | INTRODUCTION 20

1.1 Thesis Overview 20

1.2 Publications and Presentations 20

Journal Papers 20

Conference Presentations 20

1.3 Background 21

2 | LITERATURE REVIEW 23

2.1 Principles of Electrospinning 23

2.1.1 Electrospinning Setup 29

2.1.2 Parameters affecting the electrospinning process and nanofibre morphology 30

2.1.2.1 Effect of Solvent Properties 31

Solubility Parameter 31

Boiling Point 32

Dielectric Constant 33

2.1.2.2. Effect of Solution Properties 34

Concentration 34
Viscosity 34
Polymer's molecular weight 36
Surface Tension 37
Conductivity 38
2.1.2.3. Effect of Process Parameters 40
Applied Voltage 40
Flow Rate 42
Tip to collector distance (TCD) 43
Type, Shape and Size of Collector 43
Nozzle Configuration and Diameter 44
2.1.2.4. Effect of environmental parameters 45
Humidity 45
Temperature 46
2.1.3. Modelling – Control of Nanofibre Morphology 46
2.2 Conducting Polymers 48
2.2.1 Polyaniline (PANI) 50
2.2.1.1 Structures of PANI 51
2.2.1.2 Doping 53
2.2.2 Electrospinning of PANI 54
2.2.2.1 Blending with Carrier Polymers 57
2.2.2.2 Electrospinning of Pure PANI 58
2.2.2.3 Post spinning addition of conducting polymer – *In situ* Polymerization 59
2.2.2.4 Coaxial (Core-Shell) Electrospinning 60
2.2.3 Conducting Polymers in Drug Delivery 61

2.2.4 PANI for Tissue Engineering 64
2.2.4.1 PANI biocompatibility - *In vitro* studies 68
2.2.4.2 PANI biocompatibility - *In vivo* studies 72
2.3 Conclusions - Discussion 73
3 |EVALUATION OF POTENTIAL APPROACHES FOR PANI ELECTROSPINNING 76
3.1 Introduction 76
3.2 Materials & Methods 79
3.2.1 PANI Polymerization 79
3.2.2 Electrospinning Setup 80
3.2.3 Blend electrospinning - Selection of carrier polymers, solvents, doping agents and amount of doping 81
3.2.5 *In situ* Polymerization 83
3.2.6 Core-Shell Electrospinning 84
3.3 Results & Discussion 84
3.3.1 Production of blend PANI nanofibres 84
3.3.1.1 Determination of suitable carrier polymers 84
3.3.1.2 Determination of suitable solvents 88
3.3.1.3 Determination of suitable dopants 91
3.3.3.4 Investigation of Doping Effect 94
3.3.2 *In situ* PANI polymerization 98
3.3.3 Core-Shell electrospinning 99
3.4 Conclusions 101
4 | DETERMINING FACTORS FOR THE ELECTROSPINNING WINDOW OF CONDUCTING PANI/PEO BLEND 103
4.1 Introduction 103
4.2 Materials and Methods 107

4.2.1 Solution Preparation 107
4.2.2 Electrospinning Process 108
4.2.3 Experimental Design 109
4.3 Results and Discussion 111
4.3.1 Morphology 111
4.3.1.1 Effect of flow rate 112
4.3.1.2 Effect of humidity 113
4.3.1.3 Effect of voltage 115
4.3.1.4 Effect of doping level 116
4.3.2 Electrospinning Window 117
4.3.3 Data fitting 125
4.5 Conclusions 127
5 | PANI/CHITOSAN NANOFIBRE PRODUCTION – DETERMINATION OF THE ELECTROSPINNING WINDOW 129
5.1 Introduction 129
5.2 Materials and Methods 134
5.2.1 Synthesis of Chitosan Grafted Polyaniline (CHgPANI) 134
5.2.2 Preparation of electrospinning solutions & electrospinning process 134
5.2.3 Experimental Design 135
5.3 Results and Discussion 138
5.3.1 Fabrication of Chitosan Mats 138
5.3.1.1 Effect of Polymer Concentration 138
5.3.1.2 Effect of humidity 140
5.3.1.3. Effect of applied voltage 142
5.3.2 Fabrication of Chitosan grafted PANI (CHgPANI) mats 145
5.3.3 Fabrication of PANI/CH blend mats 147

5.3.4 Discussion of the current measurements and investigation of the effect of the tip to collector distance (TCD) 153

5.4 Conclusions 158

6 | EVALUATION OF THE BIOLOGICAL PROPERTIES OF ELECTROSPUN MATS 159

6.1 Introduction 159

6.2 Materials & Methods 164

6.2.1 Electrospinning of Polyaniline Blends with Chitosan and PEO 164

6.2.2 Stabilization of Electrospun Membranes 164

6.2.3 Contact Angle Measurement 165

6.2.4 Electrical Resistivity 165

6.2.5 Cell Culture 166

6.2.6 Cell Attachment and Viability Assay 167

6.2.6.1 Cell Proliferation Assay 167

6.2.6.2 Morphological Assessment 168

6.2.7 Antibacterial Properties 168

6.3 Results and Discussion 169

6.3.1 Production of PEO-Polyaniline and Chitosan-Polyaniline electrospun membranes 169

6.3.2 Stabilization of the electrospun mats 173

6.3.3 Characterization of neutralized electrospun membranes 176

6.3.4 Contact Angle 176

6.3.5 Electrical Conductivity 177

6.3.6 Evaluation of Cell Attachment and Viability 180

6.3.6.1 Cell proliferation 181

6.3.6.2 Cell Morphology Assessment 186

6.3.7 Investigation of Antibacterial Properties 190

6.4 Conclusions 192

7 | CONCLUSIONS & FUTURE WORK 195

7.1 Thesis Conclusions 195

7.2 Future Work 198

REFERENCES 200

List of Tables

Table 2.1: Methods for the production of nanofibres - Comparison 25
Table 3.1: Properties of solvents commonly used for electrospinning 82
Table 3.2: Screening for solvents and solvent systems – Solution properties and applied experimental conditions 88
Table 3.3: Screening for Dopants – Solution properties and applied experimental conditions 92
Table 3.4: Screening for best amount of doping – Solution properties and applied experimental conditions 94
Table 3.5: Electrospinning Parameters Used for Co-axial electrospinning 100
Table 4.1: Experimental runs according to three level full factorial experimental design 110
Table 5.1: 2^3 full factorial experimental design for the electrospinnability of chitosan solutions 135
Table 5.2: Mixed level factorial experimental design for the electrospinnability of PANI/CH blends 136
Table 5.3: Mixed level factorial experimental design for the electrospinnability of CHgPANI solutions 137
Table 5.4: Average nanofibre diameter for high (50%) and low (20%) values of RH. 141
Table 5.5: Comparison of average diameters and diameter distributions expressed as coefficient of variation, for each of the electrospun solutions 3% and 5% w/v, applied voltages 22.5kV and 28.5kV and at fixed RH 20%. 145
Table 5.6: Measured current on the collector brought by the fibres, with respect to solution composition and applied voltage 155
Table 6.1: Electrospinning parameters and resulting PANI/PEO nanofibre diameters at different PETA content 169
Table 6.2: Electrospinning parameters and resulting PANI/CH nanofibre diameters at different PANI content 170
Table 6.3: Measured Surface Tension for Chitosan and PANI/CH blend solutions 170
Table 6.4: Contact angle measurements for electrospun PANI/CH membranes after neutralization 177

List of Figures

Figure 2.1: The electrospinning process.....30
Figure 2.2: Effect of varying the applied voltage on the formation of the Taylor cone 41
Figure 2.3: Chemical Structure of PANI.....50
Figure 2.4: Different oxidative and protonated states of polyaniline 52
Figure 2.5: Representation of tangential (E_t) and normal (E_n) electric fields at the fluid surface with the application of high voltage [85].....56
Figure 2.6: (A) Schematic of side-by-side nozzle configuration. (B) Schematic of coaxial nozzle configuration [70].....60
Figure 2.7: A. Conventional profile of release vs desired sustained release profile 62
Figure 2.8: Schematic illustration of the controlled release of dexamethasone: (a) dexamethasone-loaded electrospun PLGA, (b) hydrolytic degradation of PLGA fibres leading to release of the drug, (c) electrochemical deposition of PEDOT around the dexamethasone-loaded electrospun PLGA fibre slows down the release of dexamethasone (d). (e) PEDOT nanotubes in a neutral electrical condition. (f) External electrical stimulation controls the release of dexamethasone from the PEDOT nanotubes due to contraction or expansion of the PEDOT [147].....63
Figure 3.1: Electrospinning Setup A: Electrospinning Chamber and Syringe Pump 80
Figure 3.2: Molecular structure of PEO.....85
Figure 3.3: Molecular structure of A: PVA, B: Eudragit S-100, C: PCL, D: PLA 86
Figure 3.4: Comparison of PANI electrospinning with different carrier polymers: A. PVA, B: Eudragit, C: PCL, D: PLA, E: PEO, Fa: Chitosan/PEO with undoped PANI, Fb: Chitosan/PEO with CSA predoped PANI 87
Figure 3.5: CSA doped PANI/PEO A: in chloroform:NMP (80:20) B: in chloroform:DMSO (80:20) C: in chloroform:DMF (80:20) 90
Figure 3.6: CSA doped PANI/PEO A: in chloroform B: in DCM C: in 50:50 chloroform/acetonitrile D: 50:50 chloroform/acetone E: in 50:50 chloroform:DCM.....91
Figure 3.7: A: undoped PANI/PEO B: DBSA doped PANI/PEO C: glutaric acid doped PANI/PEO with doping ratio 0.8:1 and D) glutaric acid doped PANI/PEO with doping ratio 4:1.....93

Figure 3.8: CSA doped PANI/PEO (1:1) in chloroform with different ratios of dopant/polyaniline A) 0:1 B) 0.5:1, C) 1,3:1, D) 3:1, E) 5:1, F) 7:1 95
Figure 3.9: Relationship between amount of doping and solution conductivity 97
Figure 3.10: A: Electrospun PLA nanofibres, B: *In situ* polymerized PANI on electrospun PLA nanofibres, C: Cross-sectioned area of the *in situ* polymerized PANI on electrospun PLA mat, D: Cross-sectioned area of the *in situ* polymerized PANI with the presence of surfactant, on electrospun PLA mat. 99
Figure 3.11: PVA-PANI core-shell fibres fabricated with 0.5mL/hr / 0.5mL.hr, 22kV, 20%RH: A SEM image, B: Confocal Fluorescence Microscope image, C: TEM image 101
Figure 4.1: Modified electrospinning setup to control environmental humidity 108
Figure 4.2: SEM images for the comparison of flow rate variation on the nanofibre morphology. The samples on each row are electrospun at same voltage and RH and at decreasing flow rate (mL/h): A, B & C at 13.5kV and 18%RH and D, E & F at 9.2kV and 25%RH 112
Figure 4.3: SEM images showing the effect of relative humidity variation on the nanofibre morphology. The samples on each row are electrospun at same voltage and flow rate and at decreasing %RH: A, B & C at 5kV and 1mL/h, D, E & F at 5kV and 2mL/h G, H & I at 13.5kV and 3mL/h 113
Figure 4.4: SEM images for the comparison of applied voltage variation on the nanofibre morphology. The samples on each row are electrospun at the same %RH and flow rate and at decreasing applied voltage. A, B & C at 18%RH and 1 mL/h, D, E & F at 18%RH and 2 mL/h 115
Figure 4.5: SEM images of electrospun 100% CSA doped PANI–PEO solution under various process parameters at 18%RH 116
Figure 4.6: Electrospinning window of 60% doped PANI-PEO solution, grouped by the flow rate, A) 1mL/h B) 2mL/h, C) 3mL/h 118
Figure 4.7: Combined effect of voltage/flow rate/relative humidity on the electrospinnability of PANI/PEO blend 119
Figure 4.8: Diameter Distribution for electrospun mats at 18% RH: A) 1mL/h, 13.5kV B) 2mL/h, 13.5kV C) 3mL/h, 13.5kV, D) 1mL/h, 9.2kV E) 2mL/h, 9.2kV and F)) 3mL/h, 9.2kV G) 1mL/h, 5kV H) 2mL/h, 5kV 121
Figure 4.9: Effect of the applied voltage on the nanofibre diameter 123

Figure 4.10: Effect of flow rate on the nanofibre diameter..... 124
Figure 4.11: Graphic representation of the fitting of the experimental data to the theoretical model. A: The terminal jet diameter, d_f shown as a function of Q/I compared to the theory. B: Direct comparison of experimental and predicted values at various flow rates..... 126
Figure 5.1: Molecular structure of chitosan..... 131
Figure 5.2: Graft polymerization of aniline on the amino group of the chitosan backbone [209]..... 132
Figure 5.3: SEM pictures of chitosan solutions of A: 5% w/v and B: 3% electrospun at 28.5kV and 45%RH, C: 5% w/v and D: 3% w/v electrospun at 23kV and 45%RH, E: 5% w/v and F: 3% electrospun at 28.5kV and 20%RH..... 139
Figure 5.4: SEM pictures of chitosan solutions of 3% w/v electrospun at A: 23kV and 20%RH, B: 23kV and 45%RH, C: 28.5kV and 20%RH, D: 28.5kV and 45% RH..... 140
Figure 5.5: SEM pictures of chitosan solutions of 5% w/v electrospun at A: 28.5kV and 45%RH, B: 22.5kV and 45%RH, C: 28.5kV and 20%RH, D: 22.5kV and 20% RH and 3% w/v solution electrospun at E: 28.5kV and 45%RH, F: 22.5kV and 45%RH, G: 28.5kV and 20%RH, H: 22.5kV and 20% RH..... 143
Figure 5.6: Electrospun CHgPANI solutions A: 3% w/v CHgPANI-40 electrospun at 26kV, B: 3% w/v CHgPANI-20 electrospun at 22kV, C: 3% w/v CHgPANI-10 electrospun at 22kV, D: 5% w/v CHgPANI-40 electrospun at 26kV, E: 5% w/v CHgPANI-20 electrospun at 22kV, F: 5% w/v CHgPANI-10 electrospun at 22kV..... 146
Figure 5.7: A, B & C: Electrospinnability window of blends with different PANI ratios, at various voltages and at fixed RH: A: 20%, B: 35%, C: 50%..... 148
Figure 5.8 A, B & C: Electrospinnability window of blends with different PANI ratios, at various RH and at fixed applied voltage: A: 22.5kV, B: 25.5kV, C: 28.5kV..... 150
Figure 5.9: Diameter Distribution of PANI-CH blends electrospun at various voltages and at fixed RH 20%..... 151
Figure 5.10: The current transferred by the fibres on the collector in relation to high (50%) and low (20%) environmental humidity values for different blends with different concentration of PANI electrospun at different voltages..... 154

Figure 5.11: SEM pictures of solutions A: 0:1 electrospun at 28.5kV, 16cm, B: 0:1 at 22.5kV, 13cm, C: 1:1 at 28.5kV, 16cm, D: 1:1 at 22kV, 13cm, E: 1:1 at 29kV, 15cm, F: 1:1 at 29kV, 10cm..... 156
Figure 6.1: SEM images of A: Chitosan, B: PANI/CH 1:3, C: PANI/CH 3:5 D: PANI/CH 1:1 electrospun membranes – Images are representative of three membranes prepared for each condition..... 171
Figure 6.2: Electrospun PEO containing membranes after crosslinking and immersion in PBS (7 and 14 days)..... 173
Figure 6.3: Electrospun chitosan containing membranes after neutralization and immersion in PBS (7 and 15 days)..... 174
Figure 6.4: Comparison chart of membrane conductivity before and after neutralization (note the different order of magnitude for the two curves)..... 179
Figure 6.5: Fluorescence LIVE/DEAD stain for PANI:CH membranes (3d in culture): A & B, E & F: Live at two different membrane regions for each blend C & D, G & H Dead staining for the same two membrane regions of each blend..... 181
Figure 6.6: Proliferation rates of A: Osteoblasts – Attachment time 1 day. B: Osteoblasts - attachment time 3 days. C: Fibroblasts – Attachment time 3 days. All bars represent mean values from triplicate experiments and the error bars represent the ranges of the measured values..... 183
Figure 6.7: Microscope Images (10X) of A: osteoblasts on TCP B: osteoblasts on glass slides, C: fibroblasts on TCP, D: fibroblasts on glass slide..... 187
Figure 6.8: Scanning Electron Microscope Images of osteoblasts A&B: on glass slide, C&D: 1:3 PANI:CH membrane, E: 3:5 PANI:CH membrane F: 1:1 PANI:CH membrane 188
Figure 6.9: Scanning Electron Microscope Images of fibroblasts - A&B: on glass slide, C&D: 1:3 PANI:CH membrane, E: 1:1 PANI:CH membrane..... 189
Figure 6.10: Antibacterial activity as evaluated by the inhibition zone (in cm) of blend mats against A: *B. subtilis* and B: *E. coli*. All bars represent mean values from triplicate experiments..... 191

Nomenclature

Abbreviations

2D	Two Dimensional
3ABAPANI	Poly(aniline-co-3-aminobenzoic acid)
3D	Three Dimensional
AB	Alamar Blue
AMPSA	2-Acrylamido-2-,ethyl-1-propanesulfonic acid
APS	Ammonium persulfate
ATP	Adenosine triphosphate
CA	Cellulose acetate
CAGR	Compound annual growth rate
CFUs	Colony forming units
CH	Chitosan
CHgPANI	Chitosan grafted polyaniline
CNT's	Carbon nanotubes
COS	Chitosan oligosaccharide
CSA	Camphorsulfonic Acid
DBSA	Dodecylbenzenesulphonic acid
DCM	Dichloromethane
DMF	Dimethyleformamide
DMSO	Dimethyl sulfoxide
EB	Emeraldine base
EF	Electric field
ES	Emeraldine salt
FTIR	Fourier transform infrared spectroscopy
GPC	Gel permeation chromatography
HCl	Hydrochloric acid
hMSC's	Human mesenchymal stem cells

HMW	High Molecular Weight
ICP	Intrinsically conducting polymers
MC	Methylene chloride
Na_2CO_3	Sodium Carbonate
NaCl	Sodium Chloride
NaOH	Sodium hydroxide
NMP	N-methyl pyrrolidone
PA	Peptide amphiphile
PABSA	p-Acetamidobenzenesulfonyl Azide
PAN	Polyacrylonitrile
PANI	Polyaniline
PBS	Phosphate buffered saline
PCL	Polycaprolactone
PEDOT	Poly (3,4-ethylene dioxythiophene)
PEG	Poly (ethylene glycol)
PEO	Poly (ethylene oxide)
PETA	Pentaerythritol triacrylate
PHT	Poly (-hexyl-thiophene)
PLA	Poly (lactic acid)
PLCL	Poly (lactide-co-caprolactone)
PLGA	Poly (lactic-co-glycolic acid)
PLLA	Poly-L-lactic acid
PMMA	Poly (methyl methacrylate)
PNIPAm-co-MAA	Poly(N-isopropyl acrylamide-co-methacrylic acid
PPV	Poly(p-phenylene-vinylene)
PSU	Polysulfone
PTFE	Polytetrafluoroethylene
p-TSA	p-toluenesulfonic acid
PVA	Poly (vinyl alcohol)

PVP	Poly(vinyl pyrrolidone)
RFU	Relative Fluorescence Units
RH	Relative humidity
SEM	Scanning electron microscopy
TCD	Tip to collector distance
TCP	Tissue culture plastic
TEM	Transmission electron microscopy
TEP	Transepithelial electrical potential
TFA	Trifluoroacetic acid
THF	Tetrahydrofuran
$Ti(OiPr)_4$	Titanium Isoproxide
TIPS	Thermally induced phase separation
XRD	X-Ray Diffraction

Symbols

C	Polymer concentration	g/mL
d	Thickness of conducting layer	mm
d_f	Fibre diameter	nm
E_n	Normal electric field	V/m
E_t	Tangential electric field	V/m
h	Terminal diameter of the jet	nm
H	Distance between needle and collector	cm
I	Current	A
K	Conductivity	S/m
L	Length of the needle	cm
Mw	Weight average molecular weight	g/mol
Q	Flow rate	m^3/s
R	Radius of the needle	mm
R_S	Sheet resistance	Ω/sq

T	Temperature	°C
V	Voltage	V

Greek Letters

ɣ	Surface tension	mN/m
η	Shear viscosity	Pa·s
δ	Solubility parameter	$MPa^{1/2}$
ε	Dielectric permittivity	
ρ	Bulk resistivity	Ω·m
σ	Surface charge density	C/l
τ_{es}	Tangential electric stress	kV /cm
χ	dimensionless whipping instability	

1 | INTRODUCTION

1.1 Thesis Overview

This thesis is divided into 7 chapters: One introductory chapter (Chapter 1), one chapter consisting the literature review (Chapter 2), where the theoretical background knowledge is discussed and the relevant published research studies are critically reviewed and linked to this thesis, four experimental chapters (Chapters 3-6), each one self-contained and focusing on different aims and research questions and a final one (Chapter 7) where the most important findings of this work are summarized, discussed and linked to future work.

1.2 Publications and Presentations

The publications and presentations derived during the conduction of this thesis are listed below:

Journal Papers

P. Moutsatsou, K. Coopman, M. B. Smith, and S. Georgiadou, "Conductive PANI fibers and determining factors for the electrospinning window," Polymer, vol. 77, pp. 143–151, Oct. 2015

P. Moutsatsou, K. Coopman and S. Georgiadou, "Novel biocompatible electrospun chitosan / conducting polyaniline nanofibers", Materials Science and Engineering C, Under Review

Conference Presentations

"Composite electrospun conducting nanofibers for biomedical applications", P. Moutsatsou, S. Georgiadou, 11th International Conference and Expo on Nanoscience and Molecular Nanotechnology, 20-22nd October, 2016, Rome, Italy

"Electrospinning of polyaniline for tissue engineering applications", P. Moutsatsou, S. Georgiadou, Joint Conference of EPSRC and MRC Centres for Doctoral Training in Tissue Engineering and Regenerative Medicine, 8th July 2016, University of Manchester, UK

"Novel electrospun chitosan fibres incorporating conducting PANI for biomedical applications", P. Moutsatsou, S. Georgiadou, ELECTROSPIN 2016, 28th June-1st July, Otranto, Italy

"PANI/PEO electrospinning - Determining factors of the electrospinning window", P. Moutsatsou, K. Coopman, M.B. Smith, S. Georgiadou, Cross Cadre Conference, 10th April, 2014, Keele University, UK

1.3 Background

Nanofibre technology is an emerging field of particular interest to the biomedical community, as current research findings orientate towards using nanofibres as a potential solution to the current biomedical challenges. In 2012 the nanofibre market was worth US$ 151.7 million, 16% of which was directed to the biomedical sector and rose to US$ 276.8 million by 2014. For the period 2015 - 2022 the compound annual growth rate (CAGR) is estimated to be 38.6% reaching from 383.7 million at 2015 to 2 billion by 2020. Healthcare & biomedical industry is expected to be the fastest growing segment of global nanofibres market, which is expected to witness a CAGR of 36.8% during the forecast period [1], [2].

Nanofibres can be applied in the biomedical field for a variety of uses: delivery of bioactive molecules such as drugs, growth factors, enzymes etc, fabrication of "smart" medical textiles, biosensors, medical implants, membranes for molecular filtration systems or as scaffolds for cell growth and tissue engineering. Their nano-structure "mimics" the native extra cellular matrix (fibrils) and offers malleability to conform to a wide range of sizes and shapes.

Nanofibres are attractive to the biomedical field for several reasons. Firstly, surface to volume ratio is much higher compared to bulk materials, which allows for loading high volume of therapeutics. Secondly, nanofibres can be fabricated into sophisticated macro-scale structures and therefore hierarchical structures that mimic those of the human body can be produced and used as scaffolds for tissue repair and regeneration purposes [1], [2], [3].

Potential applications of nanofibre matrices in tissue engineering would be for wound care and wound dressing [6], bone regeneration [7]–[9], prevention of post-surgical adhesions (e.g. abdominal laparotomy management) [10], nerve repair [11], tendon and ligament regeneration [12]–[14], vascular grafts [15]–[17], muscle tissue repair [18] and even dental composites [19].

Furthermore, bioactive compounds, such as growth factors [20], minerals [8],drugs [21] and proteins [22] can be incorporated in those nanofibre scaffolds so as to enhance cell adhesion and proliferation, and to guide cell activity. By careful selection of polymers, drug binding mechanisms can be tailored for each desired application leading to control over the release rate of these compounds, so that cell attachment and differentiation can be enhanced for tissue engineering purposes [3].

These scaffolds can also be exploited as drug delivery devices for localized delivery of, for example anticancer drugs for prevention of cancer metastasis [23] or after tumor removal [24], [25], nucleic acids for gene therapy [26], [27], antibiotics for suppression of inflammation [10], [28], antibacterial drugs [6] etc. Especially the large surface to volume ratio not only can reassure a high therapeutics take up, it can also reduce the constraint to drug diffusion leading to increases in total fraction of drug that can be released. Thus, they are considered very favorable for tissue engineering purposes and medical implants and very promising for drug delivery applications [4], [29]. Targeted local drug delivery also gives us the opportunity to efficiently use drugs, such as immunosuppressive or antitumor ones, which when delivered systemically are known to cause severe side effects but when delivered locally at adequate dosage exhibit an optimized therapeutic result [25], [30].

2| LITERATURE REVIEW

This chapter is focusing into the review of the aspects governing the electrospinning technique and the identification of the gaps in the knowledge regarding this procedure. The function, properties and potential application of conducting polymers in the biomedical sector is being investigated as well, with a main focus on polyaniline.

2.1 Principles of Electrospinning

Electrospinning is the most widely used technique for the fabrication of nanofibres because of the significant advantages it has to offer compared to other techniques (such as molecular self assembly, template synthesis, drawing or thermally induced phase separation). A short description and advantages and disadvantages for each one are summarized in Table 2.1.

The electrospinning process was patented by Formhals in 1930 and since then it has proven to be a robust and versatile technique for the fabrication of nanofibres [31]. It is simple and low cost, easily scalable method and a very wide range of materials can be used for mass production of continuous electrospun nanofibres.

As is shown in Table 2.1, the electrospinning technique helps to overcome some of the problems commonly acquainted when other techniques are used, mostly the restriction of materials than can be used and the complexity of the processes that need to be followed. The disadvantages that electrospinning presents, are not unsurmountable; for example, complete solvent removal is easy to achieve by thoroughly washing the produced fibres (a step that would be applied independently of the technique used, if the produced fibres are destined for biomedical applications and/or drying the produced fibres in a vacuum oven. Also, the extensive research in the field the past years has helped to tackle the porosity issue as well as to prepare 3 dimensional scaffolds with structural integrity, good mechanical properties and adequate porosity, that can successfully promote cell infiltration and sustain cell culture [32], [33]. Combination of electrospinning with other available techniques

(mainly 3D printing) has been reported as well towards this end and has provided some promising results for further research in the tissue engineering field, but cannot yet be used as a stand-alone method for the production of nanofibres [34]–[36].

Table 2.1: Methods for the production of nanofibres - Comparison

Method	Description	Advantages	Drawbacks
Electrospinning	See Section 2.2.1.	➢ Cost-effective ➢ Easily scalable ➢ Vast variety of materials ➢ Control over nanofibre dimensions and orientation ➢ High productivity	➢ Use of toxic solvents ➢ Poor cell infiltration into the pores of the nanofibrous mat ➢ 2D pore or microstructure arrangement [37]
Molecular Self-Assembly	Molecules, namely nucleic acids, dialkyl-chain peptide amphiphiles (PA's) arrange themselves spontaneously into structurally defined stable patterns through pre-programmed non-covalent interactions, such as hydrogen bonding, hydrophobic interactions, van der Waals forces, side – chain and electrostatic interactions [37], [38].	➢ Tailorable properties by tuning the composition of amino acid chains. ➢ Simple fabrication process ➢ Possibility for cell encapsulation during the self-assembly process. ➢ Possibility of self assembly *in vivo,* after injection in the body [9], [37]	➢ Insufficient mechanical properties for stable 3D geometries required for hard tissue engineering. ➢ High cost of PA synthesis ➢ Time consuming ➢ Limited choice of molecules that have the ability to self-assemble. ➢ Limited control on the pore size and shape within the hydrogel scaffold [5], [9]

Method	Description	Advantages	Drawbacks
Template Synthesis	A nanoporous membrane is used as a template so as to obtain the desired structure. Then, water pressure or mechanical force is used to extrude the polymer from the membrane. As soon as the polymer comes in contact with the solidifying agent, fibres with diameter correspondent to the membrane pore size are produced [39]–[41]	➢ Great range of materials ➢ Solid or hollow nanofibres can be produced ➢ Good control on fibre diameter [37], [42]	➢ Need for a post-synthesis process step, for template removal poses limitation on the fibre length, orientation and arrangement [37], [42].
Thermally induced phase separation (TIPS)	A thermodynamic process where a homogeneous multi - component system tends to separate into multiple phases to lower the system free energy. A polymer is initially dissolved in solution and then either using heat (most commonly) or by introducing a	➢ It can be incorporated with other scaffold production techniques so as to introduce macro or micro pore/channel networks within 3D nanofibrous scaffolds.	➢ Limited range of materials ➢ Poor control over the nanofibres arrangement ➢ Application possible only on laboratory scale [5], [9]

Method	Description	Advantages	Drawbacks
	non-solvent, two phases are formed: a polymer-rich and polymer-poor / solvent-rich. Upon solvent removal (achieved by the addition of water), cooling and freeze drying, the polymer-rich phase solidifies to form the polymer skeleton and the polymer-poor phase becomes the void space [9], [37], [43].	➢ No need for specialized equipment ➢ Good reproducibility [5], [9]	
Drawing	Nanofibres can be mechanically drawn by contacting a previously laid droplet of a polymer solution with a sharp tip and drawing it as a liquid fibre which is quickly solidified because of the high surface area. A suspended fibre can be formed by connecting the drawn fibre to another deposited polymer solution	➢ No special equipment needed ➢ Simple procedure ➢ Vast selection of materials	➢ Technically challenging (the diameter of the drawn fibre is affected by the continuous reduction of the polymer solution volume, resulting in nanofibres with inconsistent diameter and of limited length) ➢ Low productivity

Method	Description	Advantages	Drawbacks
	droplet [44], [45].		➢ Limited to lab-scale applications [37]
Rapid prototyping (3D printing)	This is a common name for a group of techniques that can generate a physical model directly from computer-aided design data. It is an additive process in which each part is constructed in a layer-by-layer manner [34].	➢ High control on the shape of the produced object ➢ High reproducibility ➢ Wide range of materials [34]	➢ Time consuming ➢ Still limited to lab-scale applications ➢ Limitations in the production of fibres with nano-scale diameters [46]

2.1.1 Electrospinning Setup

The method principle relies on the application of an electric field between a grounded target and a capillary tip (spinneret) containing a polymer solution or melt. When the electrostatic force becomes greater than the surface tension of the polymer, an electrified polymer jet is formed, which travels towards the grounded target. This electrified jet is subjected to stretching and whipping while at the same time the solvent evaporates, leading to the formation of a long thin thread. The final diameter of the thread can therefore be of the nanometer scale. Attracted by the grounded collector, the charged fibres are deposited on it, as a randomly oriented, non-woven mat [37], [47], [48]. More specifically, the process could be divided into three sections: 1. The Taylor cone formation 2. The jet stretching and linear travelling and 3. The whipping instability region [49]. The application of a high voltage, in the range of kilovolts, electrostatically charges the surface of the fluid droplet that is held at the edge of the nozzle, forming what is known as the Taylor cone. The droplet becomes unstable because of the electric field and when the latter reaches a certain value (so that the electrostatic forces exceed the forces related to the fluid's surface tension), a single fluid jet is drawn from the apex of the Taylor cone. The jet follows initially a linear trajectory, but it then begins to whip out at some critical distance from the nozzle. This is referred to as the bending instability, triggered by non axisymmetric perturbations of the position and velocity of the jet because of: firstly, the repulsive forces growing between adjacent elements of charge carried by the jet and/or secondly, the presence of a dipolar charge distribution induced by lateral fluctuations of the centreline of the jet as the charge on the jet surface shifts to accommodate the changes in surface geometry, screening out the electric field inside the jet. Then, as the it travels spiraling towards the collector, higher order instabilities are caused and the diameter of these spiral loops grows larger as the jet becomes longer and thinner [6], [49]–[51]. In some cases though, it has been shown that use of a solvent with low dielectric constant, can prevent the initiation of the bending instability, as it provides low charge density on the surface of the jet [6]. In Figure 2.1, the electrospinning process is depicted.

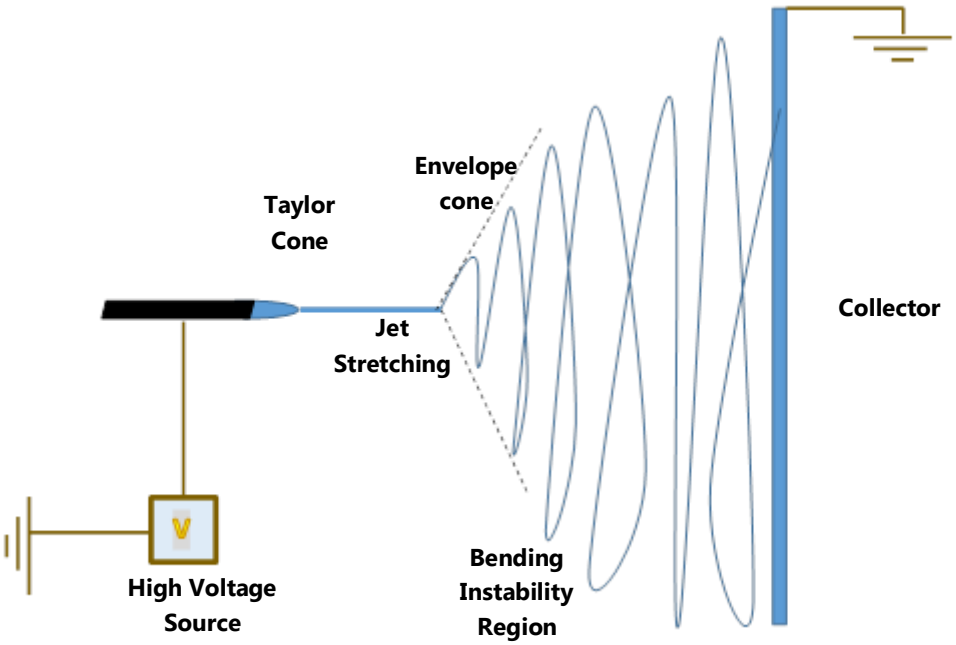


Figure 2.1: The electrospinning process

The final physical properties of electrospun nanofibres such as diameter, porosity and flexibility are highly customizable through the material choice and the process parameters (e.g. voltage, polymer solution concentration, fibre orientation, distance between spinneret and collector, spinneret diameter etc) and are examined in detail in the following sections [3], [4], [9].

2.1.2 Parameters affecting the electrospinning process and nanofibre morphology

The morphology of the electrospun fibres has been shown to be influenced by a variety of factors including solvent properties (dielectric constant, volatility), solution properties (viscosity, surface tension, conductivity, polymer concentration and molecular weight, incorporation of additives such as salts or surfactants), environmental conditions (temperature, humidity) and process parameters (applied voltage, flow rate, needle tip to collector (TCD) distance, needle diameter, type and size of collector) [52]–[56].

2.1.2.1 Effect of Solvent Properties

The choice of solvent is very important for the electrospinning process as it determines to a great extent the properties of the electrospinning solution.

Solubility Parameter

One very important property of the solvent chosen for the polymer or polymer system to be electrospun, is its suitability for dissolution of the desired polymer(s). Although it is not crucial that it is a perfect solvent for the material in question, it is necessary that the liquid to be electrospun is homogeneous for the electrospinning process to be stable and the nanofibrous mesh uniform [57]. In many cases this information can be drawn from the literature, referred to as solubility parameter for the solvent and cohesion parameter for the polymer. The most common parameter used is the Hildebrand parameter firstly defined as the square root of the *cohesive energy density (δ)*.

$$\delta = \sqrt{\frac{\Delta H_v - RT}{V_m}} \qquad (1)$$

This parameter was then divided by Hansen in three components. Specifically, each molecule is given three Hansen parameters, each measured in $MPa^{0.5}$:

- δ_d The energy from dispersion forces between molecules
- δ_p The energy from dipolar intermolecular force between molecules
- δ_h The energy from hydrogen bonds between molecules.

$$\text{so that, } \delta = \sqrt{\delta_d^2 + \delta_p^2 + \delta_h^2} \qquad (2)$$

In order for a polymer to be soluble in a certain solvent, the difference between their solubility parameters has to be as close to zero as possible [58].

It is also possible to use a system of solvents where one of them is a good solvent for the polymer to be electrospun and the other one is a non-solvent. Carefully calculated composition of this solution so as not to result in phase separation before electrospinning, can be used to produce porous nanofibres and to fine tune pore size

and surface area. The mechanism behind pore formation relies on the induction of thermodynamic instability in a polymer solution, which causes its separation to polymer rich and polymer poor phases. The polymer rich phase forms a matrix, on which the pores are formed from the polymer poor phase [59].

Boiling Point

The boiling point of the solvent is an important parameter as it affects the evaporation rate of the solvent during the jet travelling towards the collector. Solvents with very high boiling point will most likely not evaporate fully before the jet reaches the collector. This may cause flattening of the nanofibres upon impact on the collector resulting in ribbon - like morphologies or it may cause fibre fusion on point contact with other fibres or even complete loss of fibre morphology [60]. On the other hand, use of solvents with too low boiling point might cause very fast evaporation at the needle tip, causing needle blockage and disruption of the process [61]. Another effect of the use of high volatility solvent has been shown by Megelksi et al. where electrospinning of polystyrene with tetrahydrofuran (THF, boiling point: 66°C) results in porous polystyrene fibres as compared to electrospinning under same conditions with a lower volatility solvent such as dimethylformamide (DMF, boiling point: 153°C), which resulted in smooth surface nanofibres, They attribute this phenomenon to evaporating cooling occurring on the jet when the solvent evaporates fast. This causes moisture from the surrounding air to condense on the jet, leaving behind an imprint in the form of pores, signaling the importance of the solvent's vapor pressure throughout the spinning process. However, different size and shape of pores that were formed when lower concentration was used, indicated that there might be a second mechanism involved in pore formation driven by vapor induced phase separation when the solvent used was of a low boiling point [62]. In the same study, ribbon-like morphology has been observed and has been attributed to the quick formation of a skin on the surface of the jet, which when evaporation of the solvent from the centre of the fibre occurs, it causes the skin to collapse resulting in a ribbon shape. This phenomenon has been observed and verified by other studies as well [63], [64].

Dielectric Constant

The electrostatic energy required to ionize a solute is dependent on the inverse of the dielectric constant of the solution, therefore solvents with higher dielectric constant will better dissociate the electrolytic species and result in solution with higher free charge density, improving conductivity, which is essential for the initiation of the electrospinning process. Conversely, a compound which has no electrostatic charge will dissolve better in a solvent with low dielectric constant. The dielectric constant can be directly correlated with the Hildebrand solubility parameter discussed previously. However, Torres-Giner et al [65] showed that when dissolving a polyelectrolyte such as chitosan in a high dielectric constant solvent, too high charge density in the solution, introduced by the solvent can be proved hindering for the electrospinning process, by causing extensive repulsive forces between the polycations along the polymer chain, and thus preventing sufficient chain entanglements which are necessary for electrospinning. In that case a second solvent with lower dielectric constant can be added to the solution, to facilitate the process. But when electrolytes are dissolved in aqueous solvents, another phenomenon takes place as well. The dissolved electrolyte molecules cause the solvent molecules in their vicinity to orient, much reducing their freedom to respond to an applied field, and so decreasing the value of the dielectric constant below the solvent's value. This phenomenon is known as dielectric decrement. Surface tension is also known to increase when a polyelectrolyte is dissolved in solvent media [66], [67]. For these reasons, higher electrostatic repulsion for obtaining the same fiber formation conditions is required, translating into the need for higher applied voltages.

Generally, it has also been shown that a solvent with high dielectric constant can help the charges to distribute more evenly throughout the electrospun jet. More conductive solvents also contribute to higher charge repulsions on the surface of the jet during electrospinning, thus causing it to whip and stretch for longer (as the envelope cone's angle becomes wider, see Figure 2.1), providing this way fibres with less beads and of smaller diameters [68], [69].

2.1.2.2. Effect of Solution Properties

The solution properties analyzed below are interdependent and in many studies it has been proven difficult to isolate the effect of each one on the electrospinning process, as it is very challenging to vary one and keep the others fixed in the attempt to deepen the understanding of their effect on the process. For example, increasing the concentration of a solution will automatically lead to increase of its surface tension and viscosity. If the polymer used is conducting, the conductivity will follow the same trend as well. In many studies, it is usually one of the three parameters (concentration, viscosity and surface tension) measured and studied and any effect and conclusion is attributed to this specific variable.

In the following paragraphs, the distinction of the effect between the three will be attempted but the combined effect of those will also be commented and discussed.

Concentration

The polymer concentration is one of the parameters that determine the electrospinnability of a solution. For every polymer system there is a concentration threshold above which there enough polymer chain entanglements occur to assure electrospinnability instead of electrospraying [70]–[72] and while for some polymers like HMW PEO, this may be as low as 1% w/v [73], for some others like polyamide-6, it may be more than 25% w/v .

Viscosity

Many studies have concluded that solution viscosity is amongst the most important parameters affecting electrospinning and the final nanofibre morphology. Viscosity is usually studied together with elasticity when the rheological properties of a polymer solution are examined. Viscoelastic forces resist rapid changes in the shape and support the formation of fibres with smooth surfaces and fewer beads. Therefore, there is a low threshold to solution viscosity, that only above this, fibre formation is possible [65]. There is also a high threshold for viscosity above which only fibres of very large diameters (micro-scale) can be produced or other practical issues occur,

like needle blockages and lack of control over the feed rate, which prevent the electrospinning process. Generally there is a consistency between different studies with various polymeric solutions, that within the range of electrospinnability, a decrease in viscosity results in decreased nanofibre diameter and that with higher viscosity the presence of beads is less frequent. Also, when beads are present, with increasing viscosity, they tend to be formed in a more spindle-like shape and the distance between them increases [57], [74]. The formation of beads is due to the coiled polymer macromolecules being transformed by the elongational flow of the jet into oriented entangled networks that persist as the jet solidifies. The solution's surface tension tends to decrease the jets surface area, transforming it into round beads and the viscoelastic forces tend to counteract this. Therefore, as the viscosity increases, the more it overtakes the opposing the surface tension, resulting in the formation of more elongated beads. With further increase of viscosity, the beads become more and more elongated so that they finally disappear. Wang et al., in an attempt to isolate and study the effect of the viscosity added a certain amount of salt each time to a polystyrene solution of variant concentration/viscosity, in order to maintain the conductivity stable. The power law relation: $d_f \sim \eta^{0.41}$ was derived (when the solution conductivity and surface tension are fixed), where d_f: nanofibre diameter and η: shear viscosity [72].

Interestingly, when trying to examine separately the viscosity and elasticity influence of a polymer fluid, with the use of aqueous analogs of Boger fluids, Yu et al., reached the conclusion that there is no correlation between the Newtonian viscosity of the fluid and the fibre morphology and that the presence of entanglements (through achievement of critical concentration) is not a prerequisite for successful electrospinning provided that the relaxation time of the fluid is longer than the time of extensional deformation. That fluid elasticity, as measured by relaxation time, is the essential property controlling the morphology of the fibres produced by electrospinning [75]. Rošic et al., however reached the exact opposite conclusion, finding that plasticity rather than elasticity is the governing parameter for electrospinning and that concentration directly affects the jet initiation. However, it has to be noted here, that this study was conducted with chitosan and alginate as

model polymers, which are polyelectrolytes and other parameters which were not investigated in the study (such as increased Coulomb forces with increasing concentration) may have intervened with the determination of the role of the polymer's rheology [76].

Polymer's molecular weight

The molecular weight of the polymer to be electrospun is directly related to the solution's viscosity and surface tension. Torres-Guinel et al showed how the molecular weight of chitosan affects the solution's viscosity and surface tension. As a result, higher molecular weight chitosan exhibited lower surface tension and higher viscosity when compared to same concentration solutions of lower and medium molecular weight chitosan solutions. These properties rendered the electrospinning process more successful, resulting in bead-free nanofibres [65]. Nezarati et al., also showed that small changes in molecular weight of polycarbonate urethane (PCU) (Mw_{high}=241kDa vs Mw_{low}=217KDa), resulted in significant different nanofibre morphologies, mainly due to the change that the molecular weight impacted on the viscosity of the two solutions. Thus, they concluded that it is better to refer to properties like viscosity or surface tension, in order to conduct comparative studies, rather than molecular weight or solution concentration values [77]. Generally, the higher the molecular weight of the polymer, better chain entanglement is achieved, therefore electrospinning becomes feasible at lower concentrations. However, as McKee et al., successfully pointed out, sufficient intermolecular interactions can act in a similar way as polymer chain entanglements, allowing electrospinning of oligomers [78]. In their study, they showed how lecithin, a natural mixture of phospholipids and neutral lipids, can be electrospun at certain concentrations by forming cylindrical or wormlike reverse micelles in non-aqueous solutions which overlap and entangle in a similar way to that of polymer chains in semi-dilute or concentrated solutions. Water and other polar molecules serve to bridge the phosphate head groups between neighboring phospholipids through hydrogen bonds, rendering electrospinning possible.

Surface Tension

The solution's surface tension is one of the most important properties to determine the electrospinnability window of a particular solution as it tends to convert the liquid jet into one or many spherical droplets by minimization of the surface area. Generally, surface tension determines the upper and lower boundaries of electrospinning window if all other variables are held constant. Very high surface tension is more likely therefore to force the solution into beads rather than fibres. Lower surface tension on the other hand, helps electrospinning to occur at a lower electric field [65], [79].

The value of a solution's surface tension is mainly attributed to the selection of the solvent, and secondarily to the polymer's concentration. Yang et al., investigated the influence of surface tensions on the morphologies of electrospun PVP with ethanol, DMF and methylene chloride (MC) as solvents. They found that the different surface tension caused by the use of different solvent, when the concentration and all process parameters were kept fixed, lead from beaded fibres to the production of smooth fibres. Of course, in that case, lower surface tension was accompanied by higher viscosity as well, therefore the effect of the surface tension alone wasn't highlighted. It must be noted here, that the dielectric constant of the solvents also varied, although not commented by the authors, there seems to be no correlation between the dielectric constant and the existence of beads, and it must have had negligible effect on the morphology of the produced fibres [80]. Similarly, Fong et al., in another study, introduced ethanol, which exhibits low surface tension and boiling point, to an aqueous PEO solution, in an attempt to improve the morphology of produced fibres. This addition lowered the surface tension, increasing at the same time the viscosity, indeed resulting in beadless and smoother filaments [74]. But, when Zhang et al., tried as well to incorporate ethanol, as a co-solvent to an aqueous PVA (Polyvinyl alcohol) solution, they observed that instead of having a positive effect on the fibre morphology, even when incorporated at low ratios, it lead instead to the appearance of beads. This was attributed to ethanol being a non-solvent of PVA, which together with lowering the solution's surface tension, it lowered the viscosity too, subsequently leading to deteriorated fibre morphology [81].

Therefore, the effect surface tension changes have to be considered together with changes in viscosity when evaluating a solvent system for an electrospinning solution. A common practice is the addition of a surfactant in the electrospinning solution, in order to lower the surface tension and facilitate the electrospinning process. However, the addition of surfactant does not guarantee electrospinnability if other essential parameters for the onset of electrospinning, such as for example, sufficient chain entanglements are not in place first [82]. But when electrospinning is possible, the addition of non ionic surfactants, as expected, has been found to result in the refinement of nanofibres [83]. Ionic surfactants can also be added, which apart from lowering the surface tension can contribute also to increasing the conductivity of the electrospinning solution [84].

Conductivity

The two parameters affected by the solution conductivity are the surface charge density and the tangential electric field that both determine the Taylor cone formation and the ejected linear jet.

It has been generally accepted that the solution must be a leaky dielectric to be electrospun efficiently. Leaky dielectric solutions exhibit the ability of quickly conducting the charges to the surface from the interior and the ability to sustain the electric field tangential to the fluid surface. The dielectric properties of a liquid are primarily governed by the conductivity, permittivity, ionization, and polarization characteristics of the material and therefore, these have a significant effect on the electrospinnability of a solution. Thus, it is difficult or even impossible, in some cases, to electrospin solutions that are highly conductive or highly insulating though, the other properties of a polymer solution are in the required range for electrospinning [85].

In the case of highly insulating liquids with no dielectric properties, when an external electric field is applied, there are not enough free carriers at the surface of the liquid, resulting in reduced charge density, thus no Taylor cone is formed from the pending droplet, and electrospinning cannot initiate. Secondly, beyond the Taylor cone formation, during the jet thinning stage, electrostatic repulsive forces on the jet

are very important as they tend to increase the surface area, thus favoring the formation of a thin jet associated to the electrospinning process and the formation of thin fibres [65].

On the other hand, solutions with very high conductivity are also not electrospinnable because of the depleted tangential electric field along the surface of the fluid droplet, which becomes the dominant phenomenon due to the high recombination rate, which is decreasing the electrostatic force along the surface of the droplet and not allowing for Taylor cone formation either [54], [85], [86].

Angammana et al. noted that the solution conductivity and the average jet current are closely related, with the jet current initially increasing for increasing solution conductivity and then decreasing with a further increase at solution conductivity. They also demonstrated a power relationship between increasing solution conductivity and decreasing fibre diameter. These findings can be attributed to the charge distribution on the surface of the solution droplet and the tangential field applied to it (Figure 2.4). At their study they used NaCl salts to increase the solution's conductivity. The addition of NaCl salt in the solution interferes in two ways though, first it increases the number of free ions, moving towards the surface of the droplet, increasing surface charge density, and secondly it increases the conductivity of the solution, allowing for decrease of the tangential electric field applied on the surface of the solution [54]. Generally, the addition of small amount of salts in electrospinning solutions is known to contribute in the elimination of beads, by increasing the net charge density on the surface of the jet [47]. Sun et al., in another study incorporated different amounts of an organic ammonium salt to alter the conductivity and thus the free charge density of PEO-chloroform solution, proving that with increasing conductivity, the angle of the envelope cone of the jet increases, making more difficult the deposition of aligned fibres [6].

On a different note, increased conductivity may cause the formation of multiple jets from the fluid droplet and protrusions on the final fibres giving rise to a phenomenon known as jet splitting or splaying or branching, which is explained in detail in Section 4.3.1 [54].

2.1.2.3. Effect of Process Parameters

Similarly, as explained above, regarding the solution properties, many of the process parameters are interrelated and may affect the process, in multiple and sometimes contradictory ways, giving rise to different phenomena and different outcomes regarding electrospinnability and fibre morphology.

Applied Voltage

Contradicting results have been reported with regards to the effect of the applied voltage on the nanofibre morphology and diameter. Megelski et al., Wang et al. and Beachley et al., observed that increase of the applied voltage resulted in smaller nanofibre diameters and better uniformity, attributing this to the increased charge repulsions taking place when the jet is subjected to a stronger electric field [62], [72], [87]. Nezarati et al., also reported that increasing the applied voltage contributes to the refinement of the fibres but enhances the phenomenon of broken filaments [77].

Others however have found, that higher applied voltage resulted in slightly larger average diameter and/or broader diameter distribution [61], [81]. Zhang et al., attributed this phenomenon to the solution being removed from the capillary tip more quickly under the application of higher electric field, as the jet is ejected from Taylor cone, tampering the flow rate that was set from the syringe pump [81]. The exact relationship between voltage and fibre diameter is still quite vague and interdependent with other parameters such as solution properties. It has also been reported that, higher electric field can result in increased bead formation. Electric fields upon a certain threshold (which varies depending on the polymer solution and other process parameters may induce deformation of the Taylor cone's shape (Figure 2.2) and disruption of the flow rate, leading in the formation of beads [47], [88], [89].

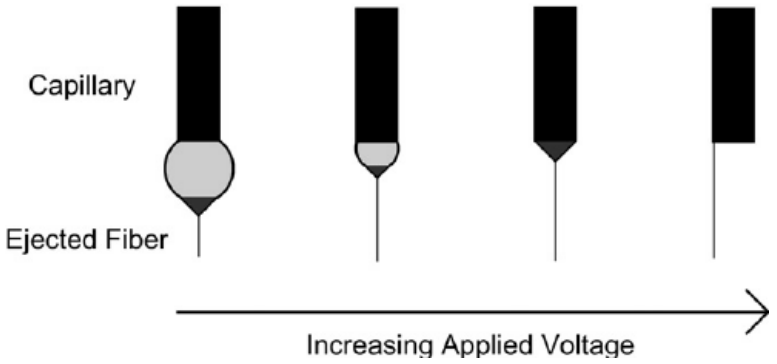


Figure 2.2: Effect of varying the applied voltage on the formation of the Taylor cone

As shown in Figure 2.2, at relatively low applied voltages a pendant drop (depicted in light gray) is formed at the tip of the capillary. The Taylor cone (depicted in dark gray) then firstly forms at the tip of the capillary and then at the tip of the pendant drop. However, as the applied voltage is increased, the volume of the pendant drop decreases until the Taylor cone is formed at the tip of the capillary. Increasing the applied voltage further, results in the fibre jet being ejected from within the capillary, which is associated with an increase in bead defects [70].

In Taylor's work [90], the minimum (critical) voltage (V_c) that has to be applied to successfully electrospin a polymer solution is calculated (Equation 3) by taking into account, only the surface tension, from the solution parameters, and some process parameters such the air-gap distance, the length of the capillary tube, and the radius of the tube.

$$Vc^2 = 4\left(\frac{H^2}{L^2}\right)\left(ln\frac{2L}{R} - 1.5\right)(0.117\pi R\gamma) \qquad (3)$$

Where H is the air-gap distance, L is the length of the capillary tube, R is the radius of the tube (units: H, L, and R in centimeters), and ɣ is the surface tension of the fluid (dyn/cm). It is shown that the higher the surface tension of the polymer solution, the higher is the voltage that has to be applied for jet initiation.

However, it must be noted here, that the above prediction equation is more likely to be in agreement with experimental results when a two plate electrospinning configuration is used, rather than the nozzle-plate configuration. Also, it is based on

the theoretical calculation that the envelope angle cone for Taylor cone formation is 49.3°. The Taylor cone angle has been independently verified by Larrondo and Manley, who experimentally observed that the semivertical cone angle just before jet formation is 50° but in another publication, it has been reported that the Taylor cone's angle should be 33.5° instead of 49.3° [91].

Flow Rate

As for the flow rate, there is consensus, generally, that the increase in flow rate can result in increased nanofibre diameter as well as increased mat porosity and sometimes in increased formation of beads; this seems to be valid for a conducting polymer blend such as PANI-PEO as well [92]. Too high flow rate normally would cause slower solvent evaporation, resulting in incomplete drying and/or bead formation. Low flow rate, on the other hand, usually results in finer nanofibres of smaller diameter and of higher homogeneity. This happens due to increase of the volumetric charge density, leading to increased stretching (provided that all other parameters such as TCD and applied voltage are maintained stable) [55], [61], [77], [92]. It has been shown that at high flow rates, the current in the jet is increased while the surface charge density is decreased, resulting in less whipping and stretching [61], [93]. However, it has also been reported that within a range, (once the flow rate applied provides enough polymer solution to the needle tip), changes at the flow rate do not influence the nanofibre diameter or length [87]. It has to be noted here though, that this range, is determined by a mass balance between the feed rate and the drawing rate that has to be achieved. For example, above that range, at quite high values of flow rate, the delivery rate of the polymer to needle tip may significantly exceed the drawing rate of the polymer by the electrostatic forces, resulting in sustained but unstable jet, either expressing as excess of polymer solution gathering at the needle tip and dripping or as formation of large beads on the final fibres [81], [87]. On the opposite end, when the drawing rate of the polymer due to electrostatic forces exceeds a lot the delivery of the polymer to the needle tip, there is unsustained Taylor cone, or even inability for Taylor cone formation and not

continuous jet formation. In that case, the flow rate value controlled by the pump would not be representative of the actual drawing [72].

Tip to collector distance (TCD)

Increasing the collector distance (given a fixed applied voltage) results in decreased electrostatic field and coulomb forces at the needle tip. The decrease of the electrostatic field this way may result in fibres of larger diameter [70], [94]. On the other hand, a longer TCD allows the jet to whip for longer, thus resulting in thinner fibres. Which of these phenomena prevail each time, is dependent on other parameters as well, such as solution properties, process properties such as voltage, and ambient variables. It should be noted here that very short TCD (>10cm) are generally avoided as, there is not enough travel time and space provided for the jet to fully solidify [21], [72]. However if the distance is too long, given the voltage/distance ratio is maintained fixed, broken fibres may be produced, due to early solidification and further stretching and whipping that they undergo before reaching the collector [61].

Type, Shape and Size of Collector

A variety of collector configurations can be used at electrospinning. The simplest and most commonly used is the square plate collector for the production of non woven mats. Usually, a metallic, conducting collector is used, as the use of non-conducting one will result in accumulation of charges on it, so further deposition of fibres will be prevented [95]. With adequate orientation or modification of the collector (e.g. spinning drum collector) aligned nanofibres can be collected, as well as other sophisticated macroscopic structures [37]. As Sutasinpromprae et al. pointed out, the use of a rotating drum collector can also be used to produce fibres of smaller diameter. When compared to the flat square one, thinner nanofibres were obtained and further increase of the rotation speed acted beneficially to the refinement of the nanofibres' morphology and not only to their alignment due to the take-up speed as they noted [96]. However, since transferring the fibres from the aluminium foil that

they are usually collected onto, to any other desirable surface for different applications, can be proved challenging, various other types of collectors have been reported including wire meshes, pins, grids, rings, plates with arrays of protrusions or ridges, parallel bars or plates, rotating rods, coagulation liquid baths, and so on [97]. Regarding the influence of the collector's size, Beachley et al. showed that when parallel plates are used to collect aligned fibres, stretching in between them, the length of the fibres can be increased without breaking when the size of the plates is increased [87].

Nozzle Configuration and Diameter

The simplest and most common nozzle configuration for electrospinning, is the single nozzle. Side by side nozzle configuration is used to simultaneously electrospin two different polymer solutions (Figure 2.5 A). As long as the two polymer solutions exhibit similar conductivities, a single Taylor cone is formed, but the ratio of the two polymers will differ along the produced fibres [98]. Coaxial electrospinning is also used to electrospin two different polymer solutions together, but this time the final product is nanofibres with distinct core and shell compositions. Core-shell electrospinning will be further analyzed in Section 2.3.2. Finally, for industrial or semi-industrial applications, multiple nozzle and nozzleless electrospinning are more commonly used.

The needle diameter is a parameter affecting final fibres' diameter but not many studies have been conducted to determine its effect as it is considered minor compared to other process parameters such as voltage, flow rate and TCD. Wang et al, noted that the needle end was completely wetted during electrospinning by the protruded pendant drop, which designated the importance of outer diameter for comparison. The size of the Taylor cone and the length of the electrified jet, increased with an increase in needle diameter. However, despite the five times difference in the needle diameter, the jet diameter was constant (ca. 4.0 μm), but the final fibre diameter was found to increase from 256 to 502 nm, accompanied by a lower drawability and less molecular orientation, for the same needle diameter difference. This is explained if the non-uniformity of the electric field, when the point to plate

configuration is taken into account. Because of a longer jet produced by the larger needle assembly, the electric field strength that the terminal jet experiences in order to undergo the bending instability deformation is evidently smaller (ca. half of that for the smaller needle), leading to less electrostatic stretching and therefore resulting in thicker fibres [99].

Sutasinpromprae et al. found that larger nozzle diameter resulted in larger fibre diameters as expected theoretically. The charged jet ejected from the larger nozzle is naturally of larger diameter as well. This leads to a longer linear distance covered by the charged jet before the bending instability phenomenon takes over, thus reducing the total path length which would be responsible for the diminution of the fibres' diameter. It maybe however, that above a certain threshold of nozzle diameter, this explanation could not still be valid as multiple jets can arise, if the needle tip is too large. Depending of course on the solution properties as well, smaller needle diameters may cause clogging [95], [96].

2.1.2.4. Effect of environmental parameters

Humidity

Humidity has been acknowledged as one of the environmental parameters, but is not always taken into account in the electrospinning models as a parameter that can significantly affect the process. On the contrary, it seems to be categorized as a minor parameter affecting the final jet diameter [52]–[56].

Studies on the effect of humidity on electrospun fibres have shown ambiguous results and will be examined in detail in Section 4.1.

Humidity variations of around 15% have been shown to have impact on the morphology of the resulting mats. The ambient relative humidity may affect the electrospinning process in various ways. First, it may decrease the solvent evaporation rate, favoring formation of thinner fibres. Also, very high humidity can cause the solvent to not fully evaporate throughout the process [88], [100]–[102]. Secondly, water absorption on the jet may induce polymer precipitation and phase separation

changing the morphology of the resulting fibres (eg fibres with porous or rough surface) [103]. Lastly, as water is electrically conducting, it may affect the charge distribution on the jet, by possibly removing charges. The latter theory though has not been yet established by systematic studies on the effect of humidity. These findings highlight that the effects of relative humidity on electrospun fibre morphology are dependent on polymer chemical structure and hydrophobicity, solvent miscibility with water and solvent vapor pressure [77].

Temperature

The change in temperature causes two main and opposing effects that have an effect on the average diameter. The first one, is the evaporation rate of the solvent. This rate decreases exponentially with decreasing temperature. Thus, at lower temperature, it takes a longer time for the jet to solidify, continuing the elongation of the jet, producing thinner fibres. The second effect is the rigidity of the polymer chains. The polymer chains move more freely at higher temperatures, resulting in lower solution viscosity and surface tension. The stretching of the polymer jet occurs due to the dominance of the stretching electric force over the surface tension and the viscoelastic forces of the polymer solution, which is thus facilitated when those decrease. Therefore, higher temperature will produce higher stretching rate and as a result thinner fibres [101], [104]. A variation of 10 degrees lower or higher of the environmental temperature (~20°C) is sufficient to affect the average fibre diameter [101]. This effect was also described by Wang et al, where not only smaller diameters were reported, but also a higher chain orientation [99].

2.1.3. Modelling – Control of Nanofibre Morphology

Several attempts have been conducted by a few groups in order to predict nanofibre morphology and more specifically nanofibre diameter by using a theoretical modelling approach. The main challenge for this type of work is to accurately describe and model the electrospinning process by using easily measured variables and parameters. For example Fridrikh et al [52] concluded with this equation

(Equation 4) after studying the motion of the electrified jet, treating it as a slender viscous object.

$$h = \left(\gamma\bar{\varepsilon}\frac{Q^2}{I^2}\frac{2}{\pi(2\ln\chi-3)}\right)^{1/3} \qquad (4)$$

This model predicts the terminal diameter of the jet (h) as a function of ε (dielectric permittivity of the medium, usually air), Q (flow rate), γ (surface tension of the solution) and I (current measured on collector); where χ is the dimensionless wavelength of the instability responsible for the normal displacements and here it is considered to equal 100. The exact value is not critical, since lnχ varies slowly [51], [52].

The terminal diameter of the jet is defined as the diameter of the jet at the late stages of whipping, where the dramatic stretching of the jet due to the whipping instability ceases. Equation (4) neglects elastic effects and fluid evaporation, and also assumes minimal jet thinning after the saturation of the whipping instability. The final diameter of the nanofibres (d_f) collected was related to the terminal jet diameter (h_t) by correcting the value for the polymer concentration (C), as sown in Equation (5).

$$d_f = h_t c^{\frac{1}{2}} \qquad (5)$$

Fridrikh et al. tested these assumptions by measuring the diameters of electrospun fibres obtained over a wide range of external conditions and from different polymer solutions (PCL in methanol, PEO in water and PANI in N, N-dimethyl formamide) [52].

Reneker et al. [50] provided a model which represents the electrified jet as a series of n beads (jet beads) with appropriate mass and charge at mutual distance l connected by viscoelastic elements which react with each other according to Coulomb's law. They are also subjected to the electrical forces produced by the applied voltage potential difference. Viscoelastic resistance and surface tension effects were taken into account in the model but aerodynamic and gravitational forces were negligible according to the analysis of the experimental data, and therefore not incorporated. Solvent evaporation was not taken into account either.

Lauricella et al. based on Reneker's analysis, took a step forward into coding an open-source computer program called JETSPIN [105], in order to incorporate Yarin's et al. [106] solvent evaporation model as this affects the viscoelastic properties of the

jet while it solidifies with time. Yarin et al. in that study, proved that solvent evaporation renders the jet more viscous with time, increasing its elastic modulous and bending stiffness, causing a significant increase of the radius of bending loops, thus improving very much the correlation of theoretical prediction models and experimental data.

The prediction of nanofibre diameter would be a more useful tool instead of the trial and error approach that is commonly used in the literature, however, still more in depth understanding of how electrified polymer solutions jets is needed, mainly because of the great variability in terms of combinations of materials and intermolecular reactions involved. Up to date, there has been no model for fibre diameter prediction or for electrospinnability of inherently conducting polymers.

2.2 Conducting Polymers

Semiconducting and metallic polymers are the fourth generation of polymeric materials as professor Bengt Rånby characteristically classified them at the Nobel Symposium (NS-81) in 1991 [107]. Natural polymers such as wood, fibres, bone and skin constitute the first generation of polymeric materials, used even in prehistoric times. Synthetic polymers constitute the second generation of polymers initiated by the work of Carothers and greatly enhanced by Ziegler and Natta. Polystyrene, polypropylene and polyethylene are typical examples of synthetic polymers, the discovery of which initiated a great breakthrough in the field of organic chemistry, with the synthetic polymers being vastly used, up to nowadays with myriad applications [107], [108]. The third generation of polymers consists of the group of polymers generally described as "engineering polymers". Those are engineered to a high level, presenting exceptional mechanical and/or thermal properties and are usually used for low-volume applications. Amide aromatic resins, polysulfones and polyurethanes are examples of the third generation polymeric materials.

Since the early work on polyacetylene conducted in the 1970's, where H. Shirakawa, A. MacDiarmid and A. Heeger actually discovered the conducting polymers and the ability to dope those over the full range from insulator to metal, till nowadays, a lot of

progress has been made in the conducting polymer science field. This initial discovery of polyacetylene signaled the first generation of semiconducting polymers, which gave way to the soluble PVP's and poly(alklylthiophenes) which are main examples of the second group of semiconducting polymers, nowadays complex molecular structures with more atoms in the repeat unit as well as copolymers constitute the third generation of semiconducting polymeric materials. Processable conjugated polymers and copolymers are already being used in various applications [108], [109].

Intrinsically conducting polymers (ICP's) are organic polymers exhibiting electrical, optical and magnetic properties similar to those of metallic materials but with the characteristic processability and mechanical properties of polymers [110]. In saturated organic polymers, all of the four valence electrons of carbon are used up in covalent bonds, but in conjugated polymers the electronic configuration is fundamentally different. In this case, the chemical bonding leads to one unpaired electron (the π electron) per carbon atom. Moreover, π bonding, in which the carbon orbitals are in the sp^2p_x configuration and in which the orbitals of successive carbon atoms along the backbone overlap, or conjugated segments are coupled with atoms providing p-orbitals for a continuous orbital overlap (e.g. N, S), leads to electron delocalization along the backbone of the polymer. This electronic delocalization provides the "highway" for charge mobility along the backbone of the polymer chain. Also, the alternation between the single and double bonds favors electron mobility and transport of electric charge within and between the polymer chains [108], [111]–[114].

The electrical conductivities of conjugated polymers can be increased by many orders of magnitude from 10^{-10}–10^{-5} to 10^{2}–10^{5} S/cm upon doping, which cover the whole insulator-semiconductor-metal range. Due to this unique nature as well as the reversible doping/dedoping process and their controllable chemical and electrochemical properties, a variety of conducting polymers (e.g., polyacetylene, polyaniline, polypyrrole, poly(p-phenylene-vinylene (PPV), poly(3,4-ethylene dioxythiophene) (PEDOT) and other polythiophene derivatives, etc.), and more specifically their 2D nanostructures such as nanotubes and nanowires, have recently received special attention in the field of nanotechnology. But it was only in the 1980's that these polymers became attractive to the medical and biological field, when it

was found that they are biocompatible with many biological molecules. Since then, they have been successfully tried on biosensors and tested as for their ability to promote cell adhesion, regulate and modulate cell differentiation, migration, protein secretion and DNA synthesis [115].

The potential of the application of conducting polymers in the field of biomedical and tissue engineering seems very promising and it has not yet been examined thoroughly, especially regarding materials in nanoscale structures. This study will be focused on conducting electrospun nanofibres and their potential application as drug delivery devices and/or tissue engineering scaffolds.

2.2.1 Polyaniline (PANI)

The term "Polyaniline" refers to a class of conducting polymers derived from the base of general composition:

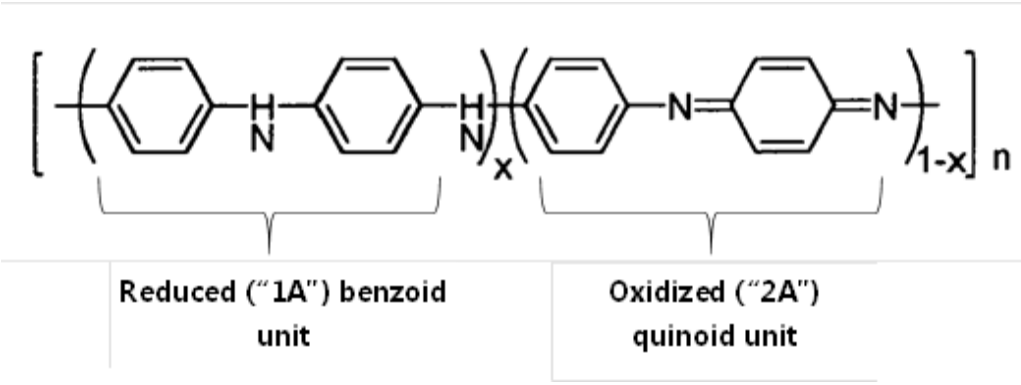


Figure 2.3: Chemical Structure of PANI

The average oxidation state is described by the parameter (1-x). This can vary from (1-x)=0, the fully reduced form known as "leucoemeraldine" form, to the fully oxidized one (1-x)=1 which would be the "pernigraniline" form. When (1-x)~0.5, the material is referred to as "emeraldine" base (EB) or salt (ES) which contains equal number of 1A and 2A units, as the case may be [116], [117]. The EB is regarded as the most useful form of polyaniline due to its high stability at room temperature, it is composed of two benzoid units and one quinoid unit that alternate and it is known to be a semiconductor [118]. In principle, the imine nitrogen atoms can be protonated in whole or in part to give the corresponding salts, the degree of

protonation of the polymeric base depending on its oxidation state and on the pH of the aqueous acid.

Compared to other conducting polymers, polyaniline presents significant advantages such as ease of synthesis, low cost of aniline monomer and good stability in environmental conditions [119]. In terms of ease of processing though, it has been reported that pure PANI films or even blend films with high polyaniline ratio present high brittleness and are not easily manipulated [120].

2.2.1.1 Structures of PANI

In Figure 2.4, the three different structures of PANI are depicted in more detail.

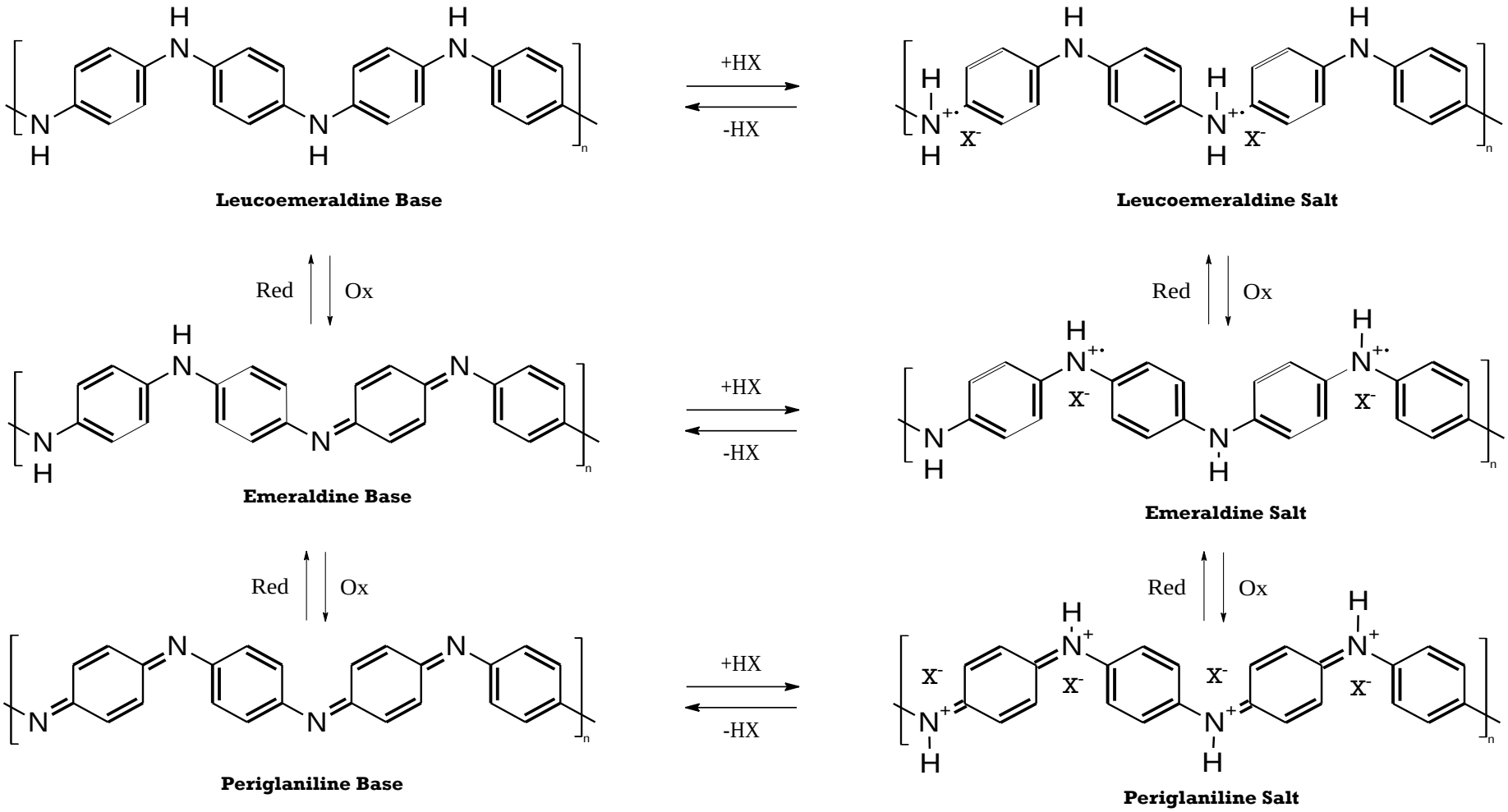


Figure 2.4: Different oxidative and protonated states of polyaniline

The properties of the polyaniline are highly dependent on the degree of oxidation and the degree of protonation. The fully reduced state of PANI, the leucoemeraldine base and salt are colorless, insulating and unstable structures. The pernigraniline base and salt are violet in color, and non conducting either. Only the emeraldine base form of PANI (colored deep blue) can be rendered conducting through a simple redox reaction, also known as doping, which gives the emeraldine salt, green in color, very stable and with tunable conductivity from 10^{-10} S/cm up to 100 S/cm which classifies the polyaniline emeraldine salt in the range of organic metals [121].

2.2.1.2 Doping

The doping reaction introduces charge carriers in the polymer chain that can move along and between the polymer chains, transforming it into a polaronic lattice and rendering it highly electrically conducting.

Doping agents are proton donors, and are therefore most usually strong acids such as hydrochloric, sulfuric, or sulfonic acids. The electrical conductivity of the doped PANI varies depending on the degree of oxidation, the type of protonic acid used for the doping, the chain length, degree of crystallization and so on [122]. Furthermore, the emeraldine salt form of PANI, which is produced upon doping renders the polyaniline soluble in some organic solvents, dependent on the doping acid too, and thus easier to process [123].

The protonation of PANI is a very straight forward procedure, usually consisting of dispersing PANI in an organic solvent and introducing the protonic acid in the solution. With adequate stirring, protonation occurs and the solvent may then be removed. Good acid dopants for the EB PANI have been found to be organic acids such as camphorsulfonic acid (CSA), Dodecylbenzenesulphonic acid (DBSA), acrylamedo-2-proparesulphic acid (AMPSA) and *p*-toluenesulfonic acid (*p*-TSA) [124].

The selection of the dopant acid is important as it influences the final product's properties and solubility [123]. The best retention of conductivity of PANI at high temperature has been found to be achieved with methane sulfonic acid as dopant amongst various organic and inorganic acids [125]. When a polymeric acid (e.g.

polyacrylic acid), is used as dopant, the conductivity at room temperature and also the retention of conductivity at 180 ◦C is higher for the dopant that has a higher molecular weight. A higher basicity of the dopant anion results in a lower conductance of PANI. In the case of organic dicarboxylic acid dopants, a greater quantity of dopant results in a lower yield and conductivity but a higher solubility of PANI [126].

The amount of doping also seems to have an effect of the properties of ES PANI. Jin et al. studied the electrical and thermal conductivity of PANI films, using CSA as dopant acid. They found that the films with a doping level of 60% have been found to possess the maximum electrical and thermal conductivity due to the formation of the most delocalized structure of PANI as revealed in the UV–visible absorption and Raman spectra. The thermal conductivity was found to be much less sensitive to the acid doping level. It is concluded that phonons (also known as lattice waves) play a more important role in the thermal transport of PANI nanoscale films, while polarons are responsible for the electrical conduction [127]. Furthermore, with the increase in the degree of doping beyond 60%, the decreased conductivity may be due to the formation of bipolarons [126].

Generally, taking into account PANI processability (mainly in terms of solubility) and acquired conductivity, CSA and secondly DBSA seem to be the most promising and versatile of the dopant acids [126].

2.2.2 Electrospinning of PANI

Compared with other synthetic approaches, the electrospinning process seems to be the only method that can mass-produce continuous long fibres with nano-scale diameters [42]. The need for nanofibrous structures has been identified by several researchers who showed how the nanofibrous topography apart from the obvious advantages such as larger surface to volume ratio, which would be beneficial to a vast variety of applications, they also seem to provide significant advantages for cell culture applications as they have been found to induce enhanced adhesion of cells when compared to flat surfaces composed of the same materials. For example, Chu et

al. showed how hepatocytes attach better on chitosan nanofibres, rather than on chitosan flat film, also exhibiting higher urea synthesis, albumin secretion and cytochrome P450 activity. Furthermore, when nanofibres are compared to microfibres they have been found to outperform those, in terms of cell activity (proliferation, excretion of extracellular matrix, maintaining their initial morphology and differentiation state) [3], [21]. Nanofibre morphology, in terms of diameter size, affects cell viability and proliferation *in vitro*, with smaller diameters (in the range of 200-400nm) consistently presenting better morphology and proliferation rates than larger ones (up to 2μm) as it was shown in numerous studies such as Hodgkinson's et. al on proliferation of human fibroblasts on silk fibroin nanofibres, Leung's et al. of lung fibroblasts on calcium alginate nanofibrous scaffold, Yang's et al. of neurites on PLA (polylactic acid) nanofibres and so on [3], [128].

However, electrospinning of highly conducting polymers such as polyaniline, is quite a challenging procedure due to the unique dielectric properties these materials exhibit. Another significant drawback is that they are principally insoluble and infusible, which has been shown by numerous experimental approaches as well as by thermodynamical theoretical approaches [114]. For a conducting polymer to be soluble, absence of interaction with neighbor chains is a prerequisite so that each polymer chain could be only surrounded by solvent molecules, which is not the case with conducting polymers due to backbone rigidity associated with the delocalized conjugated structure. The conjugated structure which is necessary for polymers to become intrinsically conducting, results in those polymers being processable only by dispersion; meaning (in the case of solids becoming dispersed in a liquid) agglomerated particles are separated from each other and a new interface, between an inner surface of the liquid dispersion medium and the surface of the particles to be dispersed, is generated [71], [112]–[114]. For these reasons, the electrospinning of pure polyaniline has been proven to be extremely challenging [123].

As it was explained in detail earlier, electrospinning is governed by a combination of Coulomb forces between charge particles on the jet surface, electrostatic force due to the application of external electric field, gravitational force, viscoelastic forces due to the solution's viscosity, surface tension force as well as air drag force due to friction

with the air. The formation of the Taylor cone, which is the first step of the electrospinning procedure, is governed mainly by the electrostatic force created by the surface charges with the application of an external electric field that can be divided into two components namely tangential field (E_t), which is tangential to the fluid surface, and normal field (E_n), which is normal to the fluid surface as shown in Figure 2.5.

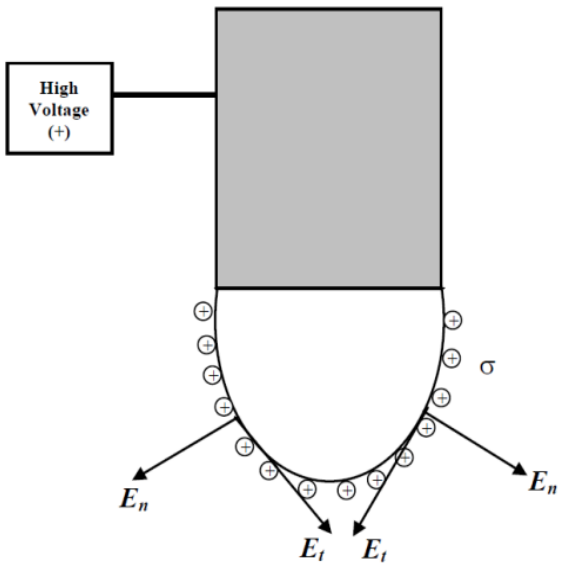


Figure 2.5: Representation of tangential (E_t) and normal (E_n) electric fields at the fluid surface with the application of high voltage [85].

So, if the surface charge density at the fluid surface is σ, the tangential electric stress τ_{es} can be calculated by the following equation [85]:

$$\tau_{es} = E_t \sigma \qquad (6)$$

In the case of a perfect conductor and in any adequately conducting ionic solution really, exposure to an external electric field, would cause the positive and negative carriers inside the droplet to move to opposite directions and in such way so as to counterbalance the external electric field. The excess charge, meaning the difference in the number of positive and negative ions in a particular volume segment of the liquid is simply considered as its charge. This, is the cause of the formation of a charged layer at the liquid-gas interface and the electrochemical equilibrium of the charge carriers is achieved by making the charge distribution such that the field is normal to the liquid surface and thus the E_t would be zero. Therefore, it is obvious that in the case of highly conducting solutions, the tangential electric field decreases

appreciably when the conductivity of the solution increases by several orders. This finally leads to the reduction of tangential electric stress, influencing the jet formation from the Taylor cone [85].

Apart from the electrostatic forces due to the application of the external electric field, Coulomb forces acting between the charges on the surface of the liquid play an important role during the elongating and thinning of the straight jet portion. It has actually been proven, that Coulomb forces constitute the main factor during the whipping instability of the jet [50].

Of course all the other relevant factors applicable for the electrospinning of non-conducting polymers that have been described in p2.2.2 apply here as well. The rheological characteristics of the electrospun solution (viscosity, plasticity vs elasticity) and its surface tension, as well as ambient factors such as temperature and humidity, play an important role on the electrospinning process and the morphology of the produced nanofibres. In the case of polyaniline, an added concern raised regarding its electrospinnability is the low molecular weights in which it is available, affecting solution viscosity and elasticity, which are very important parameters for electrospinnability as explained earlier in Section 2.1.2.2 [71].

The combination of all the above reasons, signal the necessity to use blends of polyaniline with commonly electrospun insulating polymers so as to successfully produce nanofibres [129].

2.2.2.1 Blending with Carrier Polymers

By now, composite fibres containing conductive polymers have been prepared by electrospinning, using an easily spinnable polymer in the blend: PANI/PEO [130], (PHT)/PEO [131], PHT/PLGA (polylactic-co-glycolide) [132], and PANI/PEO/CNT (carbon nanotubes), PANI-CNT/PNIPAm-co-MAA (poly(N-isopropyl acrylamide-co-methacrylic acid) [133], CSA-PANI/PLCL [134], PANI/Polystyrene [135] etc.

However, the non-conducting polymers and agents that are usually added into the spinning solution, in order to assist in the fibre formation will inevitably result in a

decrease of the conductivity of the electrospun composite fibres. Electrospinning PANI from blends will be analyzed in more depth in Section 3.1.

2.2.2.2 Electrospinning of Pure PANI

There has been a very limited number of studies focusing on electrospinning of pure PANI solutions. As this has been proven impossible by conventional electrospinning setup, Cardenas et al. used a vertical electrospinning setup on which they modified the collector, and instead of using the usual metallic one, they used a grounded electrode placed in acetone bath. This allowed them to use very high flow rate which is necessary in this case in order to provide enough polymer supply to create continuous fibres but in the same time the excess solvent that inevitably accompanies high flow rates didn't need to evaporate before reaching the collector, as it was diffused in the acetone, just before reaching the grounded electrode. This approach permitted the fabrication of pure polyaniline sub-micron and micron size fibres by electrospinning without the need to previously dope the polyaniline with high molecular weight acids or other polymer to gain stability and form the fibres. The conductivity of the resulting fibres was in the order of 10^{-3}–10^{2} S/cm [136].

MacDiarmid et al. also managed to electrospin a 20% w/v polyaniline solution in concentrated sulfuric acid by using a copper collector immersed in water. The fibres are collected either on the surface of the water or inside [135]. The pure PANI fibres exhibited conductivity values of the range of 0.1 S/cm, which wasn't higher than the one obtained when PEO was used as a carrier polymer at a ratio of 50:50, as would be expected. This was attributed to partial dedoping occuring in the water [135]. Pure polyaniline fibres from electrospinning of polyaniline in hot sulfuric acid were also produced by Yu et al. [137]. The nanofibres were collected in a bath collector as well, but instead of water, they used dilute solution of sulfuric acid avoiding thus the dedoping that would occur in the water. Pure PANI nanofibres exhibiting a very high conductivity, in the range of 50 S/cm, were produced this way. This same method was also applied by Leon et al; the polyaniline dissolved in sulfuric acid though was doped with AMPSA (2-Acrylamido-2-,ethyl-1-propanesulfonic acid) prior to electrospinning [121].

2.2.2.3 Post spinning addition of conducting polymer – In situ Polymerization

Several studies have been conducted where the conducting polymer is deposited on the surface of the already electrospun fibres, usually made from a common non-conducting polymer, such as PEO, PLGA, PLA, PCL etc. A challenge that comes along with this process is to ensure that the conducting polymer is deposited uniformly throughout the nanofibrous web as the porosity of the nanofibrous mat could impede this process. Xie et al [138] as well as J.Y. Lee et al., managed to uniformly coat PCL and PLGA electrospun fibres respectively with polypyrrole. The electrospun mat was simply immersed in aqueous solution of pyrrole monomer where the reactants were added according to polymerization protocol. It has been shown that their quantity and ratio, as well as the reaction time, influence the quality of the nanofibrous mat, either producing non-uniform, inadequate coating, or excess of polypyrrole deposited in form of aggregates on the nanofibres, both affecting negatively conductivity and uniformity of the mat [139]. Sarviet al. [140] used the same method of *in situ* polymerization of polypyrrole on PMMA (Polymethyl methacrylate) electrospun fibres, in order to finally get polypyrrole nanotubes by dissolving the core PMMA in chloroform. PANI, has also been polymerized *in situ* on PMMA nanofibres that had been prepared by electrospinning. Ji et al., in this study showed that *in situ* polymerization of PANI on PMMA fibres can lead to coaxial fibres of very smooth surface with no aggregation of PANI particles, and enhanced when the polymerizing conditions and the dopant acid are selected carefully [141]. PANI has been as well successfully polymerized on silk fibroin electrospun fibres pretreated with Methyl-orange [142]. By monitoring the morphology of the fibres at various times during polymerization, it was found that in order for a smooth coating to develop along the fibres, a minimum polymerization time of 6h is required [142].

2.2.2.4 Coaxial (Core-Shell) Electrospinning

Two different miscible or not polymer solutions may be electrospun by utilizing a co-axial setup of an inner and an outer capillary tube (Figure 2.6 B). This method is capable of producing a continuous double layer of nanofibres by co-electrospinning two materials through a facile one-step procedure [143], [144]. Thus, coaxial electrospinning is recommended when miscibility of the core-shell solution is not possible. Actually it has been reported that coaxial electrospinning is favored when miscibility is not possible because control on the electrospinning process is easier to achieve than when having miscible core and shell material. Xia and Li have demonstrated the significance of immiscibility in order to obtain a core/shell jet with uniform and continuous cross section [144], [145]. It is worth mentioning here that co-electrospinning of immiscible polymers can also be achieved by a side-by-side nozzle configuration that has been described in Section 2.1.2.3.

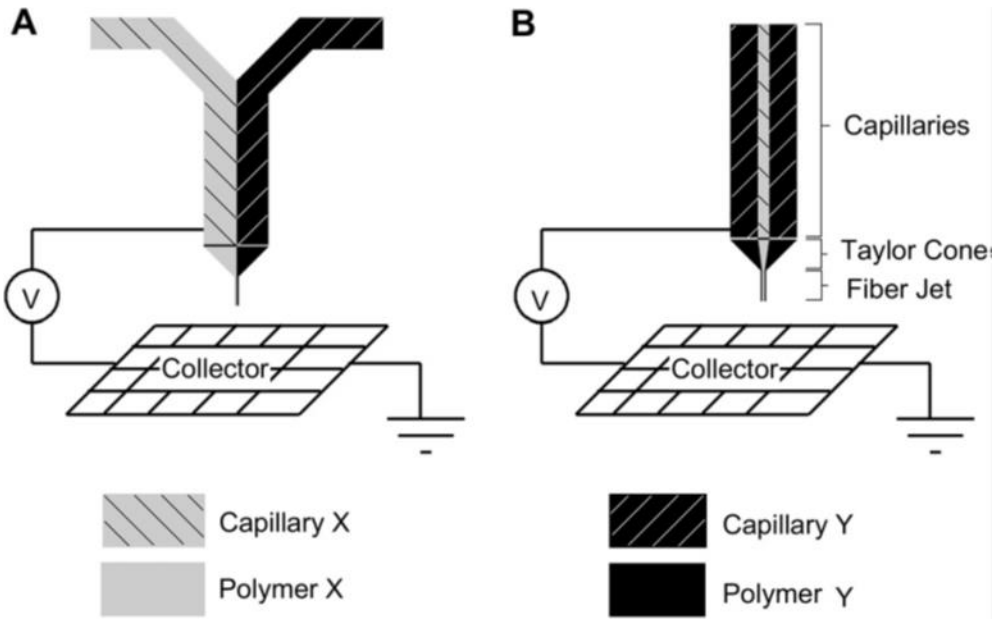


Figure 2.6: (A) Schematic of side-by-side nozzle configuration. (B) Schematic of coaxial nozzle configuration [70].

The coaxial electrospinning of conducting polymers offers great advantages, as it bypasses all the difficulties rising from the poor processability of conducting polymers. Usually, the conducting polymer is electrospun as the core material and a

biodegradable, easily electrospun polymer is used to form the sheath, and is subsequently dissolved in a suitable solvent.

On a different note, the same technique is being frequently used for the production of continuous, hollow nanofibres (nanotubes) where in this case, post to electrospinning, the nanofibrous mat is being immersed in a solvent that selectively dissolves the core polymer, so that hollow fibres of the desired material are left behind. Using this technique, Li et al. managed to attain hollow fibre from pure titania, by first co-axially electrospinning an ethanol solution of PVP and $Ti(OiPr)_4$ (shell) and heavy mineral oil (core) and subsequently dissolving the mineral oil core in octane overnight [145].

2.2.3 Conducting Polymers in Drug Delivery

Conducting polymer-based devices are being investigated to examine how they can serve as electrically controlled drug delivery devices inside the body and they seem to be quite promising for this purpose because of their unique ability to entrap and controllably release bioactive molecules [115]. Typical drug delivery systems exhibit an initial burst release of the drug which is not desirable (Figure 2.7). A major challenge of the field is to eliminate this initial burst release and to produce strictly controllable drug delivery systems either for sustained release or for pulsatile release (ON/OFF release state that allows delivery of required doses). Control over the drug delivery can be achieved by using external stimuli such as pH, temperature, electricity or magnetism and on a drug delivery system responsive to this stimulus. Therefore, electrical stimuli can be used to control the drug release rate of an electrically conducting drug delivery system.

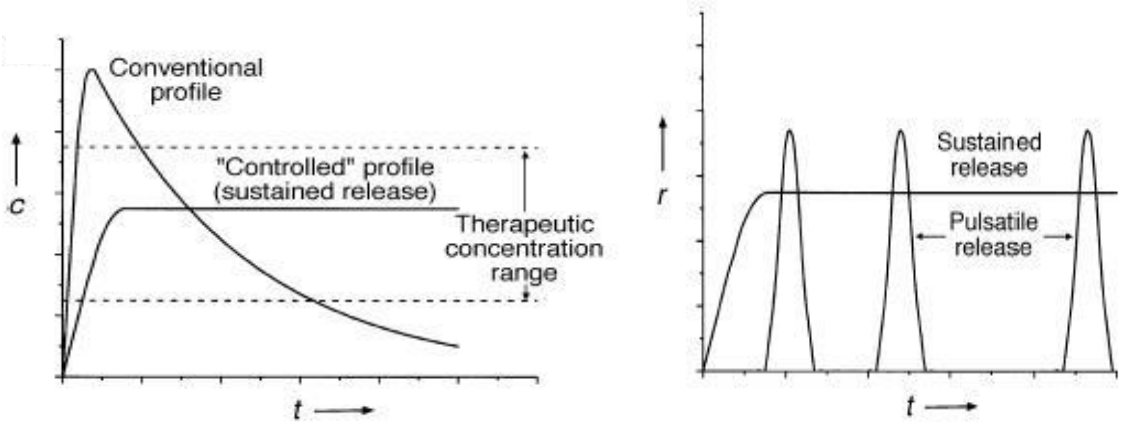


Figure 2.7: A. Conventional profile of release vs desired sustained release profile B. Alternative Pulsatile (ON/OFF) release in dosages.

The published studies, refer to either drug release from other conducting polymer electrospun matrices (such as PPy or PEDOT) or polyaniline containing hydrogels. Currently there is no work published regarding drug encapsulation and release from electrospun polyaniline nanofibres, although PANI stands out for its very good environmental stability (pH, presence of oxygen, intense light) when compared to other conducting polymers, and PANI fibres with very good mechanical and thermal stability can be produced [146].

Abidian et al. [147] reported a drug release system based on PEDOT nanotubes (Figure 2.7). In this approach, PLGA/dexamethasone fibres were formed by electrospinning PLGA, and then *in situ* polymerizing PEDOT to form nanotubes. The release characteristics of dexamethasone were studied by biasing the electrode at different voltages. Short voltage pulses applied on the electrode hosting the PEDOT/PLGA/dexamethasone fibres, were found to increase dramatically the cumulative mass release of dexamethasone. The electrically controlled release in this case was attributed to two parallel effects. First, as the oxidation state of PEDOT cladding layer is switched, a contraction force on the PLGA/dexamethasone fibre core is induced. This force squeezes the core of the fibre, affecting the mass transport as well as the kinetics of the drug molecule, translating in timed controlled small burst releases, both from the ends of the nanotubes and through nano-cracks that develop on the nanotubes surface during the switch cycles (Figure 2.8) [147]. However, in such

drug delivery systems, there is the possibility that the conducting cladding may irreversibly crack during a switch cycle, which would inevitably result in additional pathways for the drug to escape the core host, and loss of control of the release [42], [148].

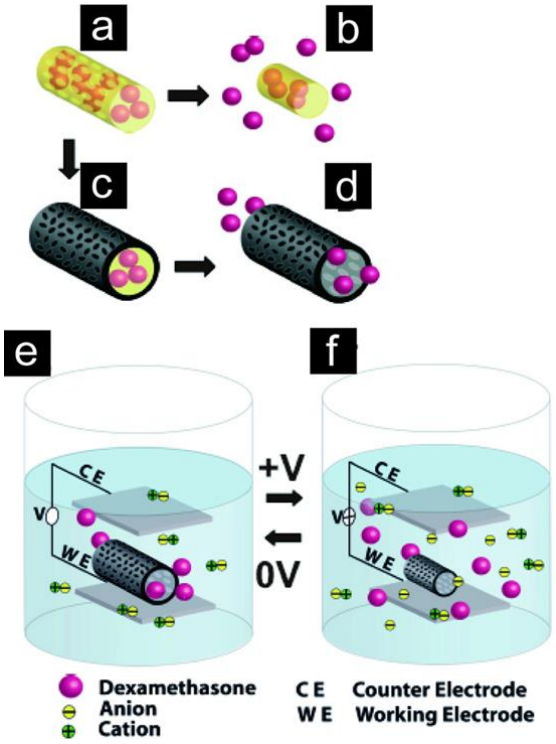


Figure 2.8: Schematic illustration of the controlled release of dexamethasone: (a) dexamethasone-loaded electrospun PLGA, (b) hydrolytic degradation of PLGA fibres leading to release of the drug, (c) electrochemical deposition of PEDOT around the dexamethasone-loaded electrospun PLGA fibre slows down the release of dexamethasone (d). (e) PEDOT nanotubes in a neutral electrical condition. (f) External electrical stimulation controls the release of dexamethasone from the PEDOT nanotubes due to contraction or expansion of the PEDOT [147].

Similarly, Tsai et. al., managed to obtain an "ON-OFF" switchable release of model drug indomethacin by periodically applying-removing-reapplying an electric potential on a crosslinked PVA hydrogel containing PANI. The dosages of the released drug were shown to be maintained the same throughout the stimulation cycles, and were found to be proportionate to the strength of the applied voltage. It

was shown that with careful selection of the degree of crosslinking, the polymeric ratio and the amount of voltage stimulation, highly controllable release and degradation rate of the scaffold could be achieved, tailorable with respect to the application [149].

As this is a field of research emerging just recently, there have only been a handful of studies dealing with release of bioactive molecules from nanofibrous structures containing conducting polymers, although a bit more work has been done with hydrogels. This must be linked with the difficulty to electrospin the conducting polymer which has been explained in section 2.3.2. Since, these studies have shown very promising results regarding the electrically driven and controlled release of drug molecules, it is concluded that pinpointing the factors that would facilitate the electrospinnability of these polymers would give a great boost to this area of research, and address a lot of the issues that other drug delivery systems (passive diffusion from encapsulated structures, thermoresponsive, pH based etc).

2.2.4 PANI for Tissue Engineering

Conducting polymers have been investigated and identified as easily programmable implantable biomaterials, biosensors, drug delivery devices, tissue engineering scaffolds etc. It has been proved in recent studies that the combination of electrical and topographical cues promotes and regulates cell attachment, proliferation and differentiation. ICP's have also been found able to transfer the charge occurring from a biochemical reaction [115].

It has been proved since the early 1990's that electrical stimulation in the range of 10mV/mm - 6V/mm and 15mA/m^2 – 5A/m^2 (depending of course on the tissue and the frequency of stimulation) can assist healing of damaged connective tissue, bone, cartilage, skin, peripheral, cranial and spinal nerves, *in vitro*, *in vivo* and in clinical studies as well [150]–[152].

For these purposes, electroactive polymers have been processed to either display permanent charges (electrets) or to generate transient surface charges (piezoelectric materials) or to generate electrical signals by electron transfer between different

polymer chains (conducting polymers). The latter category of materials can be applied by using either constant current or constant voltage. Compared to the electrets and the piezoelectric materials, they offer two major advantages: a) external control of the timing, duration and degree of the electrical stimulation and b) they don't require extensive processing to be rendered electroactive [153], [154]. To better understand the applicability of electrically responsive polymers for tissue engineering, it is useful to look into the mechanisms involved with mammalian cell function and growth.

All cells have an electrical charge across their plasma membrane, with the interior of the cell negative with respect to the exterior, which is referred to as the resting potential: The value of the resting potential varies, depending on the type of the cell.

The resting potential arises from the separation of potassium ions from intracellular, relatively immobile anions across the membrane of the cell. Because the membrane permeability for potassium is much higher than that for other ions, and because of the strong chemical gradient for potassium, potassium ions flow into the extracellular space carrying out positive charge, until their movement is balanced by build-up of negative charge on the inner surface of the membrane. Because of the high relative permeability for potassium, the resulting membrane potential is almost always close to the potassium reversal potential. In order for this process to occur, a concentration gradient of potassium ions must first be set up. This is accomplished by the ion pumps/transporters and/or exchangers and generally is powered by ATP.

Cells like neurons, muscle (skeletal, cardiac and smooth) and some endocrine cells (e.g. β-pancreatic cells) are known to be electrically excitable, meaning they can produce a rapid and reversible reversal of the electrical potential difference across the plasma membrane. In neurons for example, the membrane potential can rapidly change from its resting level of approximately −70 mV to around +50 mV and, subsequently, rapidly return to the resting level. This mechanism constitutes an important basis for information processing, propagation, and transmission and is referred to as the action potential, electrical impulse, or nervous impulse.

In non-excitable cells, electrical stimulation only temporarily alters the membrane resting potential, but does not lead to "excitation" of the cell. At the end of the depolarizing (interior voltage becoming less negative) or hyperpolarizing (interior voltage becoming more negative) pulse, the membrane potential simply returns to the resting value. This behavior is independent of the strength of the stimuli. The amplitude of the depolarization or hyperpolarization is directly proportional to the amplitude of the stimulus; and because of that reason they are called graded potentials. These graded potentials represent the passive property of the membrane to electrical stimulation.

In excitable cells, hyperpolarizing stimuli leads to the same graded responses that are seen in non-excitable cells. However, the nature of the response of excitable cells to depolarizing stimuli depends on the strength of the applied stimulus. If weak stimuli are given, the response is graded and is similar to that of a non-excitable cell. If, however, a strong enough stimulus is given such that the resulting depolarization surpasses a certain critical voltage, an action potential (the brief, about one-thousandth of a second, reversal of electric polarization of the cell's membrane) is generated. The voltage that must be surpassed in order to get an action potential is referred to as threshold. In most neurons threshold is around −40 to −50 mV. If a stimulus leads to a membrane depolarization that is more negative than the threshold value, the stimulus is said to be sub-threshold. Sub-threshold stimuli do not lead to action potentials.

Exogenous and endogenous electric fields (EFs) have been shown to have important effect on physiology and possibly be related to disease rates. Most organs (especially glands) and embryos surrounded by a layer of epithelial cells produce potential differences or transepithelial potentials (TEPs) of a few millivolts to tens of millivolts.

Endogeneous DC EFs play a significant role in major biological processes such as embryogenesis, wound healing and tissue regeneration and the electrical activation of the nervous system and the muscles. TEP is also generated by the human body ranging between 10 and 60 mV in various locations TEP values vary depending on the condition state of the tissue (physiological or pathophysiological). For example, in cystic fibrosis, which is associated primarily with impaired Cl^- transport across

epithelial membranes, the TEP of the nasal airway epithelium is hyperpolarized (–51 mV in cystic fibrosis patients, compared with –15 mV in normal nasal airway epithelium) [155]. The TEP is also active in wound healing by promoting cell migration from the wound edges. Injured epidermis is thus characterized by a TEP short circuit that gives rise to a measurable DC current efflux between 1 and 10 mA/cm^2 and an estimated current density up to 300 mA/cm^2 near the edge of the wound. This wound current corresponds to a relatively steady local EF between 40 and 200 mV/mm. The EF persists until complete wound re-epithelialization is achieved. The beneficial effect of this endogenous EF is to guide cell migration and nerve sprouting directly toward the wound edge; however, this healing process is compromised if the EF is inhibited [156]. This consists of a very promising area for application of electroactive polymers. An electroactive, biocompatible wound dressing membrane for example, could help retain and control the EF necessary for the healing of the underlying tissue, whilst providing mechanical properties, sufficient for physical protection against contamination.

Another challenge of this field, is the development of a "seamless" integration of optimized neural electrodes with the native neural tissue so as to optimize signalling to the surrounding cells. Conducting polymers are attractive candidates as interfacing electrodes with neurons because they can achieve high surface area, helping to promote effective ion exchange between recording sites and the surrounding tissue. The goal is to increase surface area of the recording site, while maintaining a sufficiently small geometric area to isolate the action potential from a single neuron. A larger surface area results in an increase in capacitance, which corresponds to a decrease in impedance, thus improving signal-to-noise ratio. Ideally, a neural probe would maximize neural signals recorded, minimize noise, maintain high capacitance, and remain conducting over the long term. In this context, polypyrrole has been used as a substrate to increase electronic interfacing between neurons and micromachined microelectrodes for potential applications in neural probes and prosthetic devices. However, even though PPy is commonly explored for coating neural probes, more recent studies have focused on the polythiophene derivative PEDOT because of its stable oxidative state and higher conductivity [115]. Polyaniline as well exhibits very

high environmental stability as well (against oxygen, water, temperature etc), and recently has also been found possible to maintain its electrical properties in alkaline pH, so it may have even better potential in that area too [157].

From all the above, it becomes obvious that electrical stimuli can directly influence the cell's physiology and activity. For excitable cells, the impact is quite straight forward, for example in neurons an action potential produces the nerve impulse, and in muscle cells it produces the contraction required for all movement. For this reason, most research that has dealt with electroactive substrates for biomedical applications, such as PANI containing cast membranes, hydrogels etc, has revolved around the investigation of applicability of these substrates in relation to excitable cells, and has given some interesting results, which will be discussed in the following paragraph. However, from clinical studies that will be discussed in more depth in Chapter 6, it has also been shown how electrical stimulation can enhance healing of non excitable tissues, such as skin for example. The application of nanofibres containing an electroactive polymer such as PANI, in this area could be very beneficial and worth investigating for that matter.

2.2.4.1 PANI biocompatibility - In vitro studies

Only a few studies have been conducted with the aim to test the biocompatibility of PANI containing nanofibrous films and study their effect on the growth *in vitro* of some types of cells.

For example, Li et. al. incorporated polyaniline in gelatin nanofibrous films in different ratios (0:100, 15:85, 30:70, 45:55) and found that all of them supported the growth of H9C2 rat cardiac myoblasts to the same degree as the standard tissue culture plastic and smooth glass surfaces [158].

Similarly, incorporation of PANI in polyethylene glycol based hydrogels has been shown to promote the cell response of PC12 (Rat adrenal gland pheochromocytoma) and hMSC's (human mesenchymal stem cells) as a result of the increase in conductivity and water retention that PANI caused [159].

Polyaniline blended with collagen has also proved to be *in vitro* biocompatible with porcine skeletal muscle cells, but in this particular study only cell attachment and growth for 2d period has been taken into consideration. Further study should be conducted to determine the biocompatibility of these substrates [160].

Wu et al. studied the proliferation and morphology of L929 fibroblast cells on electrospun PCL and PCL-PANI fibres with different ratios of contained PANI at 1, 5, 10 and 20% w/w. They concluded that no difference was observed with respect to growth rate and morphology when compared to TCP, confirming that PANI does not have any cytotoxic effect on the cells. The PCL-PANI 20% gave slightly higher number of cells at the end of the culture time (4^{th} day) [161].

L929 mouse fibroblast cells have also shown good attachment and growth when cultured on PANI coated silk fibroin nanofibres. As the surface of the nanofibres is completely covered with PANI, and in combination with the previous study, it can be concluded that PANI indeed can sustain well proliferation of L929 cells, giving final cell counts comparable and even better than standard materials such as tissue culture plastic [142].

In a very similar study, Jeong et al, showed that the growth of NIH-3T3 fibroblasts can be enhanced under the stimulation of various direct current flows when cultured on CSA doped PANI/PLCL electrospun nanofibres. In general, they concluded that increase of the electrical conductivity of a nanofibrous scaffold from commonly used biocompatible polymer, results in improvement of cell adhesion on the scaffold. The cell adhesion tests using human dermal fibroblasts, NIH-3T3 (mouse embryo fibroblasts), and C2C12 (mouse myoblasts) demonstrated significantly higher adhesion on the CPSA-PANI/PLCL nanofibres than pure PLCL ones [134].

Chen et al. reached to a similar conclusion when studying PCL nanofibres incorporated with PANI where the conducting properties of the resulting nanofibrous structures acted as electric cues for the enhancement of differentiation and proliferation of myoblasts for the formation of multi nucleated myotubes. Furthermore, the cells seeded on the mat can profit from the synergistic effect of topographical and electrical cues when aligned nanofibres are used instead of

randomly oriented ones [162]. On the same track, Prabhakaran et al. proved that an electrically conducting nanofibrous scaffold (PLLA:PANI 85:15) significantly enhanced neurite outgrowth when an electrical stimuli of 100mV/mm was applied for 60 min [163].

Polyaniline has also been used in conjunction with other conductive nanostructures, with promising results. Sharma et al. observed a positive outcome when studying the effect of the incorporation of carbon nanotubes and PANI in a PNIPAm-co-MAA nanofibrous mesh on a mice fibroblast cell line attributed to the enhanced mechanical strength and conductivity compared to the same mat before the incorporation of the polyaniline or carbon nanotubes attributing these observations to electrical stimuli provided by the PANI and mechanical strength provided by the carbon nanotubes and they proposed the use of this type of nanofibrous structures for the 3D cultures of cells *in vitro* [133]. In another study, Baniasadi et al. [164], used polyaniline in combination with graphene nanoparticles incorporated in a chitosan/gelatin scaffold, and found that the electrical stimulation which was then applied, increased the secretion of neurotrophin, a growth factor very important for nerve cell function and regeneration and resulted in delaying the degradation rate of the scaffolds and promoting good attachment and proliferation of Schwann cells.

Electrospun copolymers of PANI derivatives such as poly(aniline-co-3-aminobenzoic acid) (3ABAPANI) blended with biodegradable polymers such as PLA have been shown to also promote cell proliferation [165].

Lastly, films of pure PANI have also been tested for their biocompatibility with H9c2 cardiac myoblasts, concluding that although initially there is a delay on cell proliferation as compared to tissue culture plastic, and in agreement to the PANI-gelatin films studied by Li et al. as mentioned above [158], after 6 days in culture and when confluency is achieved PANI film cultures and controls are identical [166].

Despite these findings there have been cases as well, where PANI EB and ES powders have shown cytotoxicity against non-tumorigenic keratinocyte and human hepatocellular carcinoma cell lines. However, significant reduction of cytotoxicity was achieved through a deprotonation and reprotonation procedure, which was used as

an additional purification step after polymer synthesis, indicating that cytotoxicity might be caused rather by the reaction by-products and residues than by polyaniline itself [167].

Polypyrrole, polyaniline and polythiophene, however, are not degradable, and materials that remain in the body long-term may induce chronic inflammation and may require surgical removal [153]. One strategy to tackle this issue and to get conducting and biodegradable polymers related to polyaniline for example, is based on joining a biodegradable polymer (e.g., polyactide or chitosan) with heterocyclic oligomers of aniline. In fact, oligoanilines with well-defined chain lengths have been the model compounds for the electrical, magnetic, optical, and structural properties of PANI. Thus, many polymers containing oligoanilines as the side chains or even in the main chain have been designed and synthesized to obtain new electroactive materials [168], [169]. Although biodegradability is considered a drawback for the use of conducting polymers for some applications, it has to be highlighted here that if the biocompatibility criteria, in terms of cytotoxicity, is met, then there is worth investigating of how these materials could be scavenged by phagocytes. It has been shown that consecutive cycles of electric field application on scaffolds containing PANI and another biopolymer, can lead to erosion of the scaffold and mechanical degradation of the conducting polymer's chains, which, once broken down to a suitable size, they could then be removed by scavenger cells, in the same way as ink particles are broken and removed by the skin tissue, during tattoo removal laser procedures [149].

Lastly, and on a different note, several studies have also shown antibacterial action of polyaniline and polyaniline copolymer films *in vitro* against several Gram positive bacteria (*Streptococcus pyogenes*, *Bacillus subtilis*, *Enterococcus faecalis*, *Staphylococcus aureus* [170]–[173], gram negative bacteria (Shigella dysenteriae, *Salmonella enterica*, *Klebsiella pneumoniae*, *Pseudomonas aeruginosa*, *Escherichia coli* [171], [173]) and fungus *Candida albicans* [173]. It is worth noting that polyaniline emeraldine salt, doped with different acids has been proved a lot more efficient in inhibiting bacteria growth as compared to polyaniline base [171], [173], but further

discussion on this topic will take place on in section 6.1. Inherent antibacterial activity of polyaniline is rendering it even more appealing for biomedical applications.

2.2.4.2 PANI biocompatibility - In vivo studies

The *in vivo* biocompatibility of polyaniline films has not been vastly studied and there is no consensus in the scientific community yet regarding this.

Kamalesh et al. studied the effect of implantation of polyaniline films of all three oxidation states (emeraldine, nigraniline and leucoemeraldine) beneath the dorsal skin of rats, for a period of up to 90 weeks. No inflammation was reported for that period, nor development of neoplastic tissue surrounding the implant. XPS analysis on the films after implantation period revealed signs of hydrolysis on the surface of emeraldine and nigraniline films (=N groups converting in –NH). As leucoemeraldine film is in the fully reduced state, it didn't undergo any further hydrolysis. All three films though did undergo some surface oxidation, as increase of C–O and C=O species showed [174]. In an almost identical study though, Wang et al. investigated the in-vivo biocompatibility of PANI, by introducing under the dorsal skin of rats polyaniline in all oxidative states in both the form of powder and film, as well as EB films from graft polymerization with acrylic acid and the subsequent immobilization of collagen on it. They found signs of minimal inflammation associated with the implants, 50 weeks after surgery. The small numbers of immune response cells (mast cells) that could be observed around the other implants, were almost absent in the case of the EB film immobilized with collagen [175].

One study was focused on correlating *in vitro* cell behaviour with *in vivo* response of two group of materials: 1. Conducting and non-biodegradable ones, namely polyaniline, polypyrrole and polyimide and 2. Biodegradable such as the triblock co-polymer PLLA-PDXO-PLLA (Poly(L-lactide-b-1,5-dioxepan-2-one-b-L-lactide)). What was found was that the biodegradable copolymer that was exhibiting migratory and regenerative ability *in vitro*, was as well performing exceptionally *in vivo*, while the non-resorbable ones resulted in higher inflammatory response which was correlated

to the *in vitro* behaviour showing good cell attachment which was not accompanied though by elongation-migration which would reflect a bioactive phenotype [176].

The lack of *in vivo* studies, apart from the fact that the biomedical application of PANI and conducting polymers in general is only just now being investigated, is also due to the fact that there are *in vitro* studies that argue the biocompatibility of PANI. For progress to be achieved in this field, there is therefore a demand for more focused *in vitro* studies that would be proving where the cytotoxicity lies exactly, if any at all, and making conclusive arguments regarding the possible limitations (e.g. in terms of threshold concentrations, biodegradability etc).

2.3 Conclusions - Discussion

There is an increasing need in the tissue engineering field, for the production of highly engineered, "smart" scaffolds, that not only offer a substrate for tissue culture but that have the potential to enhance and guide cell growth and differentiation. Topographical and electrical cues and the combination of those holds big potential for the advancement of the field.

A nanofibrous structure, apart from the apparent advantages applicable to a variety of fields, has been proved to enhance cell adhesion and to provide cells with topographical cues that benefits cell migration and differentiation. It also allows the encapsulation of a range of different therapeutic molecules, hydrophobic or hydrophilic, fragile or not, loosely or tightly bound and in high concentrations if that is desired.

Among the most commonly used, available techniques for the production of nanofibres, electrospinning is easily scalable, offers better control over the final physical properties of the nanofibres and versatility regarding the polymer materials that can be electrospun.

However, the mechanisms dictating the electrospinning procedure are not fully understood or modelled as the factors affecting the process are numerous and to a high degree, interdependent. There are some systematic studies looking at the

electrospinnability of certain common polymer solutions (PEO, PCL, PVA, PLA) and attempts to model the nanofibre properties based on some of what are considered major parameters affecting the fibre morphology (such as solution viscosity, polymer concentration, voltage, flow rate etc), but none of them has looked into conducting polymer based solutions and how the incorporation of a conducting polymer affects the process. Even more, no systematic studies have been conducted so as to determine which are the major factors affecting electrospinnability when a conducting polymer is electrospun.

Blend electrospinning, co-axial electrospinning and post spinning *in situ* polymerization are some of the most straight forward methods to overcome the processability limitations of conducting polymers and produce electrospun and electroactive fibres.

Intrinsically conducting polymers have been found to be able to insinuate electrical cues to *in vitro* cell cultures on both electrically excitable and non-excitable cells when a small voltage is applied. They also provide the possibility to introduce a very specific kind of an ON-OFF controlled delivery of bioactive molecules which however has not been fully established yet.

Amongst conducting polymers, polyaniline is very promising due to its ease of synthesis, low cost, the easily tunable electrical conductivity and its stability. However, the biocompatibility of polyaniline is still debated due to the ambiguous results that some studies have presented. It is therefore still unclear, whether any reported inflammatory responses are due to the polymer itself or rather the other processing materials used, and no systematic study has been conducted yet relating any potential adverse effect with the *in vitro* culture time or the concentration of the conducting polymer in the scaffold.

This work is aiming towards addressing some of these challenges relating to the application of conducting polymers in the biomedical sector. PANI will be used as a model conducting polymer, but the findings can be considered applicable for other conducting polymers too. Firstly, in terms of processability, a focused electrospinning

study will be conducted in order to pinpoint the factors limiting the electrospinnability of conducting polymers and an assessment of how these can be addressed will be attempted. Secondly, an in-vitro study is considered necessary in order to shed light to the cause of ambiguity encountered in the literature, to investigate what are the potential limitations of the use of PANI based nanofibres for tissue engineering application (a skin tissue application was chosen for reasons explained in Chapter 6) as well as how and if those can be surpassed.

3 |EVALUATION OF POTENTIAL APPROACHES FOR PANI ELECTROSPINNING

3.1 Introduction

The complexity involved in the electrospinning of conducting polymers and thus PANI, has been analyzed in detail in Section 2.2.2. PANI's conjugative structure, together with its low solubility in common organic solvents, are the main reasons that raise the need for research into ways to bypass the problem of processability. The production of continuous, defect free conducting nanofibres is being investigated by researchers of the field, either by blending with carrier polymers which are easily electrospinnable such as PLA, PVA, PEO, PMMA etc (with or without subsequent removal of the carrier polymers), by applying alterations on the electrospinning setup (type of collector, type of needle), or by post-electrospinning depositing of a conducting polymer on the produced fibres [129].

By now, blending with carrier polymers is the most effective and convenient way to produce micro- and nano-scale fibres of polyaniline. CSA doped PANI/PEO [121], [130], [177], PANI/PNIPAm-co-MAA [133], CSA-PANI/PLCL [134], CSA-PANI/Polystyrene [121], [135], HCl-doped poly(aniline-co-3-aminobenzoic acid) (3ABAPANI)/PLA [172], CSA-PANI/PVDF [178], DBSA - PANI/PMMA [179], CSA-PANI/PMMA [177], CSA-PANI/gelatin [158], CSA-PANI/PLA [180], EB PANI/PVA [181] and more rarely, pure PANI [135], [136] have been prepared by electrospinning. Wu et al., for example, successfully produced nanofibrous scaffolds consisting of PCL (polycaprolactone) and PANI, by electrospinning blend solutions in chloroform/methanol. The incorporation of 20% w/w PANI in the blend, resulted in slight decrease of the nanofibre average diameter and also in improvement of physical properties, namely conductivity and improved hydrophilicity [161]. Then, polyvinyl alcohol (PVA) and chitosan oligosaccharide (COS) were blended into the PANI copolymer to make the electrospinning solution. XRD and FTIR data from this study displayed the existence of hydrogen bonds between hydroxyl groups in PVA and amino groups in copolymers and/or hydroxyl groups in COS (Chitosan oligosaccharide) could be indicating that the addition of PVA moderates the

interaction between COS macromolecules and PANI-co-PABSA copolymers, and improving this way the electrospinnability of the blend. Moreover, with the addition of PANI-co-PABSA (p-Acetamidobenzenesulfonyl Azide) in the PVA/COS blend fibres, superior thermal stability was obtained [182].

However, the non-conducting polymers or other non-conducting agents that are added into the spinning solution, in order to assist in the fibre formation may result in a decrease of the conductivity (10^{-1}–10^{-4} S/cm) of the electrospun composite fibres, when compared to pure polyaniline films. Zhang et al. for example, observed that the electrical conductivities of single electrospun fibres were found to increase exponentially with the weight percent of doped PANI in the fibres, with values as high as 50 ± 30 S/cm [177]. Chronakis et al., also produced PPy nanofibres with the addition of PEO to enhance processability of the polymer solution. The conductivity through the thickness of the electrospun PPy/PEO nanofibres increased by two orders of magnitude from the lowest to the highest concentration of PPy and ranged from about $4.9x10^{-8}$ to $1.2x10^{-5}$ S/cm. As expected, the higher the PPy content of the PPy/PEO nanofibres, the higher the electrical conductivity, as there is increase of the continuous domains of the conducting PPy molecules in the fibre structure, facilitating the mobility of charges within the polymeric network. Furthermore, it was noted that higher % w/v concentration of PEO in the initial solution, when the PPy:PEO ratio is maintained fixed, results in higher conductivity, attributed to the formation of a better matrix nanostructure that provides higher conducting pathways or charge-carrier mobility of PPy molecules along the fibres [83]. However, that would be interesting to further investigate, along with the distribution of fibre diameters, in order to safely conclude on the reason of this phenomenon.

It has also been found that through reducing or eliminating PEO content or embedding carbon nanotubes in the fibres, their conductivity could be increased by one or several orders of magnitude [42], [183]. Serrano et al., observed the same when they managed, by using a modified procedure, to electrospin blends of PANI and PLA, at the presence of only a very low concentration of PLA. The very low PLA concentration was vital for the production of fibres that were conductive enough to be used for the fabrication of a diode which was connected in half wave rectifier

circuit and was able to rectify low frequency ac signals with moderate efficiency [180]. Another way to increase conductivity of composite electrospun mats is a post spinning mechanical procedure of solid state drawing which allows for enhanced molecular orientation and may result to increased conductivity of the range of one order of magnitude, as it was shown by Zhang et al [177]. Chronakis et al., also pointed out that both the nature of the polymer solutions, meaning the compatibility in solution of the conducting/carrier polymer blends (owing to the low molecular weight of PPy in comparison with PEO) prior to solidification and the extremely rapid structure formation of polymer nanofibres play a significant role in diminishing the formation of phase-separated domains between conductive polymer molecules along the length of the nanofibre [83].

As mentioned in Chapter 2, another way to obtain conducting nanofibres by electrospinning is to use a co-axial needle during electrospinning. Zhang et al.[177], successfully produced continuous nanofibres of HSCA doped polyaniline (PANI), by coaxially electrospinning PANI (core) and PMMA (shell), followed by dissolution of the PMMA shell in isopropylalcohol leaving smooth and uniform pure PANI nanofibres. Despite the fact that some of the dopant is lost during the PMMA dissolution, the electrical conductivities of these mats were significantly higher than the one of the blend mats (electrospinning of PANI-PMMA blend) reaching the value of 50 ± 30S/cm.

In situ polymerization was used by Dong et al. [69], for the production of core-shell fibres of PMMA (core) and polyaniline (shell). The coated fibres exhibited higher conductivities when compared to those made by electrospinning the corresponding PANI blend. In another study, Chen et al. also successfully deposited nanoparticles (<50nm) of polyaniline on electrospun polyimide fibres, by *in situ* polymerization of aniline monomer, producing uniform polyaniline coated fibres, with improved mechanical and electrical properties. The mat is pH sensitive as well, due to the easily changeable protonation degree, by simply immersing the mat in a suitable acid/base solution [146].

In this chapter, based on the literature, a wide range of experiments will be conducted, the evaluation of different approaches and materials in order to achieve

the production of fibres containing PANI, with diameters up to 500nm will be evaluated and discussed.

3.2 Materials & Methods

3.2.1 PANI Polymerization

Polyaniline was produced from aniline monomer by following the polymerization process described by Stejskal et al. [1]. The synthesis was based on mixing aqueous solutions of aniline hydrochloride and ammonium persulfate at room temperature, followed by the separation of PANI hydrochloride precipitate by filtration under vacuum and drying at 60°C for 4 hours. The handling of solid aniline salt is preferred to liquid aniline from the point of view of toxic hazards. Persulfate is the most commonly used oxidant and its ammonium salt was preferred to the potassium counterpart due to its better solubility in water.

The resulting polyaniline emeraldine salt was treated with ammonium hydroxide of 1M for 24h at room temperature to receive the polyaniline emeraldine base form. The resulting polymer was then washed with water and acetone to remove oligomers and filtered under vacuum. The precipitate was dried under vacuum at room temperature for 24h [2]. Ammonia solution 35%, was purchased from Fisher Scientific Ltd. All other chemicals were purchased from Sigma-Aldrich Inc.

This home-made polyaniline was used to conduct all initial experiments. It has to be noted here that the molecular weight of the produced polymer was not determined as a main issue reported with aniline polymer is that because of the very low solubility emeraldine base form in organic solvent, the GPC (gel permeation chromatography) technique which is commonly used for the determination of molecular weights of polymers cannot be reliable, firstly because only the soluble part of the sample is characterized and secondly the solution has a colloidal rather than molecular character [185]. In general, solutions of polyaniline cannot exist, only very good dispersions and therefore, any method of molecular weight determination

would not be reliable. However, for the purpose of the screening experiments in this chapter, it is judged that the procedure described above is fairly reproducible and the polymer obtained, consistent, especially when the washing/filtration step is followed thoroughly.

3.2.2 Electrospinning Setup

The electrospinning equipment that was used for all experiments is the custom made device shown in Figures 3.1 A & B. The electrospinning chamber (Figure 3.1 A) consists of polystyrene walls and a plexi-glass door incorporating a safety switch at the upper left side.



Figure 3.1: Electrospinning Setup A: Electrospinning Chamber and Syringe Pump B: High Voltage Source

The blends were fed through a plastic syringe to the needle tip (18G diameter) and electrospun under different voltages, produced by the high voltage source (Glassman High Voltage Inc.) (Figure 3.1 B). The nanofibres were collected on an aluminium foil covered grounded collector, which was either a flat rectangle or a rotating cylinder.

The flow rate of the solutions was controlled by the syringe pump (Harvard Apparatus) (Figure 3.1 A) , and varied from 1 to 10 mL/h, depending on the nature of the electrospun solution. The environmental conditions (namely humidity and temperature) in the electrospinning chamber were monitored using a temperature and humidity meter ST-321.

The conductivity of the solutions was measured with a 470 Jenway Conductivity Meter.

The morphology of the electrospun mats was examined with the use of Carl Zeiss (Leo) Scanning Electron Microscope (Model 1530VP).

3.2.3 Blend electrospinning - Selection of carrier polymers, solvents, doping agents and amount of doping

The produced polyaniline base or its acid doped form was used in all blends as the conducting polymer. CSA ((1R)-(-)-10-camphor-sulfonic acid), DBSA and glutaric acid, were purchased from Sigma-Aldrich Inc. and were investigated as possible polyaniline dopants. PEO of two different molecular weights (Mw=300 000, & 600 000) and purchased from BDH Ltd, chitosan (of Mw=600 000 was purchased from AcrÕs Organics), and other biodegradable polymers that can be easily electrospun in a variety of solvents [186] and are also commonly used in the biomedical industry [3], such as PCL (Mw 80 000), PVA (Mw 70 000, 98% hydrolyzed) and Eudragit S-100 (Figure (copolymer based on methacrylic acic and methyl methacrylate with Mw~34 000) all purchased from Sigma Aldrich Inc were chosen as carrier polymers in the blend solutions. Several solvents (see Table 3.2 in Section 3.3.1.1), all purchased from Sigma-Aldrich Inc., were investigated for their suitability as for the dissolution of polyaniline and the electrospinning procedure requirements.

Looking at suitable solvents and solvent systems for PANI blends, the first requirement is the use of a solvent or solvent system that successfully disperses the polyaniline and dissolves the carrier polymer. It is equally important that the boiling

point of the main solvent is not too high, so as to avoid non evaporation during the process and a medium to high dielectric constant. So, after searching the literature for solvents that are currently used for polyaniline and possibly other suitable ones, the screening electrospinning experiments presented in Table 3.2, were performed.

It has to be noted here that the values of the process parameters applied during the electrospinning experiments were mostly determined by practical factors. For example, for some solutions the flow rate had to be increased, as the drop at the needle tip would dry too fast, if the solvent was more volatile than in other solutions. Also depending on the conductivity and surface tension of the solution, sometimes higher voltage field had to be applied in order to get the formation of Taylor cone and so on, or some other times high PANI content would cause intense corona discharge and sparks, not allowing for electrospinning at higher voltages. During this screening procedure, several solutions were prepared as shown in Table 3.2, using solvents with a wide range of different properties. Table 3.1 summarizes the properties of commonly used solvents as they are found in the literature based on which the solvent selection was performed.

Table 3.1: Properties of solvents commonly used for electrospinning

Solvent	Boiling Point (°C)	Dielectric Constant (ε)	Polar	Protic/ Aprotic	Surface Tension (mN/m)	Solubility Parameter (δ) $(cal/cm^3)^{1/2}$
Acetic Acid	118	6.15	Y	Protic	27.12	10.5
Acetone	56.3	20.7	Y	Aprotic	25.2	9.9
Acetonitrile	81.6	37.5	Y	Aprotic	29.3	11.9
Benzene	80.1	2.27	N			9.2
Chloroform	61.7	4.81	N		27.5	9.3
m-Cresol	191	5.0	Y	Protic	24.95	11.1
Dichloroethane	84	10.6	Y	Aprotic	33.3	9.1
Dichloromethane	39.8	8.93	N		26.5	9.9
Diethyl Ether	34.6	3.1	N			7.4

Dimethylformamide	153	36.7	Y	Aprotic	37.1	12.1
Dimethyl Sulfoxide	189	46.7	Y	Aprotic		12.0
Ethanol	78.5	24.5	Y	Protic	22.1	12.92
Ethyl acetate	77	6.02	N			9.1
Formic Acid	101	58.5	Y	Protic	37.03	12.2
Hexane	69	1.89	N			7.3
Isopropyl Alcohol	82	17.9	Y	Protic		8.8
N-methyl pyrrolidinone	202	32	Y	Aprotic	40.79	11.2
Methanol	64.6	32.7	Y	Protic	22.7	14.5
2-Propanol	82.4	18.3	Y	Protic		11.6
Pyridine	115.2	12.4	Y	Aprotic	38	10.7
Tetrahydrofuran	66	7.58	Y	Aprotic	26.4	9.4
Toluene	110.6	2.38	N		28.4	8.9
Trifluoroacetic Acid	72	8.55	Y	Protic	13.63	10.7
2,2,2-trifluoroethanol	79	26.5	Y	Protic	21.1	11.7
Water	100	80.1	Y	Protic	72.8	23.4

3.2.5 *In situ* Polymerization

Another possible method to obtain PANI nanofibres is the *in situ* polymerization of polyaniline on already electrospun nanofibres made from other easily electrospinnable polymers [138]. In this case electrospun polylactic acid (PLA) nanofibres were used as a template. The PLA (PLA 4060D purchased from Nature Works with an L-lactide content of around 88 %weight) was dissolved in a mixture of acetone:DMF (80:20). The PLA electrospun fibres were then immersed in aniline hydrochloride solution and the same polymerization procedure was followed (as described in paragraph 3.2.1), under continuous gentle stirring.

3.2.6 Core-Shell Electrospinning

For core shell electrospinning, the same apparatus was used as described in 3.2.2, but a second pump from the same manufacturer was added, and a coaxial needle (Linari Engineering S.r.l) with 0.5mm inner diameter and 0.8mm outer diameter was used.

3.3 Results & Discussion

3.3.1 Production of blend PANI nanofibres

Here, the steps that were followed, in order to explore the possibilities of PANI blend electrospinning in terms of solution preparation are explained and discussed in detail.

3.3.1.1 Determination of suitable carrier polymers

As mentioned in Chapter 2, PEO can be used as a carrier polymer to facilitate electrospinning of conducting polymers. When blended with polyaniline it has been reported to successfully give, bead free, homogeneous nanofibres [92], [119]. It is available in a very wide range of molecular weights varying from 10 000 till up to 9 000 000; this gives great freedom to tailor the quantity of the PEO used in the blend as high molecular weights allow for sufficient chain entanglement, which is necessary to achieve electrospinnability, even when at very low quantity (in terms of mass) of the polymer is used. This allows the usage of less mass in the blend, allowing higher ratio of polyaniline in the final mat rendering the aforementioned advantages of polyaniline more evident in the electrospun mat [3].

Furthermore, it can be easily processed as it is soluble in a wide variety of organic solvents and lastly, PEO is an FDA approved material, which renders it suitable for the applications aimed at the present study. Its structure is depicted in Figure 3.2.

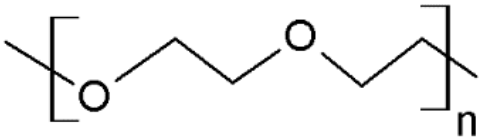


Figure 3.2: Molecular structure of PEO

Chitosan (see Figure 5.1 in Chapter 5) was selected as a second carrier polymer due to its known biocompatibility, non-toxicity and its inherent antibacterial properties, rendering very attractive for biomedical applications. It has also received lately a lot of attention for application in drug delivery systems [4]. Chitosan is generally insoluble in common organic solvents; that is the reason why the chitosan was first dissolved in an acidic agent and then added to the PANI/PEO blend, or electrospun in only acidic solvents. The polyaniline was either doped with CSA as usual or dopes by the acid used as solvent. Chitosan solutions are more conducting as compared to PEO due to the polycationic nature and positive charges on the polymer chains. However, this interferes with the electrospinning process as it creates repulsive forces between the chitosan chains, causing jet instability [187].

It has been shown by Geng et al.[188], that the increase of acetic acid concentration and decrease of water amount in the chitosan solution critically affects the electrospinning process. The decrease of the surface tension that is caused by the acid abundance significantly facilitates the electrospinning.

The molecular structures of PVA, Eudragit S-100, PCL and PLA are shown in Figures 3.3 A, B, C & D.

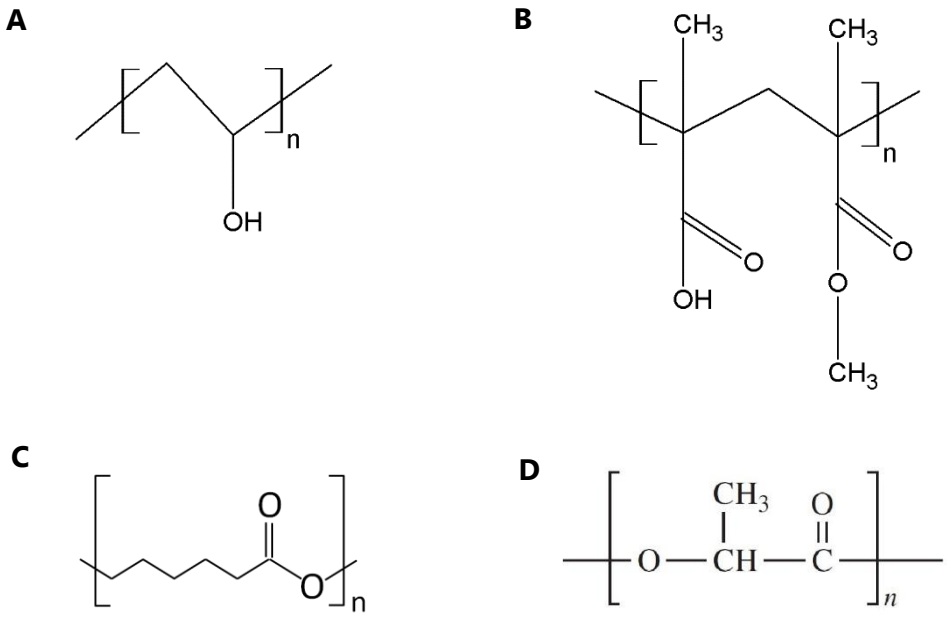
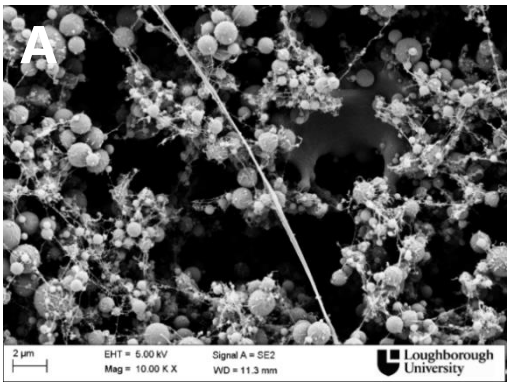


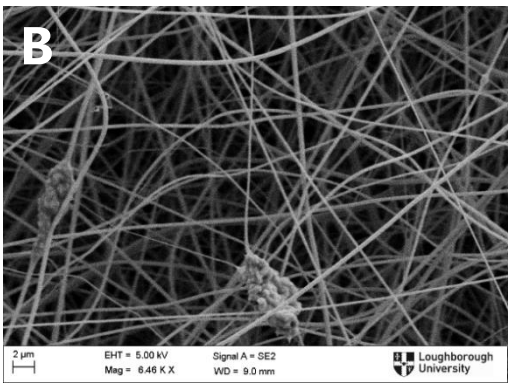
Figure 3.3: Molecular structure of A: PVA, B: Eudragit S-100, C: PCL, D: PLA

When those were used as carrier polymers, the PANI ratio (in the final dry nanofibrous mat) could not exceed 10% w/w, as those polymers are only electrospinnable in high concentrations (>10% w/v), and PANI solubility in those solvents is very low. Although some of them succeeded in producing acceptable nanofibrous structures (Figures 3.4 A, B, C & D), the limit of 10% of PANI concentration was considered too low for the application in question. When PEO and chitosan (Figures 3.4 E & F) were used as carrier polymers, higher ratios of PANI incorporation could be achieved for two different reasons in each case. In the case of PEO, its high molecular weight can give electrospinnable solutions at a concentration as low as 0.9% w/v. When chitosan was added into the mix, it allowed for further increase of the PANI concentration, as chitosan is a polyelectrolyte and also the concentrated acetic acid in which it dissolves, also helped PANI dispersion. It should be noted here, that both undoped PANI and CSA doped PANI were successfully electrospun with chitosan as a carrier polymer. This is attributed though more to the acetic acid that was used as a co-solvent for the dissolution of chitosan and it partially doped the PANI base, when the latter was used as such. However, the distinct bead formation (Figure 3.4 F b) shows that acetic acid doesn't adequately assist with PANI dissolution. At a later stage, trifluoroacetic acid was identified as a

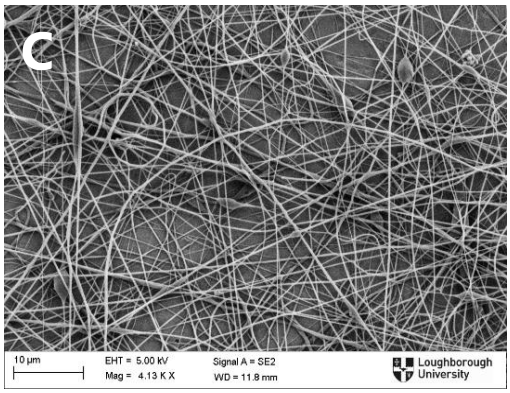
more suitable solvent for electrospinning of chitosan as it enabled electrospinning of pure chitosan (without PEO addition) and it will be discussed in detail in Chapter 5.



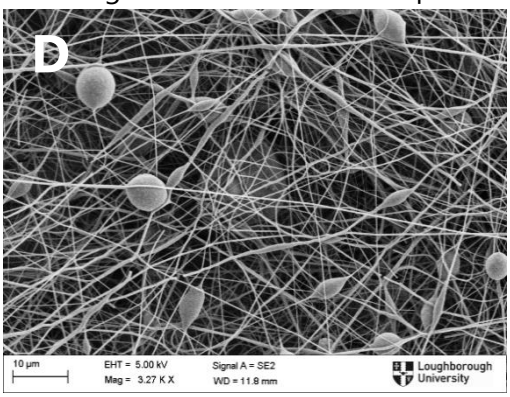
10% PVA + 1% CSA doped PANI



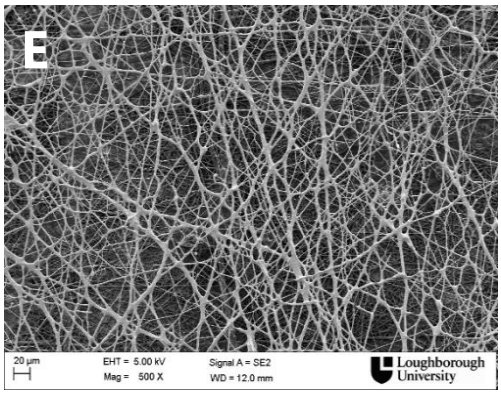
13% Eudragit S-100 + 1.3%CSA doped PANI



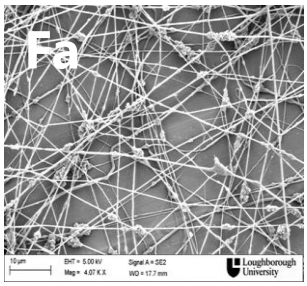
13% PCL + 1.3%CSA doped PANI



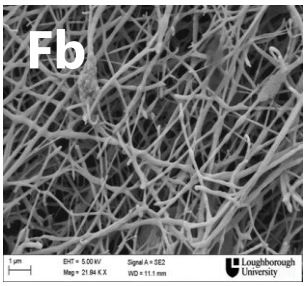
13%PLA + 1.3% CSA doped PANI



1,3% PEO + 1.3%CSA doped PANI



0.9% PEO + 0.9 Chitosan + 2% undoped PANI



0.7% PEO + 0.7% Chitosan + 2.8%CSA doped PANI

Figure 3.4: Comparison of PANI electrospinning with different carrier polymers: A. PVA, B: Eudragit, C: PCL, D: PLA, E: PEO, Fa: Chitosan/PEO with undoped PANI, Fb: Chitosan/PEO with CSA predoped PANI

3.3.1.2 Determination of suitable solvents

In Table 3.2, the solvent screening electrospinning experiments are presented. Together with the process parameters applied, the measured conductivity is given as well for reference.

Table 3.2: Screening for solvents and solvent systems – Solution properties and applied experimental conditions

Solution Recipe			**Conductivity (µS)**	**Electrospinning Procedure**		
Polymers and dopants	**Solvent/Solvent System**	**Final Polymer Concentration (w/v)**		**Conditions (Humidity – Temperature) *0.8mm needle* unless stated otherwise**	**Flow Rate (mL/h)**	**Voltage (kV)**
1:1 CSA Doped PANI:PEO	chloroform	4.5%	**5.89**	44% - 21.8°C	1-5-10	8-10
1:1 PANI:PEO	chloroform	4%	**0.14**	44% - 21.8°C	2 – 5	7-10
1:1 PANI:PEO	DMF	4%	**308**	44% - 21.8°C	1 – 2 - 5	8-10
PANI	Chloroform	2%	**0.03**	44% - 21.8°C	1-10	0-15
PANI	DMF	2%		44% - 21.8°C	1-10	0-15
PANI	Toluene	2%		44% - 21.8°C	1-10	0-15
1:1 PANI:PEO	NMP	4%		44% - 21.8°C		
1:1 PANI:PEO	THF	4%	**0.15**	44% - 21.8°C	1-10	0-15
1:1 CSA Doped PANI:PEO	DMF	4%	**116.1**	44% - 21.8°C	1	7-15
PANI	NMP	2%	**10.76**	26% - 21.6°C	-	-
CSA doped PANI	chloroform	4.5%	**4.08**	26% - 21.6°C	5	7-15
1:1 PANI:PEO	80:20 chloroform: NMP	4%	**0.95**	28% - 20.2°C	5	8.5 – 10 – 15 – 18

1:1 CSA Doped PANI:PEO	chloroform	6.5%	**5.49**	28% - 20.2°C	5	8-12-15
1:1 PANI:PEO	DCM	4%	**12.3**	29%, 20.9°C	5-7-8-10	8-12-14
1g doped PANI with 2.4g CSA + 1g PEO	chloroform	8.8%	**9.65**	29%, 20.9°C	3-5-8	6-11-15
1:1 CSA Doped PANI:PEO	THF	6.5%	**4.13**	29%, 20.9°C	3	7-12
PEO (Mw 300 000)	chloroform	4%	**0.24**	29%, 21.8 °C	3	8-10-12.5-20-25
1g CSA doped PANI +1g PEO	80:20 chloroform: NMP	6.5%	**141.1**	29%, 21.8 °C	1-5	7-15
1:1 CSA Doped PANI:PEO	THF	6.5%	**4.13**	29%, 21.8 °C	3	7-12
PEO (Mw=600 000)	chloroform	4%	**0.22**	25%, 22.7°C,	1-3	8-10-15-20
1:1 CSA Doped PANI:PEO	1:1 chloroform: DCM	6.5%	**6.00**	29%, 23.1°C	8 - 10	8 – 10.5 - 12
0.5g PANI + 1.5g CSA + 0.5g PEO	DCM	5%	**52.27**	31%, 23.1°C	3	15 – 20 - 25
0.5g PANI + 1.5g CSA + 0.5g HMW PEO	chloroform	5%	**8.87**	32%, 23.3°C	3	15 – 20 -25
0.5g+1.5g CSA + 0.5g PEO	chloroform	5%	**6.22**	38%, 21.9°C	3	8.5 – 15 – 18 – 22.5
1:1 CSA	1:1	6.5%	**34.23**	38%, 21.9°C	3	8.5 –

Doped PANI:PEO	chloroform: acetone					15 - 20
1:1 CSA Doped PANI:PEO	1:1 chloroform: acetonitrile	6.5%	**82.7**	38%, 21.9°C	3	8 – 10 – 15 -20
0.5g PANI + 0.88g CSA + 0.5g PEO	chloroform	~3.7%	**2.93**	40%, 20.7°C	3	10

Through the experiments it was confirmed as expected from theory that the boiling point of the solvent is a crucial parameter for the electrospinning process. Solvents with high boiling points (eg. NMP, DMSO, DMF) are not suitable at all, as their evaporation rate is too low or they don't evaporate at all, even when they are used in solvent mixture with more volatile solvents such as chloroform (Figures 3.5 A, B & C).

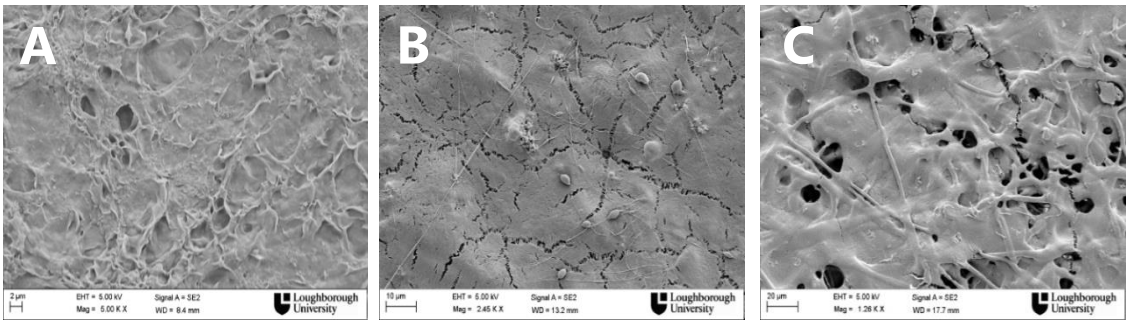


Figure 3.5: CSA doped PANI/PEO A: in chloroform:NMP (80:20) B: in chloroform:DMSO (80:20) C: in chloroform:DMF (80:20)

Polyaniline is practically insoluble in any solvent, however, when chloroform and dichloromethane were used as solvents, more uniform dispersions were received allowing the electrospinning process to be conducted smoothly and without interruption. Some representative SEM pictures are given in Figure 3.6. This was not the case when THF, acetone or acetonitrile were used, where the needle was frequently being blocked by undissolved polyaniline particles. As can be seen in the SEM pictures below, nanofibres in Figure 3.6 A seem to be more uniform in terms of polyaniline dissolution and distribution. On the contrary, in Figure 3.6 D there are many polyaniline particles of the size of tens of micrometers and therefore unsuitable for the desired purpose.

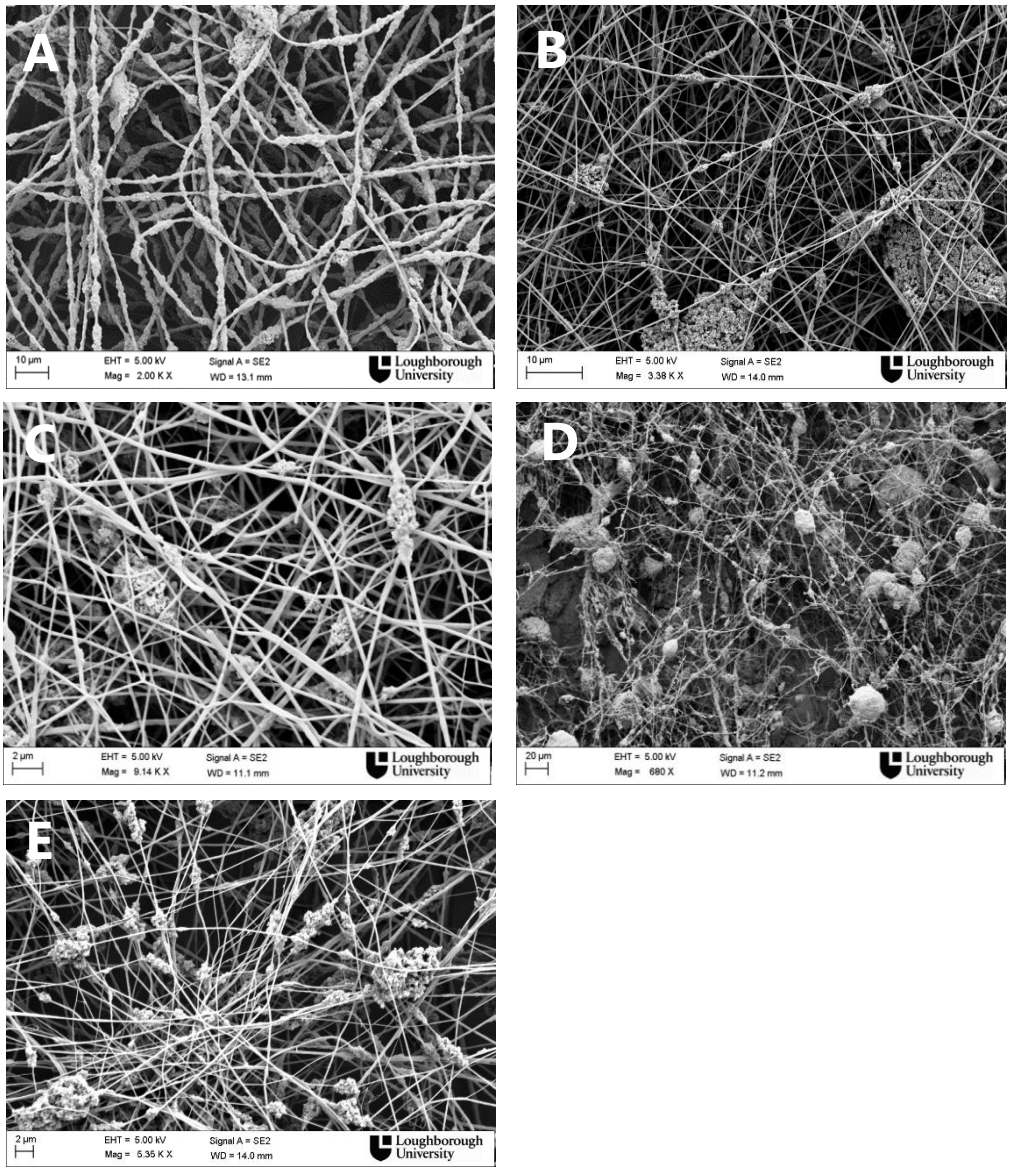


Figure 3.6: CSA doped PANI/PEO A: in chloroform B: in DCM C: in 50:50 chloroform/acetonitrile D: 50:50 chloroform/acetone E: in 50:50 chloroform:DCM

3.3.1.3 Determination of suitable dopants

Doping of the polyaniline emeraldine base with other acids other than the commonly used CSA, was attempted, in order to investigate if this would facilitate the electrospinning procedure and if morphologically better nanofibres (defect free) would be obtained. Dodecylbenzenesulphonic acid was used as it is another common polyaniline dopant in literature. Glutaric acid was chosen because of its biocompatibility, availability and similar pKa to the ones that are usually used as polyaniline dopants (CSA, DBSA).

Table 3.3: Screening for Dopants – Solution properties and applied experimental conditions

Solution Recipe			**Conductivity (μS)**	**Electrospinning Procedure**		
Polymers and dopants	**Solvents**	**Final Polymer Concentration (w/v)**		**Conditions (Humidity – Temperature) *0.8 mm needle* unless stated otherwise**	**Flow Rate (mL/h)**	**Voltage (kV)**
1g PANI doped with 0.82g glutaric acid (still blue solution)	chloroform	3.6%	**0.06**	29%, 20.9°C	3	8 – 10 - 20
0.5g PANI + 2g glutaric acid + 0.5g PEO (still blue solution)	chloroform	6%	**0.17**	34%, 24.6°C	3	8 – 15 - 20
0.5g PANI + 2.27g DBSA +0.5g PEO	chloroform	6.5%	**8.1**	52%, 18°C	3	8.5 – 15 - 20

Although DBSA is extensively used in literature as a very good polyaniline dopant [189], uniform nanofibres weren't produced when DBSA was used as a dopant. Big particles of undissolved DBSA can be seen in the nanofibrous mat (Figure 3.7 B). However, no distinct polyaniline particles similar to those observed when undoped PANI was attempted to be electrospun (Figure 3.7 A) were present in this case, meaning that DBSA assists polyaniline dispersion. In addition, the environmental conditions were not ideal at the time of these experiments, meaning that relative humidity was higher than usual (~50%) and the temperature, lower than usual (<20°C) therefore no definite conclusions should be drawn at this point. However, this inconsistency with the literature was a cause of further and systematic investigation of the environmental parameters affecting the electrospinning. In any case though, DBSA was not brought forward for further experiments as its physical state (very viscous liquid) was difficult to handle.

In the case of glutaric acid, the equivalent molar quantity with previously used CSA was used to dope the polyaniline, but it was evident even macroscopically that the amount wasn't enough as the solution color didn't take the characteristic green color of emeraldine salt. The nanoscale morphology of the produced nanofibres wasn't acceptable either, as the existence of large beads with short distance from another indicates (Figure 3.7 C). By gradually increasing the glutaric acid : polyaniline ratio from 0,8:1 to 4:1, only slight improvement was shown in terms of fibre morphology. It has to be noted here that although the environmental parameters weren't controlled, it can be safely assumed that glutaric acid is not a suitable dopant because as is shown in Figure 3.7 D, it doesn't solubilize well in the polymer blend and macroscopically, the addition of extra amount glutaric acid didn't have any effect on the color of the solution, which is a strong indicator that the doping was not successful. Further addition of glutaric acid in the blend, in an attempt to achieve complete doping, would result in precipitation of glutaric acid crystals, as it was macroscopically observed after having let the prepared solution to sit overnight. Presence of undispersed solids, is a factor that causes disruptions to the electrospinning process.

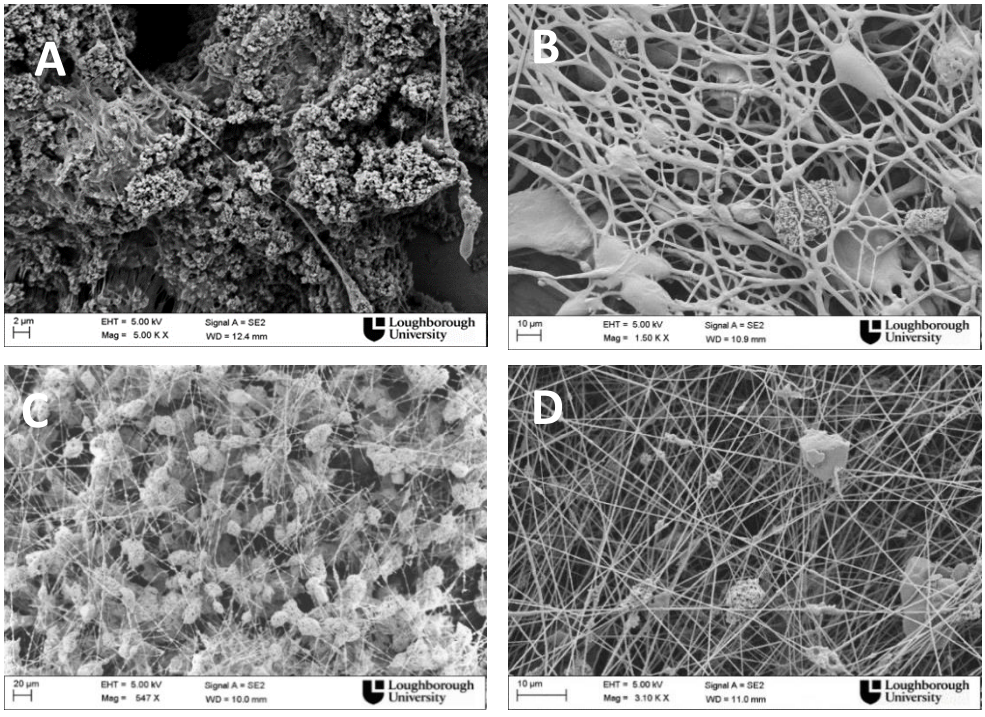


Figure 3.7: A: undoped PANI/PEO B: DBSA doped PANI/PEO C: glutaric acid doped PANI/PEO with doping ratio 0.8:1 and D) glutaric acid doped PANI/PEO with doping ratio 4:1

3.3.3.4 Investigation of Doping Effect

As CSA was proved to be a suitable dopant for polyaniline and chloroform the most suitable solvent, in agreement with the literature as well, the effect of the amount of dopant was investigated. It has been reported, that the amount of doping has significant effect on the properties of the final PANI material, namely the electrical and thermal conductivity [127]. For that reason, the following series of experiments (Table 3.4) were conducted in order to investigate the effect of the doping acid ratio, on the electrospinning procedure and the resulting nanofibres. The polyaniline and solvent quantities were kept constant and different amounts of CSA were added each time.

Table 3.4: Screening for best amount of doping – Solution properties and applied experimental conditions

Solution Recipe			**Conductivity (μS)**	**Electrospinning Procedure**		
Polymers and dopants	**Solvents**	**Final Polymer Concentration (w/v)**		**Conditions (Humidity – Temperature) *0.8mm needle* unless stated otherwise**	**Flow Rate (mL/h)**	**Voltage (kV)**
1g PANI doped with 0.5g CSA + 1g PEO	50mL chloroform	5%	**0.57**	26%, 23.9°C	3 – 5 – 7	8 – 10 – 15 – 28
1g PANI doped with 1.3g CSA + 1g PEO	50mL chloroform	6.5%	**2.05**	26%, 23.9°C	3- 5	8 – 10 – 18
1g PANI with 2.4g CSA +1g PEO	chloroform	8,8%	**9.65**	29%, 21.8 °C	3-5	6 – 8 – 12 – 20
1g PANI doped with 5g CSA + 1g PEO	chloroform	14%	**21.28**	26%, 23.9°C	5	11 –15 – 20 – 25 – 30
1g PANI doped with 7g CSA + 1g PEO	chloroform	18%	**41.97**	26%, 23.9°C	3	10 – 12 – 20 -30

Characteristic SEM pictures of the electrospun solutions are presented in Figure 3.8.

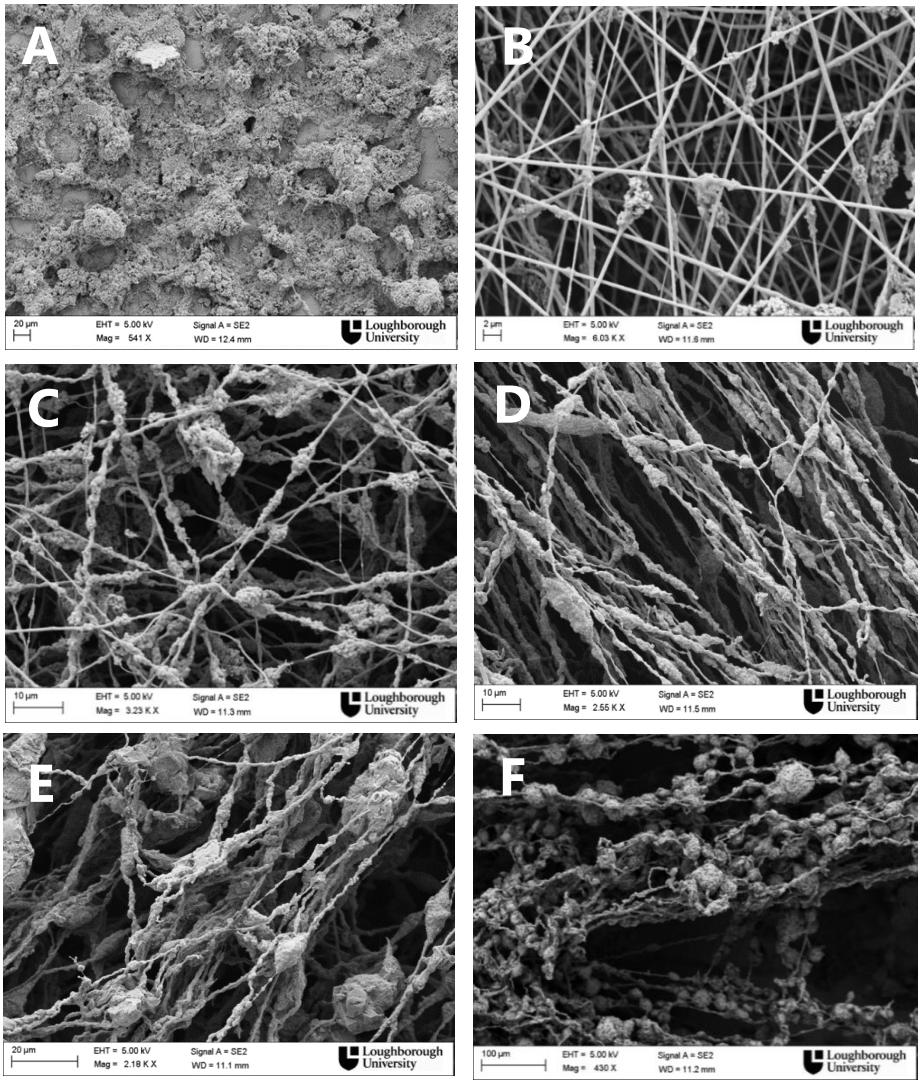


Figure 3.8: CSA doped PANI/PEO (1:1) in chloroform with different ratios of dopant/polyaniline A) 0:1 B) 0.5:1, C) 1,3:1, D) 3:1, E) 5:1, F) 7:1

As can be seen in Figure 3.8 A, the solution of undoped PANI/PEO in chloroform could not be electrospun under the given humidity and temperature conditions, although in previous experiments using DCM as a solvent, the electrospinning was successful.

The best nanofibre morphology is achieved when the dopant to polyaniline ratio is 1,3:3 and 3:1 (Figures 3.8 C & D). This result is in agreement with most of the published studies, indicating that PANI upon doping becomes easier to dissolve in organic solvents and to further process. Here, it is observed that with gradual

increase of the dopant, the nanofibre surface appears to be more uniform, with less distinct beads. Experimental observations indicate that the camphorsulfonic acid solubilizes better in the solvent than the pure polyaniline, causing a final better distribution. Also, it has been reported by other researchers that dissolving first the CSA in chloroform and then adding the undoped PANI, helps the preparation of the solution [119], [123]. Two explanations can be given for this phenomenon. Firstly, the presence of dissolved CSA in the solvent, "guides" the dispersion of PANI in the solvent when this is added, allowing for PANI chains to unfold and disperse in a more homogenous way, as the long alkyl chains of the CSA are guiding the PANI chain through its amine sites with which the acid interacts in order for protonation to occur [94]. On the contrary, when undoped PANI is added in the solvent first, aggregation is obvious even macroscopically, so that then even when the CSA is finally added, it takes longer for the solution to become homogenous. Secondly, as it has been reported in the case of DBSA as doping acid, the excess of DBSA that doesn't take part in the doping process probably acts as a plasticizer in the solution and that is a plausible reason on why more uniform fibres are obtained [190]. However, when the ratio is 5:1 or above, the nanofibre morphology disappears under the given humidity and temperature conditions. This was observed macroscopically as well; on the aluminum foil rather than a uniform mat, the polymer seems to be disposed vertically in the shape of short capillaries making it very difficult to manipulate, peel off and gold coat. This is due probably to the high conductivity of the solution, hindering the electrospinning process and the higher ratio of solids in the solution, resulting in increase of viscosity and thus making the jet formation more difficult. A macroscopically physically strong, elastic and easy to peel off mat was produced from the 1,3:1 solution which however, in the nanoscale appeared to have many distinct beads suggesting poor polyaniline dissolution.

There was found to exist a power relationship between doping amount and solution conductivity as shown in Figure 3.9.

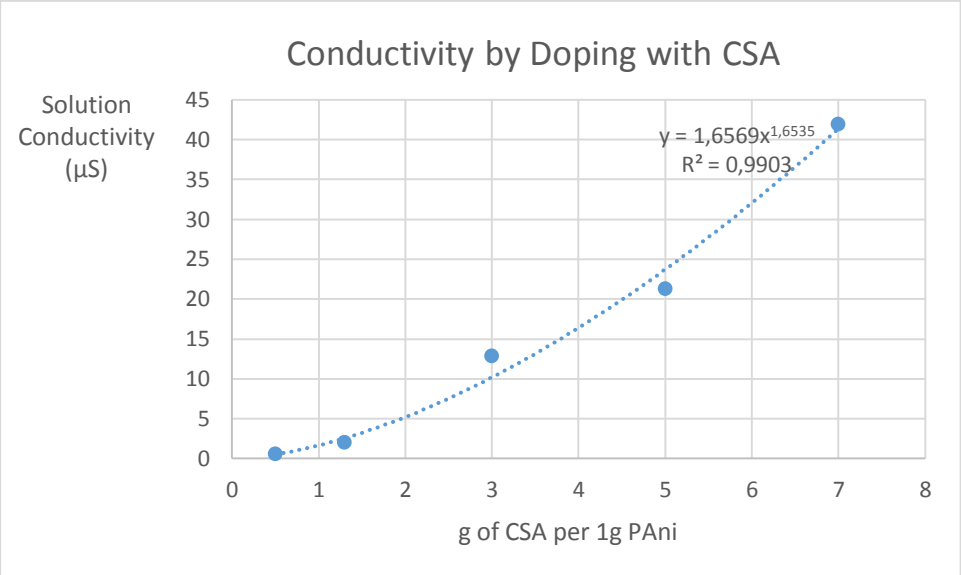


Figure 3.9: Relationship between amount of doping and solution conductivity

Figures 3.8 and 3.9, show that as the conductivity of the solution rises with the increase of the doping amount, the more difficult the electrospinning procedure becomes, causing the forming nanofibres to be attracted towards the needle tip, producing sparks, sometimes that intense that the experiment had to be interrupted. For that reason and in order to overcome that hindrance, the rotating drum collector was used at a low speed, and the produced nanofibres were carried off away from the needle tip because of the rotation movement [3]. A certain level of alignment is shown when the rotating drum is used (Figures 3.8 D, E & F). A certain level of alignment is noted also in some cases where the flat collector is used. This has happened for the solutions mentioned above where the produced fibres are attracted together and towards the needle tip. As the fibres are don't get deposited on the collector and are suspended between the needle and the collector, they form a yarn which is stretched under the electric filed. When the voltage is reduced to 0, they then sit on the aluminum foil as a thick string, and as a consequence of the stretching it had undergone, the fibres constituting it present some alignment.

3.3.2 *In situ* PANI polymerization

As shown in Figure 3.10 C, the polyaniline polymerization took place only on the surface of the nanofibrous mat, failing to infiltrate and coat the fibres laying underneath the surface. As the polymerization is taking place in aqueous media, this is attributed to the PLA's hydrophobicity. For that reason a second method was attempted, this time including prewetting the membrane with aqueous solution of Tween85. As shown in Figure 3.10 D, the dissolved aniline could better infiltrate the porous nanofibrous mat and polymerize on the nanofibres. However, even after several trials of polymerization times and initial monomer concentrations, no distinct nanofibrous structure could be achieved, indicating the difficulty of adequately controlling the *in situ* polymerization on a nanofibrous substrate. For that reason, this method was not brought forward at this stage, as the PANI blending in the electrospinning solution was proved a more reliable process, easier to control and as mentioned in the literature, more promising for biomedical applications, offering ground for deeper investigation and understanding of the effect of the PANI addition in a nanofibrous mat as more parameters can be controlled and different ratios of PANI content can be examined.

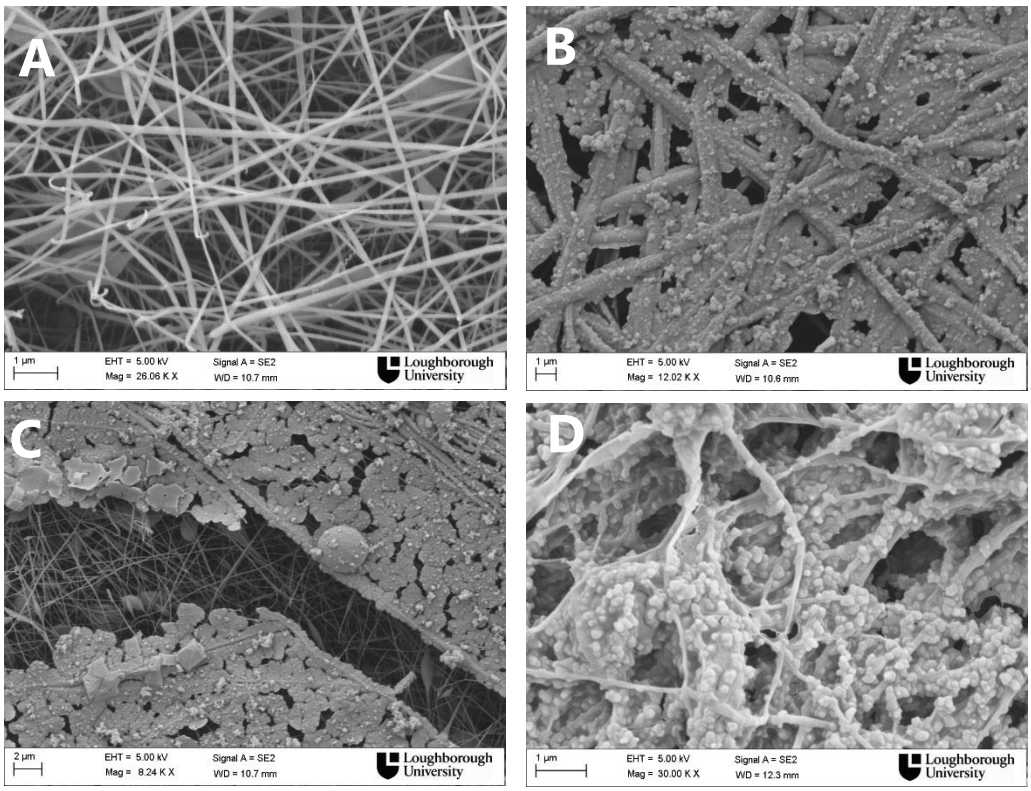


Figure 3.10: A: Electrospun PLA nanofibres, B: In situ polymerized PANI on electrospun PLA nanofibres, C: Cross-sectioned area of the in situ polymerized PANI on electrospun PLA mat, D: Cross-sectioned area of the in situ polymerized PANI with the presence of surfactant, on electrospun PLA mat.

3.3.3 Core-Shell electrospinning

During this set of experiments core-shell electrospinning was investigated. While usually the core solution consists of a low elasticity, non-electrospinnable solution and the outer shell of an easily electrospinnable polymer solution, which shields the non spinnable polymer inside, giving it the nanofibrous morphology and is then removed afterwards either by using an appropriate solvent or by thermal degradation [177], here the possibility to obtain PANI fibres by using a core of an easily spun solution and PANI on the outer shell, was investigated. The reason this trial was performed, was firstly to examine the potential of the process, since the shell solution would be green colored, indicating macroscopically if core-shell fibres are obtained. Secondly, that approach would allow for potential further investigation, which would be based on the production of fibres with PANI at the outer shell, which could then

be converted to nanotubes, by removing the core material, or incorporate bioactive substances in the core and examine how application of electrical current on the outer shell, would affect the release kinetics. To that end, an aqueous PVA solution 10% w/v was prepared and used as the core solution and a CSA doped PANI in chloroform was used as the shell solution. Since PANI was the shell solution, a small amount of PEO (0.5% w/v) had to be added, in order to make it slightly viscous and avoid spillages, when the voltage is applied during the electrospinning process. For core-shell electrospinning it is very important that the two different solvents are not miscible, so that they don't blend at the needle tip and during the Taylor cone formation. Confocal fluorescence microscopy was used initially as a method to prove if a continuous core is obtained, by adding a 2.5%v/v of fluorescein dye in the PVA polymer solution. To draw safe conclusions though on the quality of the core-shell fibres, the successful samples were also characterized by Transmission Electron Microscopy (TEM).

The settings listed in Table 3.5 were used, in order to obtain core-shell nanofibres

Table 3.5: Electrospinning Parameters Used for Co-axial electrospinning

Sample name	Voltage (kV)	Distance (cm)	FR core (mL/h)	FR shell (mL/h)	RH%	Observations
1	22.5	15	0.5	0.5	20	Good collection– Green fibres
2	22.5	15	0.25	0.75	20	Good Collection
3	22.5	15	0.75	0.25	20	No collection
4	22.5	15	0.2	0.4	20	No collection

After various combinations of electrospinning parameters were tried, the successfully electrospun mats were visualized with three microscopic methods, as shown in Figure 3.11.

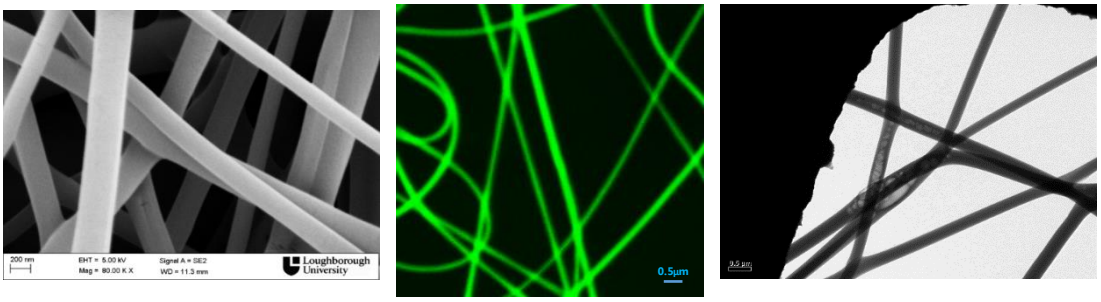


Figure 3.11: PVA-PANI core-shell fibres fabricated with 0.5mL/hr / 0.5mL.hr, 22kV, 20%RH: A SEM image, B: Confocal Fluorescence Microscope image, C: TEM image

The fibres obtained by core-shell electrospinning macroscopically had the characteristic green color of PANI, indicating the presence of a continuous PANI shell, presented good nanofibrous morphology when examined under the SEM (Figure 3.11 A) and the presence of a continuous PVA core was confirmed under the fluorescence confocal microscope (Figure 3.11 B), since the core had been dyed with fluorescein dye. However, when the samples were examined under the TEM, it is evident that there is no continuous, core-shell structure, except for just few fibres and moreover at parts there seem to be air-bubbles trapped in the structure.

3.4 Conclusions

Based on this general screening study of the electrospinning of polyaniline, the coaxial electrospinning and the *in situ* PANI polymerization on already spun fibres were set aside as potential methods for the fabrication of PANI fibres, mainly because of the complexity of the first and the limited control over the second. In any case, for the application towards which this study is oriented, where the conductivity of the mat doesn't have to be on the metallic regime and the presence of another polymer together with polyaniline, which is already proven to be biocompatible and biodegradable is advantageous, the blend solution electrospinning seems to be the most promising. High molecular weight PEO and chitosan were identified as the best carrier polymers to focus on. Chloroform and organic acidic solvents (acetic or trifluoroacetic acid) were identified as the best solvents for the electrospinning of PANI when PEO and chitosan are used as carrier polymers respectively. Camphorsulfonic acid was found to be the best dopant for that process as it

increases PANI solubility and facilitates electrospinning when added at a ratio 1.3:1 (CSA:PANI) more specifically. To tackle the problem with the undissolved PANI particles that are present in most cases, the PANI solutions will be passed through PTFE filters prior to addition of the carrier polymer. Humidity control was also found to be necessary to be incorporated in the device, so as to ensure stable and consistent electrospinning conditions, since it varies a lot on a daily basis and in order to study its effect on the process, at a second stage (Chapters 4 & 5).

4 | DETERMINING FACTORS FOR THE ELECTROSPINNING WINDOW OF CONDUCTING PANI/PEO BLEND

4.1 Introduction

Poly(ethylene oxide) is a polymer of ethylene oxide like the very widely used polyethylene glycol, but which usually refers to larger length polymer chains, above 20 000 g/mol whilst the term PEG is mostly used for molecular weights smaller than 20 000 g/mol. From the scanning experiments, it was identified as a polymer suitable to aid with the electrospinning of PANI as it also has been shown in the literature is a polymer that when blended with polyaniline can give bead free, homogeneous nanofibres (see Section 3.2). From the variety of molecular weights that it is available at, in this chapter all the experiments will be conducted with PEO of 2 000 000 g/mol, as it showed very good processability during the screening experiments. PEO and PEG are biocompatible and biodegradable, which renders them safe for biomedical applications, as numerous studies have shown [191], [192].

As has been discussed in detail in Section 2.2.2, the morphology of the electrospun fibres is influenced by a variety of factors including solvent properties (dielectric constant, volatility), solution properties (viscosity, surface tension, conductivity, polymer concentration and molecular weight, incorporation of additives such as salts or surfactants), environmental conditions (temperature, humidity) and process parameters (applied voltage, flow rate, needle TCD, needle diameter, type and size of collector). In this chapter, all the solution properties will be kept constant and emphasis will be given on two of the process parameters, namely the voltage and flow rate and one of the environmental ones, the humidity, which was identified as an important one to influence reproducibility of experiments conducted during the initial screening experiments.

Humidity has been acknowledged as one of the environmental parameters, but is not always taken into account in the electrospinning models as a significant parameter affecting the process. On the contrary, it seems to be categorized as a

minor parameter affecting the final jet diameter [52]–[56]. It is worth noting here, that during the present study, the environmental humidity in the lab where the study was conducted (East Midlands, UK) was varied from around 40%, during the winter time, when the central heating was on and up to 70% on rainy days during spring and summer.

Studies on the effect of humidity on electrospun fibres have shown contradicting results. Electrospinning of cellulose acetate (CA) exhibited an increase in nanofibre diameter with increasing humidity, while Poly-vinylpyrrolidone (PVP) showed the opposite trend. In PVP, the absorption of the surrounding water in higher relative humidity causes slower solidification of the jet, longer elongation time and as a result smaller fibre diameters. However, at high RH above 60%, PVP nanofibres begin to fuse. This is probably due to loss of surface charges, as water vapors surrounding the jet, are electrically conductive, thus resulting in apparently larger diameters. In the case of CA, as relative humidity increased, more absorption of water caused faster precipitation and therefore, larger fibre diameters. It has to be noted here that PVP is soluble in water, whilst CA not [88], [101]. Ya et al. examined the electrospinning of PEO/water solution and concluded that with increasing humidity the fibre diameter decreases. They attributed this to the slower solidification rate which lead to longer whipping of the jet. After having examined a series of single polymer solutions and polymer blends, Pelipenko et al. also concluded that higher environmental humidity in general, results in thinner average nanofibre diameter but with higher values of relative standard deviation. However, above a certain threshold of relative environmental humidity, which differs depending on the polymer, only beaded nanofibres are collected. Even if for all the solutions examined in that particular study, the general trend of how the relative humidity affects the process was the same, there were discrepancies regarding the thresholds and quantitative results which they attributed to different polymer characteristics [193]. In a more in depth study though, performed by Huang et al., on polyacrylonitrile (PAN) and polysulfone (PSU), it was demonstrated that the fibre size of both PAN and PSU increased with increasing RH, which comes to contradiction with the previous studies mentioned. It was also observed that the PAN fibres were relatively uniform throughout the range of RHs (0,

20, 40, and 60%) examined, while, PSU, on the other hand, maintained uniformity at lower RH, but formed both very large and very small fibres at higher RH. The resulting fibre diameter distributions were broad and bimodal and the jet was reported to be unstable during the process when observed macroscopically. This resulted in broken fibres that varied in diameter along their length. This difference in uniformity was attributed to different polymer hydrophilicities. PSU, being hydrophobic has less tolerance to water and thus experiences a faster phase separation. Humidity was also found to impact the mechanical properties of both polymer fibre mats. Generally, electrospun fibres at low RH exhibited higher tensile strength than those at high RH. Fibres spun at high RH underwent partial phase separation, resulting in a skin layer which hindered fibre–fibre bonding in the mat. This impacted PSU nanofibres to a greater extent due to PSU's rapid phase separation in the presence of water vapor [194].

In partial agreement with the findings of Huan et al, are the observations of Nezarati et al., where high humidity was again reported to cause fibre breakage and loss of poly-ethylene glycol fibre morphology, as a result of increased water absorption [77].

High relative humidity can also cause surface pore formation on the electrospun fibres, as was demonstrated on PCL fibres by Nezarati et al. [77], possibly through vapor-induced phase separation. It is also expected that porosity and pore diameter tend to increase with further increase of relative humidity. Casper et al. observed the same relationship between humidity and pore formation on the fibres when electrospinning polystyrene fibres with THF used as a solvent. Apart from vapor induced phase separation, they attributed this phenomenon to breath figure formation as well. The evaporative cooling that occurs as a result of solvent evaporation causes the surface of the jet to cool and water from the surrounding air to condense on the surface of the fibre. As the fibre dries, the water droplets leave an imprint behind in the form of pores.

Going back to Nezarati's et al. study, in the case of electrospinning poly-carbonate urethane, fibre collection dropped at high humidity, most likely due to increased electrostatic discharge. In the same study, humidity below 50% resulted in fibre

breakage due to decreased electrostatic discharge from the jet for all three polymers that were electrospun (Polyethylene glycol, poly carbonate urethane and polycaprolactone) [77], [88], [102]. Tripatanasuwan et al. concluded that there is a linear decrease of the diameter of PEO fibres with increasing humidity. It was also found that above 50% of relative humidity, beaded fibres are collected, with the size of the beads systematically changing with further increase of humidity [102].

Generally, the ambient relative humidity may affect the electrospinning process in three ways. First, it may affect the solvent evaporation rate, with high humidity causing slower solidification of the jet and therefore causing the jet to elongate longer, producing thinner fibres. Very high humidity can cause the solvent to not fully evaporate throughout the process [88], [101], [102]. Secondly, as water vapor is electrically conducting, it affects the charge distribution on the Taylor cone and on the elongated jet, mainly by removing charges from the jet. In this case the surface charge density decreases leading to the formation of fibres with larger diameters. Finally, water absorption on the jet may induce polymer precipitation and phase separation changing the morphology of the fibres. These findings highlight that the effects of relative humidity on electrospun fibre morphology are dependent on polymer chemical structure and hydrophobicity, solvent miscibility with water, and solvent volatility and the results are not always predictable. Especially with regards to the electrospinning of conducting polymers, the role of humidity has not been fully explored nor understood yet. Despite their numerous potential applications, very few studies have been reported on electrospinning of conducting polymers. Sisi Li et al., studied through a wide lens, the process and solution parameters as well as environmental factors on the electrospinning of PANI-PEO blends. Two humidity conditions, 38% and 60%, were directly compared and it was found that at high relative humidity (>60%) no fibres were formed. Low flow rate and high applied voltage appeared to have a synergistic effect to the stretching of the jet and the production of thinner nanofibres [92].

Contradicting results have also been reported with regards to the effect of the applied voltage and were extensively discussed in p 2.1.2.3.

As for the flow rate, there is consensus, generally, that the increase in flow rate can result in increased formation of beads and this seems to be valid for PANI-PEO blends as well. Low flow rate, on the other hand, usually results in nanofibres of smaller diameter [55], [77], [92].

Aim of this study is the examination of the effect of different parameters (flow rate, applied voltage, ambient humidity, doping level), with regards to the morphology of the nanofibrous structure and the nanofibre diameter distribution. The electrospinning window will be defined and analyzed and the effect of polymer conductivity on the jet behavior and the diameter distribution will be determined.

4.2 Materials and Methods

Polyaniline emeraldine base (PANI, Mw=50 000), (1R)-(-)-10-camphor-sulfonic acid (CSA), poly (ethylene oxide) (PEO, Mw=2 000 000) and chloroform were purchased from Sigma Aldrich Inc. and used without further purification.

4.2.1 Solution Preparation

Camphorsulfonic acid was first fully dissolved in chloroform. An adequate amount of polyaniline base was dispersed in the solution. It was first sonicated for 5minutes and kept under stirring overnight at room temperature. Sonication was repeated twice more during the stirring time and the solution was filtered through a 0.45um PTFE syringe filter. Polyethylene oxide was then added to the solution which was stirred for an additional 4hours. Three blends of different doping level, 20%, 60% and 100% were chosen to be used for electrospinning. The doped polyaniline concentration was kept the same for all solutions. Gravimetric measurements of the filters were performed to determine the final PANI content and a solution of final concentration 1,8% w/v doped PANI/PEO (ratio 50:50) was produced for electrospinning. The surface tension of the final solutions was measured with a surface tension balance (White Electric Instrument Co).

4.2.2 Electrospinning Process

The blends were fed through a plastic syringe to the needle tip (20G diameter) and were electrospun under different voltages, produced by a high voltage source (Glassman High Voltage Inc.). The nanofibres were collected on a flat grounded collector covered with aluminum foil. The needle TCD was fixed at 12cm at a horizontal orientation. The flow rate of the solutions was controlled by a syringe pump (Harvard Apparatus).

In order to control the humidity, a modification was made on the electrospinning setup, which consisted of drilling a hole on the bottom of the electrospinning chamber and passing through it compressed dry air. Another floor was added at a distance of around 2cm so that the air flow would split and pass from the perimeter of the floor, behind the nozzle, as well as behind the collector, moving upwards towards the extraction. With this modification, any evaporating solvent building up around the nozzle was removed as well. The schematic is presented in Figure 4.1.

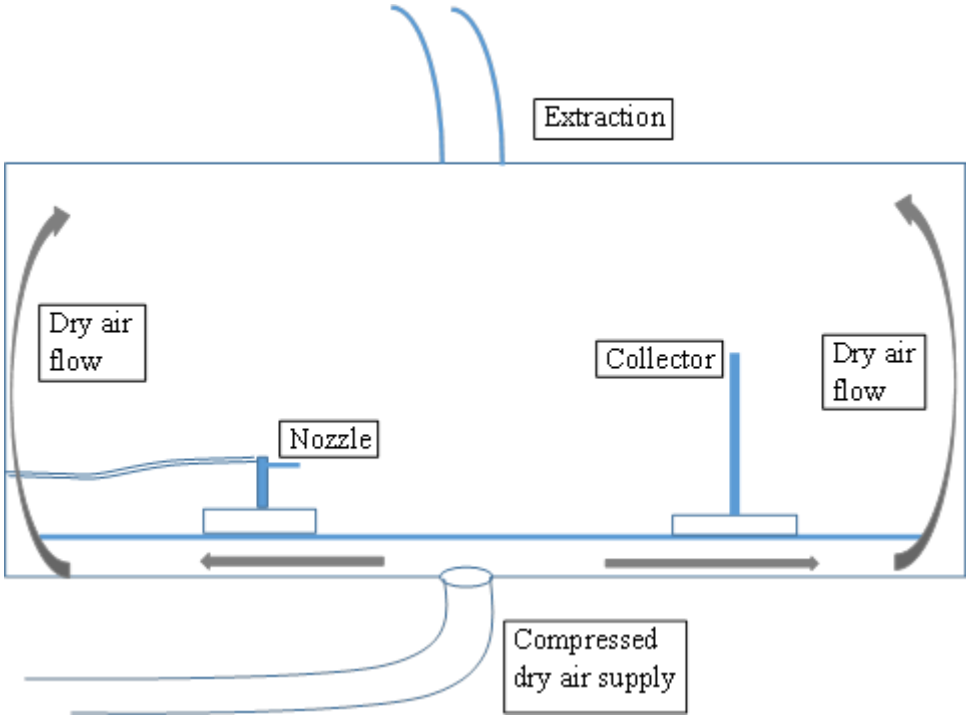


Figure 4.1: Modified electrospinning setup to control environmental humidity

This way, the humidity in the electrospinning chamber was regulated by a constant dry air flow and monitored using a temperature and humidity meter ST-321. The temperature was monitored by the same device.

Finally, a Fluke 287 digital multimeter was interposed between the collector and the ground so as to allow the measurement of the current that is transferred by the jet on the collector for each experimental run.

The morphology of the electrospun mats was then examined with the use of Carl Zeiss (Leo) Scanning Electron Microscope (Model 1530VP). The SEM images presented in the results and discussion section are representative of three electrospinning runs and at least three different areas of each mat. For the determination of the average diameter of the fibres and for the generation of charts and plots, AxioVision and Matlab R2016a software were used respectively.

4.2.3 Experimental Design

A three-level full factorial design was used in order to determine the electrospinning window for the two specific PANI-PEO solutions in randomized runs. The maximum and minimum values for each parameter were determined from some initial scanning experiments that are not presented here. Especially for the voltage range, 13.5kV was used as higher value, as higher voltages resulted in short circuit of the device due to the high conductivity of the solution. As low voltage setting, the lowest one allowing Taylor cone formation was used, which would indicate the potential formation of a jet. The runs performed are summarized in Table 4.1.

Table 4.1: Experimental runs according to three level full factorial experimental design

Run	Flow Rate (mL/h)	% Relative Humidity	Voltage (kV)
1	3	32	13.5
2	2	32	13.5
3	1	32	13.5
4	3	25	13.5
5	2	25	13.5
6	1	25	13.5
7	3	18	13.5
8	2	18	13.5
9	1	18	13.5
10	3	32	9.2
11	2	32	9.2
12	1	32	9.2
13	3	25	9.2
14	2	25	9.2
15	1	25	9.2
16	3	18	9.2
17	2	18	9.2
18	1	18	9.2
19	3	32	5
20	2	32	5
21	1	32	5
22	3	25	5
23	2	25	5
24	1	25	5
25	3	18	5
26	2	18	5
27	1	18	5

The charts illustrating the electrospinning windows of the 60% doped PANI- PEO solution, were plotted with the use of the Matlab R2016a software. As electrospinning window hereby, is defined the combination of the parameters, in this case applied voltage, flow rate and relative humidity, which allow for the electrospinning process to run smoothly, regardless of the morphology of the resulting fibres (diameter size, presence of beads or not).

4.3 Results and Discussion

The results obtained from this systematic experimental study will be used to determine the electrospinning window of a conducting polymer solution and to analyze the combined effect of major process and environmental parameters on the behavior of a conducting polymer jet during electrospinning. This will be compared with the behavior of non conducting polymer jets reported in the literature by fitting the data obtained during this study in an existing mathematical model. The effect of the level of doping on the fibre morphology will also be discussed.

4.3.1 Morphology

The combined effects of the examined parameters on the fibre morphology show that the prevailing phenomena during electrospinning are related to the conducting character of the polymer.

4.3.1.1 Effect of flow rate

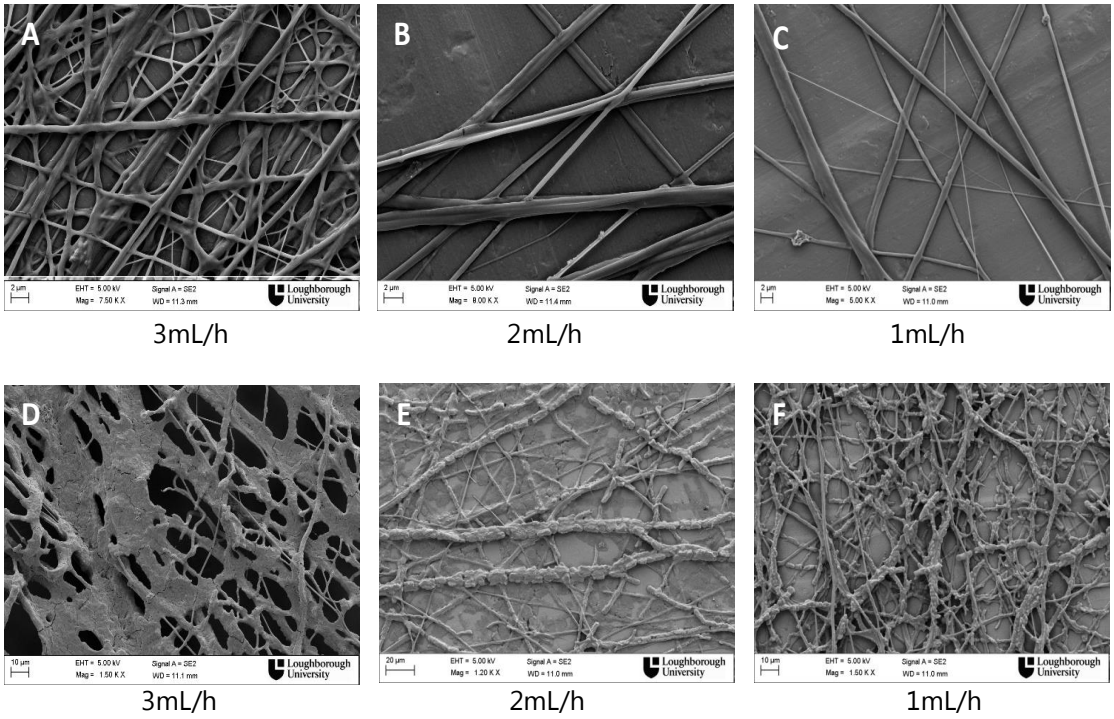


Figure 4.2: SEM images for the comparison of flow rate variation on the nanofibre morphology. The samples on each row are electrospun at same voltage and RH and at decreasing flow rate (mL/h): A, B & C at 13.5kV and 18%RH and D, E & F at 9.2kV and 25%RH

In terms of flow rate, the SEM images obtained (Figure 4.2) show a trend that was expected, based on the literature. Higher flow rates generally resulted in higher productivity and in some cases the nanofibres were not completely dry when they reached the collector. This was observed for different voltages and different levels of relative humidity, and could be attributed to the fact that, longer time would be required for the solvent to fully evaporate at higher flow rates and constant TCD. However, when the highest value of voltage was applied, the process became more stable at high flow rates. Low flow rates resulted in the formation of some very fine fibres, as shown in Figure 4.2 C, probably due to the high surface charge density which may have caused splitting of the jet [91].

4.3.1.2 Effect of humidity

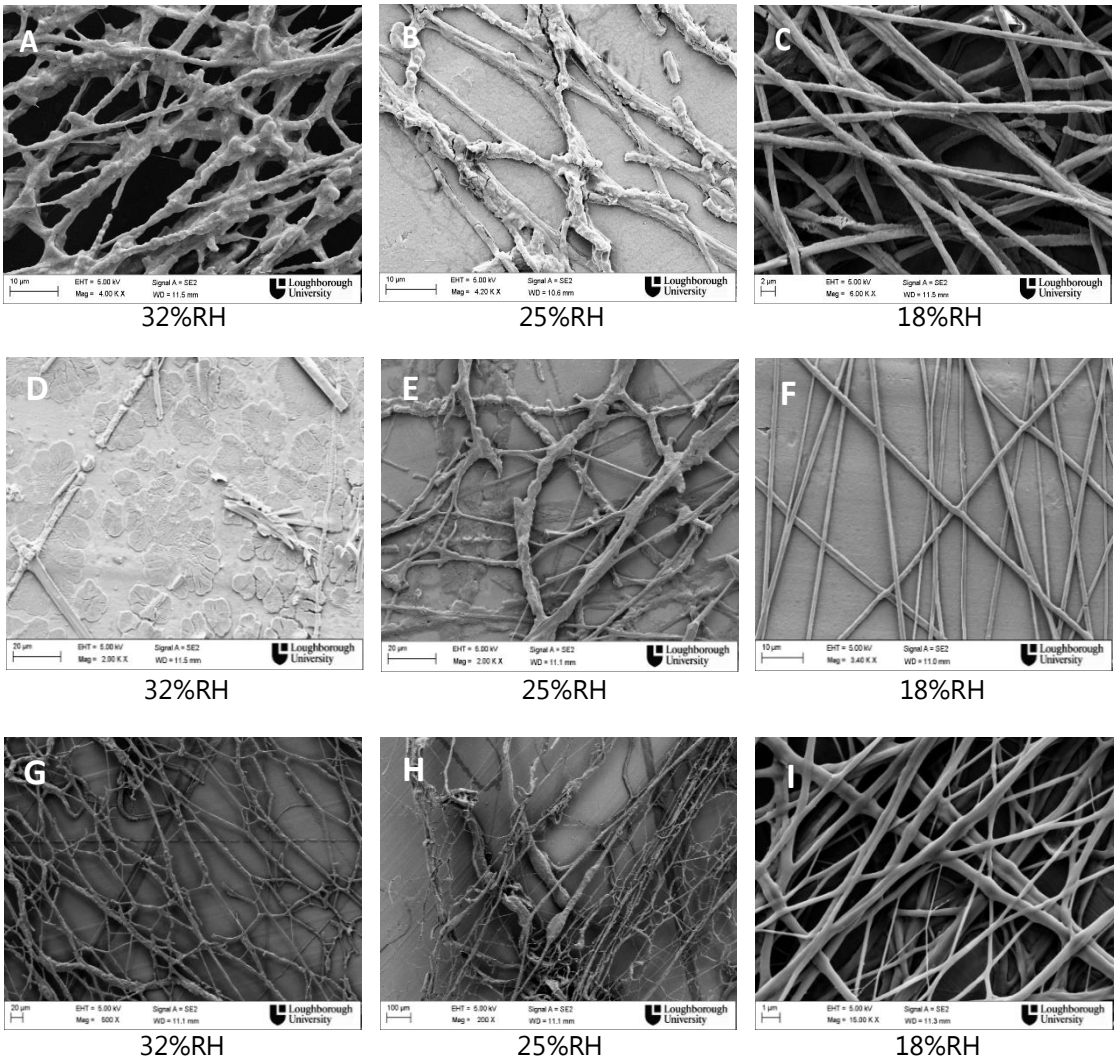


Figure 4.3: SEM images showing the effect of relative humidity variation on the nanofibre morphology. The samples on each row are electrospun at same voltage and flow rate and at decreasing %RH: A, B & C at 5kV and 1mL/h, D, E & F at 5kV and 2mL/h G, H & I at 13.5kV and 3mL/h

Humidity was found to play a crucial role in electrospinnability and mat morphology. As shown on the SEM images in Figure 4.3, only low ambient humidity allows the formation of defect free nanofibres throughout the whole range of applicable voltages. When the humidity increases to 25%, the fibres start to break and irregular and uneven surfaces are formed, whereas electrospinning was not feasible at relative humidity higher than 40%. The roughness of the surface occurring at higher humidity (Figure 4.3 A), could be explained by phase separation that potentially occurred during the jet stretching caused by the absorption of water vapour by PEO. The

electrospun solution consists of PEO which is a highly hydrophilic polymer, polyaniline which is insoluble in water and chloroform which is immiscible with water, therefore water absorption by the PEO could result in phase separation, precipitation of PANI and hence in uneven and rough nanofibre surface. Huang et al, reported the same phenomenon during electrospinning of polyacrylonitrile at elevated humidity. They concluded that during solvent evaporation, the surface cools and causes thermally induced phase separation, forming a skin layer on the spinning fibre. This effect is exacerbated by the presence of surrounding water, since in that case water was a nonsolvent. This formation of the skin layer effectively locks the fibre into a larger diameter while dissolved polymer solution remains trapped in the core. Eventually, the solvent molecules in the core evaporate through the skin layer, leaving behind an uneven surface [192].

These observations could be directly compared with Knopf's, who studied the effect of variation of environmental humidity during electrospinning of PEO solution in the same solvent. That study showed that relative humidity didn't have an effect on the electrospinning process or nanofibre morphology. On the contrary, in this case, the addition of polyaniline in the same PEO-chloroform solution resulted in humidity becoming a major factor for electrospinning [195]. The strong dependence of electrospinnability on the humidity for PANI solutions, except from the insolubility of PANI in water, could also be attributed to its conductivity. Higher humidity can remove surface charges from the jet or the solution surface at a higher rate, resulting in an increased discharge of the solution surface, which can either hinder the formation of a jet and impede electrospinnability or cause defects on the fibre surface. Angammana and Jayaram showed that the solution conductivity and the average jet current are closely related, with the jet current initially increasing for increasing solution conductivity and then decreasing with a further increase at solution conductivity. This was attributed to the decrease of the tangential electric field occurring at increased conductivity which causes the electrostatic force along the surface of the fluid to diminish [54]. Therefore, the high conductivity of PANI could lead to a decrease of the electric field. This, combined with the increased discharge rate of the jet at higher humidity, gives rise to synergistic effects that exert very strong

effects on PANI solutions, rendering them very sensitive to humidity effects and set the relative humidity threshold for electrospinnability lower than for most polymers. This suggests that polymer conductivity can significantly affect the electrospinnability of a polymer solution in relationship to humidity variations. It can be suggested that by increasing the environmental humidity there is a charge unbalance taking place on the polymer jet, as charges can be exchanged from the polymer itself to the surrounding water vapors more easily than in the case of a non conducting polymer solution. The conductivity of the polymer might be facilitating this way, the transfer of charges from the centre of the jet towards the surface, thus accelerating the discharge rate and rendering the impact of surrounding water vapors more important.

4.3.1.3 Effect of voltage

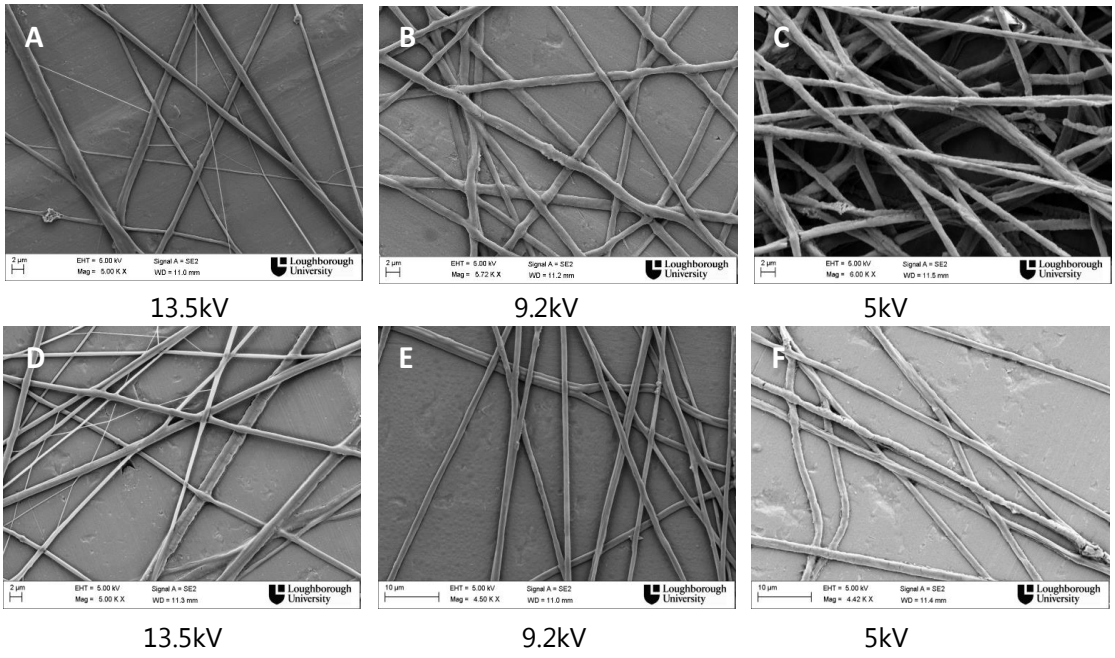


Figure 4.4: SEM images for the comparison of applied voltage variation on the nanofibre morphology. The samples on each row are electrospun at the same %RH and flow rate and at decreasing applied voltage. A, B & C at 18%RH and 1 mL/h, D, E & F at 18%RH and 2 mL/h

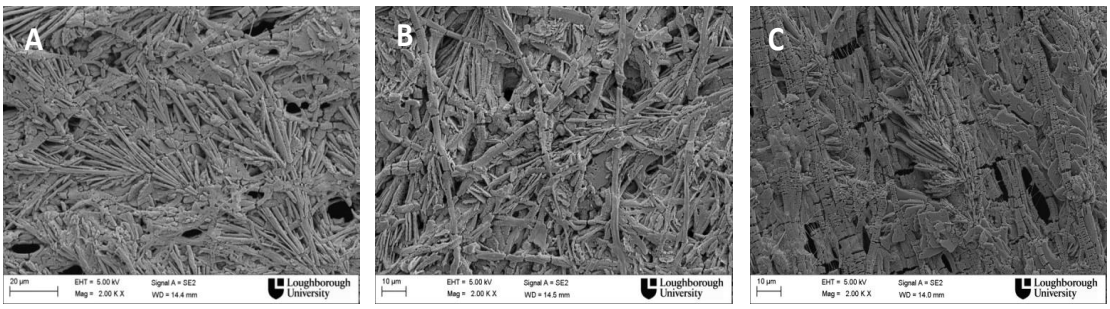
As a general trend it seems that higher voltages produce thinner nanofibres but also a bigger diversity in diameters and a broader diameter distribution which will be discussed in the next section. Especially at 13,5kV, for all flow rates, some very thin nanofibres can be seen within the mat, as shown in Figure 4.4 A and 4.4 D, indicating

splitting of the jet. It has been reported that the jet may undergo splitting into multiple subjets in a process known as splaying or branching. This happens as a result of changes occurring in the shape, and charge per unit area of the jet during its elongation and the solvent's evaporation. The balance between the surface tension and the electrical forces may be shifted, usually, if the excess charge density on the surface of the jet is high causing undulations on the jet. These undulations may grow big enough to cause instability and then, in order to regain balance and to reduce the local charge per unit area, branches are initiated outward of the spinning jet. The formation of branches in jets and fibres usually occurs in more concentrated and viscous solutions and also when relatively high electric fields are applied [91], [196].

It is also observed, that provided a low humidity, all the range of applied voltages results in defect free fibres indicating that the applied voltage is not a major factor affecting nanofibre formation.

4.3.1.4 Effect of doping level

The 20% doped solution was proved to be inappropriate for electrospinning as the inadequate doping rendered the solubility of the polyaniline in chloroform extremely low, and after the filtration there was practically no polyaniline left in the solution.



1mL/h, 9.2kV 3mL/h, 9.2kV 3mL/h, 13.5kV

Figure 4.5: SEM images of electrospun 100% CSA doped PANI–PEO solution under various process parameters at 18%RH

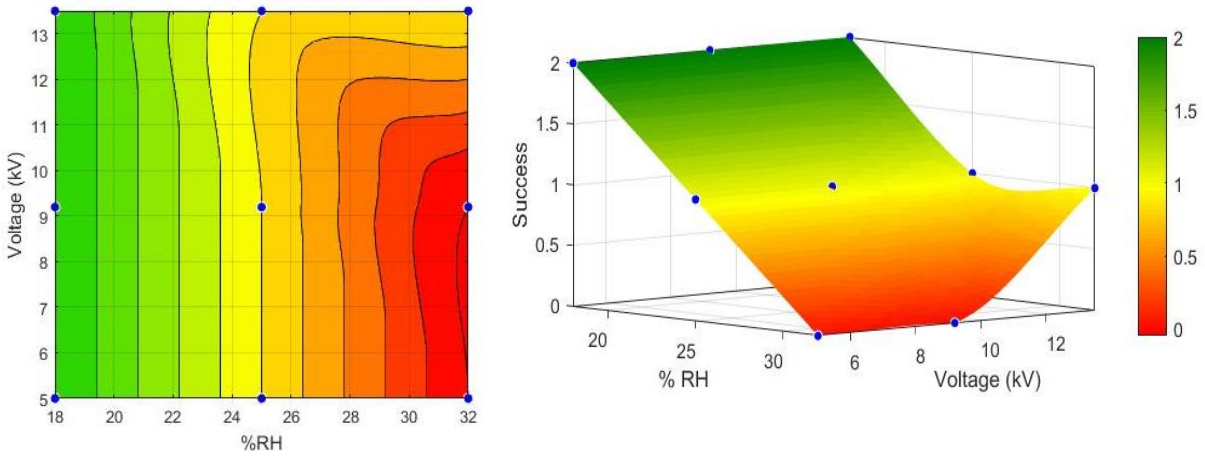
The solution containing PANI doped at a greater extent (100%) produced structures of very high crystallinity and orientation but not nanofibrous mats (Figure 4.5). The experimental design that was used covers low, medium, and high values of flow rate, voltage and environmental humidity, so it can safely be concluded that the PANI

(100%doped) - PEO solution 1,8% w/v is not electrospinnable. The amount of CSA that was added in order to increase the doping level seemed to cause the formation of crystalline structures during spinning that had a certain orientation as shown in Figure 4.5, for several flow rates and voltages. This morphology could be attributed to the CSA that is present in excess in the solution. It has also been proven in the literature that casting of CSA doped polyaniline solutions results in crystalline structures as the acid hydrogen ion bonds to the imine sites of the polymer chain [189], [197], [198]. The reason why this morphology is obtained at high doping levels, is most likely due to the fact that the excess amount of CSA added in the solution increases the boiling point of the solvent, thus hindering the evaporation of the solvent within the range of parameters tested here, resulting in a wet mat, with no nanofibre structure but with the crystalline morphology reported at the above mentioned studies on film casting.

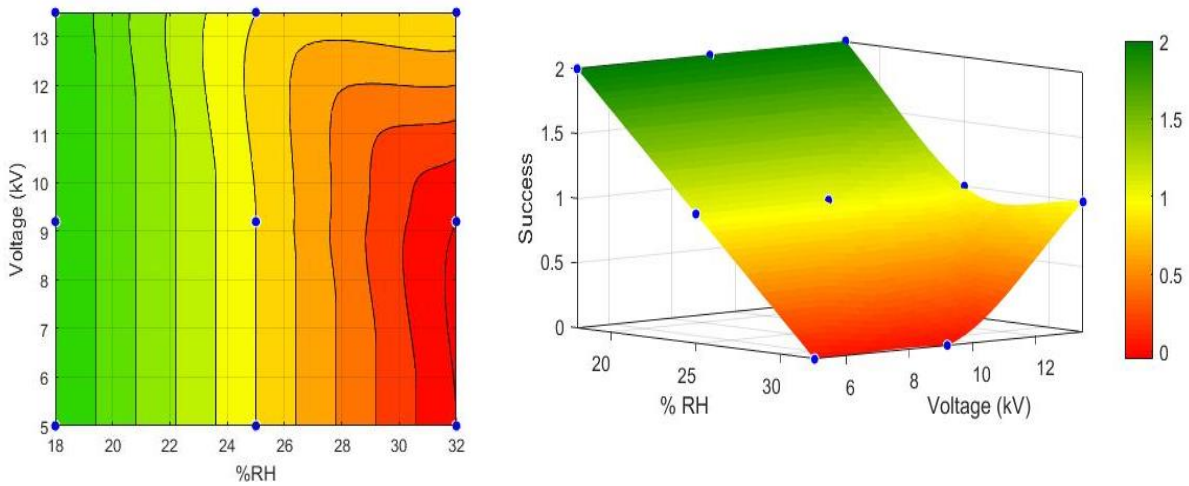
4.3.2 Electrospinning Window

After analyzing the SEM pictures obtained, the following contour plots and charts were created on Matlab as described in Section 4.2.3. More specifically, the coding that was used to define the electrospinning window is as follows: 0 (red color): electrospinning was not possible/no fibres collected, 1 (yellow color): electrospinning was possible – fibre-like morphology but with defects (beaded fibres, broken fibres, wet mat), 2 (green color): defect free nanofibre morphology.

A. Contour and Surface Plots of Success vs RH & Voltage at Flow Rate 1mL/h



B. Contour and Surface Plots of Success vs RH & Voltage at Flow Rate 2mL/h



C. Contour and Surface Plots of Success vs RH & Voltage at Flow 3mL/h

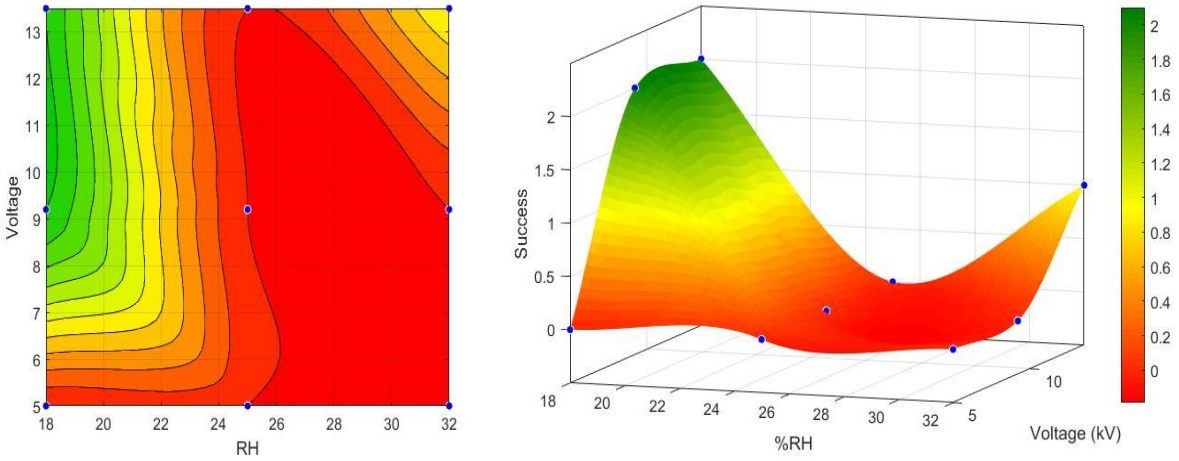


Figure 4.6: Electrospinning window of 60% doped PANI-PEO solution, grouped by the flow rate, A) 1mL/h B) 2mL/h, C) 3mL/h

The electrospinning window at a flow rate of 1mL/h is identical to the one at flow rate of 2mL/h (Figures 4.6 A & B), suggesting that although the flow rate affects the process, it is not the key parameter in terms of electrospinnability. Green areas, in Figure 4.6, depict the conditions where a stable jet formed and defect free fibres were produced (level 1-2) and the red areas depict the conditions where electrospinning was hindered, thus producing fibres with defects or where electrospinning could not be conducted at all (level 0-1). It is shown that at flow rates of 1 and 2mL/h, the electrospinning window is wider than at 3mL/h, allowing formation of nanofibres at a wider range of conditions. Similarly when 18%RH is applied, the electrospinning window is bigger allowing the formation of nanofibres over a broader range of conditions and of combinations of the other two parameters (flow rate and voltage).

In Figure 4.7, the combined effect of the three parameters on the electrospinning window is depicted in a 3D plot. Green points represent the conditions were electrospinning is undisrupted and results in defect free fibres, yellow points represent the conditions where electrospinning was possible but the collected fibres have some type of defect (beads, wet, stuck together, rough surface) and red points represent the conditions were electrospinning was not possible at all.

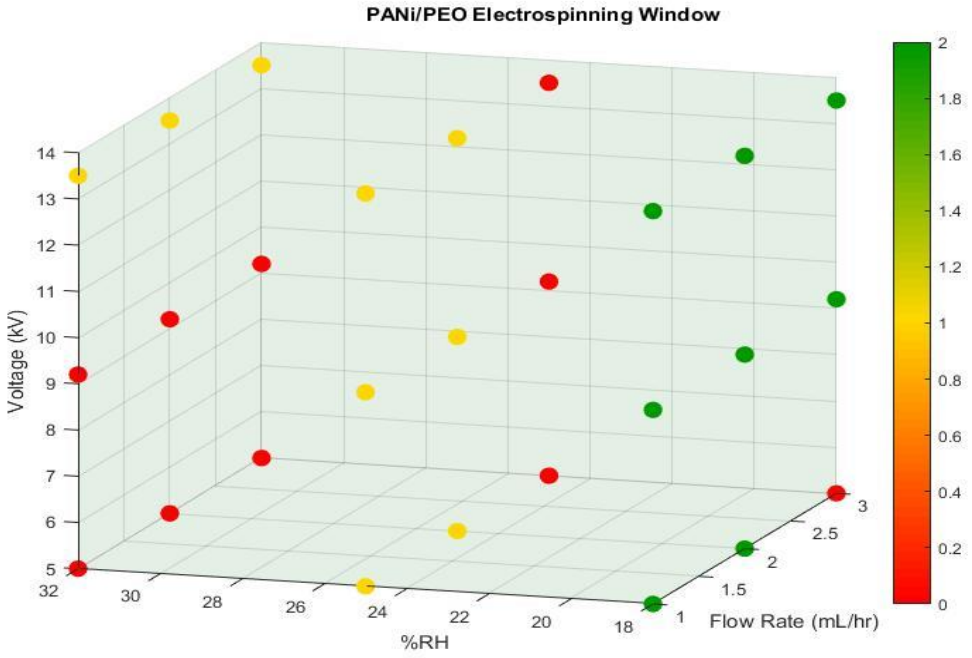


Figure 4.7: Combined effect of voltage/flow rate/relative humidity on the electrospinnability of PANI/PEO blend

It is quite clear, that the role of humidity is crucial. It is almost only at low humidity that defect free nanofibres could be collected. This indicates that humidity higher than 20% may hinder the electrospinning process in a number of ways. At higher humidity, water vapor removes surface charges, that drive the jet elongation, leading to discharge of the jet and hence to smaller electrostatic forces between surface charges. This might hinder the formation of a Taylor cone or the extrusion of the jet from the Taylor cone, or lead to the formation of beads and defects on the fibres. Also, at higher humidity, water vapor can be absorbed by the PEO in the jet which can cause phase separation as PANI is not soluble in water. Finally, high humidity may result in slower solidification of the jet.

For the combinations of these three parameters that resulted in the production of defect free nanofibrous mats, a further investigation regarding the nanofibres diameter was conducted to determine the effect of the process parameters on the mean diameter and diameter distribution. Results were based on measuring the diameter on 150 nanofibres for each sample and are summed up on the diagrams of Figure 4.8. The count of 150 fibres was decided after trial and error calculation of average diameters and standard deviations of initially 100, 125, 150 and 175 nanofibres. It was found that for the samples with higher standard deviation, namely A and B, the average diameter and standard deviation value was the same when 150 and 175 nanofibres were measured. As a result, a minimum count of 150 fibres was used for all samples.

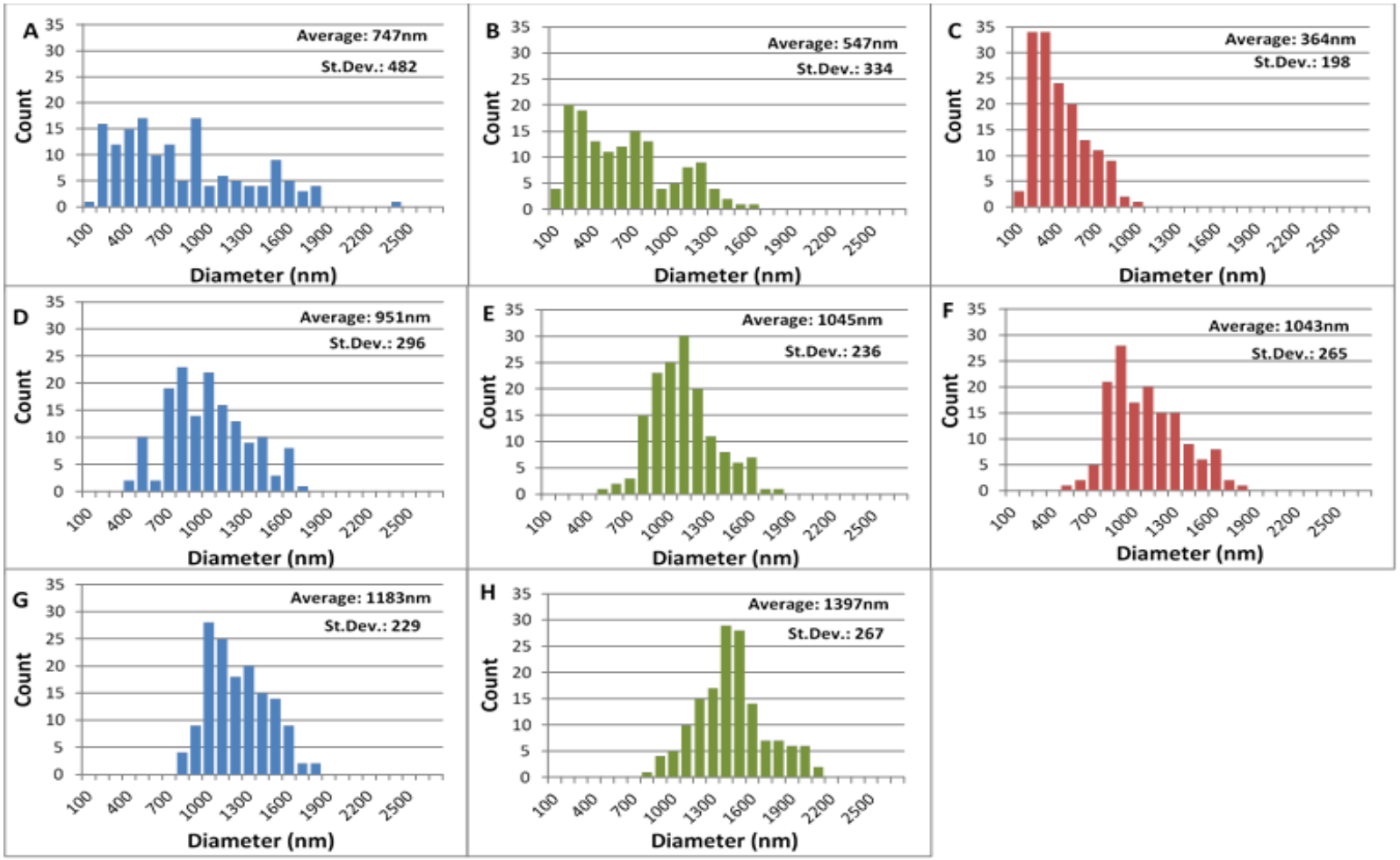


Figure 4.8: Diameter Distribution for electrospun mats at 18% RH: A) 1mL/h, 13.5kV B) 2mL/h, 13.5kV C) 3mL/h, 13.5kV, D) 1mL/h, 9.2kV E) 2mL/h, 9.2kV and F)) 3mL/h, 9.2kV G) 1mL/h, 5kV H) 2mL/h, 5kV

High voltage combined with low flow rate results in relatively thin nanofibres based on average diameter measurements, but the distribution range is very wide, indicating splitting of the jet, probably because of very high surface charge density. At constant voltage (13,5kV), as the flow rate increases (Figures 4.8 A-C), the mean diameter and the distribution range (or the width of the diameter distribution) decrease, which is shown by the graphs and the decreasing standard deviation values. At constant flow rate the diameter distribution shifts to larger diameters and becomes more narrow and uniform for decreasing voltage (Figures 4.8 A, D, G) indicating that splitting of the fibres ceased. At lower voltage of 9.2kV (Figures 4.8 D-F) the mean diameters increase and the distributions shift to bigger diameters at all flow rates. The shape of the distribution also changes and becomes more uniform at flow rates of 1mL/h and 2ml/h indicating a more stable process. The narrowest distribution was obtained at the applied conditions: [13.5kV, 3mL/h, 18%RH] followed by the [1mL/h, 5kV, 18%RH] and [2mL/h, 9.2kV, 18%RH]. However, as the average diameter obtained by electrospinning at the latter conditions was higher than the range usually proposed for cell culture, which has been found to be 400nm or less [128], the conditions of 13.5kV, 3mL/h and 18%RH were considered more suitable to bring forward for future experiments.

The combined effects of the process parameters on the mean fibre diameters are shown in Figures 4.9 and 4.10, where the variation of the average diameter in relation to the voltage and the flow rate is shown respectively.

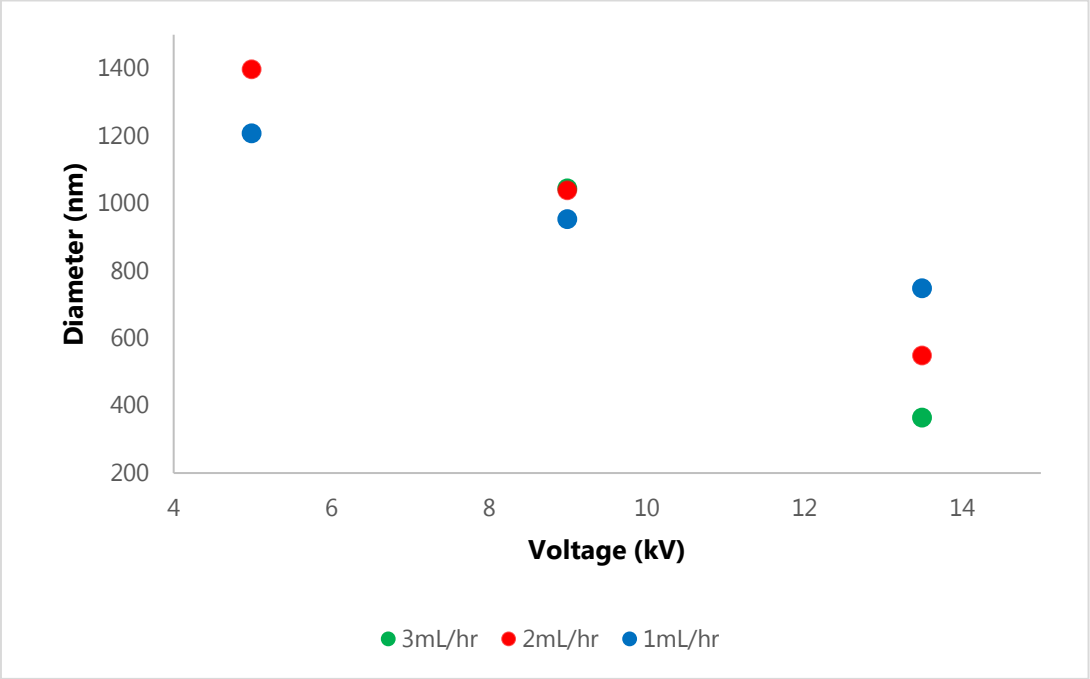


Figure 4.9: Effect of the applied voltage on the nanofibre diameter

Regarding the effect of the voltage, Figure 4.9 shows consistency on the way the voltage affects nanofibre diameter. Application of higher voltage, in general, produces thinner nanofibres at all flow rates. The impact of this though is more pronounced at higher flow rates, as shown in Figure 4.9, almost doubling for each different flow rate used. The reason that the impact of voltage is more pronounced at higher flow rates could be understood considering the dual effect of the voltage on the jet. Firstly, higher voltage provides more thermal energy to the jet and hence accelerates the solvent evaporation leading to faster solidification of the jet. Secondly, higher voltage provides higher surface charge density and stronger repulsion between the surface charges, hence more stretching of the jet. The combination of these two factors, result in a different slope in Figure 9 for different conditions. At low flow rates, faster jet solidification prevented further stretching of the jet compared to higher flow rates, where the jet solidified slower and stretching occurred to a greater extent, hence the second effect was more pronounced. These findings contribute to clarifying the controversy encountered in the literature about the effect of the voltage on various solutions and under various electrospinning conditions.

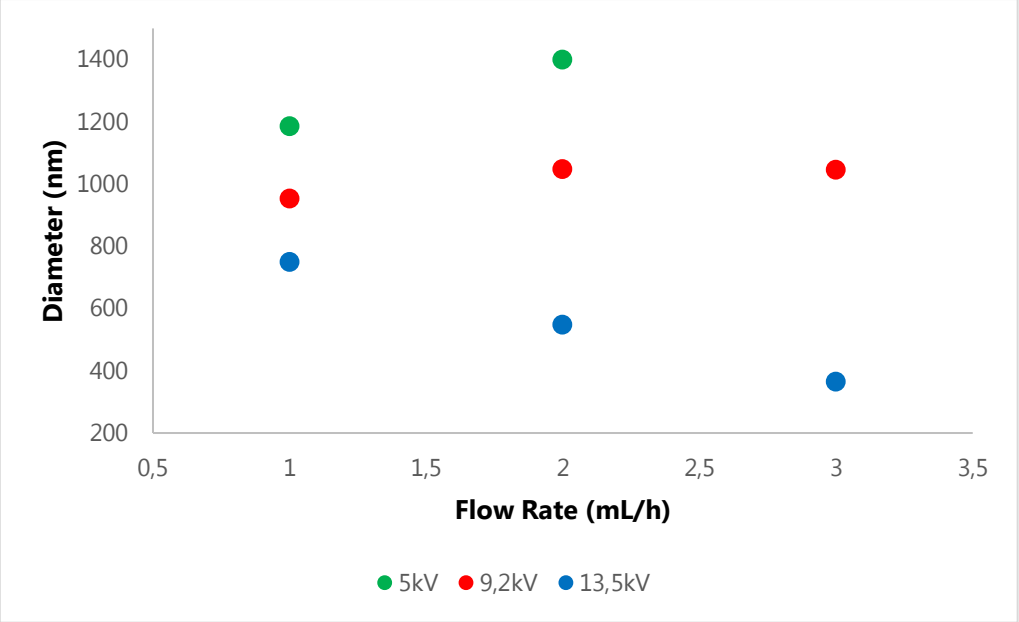


Figure 4.10: Effect of flow rate on the nanofibre diameter

With regard to the flow rate, its effect on the average diameters depends on the voltage. At a higher voltage, the average diameter decreases as the flow rate increases. At medium voltage, it doesn't change significantly, meaning that the effect of the flow rate is counterbalanced by the voltage increase resulting in a steady diameter, and at low voltage the relationship seems to get reversed. Although at high flow rate it wasn't possible to electrospin at 5kV and therefore the average diameter could not be calculated, the trend is evident. This opposes the majority of findings reported in the literature regarding the effect of the flow rate on the final nanofibre diameter [55], [61].

These observations could be explained by taking into consideration the effect of the voltage on the evaporation rate of the solvent and the jet's solidification rate. Application of higher voltage causes the temperature of the jet to increase, and therefore the solvent to evaporate faster. Fast solvent evaporation means fast jet solidification which in turn prevents further stretching of the jet leading to bigger fibre diameters at low flow rates. As the flow rate increases at the same high voltage, the jet solidifies slower and hence it is subjected to more stretching leading to the formation of finer fibres. This explains why, at high voltage, the diameter decreases with increasing flow rate. It is worth noting that these findings also depend on the volatility of the solvent. At low voltage however, different phenomena prevail. At low

voltage the strength of the electric field is not sufficient to cause further stretching of the jet for increased flow rate, hence as the flow rate increases the fibre diameter also increases. At medium voltage values, the combined action of the two competing phenomena lead to insignificant differences in the jet diameter with increasing flow rate.

4.3.3 Data fitting

For the combination of the experiment parameters that resulted in measurable nanofibres, how the data fit on the diameter prediction equation (Equation 4, Section 2.1.3) proposed by Fridrikh et al. was examined [52].

$$h = \left(\gamma\bar{\varepsilon}\frac{Q^2}{I^2}\frac{2}{\pi(2\ln\chi-3)}\right)^{1/3} \qquad (4)$$

Equation 4 was used to calculate all theoretical diameters for the electrospun 60% doped PANI-PEO solutions. The surface tension of the solution was measured to be 30.2mN/m, the dielectric constant of chloroform is found in the literature [199] and the current values were measured for each of the process parameters combination at 18%RH. Figure 4.11 presents how the predicted and measured nanofibre diameters compare. The application of the proposed model resulted in an underprediction of the resulting nanofibres for all combinations of parameters except for the data points corresponding to high flow rate, which show good agreement with the model.

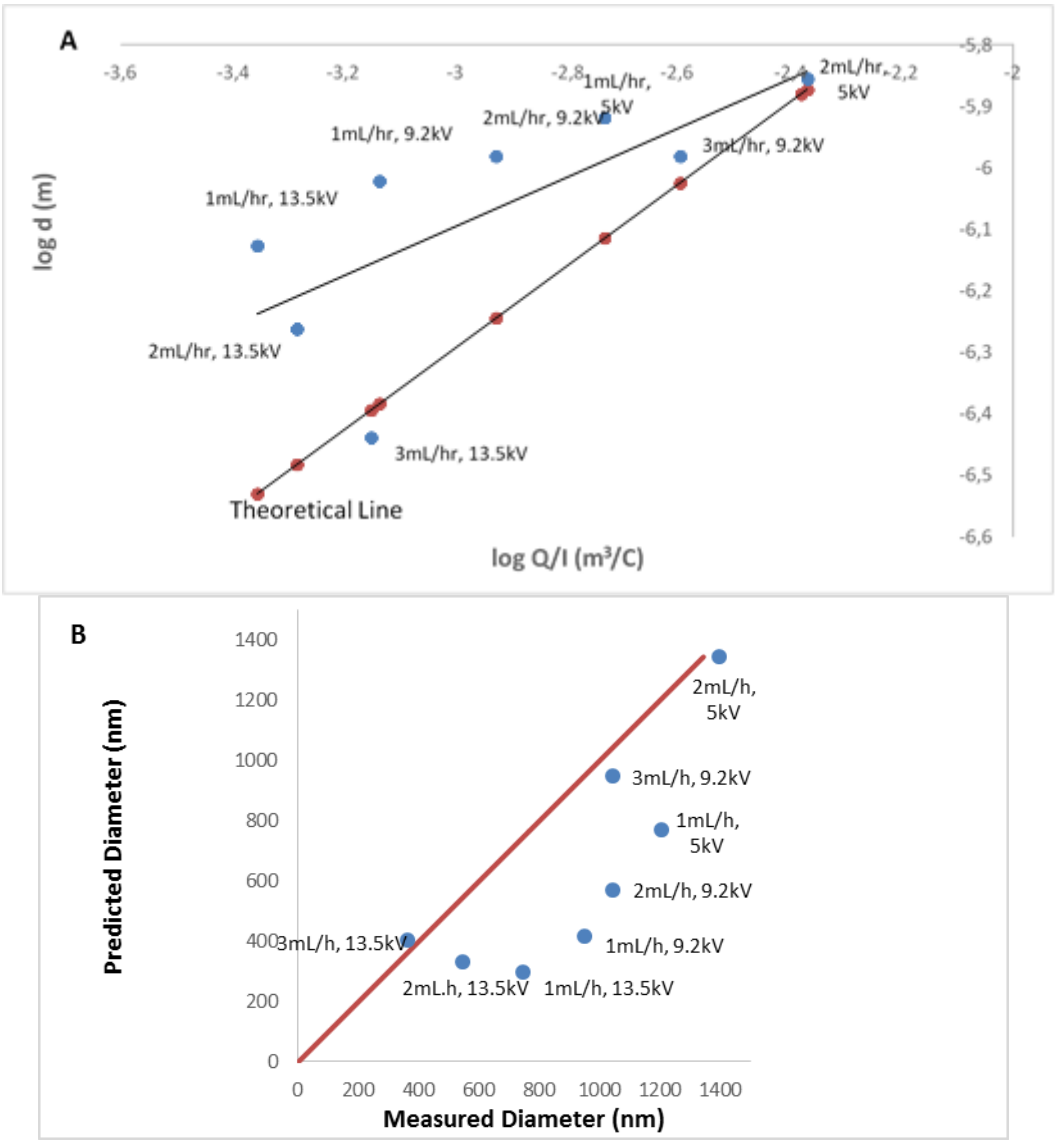


Figure 4.11: Graphic representation of the fitting of the experimental data to the theoretical model. A: The terminal jet diameter, d_f shown as a function of Q/I compared to the theory. B: Direct comparison of experimental and predicted values at various flow rates

The deviation of the predicted from the actual diameters could be attributed to the conductivity of the polymer, the complex relationship between conductivity, jet current and fibre diameter, and the evaporation rate of the solvent. The solutions studied and reported in the literature refer to non-conducting polymers, where the conductivity of the jet is mainly due to the conductivity of the solvent. The conductivity affects the distribution of surface charges and the tangential electric

field forces exerted on the jet. As the solvent evaporates the distribution of surface charges on the jet surface will be different for a conducting polymer compared to a non-conducting one resulting in a deviation from the expected values. The jet current increases with conductivity within certain range and then it decreases with conductivity [54]. This complex relationship between conductivity, jet current and the fibre diameter has not been taken into account. According to the model the relationship between jet current and fibre diameter is monotonic. However Angammana et al showed that the fibre diameter decreases with increasing jet current within a range of conductivities but increases with increasing jet current for higher conductivities. Figure 4.11 A shows that for the same Q/I the experimental data agree with the predicted behavior at high flow rates but deviate at low flow rates. This deviation may be attributed to a great extent to the effect of solvent evaporation which can be more pronounced at lower flow rates and more importantly, at the higher rate of the discharge of the jet, since at low flow rate, the jet is in theory thinner [53].

4.5 Conclusions

Humidity was shown to be the -most important parameter affecting electrospinning and defining the electrospinning window for PANI solutions. Only at very low humidity, electrospinning was feasible, indicating that for conducting polymers, the effect of humidity may be significantly greater compared to that of non conducting polymers. To our knowledge this is the first study examining the importance of environmental humidity on electrospinning of a conducting polymer in an organic solvent. Higher ambient humidity disrupted the electrospinning process and resulted in irregular and rough fibre surfaces.

Flow rate and strength of electric field were found to have an impact on the final nanofibre diameter. Higher values of applied voltage resulted in thinner nanofibres at all flow rates. But when high voltage was combined with low flow rate, the phenomenon of branching of the jet was observed, resulting in broader diameter distribution. The impact of the flow rate was found to be dependent on the applied voltage which is an observation reported for the first time, shedding light to

discrepancies that are encountered in the literature regarding the effect of voltage. At high applied voltage, the nanofibre diameter decreases with the increase of flow rate while at low voltage the opposite trend is observed. At medium values of applied voltage the effect of the flow rate is counter balanced by the increased voltage. Low doping level rendered the polyaniline insoluble in chloroform and a high one caused the doping acid to crystallize and totally alter the morphology of the final mat. Finally, the diameter data were fitted to Fridrikh's et al. prediction model which showed under-prediction of the diameters in most cases probably due to the effects of the solvent evaporation and conductivity of the polymer blend.

These findings contribute significantly to the knowledge on how electrified jets behave during electrospinning and specifically conducting polymer solutions which are vastly investigated as a more straight forward way to electrospin the polyaniline. These blends are already being used to fabricate membranes with high conducting properties finding applications as gas sensors and supercapacitors [186]. By taking into account the parameters that affect the process, it is anticipated that this will facilitate further their fabrication by increasing the productivity and eliminate disruptions that are caused due to these factors.

5 | PANI/CHITOSAN NANOFIBRE PRODUCTION – DETERMINATION OF THE ELECTROSPINNING WINDOW

5.1 Introduction

Chitosan is a N-deacetylated derivative of chitin, a biopolymer encountered in nature, in many crustaceans and insects as a main component of the exoskeleton. It is a biocompatible material, biodegradable, soluble in slightly acidic aqueous media and can be easily cast as a film, for hydrogel formation or to be electrospun with the presence of other polymers. It has also been found to exhibit antibacterial, antifungal, mucoadhesive, immunological, hemostatic [200] and wound healing properties as well as to promote cell adhesion and proliferation [201]–[203].

However, the electrospinning of pure chitosan solutions has proved challenging. Chitosan aqueous acidic solutions are very viscous with high surface tension which puts an obstacle on the production of uniform nanofibrous mats. In addition to that, the protonation of its free amino groups that takes place when chitosan is dissolved in acidic media, renders it a polyelectrolyte. Therefore, the repulsive forces between ionic groups within the polymer backbone that arise due to the application of a high electric field during electrospinning restrict the formation of continuous fibres and hinder the electrospinning process [204]. However, it is that exact property that makes it very attractive as an additive in the electrospinning solution as it is not uncommon to add salts, ionic surfactants and ionic polyelectrolytes to enhance charge density on the surface of the ejected jet, and therefore the whipping instability, in an attempt to produce bead free fibres of smaller diameters [204].

Geng et al. successfully electrospun pure chitosan from concentrated acetic acid solution and found that as the acetic acid concentration increased from 10% to 90%, the surface tension decreased from 54.6 to 31.5 dyn/cm without significant viscosity change, rendering the solution electrospinnable. The net charge density of the solution also increased with increasing acetic acid concentration in water resulting in more charged ions available for charge repulsion [188]. Pure chitosan nanofibres can

also be produced from trifluoroacetic acid solutions (TFA). Hasegawa et al. studied the dissolution of chitosan in TFA and concluded that dissolution occurs due to the formation of amine salts at the amino groups of C_2 with TFA and also noted that no trifluoroacetylation occurs at the hydroxyl groups of chitosan [205]. The salts formed seem to help decrease intermolecular interaction between chitosan molecules and therefore facilitate the electrospinning process [169], [206]. TFA has also low boiling point and low surface tension which renders it a suitable solvent for electrospinning. It has also been shown that addition of a small proportion of DCM facilitates even further the electrospinning of chitosan as it further reduces the boiling point of the solvent system and also reduces the extremely strong charge density originated by the TFA [65]. Recently it has been used as a solvent for polyaniline as well, in a thin film production process using a drop casting technique [207]. For these reasons a TFA:DCM (80:20) solvent system was selected in the present study to produce polyaniline-chitosan composite blend solutions and electrospin them into nanofibrous structures.

Another way to successfully electrospin and generally widen the applications of chitosan, is by graft copolymerization of another polymer on chitosan's backbone [203]. There are two main reactive groups on its backbone that can be grafted, first, the free amine groups on deacetylated units and secondly, the hydroxyl groups on the C_3 and C_6 carbons on acetylated or deacetylated units (Figure 5.1). Apart from the benefit of increasing its solubility, the grafting of the chitosan molecule can result in enhanced antibacterial and antioxidant properties, increased biocompatibility, mucoadhesivity as well as in improvement of chelating, adsorption and complexation properties [208].

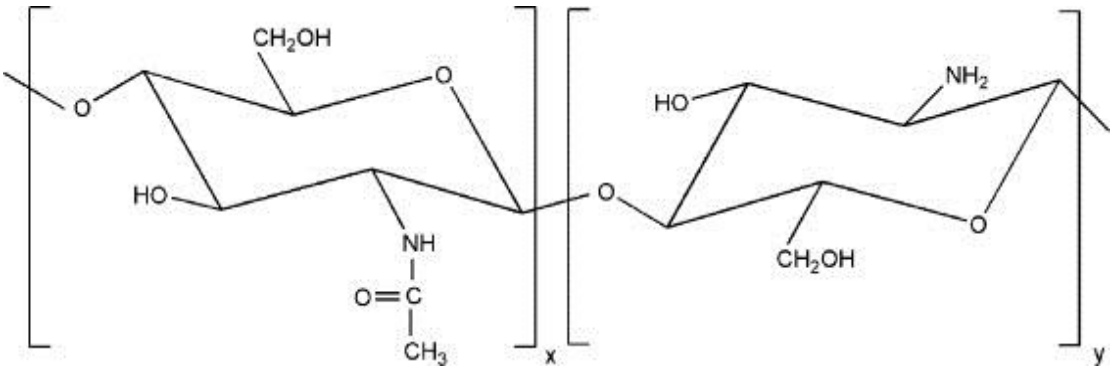


Figure 5.1: Molecular structure of chitosan

On the other hand, grafting a conductive polymer on the backbone of another, suitable one, is a way to increase processability. Chitosan is a polymer that can be used for this purpose as its properties render it stable during the aniline polymerization process and its amines are known to behave normally with respect to protonation in aqueous solution. The polymer is remarkably stable in acid at 25 °C or below, presumably because it does not have the cis -OH groups on the glucose unit that are responsible for acid hydrolysis of many polysaccharides [209]. The grafting of polyaniline on the chitosan molecule is a free-radical initiated polymerization and grafting occurs on the free amine groups of chitosan's deacetylated units [203], therefore the chitosan that is more suitable for grafting is one with high degree of deacetylation. Furthermore, it has been proved [210] that using the method of oxidative polymerization of aniline in the presence of chitosan, the aniline grafting on the chitosan backbone is favored against the homopolymerization of PANI, resulting in fully grafted chitosan molecules rather than a mixture of chitosan and polyaniline. In Figure 5.2, the grafting reaction of PANI on the chitosan back bone is depicted.

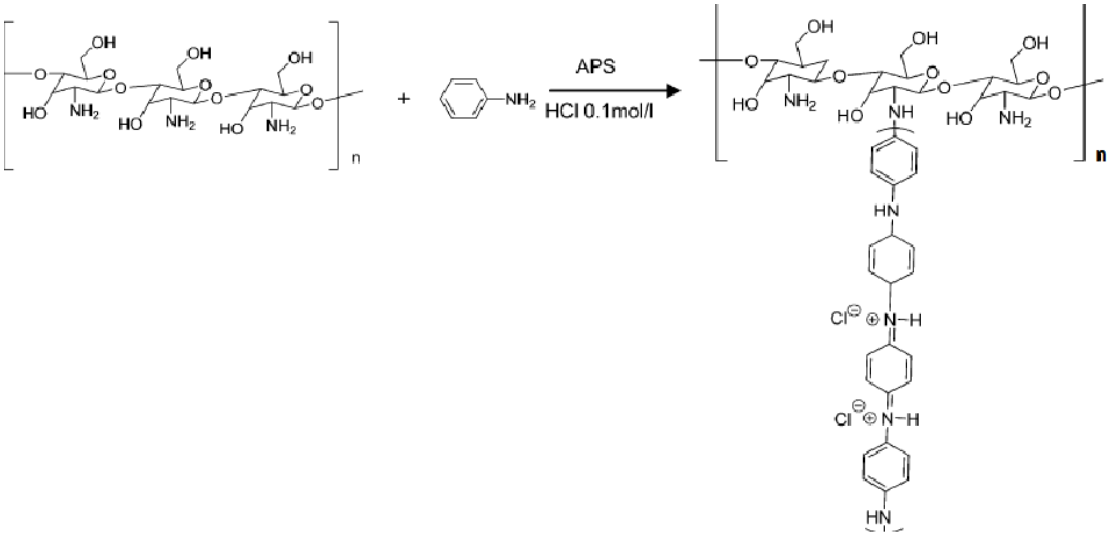


Figure 5.2: Graft polymerization of aniline on the amino group of the chitosan backbone [210]

Tiwari & Singh studied extensively the effect of the grafting extent of polyaniline on the chitosan backbone, in terms of electrical conductivity of the resulting chitosan grafted PANI (CHgPANI also referred to as chitaline) film and they concluded that conductivity increases with the increase of grafting percentage. They also tuned the polymerization parameters (eg. concentrations of oxidizing agent, aniline monomer, chitosan concentration, reaction time and temperature). The optimum grafting efficiency was observed at [$(NH_4)2S_2O_8$] 0.125M, [aniline] 0.015M, [hydrochloric acid] 0.5M, [chitosan] 1.0 g/l, temperature 25±0.2°C and reaction time 100 min. The grafted biomaterial exhibited electrical conductivity with pH responsive behavior like PANI, which was found to be dependent on the extent of grafting as well [211]. Marcasuzaa et al. [202] used the same method to graft polyaniline onto the chitosan backbone, but they report higher values of conductivity (10 to 100 times higher for the same grafting ratio) than the study by Tiwari & Singh. They attribute this to the different procedure they used with respect to measuring the conductivity which was on a casted film rather than pressed pellets from powder that Tiwari and colleagues performed. Casted films are known to offer more percolation efficiency as they allow for better chain orientation. Likewise, nanofibres are known to allow for even better orientation as compared to casted films, since the electrospinning process itself due to the coulombic forces it exerts on the polymer solution, forces the polymer to

orientate at a molecular level [177], [212]. They also confirmed the hypothesis of the resulting product's combined properties and showed that hydrogels fabricated from chitosan grafted PANI successfully combine the swelling properties of chitosan and the electroactivity of polyaniline.

The aim of the present study is to investigate the possibility of electrospinning mats containing both chitosan and polyaniline, and the fabrication of defect free homogenous nanofibrous mats exhibiting the advantageous properties from both materials (electrical conductivity and good biocompatibility) for their potential application in the biomedical field, as cell culture substrates, tissue engineering scaffolds and/or wound healing patches. The hypothesis currently tested by tissue engineering studies is that the incorporation of conducting PANI in polymeric scaffolds made by widely used, inherently insulating biomaterials will have an additional effect on the cell attachment. If this is true, a different approach towards encapsulation and release of bioactive molecules will become possible, such as the On/Off release described in detail in Section 2.2.3, as well as potential for using external electric field to electrically guide cell growth [164], [169], [213].

To this end, two approaches were followed: Firstly, the investigation of electrospinnability and the determination of the electrospinning window of chitosan grafted with PANI (CHgPANI) and secondly the one of PANI/CH blends. The effect of the PANI ratio either on the grafted chitosan or in the blends was investigated.

Based on some preliminary experiments and the literature, TFA was identified as the only suitable solvent for studying the electrospinnability of these blends, due to its effectiveness as PANI, chitosan and CHgPANI common solvent. Also its properties as found in the literature, are expected to be most appropriate for electrospinning. DCM was also used as a second solvent at a lower ratio (20%) as it's high volatility has been proved to favor the electrospinnability of chitosan when combined with TFA at a ratio of 80:20 [206].

5.2 Materials and Methods

Polyaniline emeraldine base (PANI, Mw=50000), ammonium persulfate (APS), aniline hydrochloride, and (1R)-10-camphor-sulfonic acid (CSA) were purchased from Sigma Aldrich Inc. Trifluoroacetic acid, 1-Methyl-2-pyrrolidinone (NMP), chitosan of Mw: 600 000 - 800 000 and 90% degree of deacetylation, were purchased from AcrÕs Organics. All materials were used without any further purification.

5.2.1 Synthesis of Chitosan Grafted Polyaniline (CHgPANI)

The procedure used was based on the work of Tiwari et al. with slight modifications [211]. Briefly, a known amount of chitosan (3g) was dissolved in 2L of 0.1M HCl aqueous solution. A calculated amount of aniline hydrochloride (AnHCl) $5* 10^{-3}$M was added to this, corresponding to 10%, 20% and 40% grafting of aniline to the chitosan backbone each time. APS was added dropwise to this solution to a final concentration $7*10^{-3}$M. The reaction was left to proceed for 12hrs at room temperature. The solution was then neutralized with NaOH 1M and filtered under vacuum. The precipitate was washed repeatedly with acetone and NMP, until a clear filtrate was seen, in order to remove aniline oligomers and free polyaniline residues. The precipitate was then dried in a vacuum oven at 60°C for 3 days. The resulting copolymers were named as CHgPANI-10, CHgPANI-20 and CHgPANI-40 corresponding to the amount of grafting attempted each time.

5.2.2 Preparation of electrospinning solutions & electrospinning process

The following solutions were prepared for electrospinning: A. 3% w/v chitosan in TFA:DCM (80:20), B. 5% w/v chitosan in TFA:DCM C. 5% PANI/CH blends (3 different ratios 1:3, 3:5, 1:1) in TFA:DCM (80:20) and D. 3% CHgPANI in TFA:DCM.

The conductivity of the solutions was measured with a 470 Jenway Conductivity Meter and the surface tension with a surface tension balance (White Electric Instrument Co). The same electrospinning procedure and morphology

characterization methods were used as described in Section 4.2. Finally, a Fluke 287 digital multimeter was interposed between the collector and the ground so as to allow the measurement of the current that is transferred by the jet on the collector for the final set of experimental runs. All the values reported are the mean values out of 25 measurements of the current.

5.2.3 Experimental Design

In order to determine the solution concentrations and the electrospinning conditions that would result in successfully electrospun PANI/Chitosan (PANI/CH) composite mats, a thorough study of the electrospinning window of pure chitosan was judged necessary, since there is no relevant detailed study in the literature. There are studies reporting the successful electrospinning of chitosan in TFA, but most of them focus on the molecular weight and degree of deacetylation of the chitosan and not on the solution concentration or the electrospinning parameters and how these affect electrospinnability [65], [206].

For this reason a two-level three factor full factorial design (2^3) was implemented for the investigation of the electrospinning of chitosan in TFA:DCM (80:20) solvent (Table 5.1).

Table 5.1: 2^3 full factorial experimental design for the electrospinnability of chitosan solutions

Concentration (% w/v)	Relative Humidity (%)	Voltage (kV)
3	50	28.5
3	50	23
3	20	28.5
3	20	23
5	50	28.5
5	50	23
5	20	28.5
5	20	23

After the effect of the chitosan concentration was evaluated, and one concentration was chosen, further experiments were carried out for the investigation of the combined effect of the PANI ratio, the applied voltage and the humidity on the electrospinnability of PANI/CH blends, by using a mixed level full factorial experimental design was used as shown in Table 5.2:

Table 5.2: Mixed level factorial experimental design for the electrospinnability of PANI/CH blends

Run	PANI:CH ratio	Humidity (%)	Voltage (kV)
1	0:1	50	23
2	0:1	50	26
3	0:1	50	28,5
4	0:1	35	23
5	0:1	35	26
6	0:1	35	28,5
7	0:1	20	23
8	0:1	20	26
9	0:1	20	28,5
10	1:3	50	23
11	1:3	50	26
12	1:3	50	28,5
13	1:3	35	23
14	1:3	35	26
15	1:3	35	28,5
16	1:3	20	23
17	1:3	20	26
18	1:3	20	28,5
19	3:5	50	23
20	3:5	50	26
21	3:5	50	28,5

22	3:5	35	23
23	3:5	35	26
24	3:5	35	28,5
25	3:5	20	23
26	3:5	20	26
27	3:5	20	28,5
28	1:1	50	23
29	1:1	50	26
30	1:1	50	28,5
31	1:1	35	23
32	1:1	35	26
33	1:1	35	28,5
34	1:1	20	23
35	1:1	20	26
36	1:1	20	28,5

For the electrospinning of CHgPANI the following experimental design was followed:

Table 5.3: Mixed level factorial experimental design for the electrospinnability of CHgPANI solutions

Grafting Percentage	Concentration (% w/v)	Voltage (kV)
CHgPANI10	3	28.5
CHgPANI10	3	23
CHgPANI20	3	28.5
CHgPANI20	3	23
CHgPANI40	3	28.5
CHgPANI40	3	23
CHgPANI10	5	28.5
CHgPANI10	5	23
CHgPANI20	5	28.5
CHgPANI20	5	23

CHgPANI40	5	28.5
CHgPANI40	5	23

For all three experimental designs, as can be seen in Tables 5.1, 5.2 & 5.3, the maximum and minimum values for each parameter were determined. The chitosan concentration values were chosen based on the literature [8], [169]. Higher concentration (7% w/v) has also been examined in preliminary experiments, but yielded highly viscous solutions that were not suitable for electrospinning. As for the voltage range, the upper limit of 28.5kV was defined by the technical limitations of the equipment. As low voltage setting, the lowest one allowing Taylor cone formation was used, which would indicate the potential formation of a jet. When it comes to the humidity, as maximum level, the ambient humidity value without dry air flowing inside the chamber was used, and as minimum level, again the lowest humidity value that could be attained by the dry air flow was used.

5.3 Results and Discussion

5.3.1 Fabrication of Chitosan Mats

Nanofibrous chitosan mats where prepared after electrospinning solutions of 3% w/v and 5% w/v of chitosan and according to the experimental design described above. The morphology of the mats was studied under the Scanning electron microscope and the results are grouped and summarized in the following figures.

5.3.1.1 Effect of Polymer Concentration

In Figures 5.3 A-1F, the nanofibre morphology obtained for the electrospun 5% w/v and 3% w/v solutions at different combinations of applied voltage and humidity are presented.

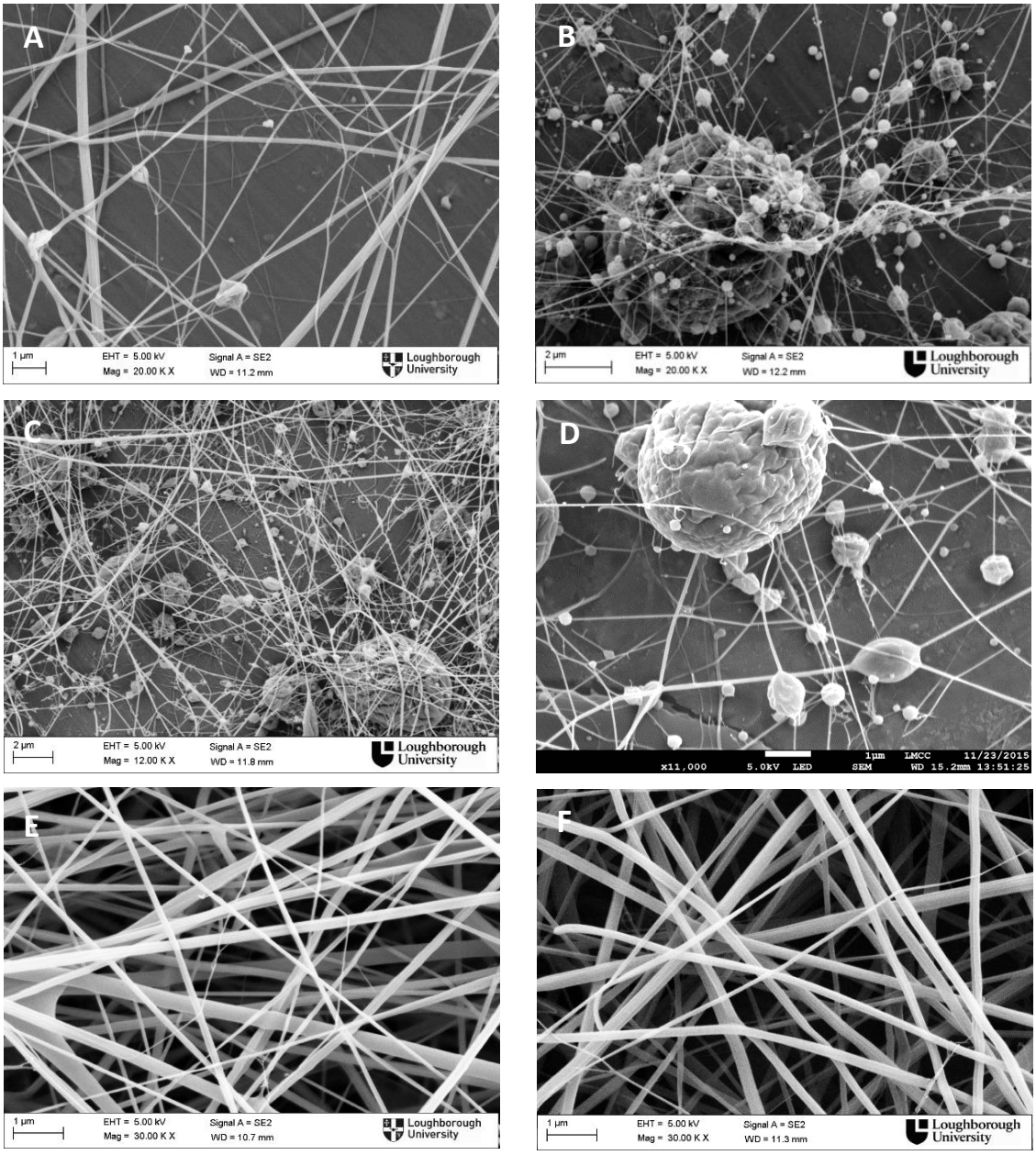


Figure 5.3: SEM pictures of chitosan solutions of A: 5% w/v and B: 3% electrospun at 28.5kV and 45%RH, C: 5% w/v and D: 3% w/v electrospun at 23kV and 45%RH, E: 5% w/v and F: 3% electrospun at 28.5kV and 20%RH

As shown in Figure 5.3, good nanofibre morphology is obtained at both concentrations when the applied voltage is high (28.5kV) and the relative humidity low (20%). However, the solution with higher concentration of chitosan (5% w/v) seems to be more easily electrospun as shown in Figure 5.3 A where good nanofibre morphology is obtained for the 5% w/v solution even at higher humidity versus Figure 5.3 B (3% w/v) where mostly beads are formed when the same electrospinning

parameters are used. This constitutes an indication that the 5% w/v solution is electrospinnable at a wider range of combined parameters. This is expected, as it was shown in Section 2.1.2.2 that higher polymer concentration, generally results in more polymer chain entanglements and therefore in solutions that are easier to electrospin.

5.3.1.2 Effect of humidity

In Figure 5.4, the nanofibre morphologies of 3% w/v chitosan solutions electrospun at different voltages and at values of high and low humidity are compared, in an attempt to examine if and how the relative humidity affects the final nanofibre morphology.

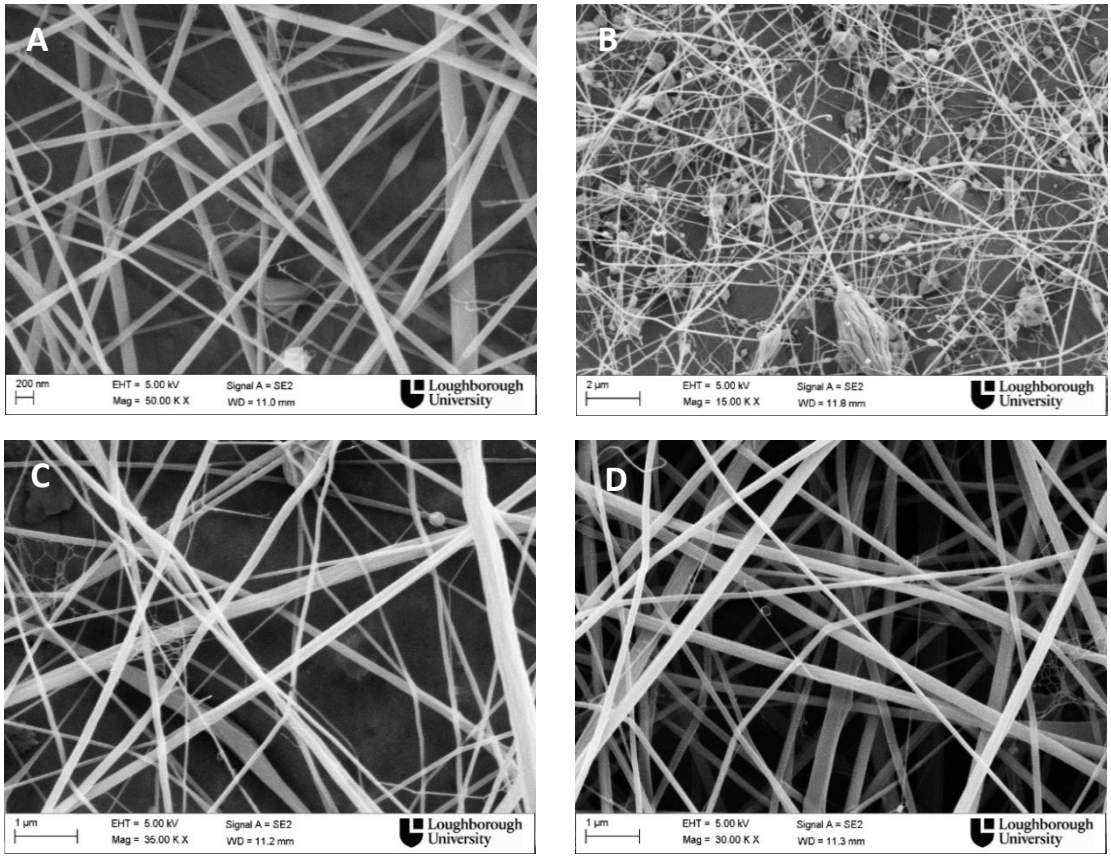


Figure 5.4: SEM pictures of chitosan solutions of 3% w/v electrospun at A: 23kV and 20%RH, B: 23kV and 45%RH, C: 28.5kV and 20%RH, D: 28.5kV and 45% RH

As can be seen in Figure 5.4, humidity appeared to have an impact on the electrospinnability of chitosan solutions only when low voltage was applied for both

solution concentrations (Figures 5.4 A & B). Humidity is expected to have an influence on the electrospinnability of chitosan, as it was explained in detail in the previous chapter, by removing charges from the jet, thus hindering the process. Also, higher humidity leads to slower solidification rate. As it has been pointed out by Pelipenko et al. [193], at higher humidity values, since the solidification rate is lower, the jet gets concentrated and stays this way for longer, allowing enough time for the elastic forces to overcome the plastic ones, thus leading into gradual appearance of beads. The slower solidification rate was as well responsible for the larger fibre diameters observed at low humidity, as is shown in Table 5.4. The way that increased humidity affects the nanofibre morphology is also due to the fact that TFA is miscible with water and that chitosan is hydrophilic. Otherwise, phase separation, resulting in rough nanofibre surface or pore formation would be more likely to be observed at high humidity.

Table 5.4: Average nanofibre diameter for high (50%) and low (20%) values of RH

Polymer Concentration (w/v)	Applied Voltage (kV)	Relative Humidity	Average Diameter (nm)
3%	26	50%	85
3%	26	20%	96
3%	28.5	50%	96
3%	28.5	20%	149
5%	26	50%	64
5%	26	20%	148
5%	28.5	50%	85
5%	28.5	20%	180

In Table 5.4, the way the humidity influences fibre diameter is evident. For both solution concentrations when the humidity is increased whilst all the other electrospinning parameters, including the applied voltage are maintained the same, the average diameter drops, in accordance with observations of others in the literature [101], [193]. This phenomenon seems to be more pronounced in the case of the solution with the higher polymer concentration, for both applied voltages. As the

solution is more concentrated, the solution viscosity increases and thus, the jet diameter is expected to be larger. At low humidity, the fast solidification causes the jet to solidify before having undergone adequate whipping, and therefore resulting in large diameter fibres. At high humidity, and since the distance used for these experiments is long (16cm is empirically considered long for electrospinning), the jet undergoes extensive whipping, having adequate time to solidify before reaching the collector and although the final diameters at high humidity are smaller as well for the lower concentration solutions of 3% w/v, the differences now seem to be less obvious when compared to those at low humidity.

5.3.1.3. Effect of applied voltage

In the following SEM pictures, the morphology of electrospun 3% w/v and 5% w/v chitosan solutions, at different voltages is depicted.

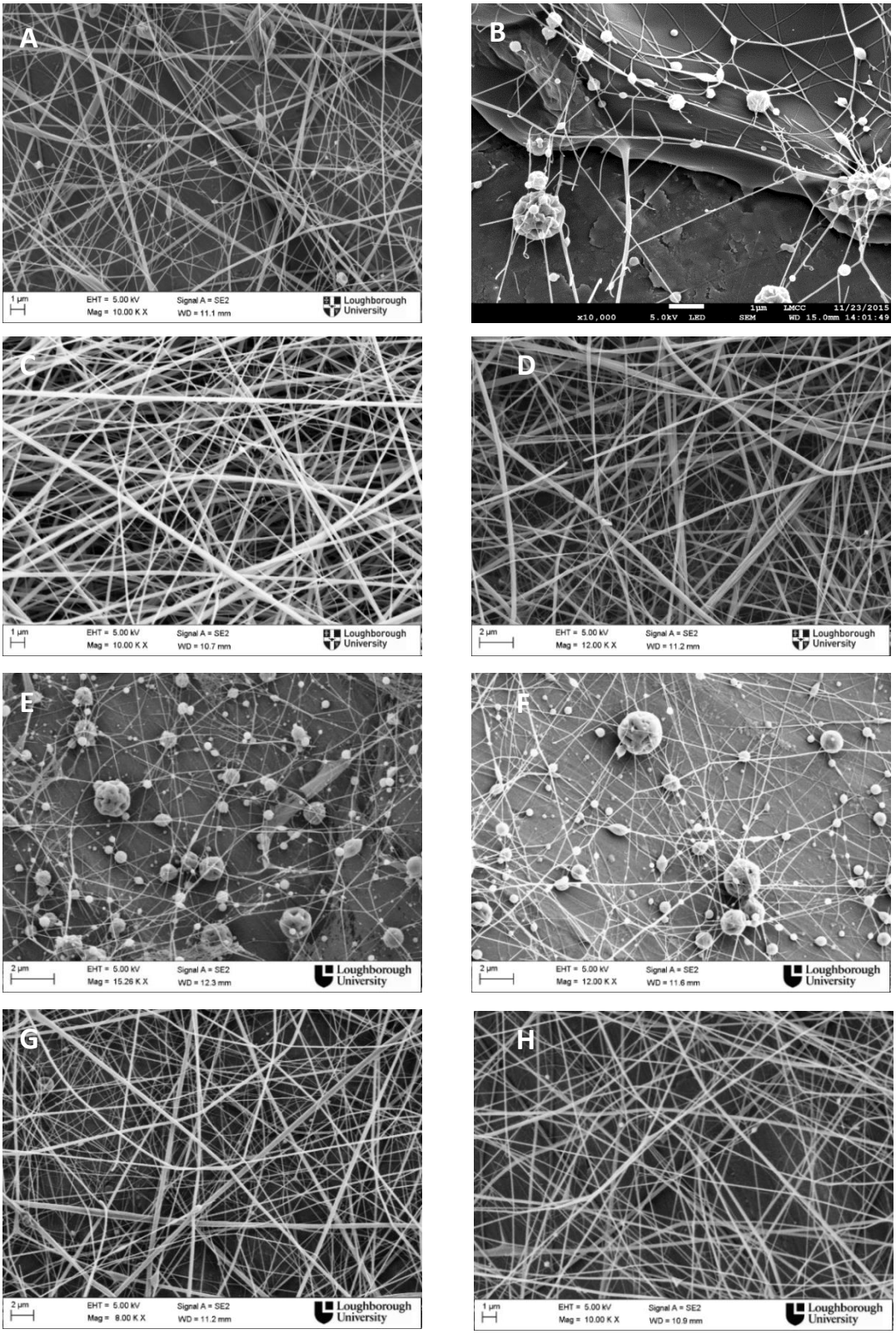


Figure 5.5: SEM pictures of chitosan solutions of 5% w/v electrospun at A: 28.5kV and 45%RH, B: 22.5kV and 45%RH, C: 28.5kV and 20%RH, D: 22.5kV and 20% RH and 3% w/v solution electrospun at E: 28.5kV and 45%RH, F: 22.5kV and 45%RH, G: 28.5kV and 20%RH, H: 22.5kV and 20% RH

When grouping the SEM pictures in an attempt to examine the effect of the applied voltage, it becomes obvious that the voltage affects the electrospinnability of chitosan solutions, but it seems to be a secondary parameter when the solution concentration is low (3%). For example, the morphology in Figure 5.5 E does not differ from 5.5 F where mostly beads are observed and Figure 5.5 G does not differ from Figure 5.5 H, both showing good nanofibre morphology. In the case of low concentration, the increase of the applied voltage doesn't seem to influence the electrospinnability of the solution. On the contrary, for higher polymer concentration, the voltage seems to be a determining factor in order to improve nanofibre morphology from beaded fibres (Figure 5.5 B) to homogenous defect free fibres (Figure 5.5 A) at high RH. When low RH is used, both applied voltages yield good nanofibrous structure, but some broken fibres appear at high voltage (Figure 5.5 D). This may be due to the fact that at increased voltage, the polymer jet undergoes extensive whipping and due to the low humidity, it may solidify before reaching the collector, thus the further whipping caused by the high electric field, may cause breakage of the solidified jet.

Comparing the electrospinning windows for the two different concentrations, as a general conclusion it can be said that both solutions (of different concentrations), are electrospinnable under the conditions examined with the experimental design and result in similar fibre morphology when same conditions are applied. One only exception is observed at high voltage and high RH, where electrospinning of the more concentrated solution (5%) results in well formed nanofibres with minor defects (Figures 5.5 A, B, C & D), while the 3% solution results in a string on bead morphology, where mostly beads of various sizes are formed during the process (Figures 5.5 E, F, G & H), because of the better chain entanglement that higher concentration allows for. Therefore, in order to safely decide on the most suitable solution concentration that will be used in further experiments, the average diameter was calculated after counting the diameters of 200 nanofibres for each sample, as well as their distributions and compared in Table 5.5.

Table 5.5: *Comparison of average diameters and diameter distributions expressed as coefficient of variation, for each of the electrospun solutions 3% and 5% w/v, applied voltages 22.5kV and 28.5kV and at fixed RH 20%.*

	Average Diameter (nm)	Coefficient of Variation
3%, 22.5kV, 20%RH	94	0.61
3%, 28.5kV, 20%RH	96	0.58
5%, 22.5kV, 20%RH	104	0.53
5%, 28.5kV, 20%RH	145	0.54

As is shown in Table 5.5, the electrospinning of 5% solution results in thicker nanofibres for the same conditions, when compared to the 3% solution. This is expected, since it has been shown in many research studies that the polymer concentration directly affects the size of the produced nanofibres [21], with denser solutions resulting in thicker fibres. It is worth noting here that all the counted diameters fall in the nanoscale. For the intended applications nanofibres up to 800nm have shown to be advantageous, as the fibres found within the native extracellular matrix are of the range of 270 to 710 nm [21]. As for the coefficient of variation, the nanofibrous mats produced by use of 5% solution seem to be slightly more uniform in terms of nanofibre diameters than when a 3% w/v solution is used. For those reasons, the 5% w/v chitosan concentration will be used for further experiments, where PANI is incorporated in the blend.

5.3.2 Fabrication of Chitosan grafted PANI (CHgPANI) mats

After electrospinning various CHgPANI mats, with different amounts of grafted PANI, different concentrations and various values of applied voltage, the following morphologies were obtained as shown in Figure 5.6:

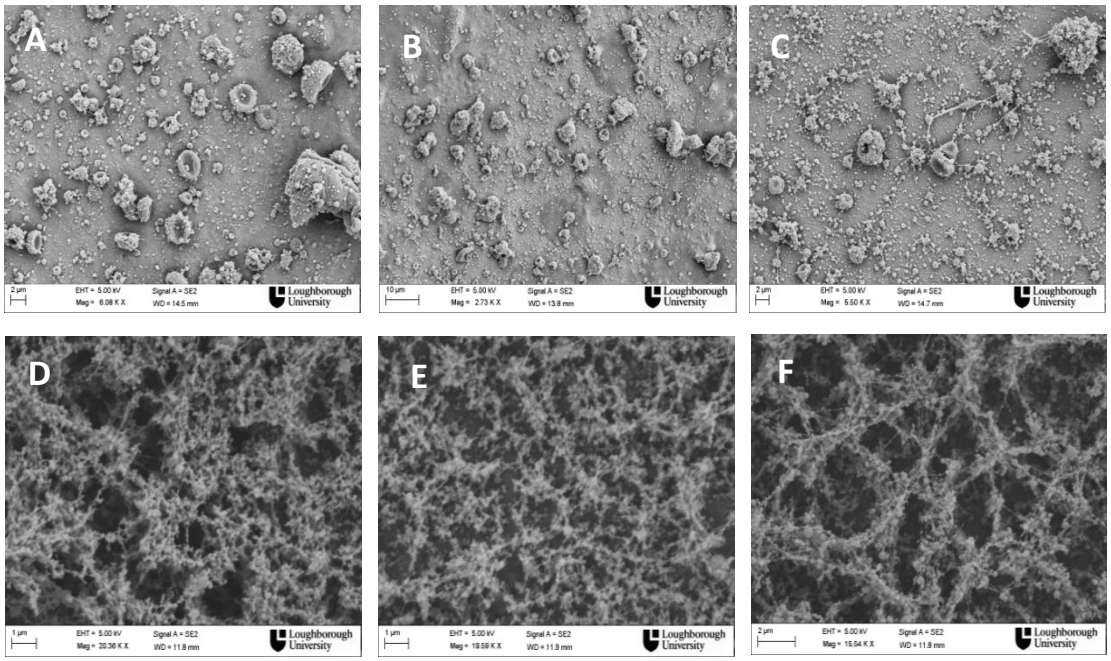


Figure 5.6: Electrospun CHgPANI solutions A: 3% w/v CHgPANI-40 electrospun at 26kV, B: 3% w/v CHgPANI-20 electrospun at 22kV, C: 3% w/v CHgPANI-10 electrospun at 22kV, D: 5% w/v CHgPANI-40 electrospun at 26kV, E: 5% w/v CHgPANI-20 electrospun at 22kV, F: 5% w/v CHgPANI-10 electrospun at 22kV

The electrospinning of CHgPANI solutions was unsuccessful, at a broad range of parameters. Some of the more characteristic morphologies obtained are depicted in Figure 5.6. These nanostructures are far from the typical nanofibrous structures with defects (e.g. string on bead, bead on string, fused fibres morphologies) which would indicate that a slight modification of one or more parameters would result in defect free nanofibrous structure. In this case, the electrospinning window for these solutions seems to be unattainable within the range of possible parameter tuning, as framed by the technical limitations of the experimental setup. This can be explained by taking into account the geometry of the grafted chitosan molecule as shown in Figure 5.2.

The PANI chain grafted on the nitrogen atom of the chitosan backbone, is the cause of more chain entanglement, and also may render the molecule rigid, thus preventing spontaneous orientation when a high voltage is applied, resulting in the above morphology. Lower polymer concentration or higher voltage could be beneficial for the free orientation of the chitosan molecules, but as shown in Figures 5.6 A, B & C

this was not the case. Higher voltages could not be applied, because of limitation of the electrospinning device. The formation of continuous jet is unachievable at lower concentration, resulting in electrospraying. Those results are worth to be compared with Ma et al. [169], who managed to successfully electrospin solutions of aniline tetramer grafted chitosan in the same solvent system. It seems like the aniline tetramer molecule is small enough that when grafted on the chitosan backbone does not cause this hindrance during electrospinning, and only in high proportions of grafted aniline tetramer did they notice the same problems. Therefore, because of the reasons listed above, the electrospinning of CHgPANI solutions was not brought forward in the current study.

5.3.3 Fabrication of PANI/CH blend mats

In Figures 6 A, B & C the contour and surface plots of the electrospinnability of PANI/CH blends of different ratios is plotted in relation to the applied voltage.

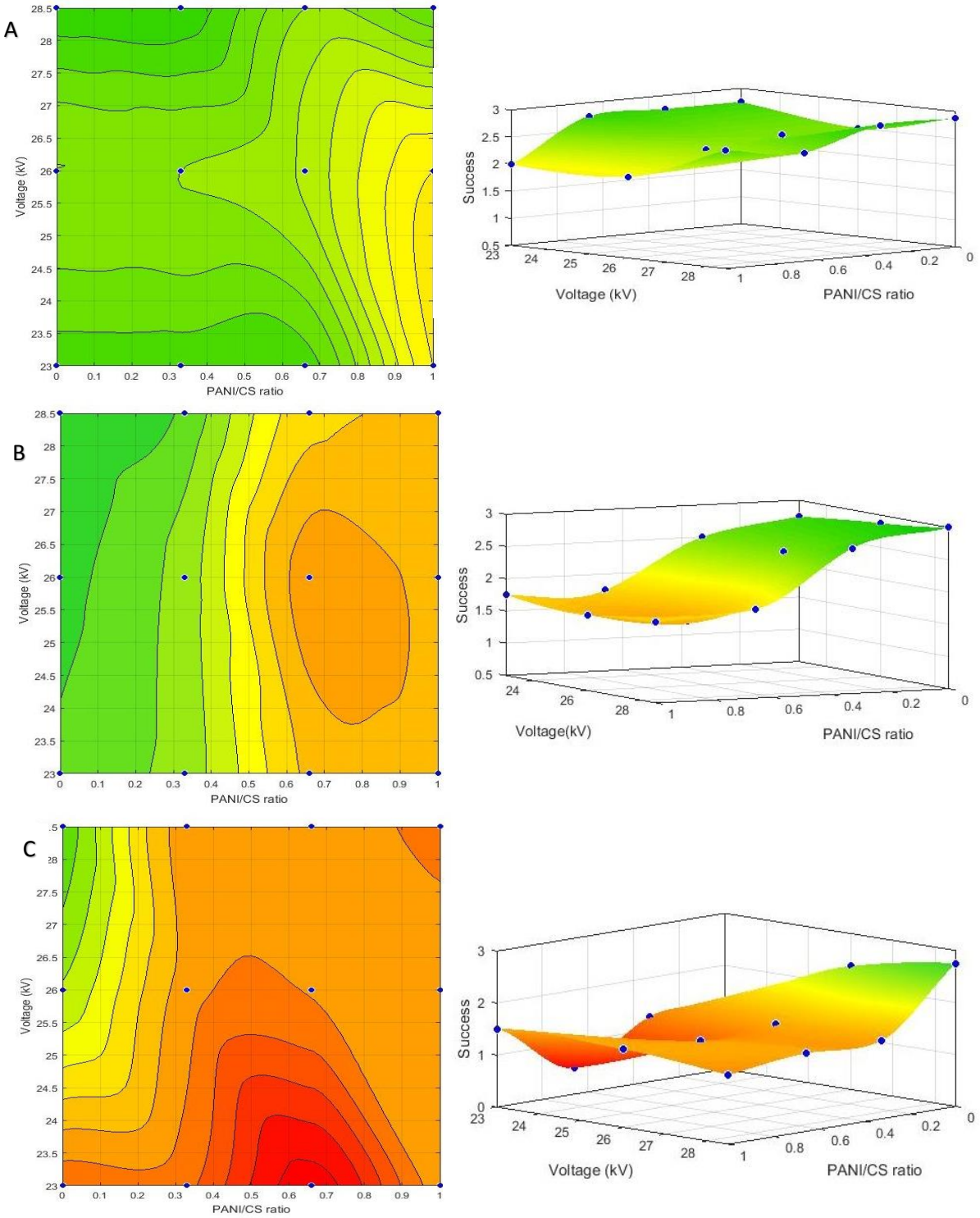


Figure 5.7: A, B & C: Electrospinnability window of blends with different PANI ratios, at various voltages and at fixed RH: A: 20%, B: 35%, C: 50%

0 (red color): electrospinning was not possible/no fibres collected,

1 (yellow color): electrospinning was possible – fibre-like morphology but with defects (beaded fibres, broken fibres, wet mat)

2 (green color): defect free nanofibre morphology

As shown in Figure 5.7, electrospinning becomes increasingly hindered as the RH increases. At 20%RH (Figure 5.7 A), defect free nanofibres are produced for all the blends. Some beads appear only at high PANI ratio and low applied voltage. As the RH increases, it is observed that the electrospinning becomes less and less successful with the higher PANI ratio blends being more influenced by the RH increase. At high RH (50%) (Figure 5.7 C), the only defect free nanofibres are obtained by electrospinning chitosan solutions without any PANI, highlighting the importance of the environmental humidity when electrospinning solutions incorporating a conducting polymer.

Comparing Figures 5.8 A, B and C contour and surface plots, it is obvious that the applied voltage affects the electrospinnability of PANI/CH blends. In general, as the applied voltage is increased, the electrospinning process is facilitated, especially for the PANI/CH blends with high PANI ratio, where defect free electrospun fibres are only obtained at high voltage and only for low values of relative humidity.

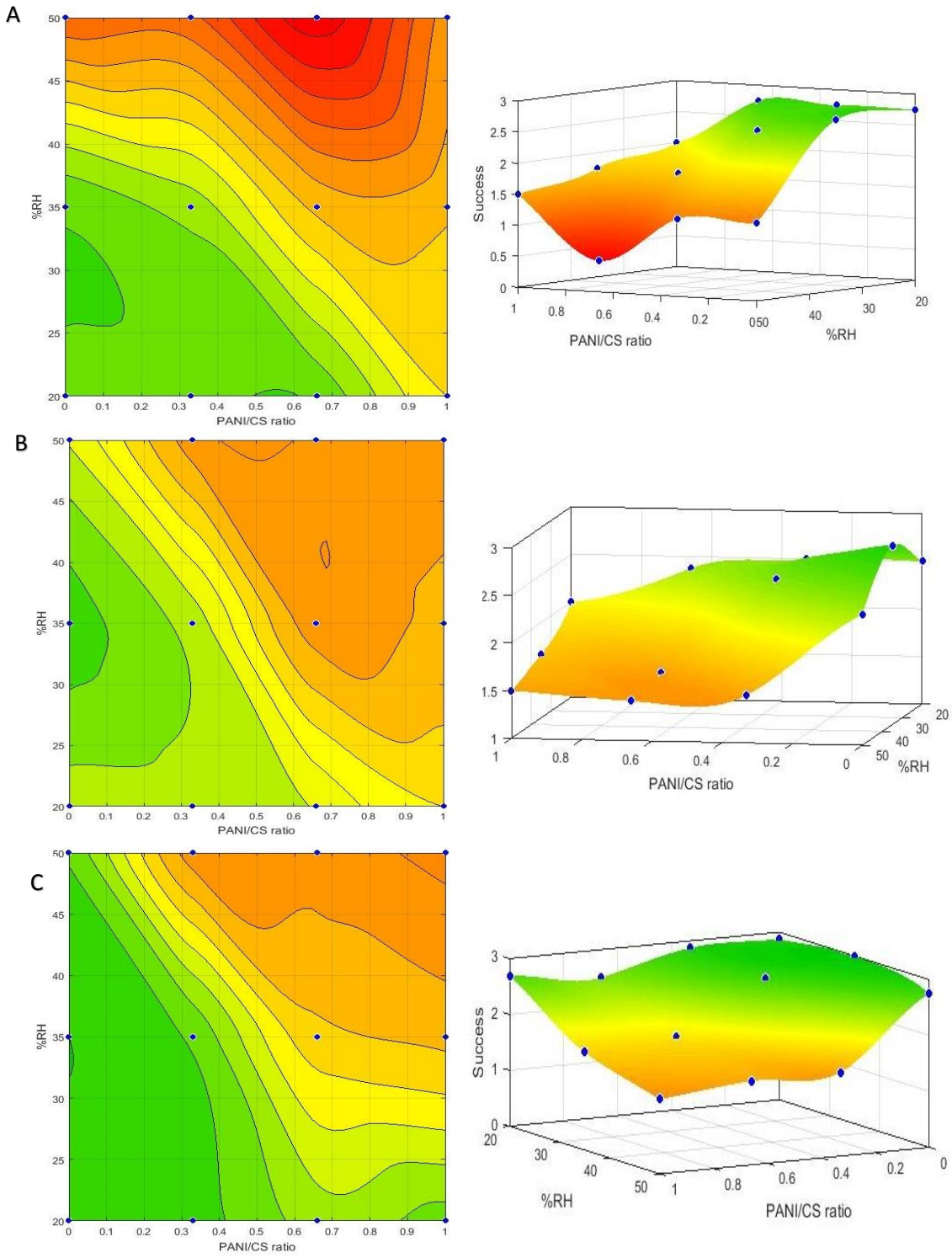


Figure 5.8 A, B & C: Electrospinnability window of blends with different PANI ratios, at various RH and at fixed applied voltage: A: 22.5kV, B: 25.5kV, C: 28.5kV

In Figure 5.9, the diameter distributions of the nanofibres produced from electrospinning PANI/CH blends at 20% RH are presented.

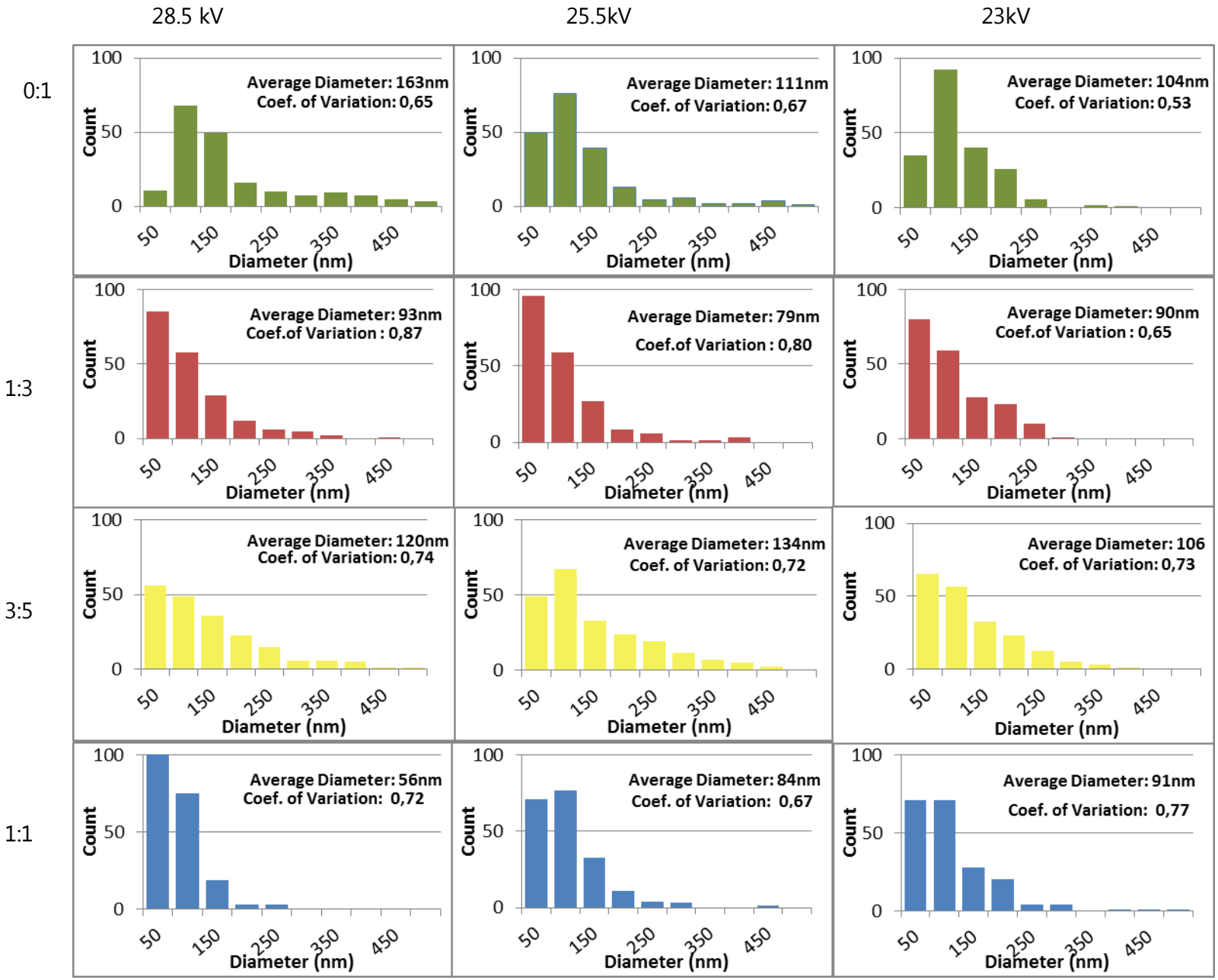


Figure 5.9: Diameter Distribution of PANI-CH blends electrospun at various voltages and at fixed RH 20%

Figure 5.9 provides some interesting observations regarding the diameter distribution of PANI/CH blends when electrospun at 20%RH. Horizontally, the diameter distributions for each one of the different blend ratios (PANI:CH 0:1, 1:3, 3:5 and 1:1) are depicted, when electrospun at different voltages. Vertically the effect of the different PANI ratio, is shown when the same voltage is applied (either 28.5kV, 25.5kV, or 23kV) Firstly, it is obvious that the incorporation of PANI in the blend results in thinner diameters, as the count of nanofibres up to 100nm increases, and the count of the larger ones decreases evidently, when comparing the 0:1 blends (no PANI), to the rest of the blends, for all the applied voltages. This is depicted on the average diameter as well, which is lower for the solutions that are incorporating PANI when compared to the pure chitosan one (0:1). Another observation is that higher voltage results in thinner nanofibres for the blend containing the bigger ratio of PANI, whilst for the other blends, the average nanofibre diameter only fluctuates a little for each voltage but does not change significantly. In the case of the pure chitosan solution, the exact opposite trend is observed, meaning that the average diameter is evidently larger for higher voltage and decreases with decreasing voltage. This observation agrees with the observations by Zhang et al, and Meechaisue et al., who both attributed this phenomenon to the solution being removed from the capillary tip faster at higher voltages, increasing the polymer's flow rate [81], [214]. However, the discrepancy between the electrospun solutions regarding how the applied voltage affects the average nanofibre diameter, points to a conclusion that there are opposing phenomena taking place. Apart from the increase of flow rate leading to larger diameters, there is also higher electrostatic repulsion within the polymer jet leading to reduction of the average diameter. When a conducting polymer is introduced in the solution, it seems to have a significant effect on this electrostatic repulsion, counteracting the increase on the flow rate. Furthermore, as the PANI ratio increases in the blend, the total polymer concentration increases as well, which would normally lead to larger diameters, but this as well seems to be counteracted by the strong electrostatic repulsions, highlighting the influence of the introduction of PANI in the blend.

Finally, the distribution range, is obviously larger when electrospinning at 28.5kV rather than at 25.5kV or 22.5kV. The polarity of the chitosan itself must be taken into account here. Chitosan is a positively charged molecule and it has been reported that when electrospun under positive high voltage (like in the present study) multiple jets are formed, instead of one, indicating process instability [215]. The addition of PANI, seems to be counteracting this phenomenon. This happens probably not because of the PANI itself, but the dopant acid used, in this case CSA. The higher content of CSA in the solution seems to have an effect on the positively charged chitosan molecule. It has been shown that sulfonic acids act as hydrogen donors to the nitrogen atom in between the phenyl rings of the PANI molecule, forming hydrogen bonds [216]. Moreover, the possibility of a single CSA molecule bonding two PANI chains by double hydrogen bonds has been shown to be high [217], leaving thus the sulfonate group negatively charged and possibly counterbalancing the charge of the chitosan molecule which is known to be positively charged under acidic conditions, preventing in that manner excessive charge repulsions and thus stabilizing the jet and resulting in more homogeneous distribution of nanofibre diameters. Indeed it has been reported that in polyelectrolyte solutions the ratio of the -COOH group of the polyanion to the $–NH_3$ group of the polycation affects the electrospinnability, leading to decreased electrospinnability when it is above 1 [218]. In this case, instead of –COOH group there is the $-S(=O)_2-OH$ group (sulfonyl hydroxide) group of the CSA but the same principle can be applied in order to explain the electrospinning instability occurring at higher chitosan ratios.

5.3.4 Discussion of the current measurements and investigation of the effect of the tip to collector distance (TCD)

In order to investigate further how the humidity affects the electrospinning of chitosan and PANI/CH blend solutions, the current transferred by the fibres on the collector was measured. In an attempt to investigate further on how the applied voltage and TCD affects the process, the current was measured by keeping the ratio V/dist. stable but changing the values of the voltage and the distance. In many

studies the applied voltage is expressed as V/cm. In the present study and up until this point, the distance was kept constant, and only the applied voltage was altered, in order to investigate the voltage effect. However, since the electrospinning of conducting polymers has not been studied in depth in the literature, the effect that longer distance in combination with different values of humidity would have in the process, was judged necessary for deeper understanding of the electrospinning of conducting polymers.

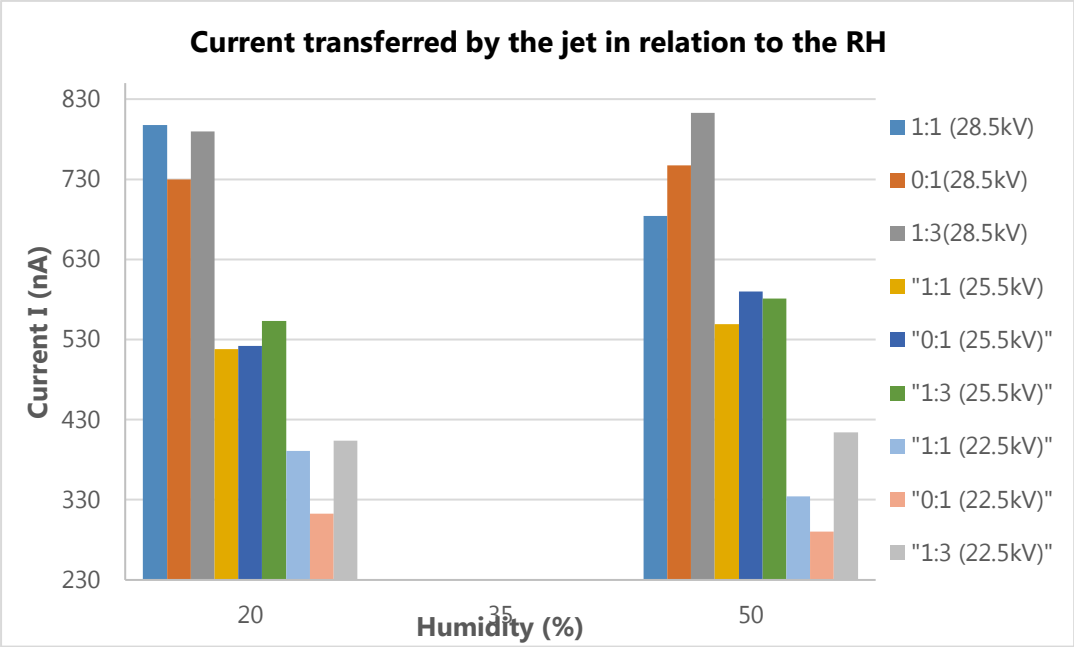


Figure 5.10: The current transferred by the fibres on the collector in relation to high (50%) and low (20%) environmental humidity values for different blends with different concentration of PANI electrospun at different voltages.

As shown in Figure 5.10, the current decreases with decreasing applied voltage, for all blends and independently from the relative humidity, which is of course expected. In fact, the measured current values for each voltage are distinct from the values at other voltages (no overlapping) independently from the RH. This constitutes a verification, that indeed, the voltage is the main parameter affecting the amount of charge that the jet carries. Humidity seems to also have an effect on the current. At lower values of applied voltage (22.5kV), it remains at the same level for the 0:1 and 1:3 blends but it significantly drops (p value = 0.43) as the PANI ratio in the blend increases to 1:1. The same phenomenon is observed at high voltage (28.5kV). This observation confirms the initial hypothesis and proposal of the mechanism that has

been explained in Chapter 3, that increased humidity leads to removal of charges from the jet when the electrospinning solution contains a conducting polymer. However, at medium value of applied voltage (25.5kV) this phenomenon is not observed, where a slight increase in the current seems to take place for all three blends. It has to be noted here though, that since the current measurements are characterized by fluctuation, this increase is small and can be due to fluctuation of the equipment, not being indicative of a trend. For the blends that have low (1:3) or none at all (0:1) concentration of conducting polymer, the humidity seems to have no effect on the current transferred by the fibres. This is in agreement with Figure 5.4 D where good nanofibrous structures are obtained even at high humidity for the blend without polyaniline. In the case of chitosan electrospinning, water is a solvent for chitosan, in fact chitosan behaves as a polyelectrolyte in aqueous acidic solutions as it has been noted earlier, so presence of water vapors, shouldn't cause disruption of the process. In fact, it might even act as another factor contributing to higher repulsion of the surface charges.

In Table 5.6, the average electric field is given (as it has been calculated from the applied voltage and the TCD) for the 0:1 and 1:1 blends with relation to the measured current at the collector.

Table 5.6: Measured current on the collector brought by the fibres, with respect to solution composition and applied voltage

Solution Composition	Applied electric Field (kv)	Distance (cm)	Average Electric Field (kV/cm)	Relative Humidity %	Measured Current (nA)
CS 5%	28.5	16	1.78	20	466
CS 5%	23	13	1.77	20	313
PANI/CH 1:1	28.5	16	1.78	20	449
PANI/CH 1:1	23	13	1.77	20	329

In Table 5.6 it is shown that for the same average electric field, different values of measured current are obtained both for high PANI concentration and low PANI concentration blends, when the distance is shifted from 16cm to 13cm and the voltage from 28.5kV to 23kV respectively. This discrepancy is also verified by the respective obtained morphologies which are shown in Figure 5.11.

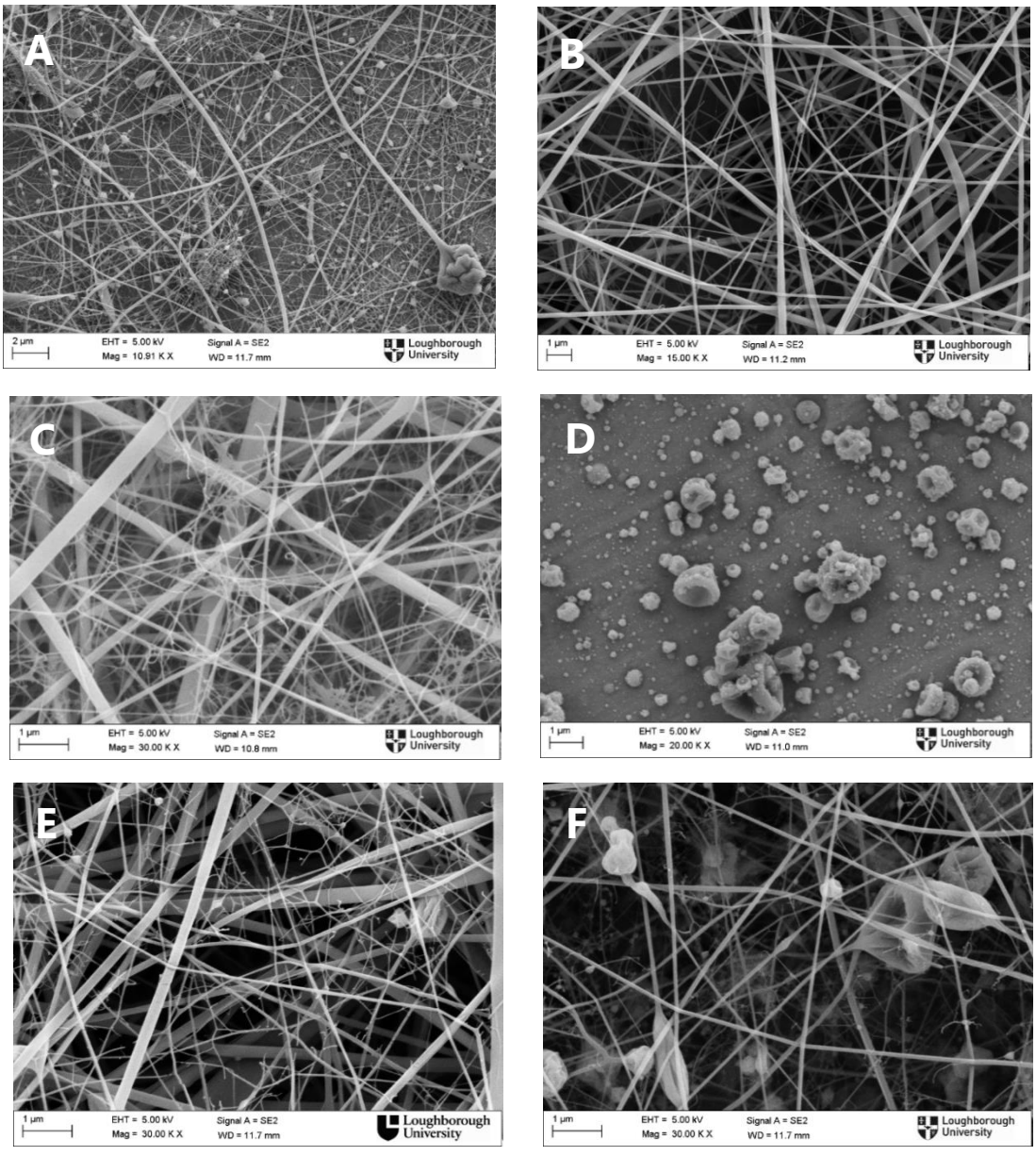


Figure 5.11: SEM pictures of solutions A: 0:1 electrospun at 28.5kV, 16cm, B: 0:1 at 22.5kV, 13cm, C: 1:1 at 28.5kV, 16cm, D: 1:1 at 22kV, 13cm, E: 1:1 at 29kV, 15cm, F: 1:1 at 29kV, 10cm

When electrospinning pure chitosan and changing the TCD (Figures 5.11 A & B), what can be observed is that although the Voltage/cm value is maintained stable, the morphology of the obtained fibres is noticeably better at lower voltage and shorter distance. All small and larger beads disappear and the mat is a lot more uniform overall. This could be an indication that the effect of the applied voltage may not be uniform and proportional throughout the electrospinning distance. The produced fibres have a morphology that they would if the applied voltage was higher, meaning that shorter distances may in general be preferable for electrospinning. However, this does not seem to apply to the more conductive PANI:CH solutions, where smaller distances seem to have an adverse effect, resulting in fibres with more beads. Remarkable is the case of the 1:1 solution (Figures 5.11 C & D) where at small distance and high voltage there is only electrospraying, while when increasing the distance, defect free fibres are produced. However, it has to be noted here that according to Reneker et al., the actual electric field close to the tip of the nozzle may be significantly higher than the average electric field, due to the geometry of the electric field lines. Therefore the discrepancy observed between the two cases of solution compositions, although the average electric field is the same, may be attributed to this [196]. This is a new insight regarding the electrospinning process, where generally it is believed that high Voltage/distance ratio results in less beads and defects.

These results agree with the observations of Deitzel et al. [89]. It is possible that when this ratio exceeds a certain threshold, which in the case of Deitzel's study coincided with a change of the slope of the current/voltage ratio. The high voltage prevents the formation of a smooth Taylor cone and jet, causing more polymer to be removed by the needle tip, which is travelling too fast towards the collector resulting in increased bead formation or even electrospraying. Thus, by monitoring the current, it may be possible to predict the morphology of the electrospun fibres. Further study on this phenomenon should be conducted in order to investigate why the opposite is observed in the more conducting solution, and better morphology is obtained when the recorded current is lower (but still corresponding to lower voltage and shorter distance).

5.4 Conclusions

An extensive study has been conducted on the electrospinning of chitosan and of PANI/CH solutions. Chitosan can be electrospun successfully when diluted at TFA:DCM (80:20) solvent system, at a concentration of 5% w/v and at several combinations of electrospinning parameters (applied voltage, TCD, environmental humidity etc). Solutions from chitosan grafted PANI, have been found to be not electrospinnable at a wide combination of electrospinning parameters that were attempted. This was attributed to the high rigidity of the polymer's chain, because of the repulsion built between the PANI molecules grafted on the chitosan backbone. On the other hand, solutions made from blending chitosan and PANI and different ratios were successfully electrospun, as in this case the PANI and chitosan molecules can freely move and orientate when high voltage is applied, thus formation of a continuous jet is rendered possible. The TFA:DCM (80:20) solvent system was found to be suitable for the electrospinning not only of chitosan solutions, which was expected, but for PANI solutions too, as it was found to dissolve CSA doped PANI very well. This can be attributed to a more expanded conformation that PANI molecules exhibit when dissolved in TFA, in opposition to most commonly used solvents such as chloroform where a more compact-coil conformation is observed [207]. In practice, this eliminates the need for removal of undispersed particles by filtration, even at high PANI concentrations, as it is the case for chloroform, which is currently the most common solvent for electrospinning of PANI based solutions.

It was found that applied voltage is the dominant factor affecting the electrospinning of such solutions and as the ratio of PANI in the blend increases, humidity becomes an important parameter affecting electrospinnability. This was further confirmed with the measurement of the current transferred by the jet, since at high RH values and high PANI content, suggesting removal of electrical charge from the jet, the current drops when all other parameters are maintained stable. As for the effect of the incorporation of PANI in the blend, on the diameter of the produced nanofibres, it was observed that the incorporation of PANI in the blend results in thinner diameters. Higher applied voltage, also generally results in higher counts of thinner nanofibres for the blends containing higher amount of PANI.

6 | EVALUATION OF THE BIOLOGICAL PROPERTIES OF ELECTROSPUN MATS

6.1 Introduction

Electrical stimuli have been shown to have a positive impact on *in vitro* cell cultures of electroactive tissues, promoting cell adhesion, alignment, regulating and modulating cell differentiation, migration, protein secretion and DNA synthesis [115], [122]. The response of fibroblasts and osteoblasts to electric stimulation with a view to enhancing wound and bone fracture healing has only recently been assessed *in vitro* [156], [219], *in vivo* [220], [221], and in some clinical studies [150], [151], indicating the potential advantages of electrical stimulation of these specific tissues even though they are not generally classified as electroactive (when compared to muscle and nerve for example). These *in vitro* and *in vivo* studies refer to electrical stimulation of the tissue usually through the use of a hydrogel or an electroactive flat membrane produced by film casting, whereas in clinical studies, the electrical stimulation is achieved with direct attachment of electrodes on the wounded area or with the use of aluminum foil. The latter procedure though may increase the risk for contamination of the wound, being disruptive to the healing process [222]. A porous, conducting wound dressing would be ideal to apply electric current at required intervals, without the need to expose the wound. A wound dressing that could hold pre-seeded cells for the introduction of cytokines, collagen and growth factors to the wound bed [223], or the encapsulation and controlled release of bioactive molecules from the wound dressing would further assist and accelerate the healing process. A nanofibrous structure would add value to such wound patch, by increasing the surface to volume ratio, and thus the quantity of the loaded molecules. Furthermore, the need for nanofibrous structures has been highlighted by several researchers who showed how the nanofibrous topography apart from the obvious advantage of the large surface to volume ratio, also seems to provide significant advantages for cell culture applications as they have been found to induce enhanced cell activity when

compared to flat surfaces composed of the same materials as explained in Section 2.2.2. From all the above, it becomes obvious that a nanofibrous structure made of electroactive polymer would be very beneficial for the enhancement of new skin tissue formation.

Polyaniline (PANI) is a polymer whose conjugative structure allows the mobility of electrons on its chain, rendering it electrically conducting as it has been explained in Section 2.2. Preliminary studies on polyaniline are showing that it could be a potential medium for the transfer of electrical stimuli to tissues, enhancing the control over differentiation and orientation of specific types of cells such as skeletal muscle, nerve and cardiac tissue [122], [152]. However, preliminary *in vitro* and *in vivo* biocompatibility studies of polyaniline have shown some contradictory results. For example, Zhao et al [213], found that the electroactive quaternized chitosan hydrogels containing polyaniline could significantly enhance the proliferation of C2C12 myoblasts compared to the pure quaternized chitosan hydrogel. Similarly, incorporation of PANI in polyethylene glycol based hydrogels has been shown to promote the cell response of PC12 (pheochromocytoma of the rat adrenal medulla cells) and hMSC's (human mesenchymal stem cells) as a result of the increase in conductivity and water retention that PANI caused [159]. More *in vitro* evaluation of nanostructures containing PANI have been discussed in Section 2.3.4. It should be noted that for wound healing purposes, the use of nanofibres as opposed to hydrogels can be proved advantageous, as although the first are known to ensure wound hydration [224] they are outperformed by 2-D nanofibrous meshes as for hemostasis, cell respiration, and gas permeation when implanted onto open wounds [225]. Additionally, water accumulation due to the hydrogel can cause maceration and bacterial proliferation [226].

Wu et al. studied the proliferation and morphology of L929 fibroblast cells on electrospun PCL and PCL-PANI fibres with different ratios of contained PANI at 1, 5, 10 and 20% w/w and they concluded that no difference was observed with respect to growth rate and morphology when compared to TCP, suggesting that PANI does not have any cytotoxic effect on the cells. The PCL-PANI 20% gave slightly higher number of cells at the end of the culture time (4th day) [161]. In most of these studies though,

the amount of reproducibly incorporated PANI in the structure, doesn't exceed 5% w/w, which is a limitation caused by PANI's lack of processability. This is important, as it is expected that incorporation of higher PANI contents, would increase percolation in the nanofibrous structure and provide higher conductivity for the induction of electrical stimuli and improved electrical properties for controlled release applications and in general better control over the electrical properties of the produced composite. When higher concentrations of conducting polymer are being used though, there is the possibility of an adverse effect regarding biocompatibility as indicated in the study of Ma et al. [169], for example. In this study, cast film of chitosan grafted with electroactive aniline tetramer was found to enhance cell proliferation of chondrocytes and C2C12 myoblasts as compared to the pure chitosan one, but high content of grafted aniline tetramer had an adverse effect in terms of cell viability. It is possible though that the adverse effect caused by the use of aniline tetramer instead of polyaniline, as it has been shown (Zhang et al. [227]) that PANI oligomers may show cytotoxicity towards certain types of cells such as the NIH-3T3 fibroblasts that were used in that study, even though in a different study the same type of cells was proven to be positively affected by subjection to various current flows [134]. There have also been cases where *in-vivo* implantation of PANI scaffolds has resulted in inflammation and poor biocompatibility [175], although this could be potentially attributed to the remaining aniline monomers and oligomers, but also because of remaining solvents and acids used during the polymerization or the processing of PANI and not because of the polymer itself [122], [167].

The matter of PANI biocompatibility is still open for investigation within the scientific community and therefore there is a need is to determine firstly if the presence of PANI compromises cell viability and at a second stage, whether the incorporation of conducting PANI in polymeric scaffolds and wound dressings can be proven beneficial to cell attachment and proliferation. If this is true, encapsulation and release of bioactive molecules in a pulsatile ON/OFF way will be possible, as well as the potential for using external electric field on polymeric biodegradable scaffolds to electrically guide the cells.

On the other hand, potential antibacterial activity of the biomaterials investigated for the use in biomedical engineering, is a property that is considered advantageous if they are intended to be used as implantable scaffolds, cell culture substrates, biosensors etc but it is of crucial importance if they are intended to be used for wound healing applications.

There has been extensive study on chitosan and its derivatives with respect to its antimicrobial activity, against several bacteria, (namely *Agrobacterium tumefaciens*, *Bacillus cereus*, *Corinebacterium michiganence*, *Erwinia sp.*, *Erwinia carotovora* subsp., *Escherichia coli*, *Klebsiella pneumoniae*, *Micrococcus luteus*, *Pseudomonas fluorescens*, *Staphylococcus aureus*, *Xanthomonas campestris* etc) [228]. Two mechanisms are generally used to explain the antimicrobial activity of chitosan. Firstly, chitosan is believed to be chelating nutrients and minerals that are essential for bacteria growth [229], and secondly, as a cationic polyelectrolyte it is believed to be electrostatically interacting with the bacterial cell's membrane, thus impeding proper cell membrane function, leakage of proteinaceous and other intracellular constituents, cell lysis and death [228], [230]. This was confirmed by a study conducted by Y. Andres et al. [231], where the potassium ion concentration in a solution where suspended chitosan powder was tested for its inhibitory effect against *E. coli* was monitored. The potassium ion concentration in the solution was found to correlate with the bacterial inactivation, and as it could only be released from the intracellular medium, it proves the effect of chitosan on the cell's membrane. However, although chitosan and its derivatives present in general antibacterial and antifungal properties, there is quite a lot of discrepancy depending on the molecular weight, degree of deacetylation, the pH of the medium/broth, the type of the chemical structure of the derivatives (e.g. quaternized chitosan, chitosan lactate, chitosan hydroglutamate, grafted chitosan, etc), and the particular characteristics of each microbial strain [228].

It has been shown that chitosan in its neutral form, where the amine groups are deprotonated exhibits no antibacterial properties when tested against a variety of bacterial strains. This can be due to two reasons: 1. The uncharged amino groups due to deprotonation in neutral pH don't interact with the cell membrane and 2. The poor

solubility that chitosan presents in non acidic pH [228]. In the same study however [232], it was shown that chitosan grafted with polyaniline exhibited higher antibacterial activity (measured with the inhibition zone method) than PANI alone. This enhancement was attributed to the grafting process, during which, chitosan is protonated under acidic conditions and it can react with the negatively charged bacterial surface, so that the copolymer in the end exhibits an improved antibacterial activity because of the synergistic effect of chitosan and PANI. The same phenomenon was observed for the other two grafted conducting polymers as well (polypyrrole and polythiophene). It was also proposed that the grafted polymers on the chitosan's backbone provided sustained release of ionic groups resulting in enhanced antibacterial activity.

It has also been reported in the literature that the conductive state of PANI exhibits an antibacterial effect against both gram negative *E. coli* and gram positive *S. Aureus* [233]. However, in that particular study, the PANI was polymerized straight on the substrate that was used further for the evaluation of its antibacterial properties, without providing any details on the removal of chemical residues that occur during this process. In another study performed by Kucekova et al., the antibacterial effect of both doped and undoped PANI was studied against the same model microorganisms. It was found that PANI base had only a marginal antibacterial effect against *S. aureus* and none against *E. coli*, while PANI salt exhibited significant antibacterial activity against both microorganisms [171]. Since the PANI salt is more conductive than the PANI base, again here no definitive conclusion can be drawn as to if the antibacterial effect is due to electrostatic interaction of the positively charged molecule and the negatively charged bacteria's cell wall as it has been proposed by Gizdavic-Nikolaidis et al. [170], which causes eruption of the cell wall, lysis and death.

For those reasons, the debate is still open, as on whether the antimicrobial action observed is a result of the agents, that are used during the processing of these materials, usually toxic and detrimental to bacteria and cells alike [167].

This study is therefore focusing on answering the question of whether the incorporation of high amounts of PANI in a biocompatible substrate, affects biocompatibility in terms of cell attachment, growth and spreading as well as the

physical and antibacterial properties of the membranes. In order to avoid remaining aniline monomers that could tamper with the results, commercial PANI was used in this study, and all cell biocompatibility assays were performed after thorough washings of the PANI containing membranes. This is determined by means of successfully electrospinning novel composite PANI/Chitosan and PANI/PEO nanofibres, and more importantly at high PANI ratio (50:50), which could find applications in other fields too, where engineering nanofibres with high amounts of conducting polymer is of fundamental importance.

6.2 Materials & Methods

6.2.1 Electrospinning of Polyaniline Blends with Chitosan and PEO

A blend solution of PANI and PEO was prepared and electrospun as described in Chapter 4. The only modification was the addition of a known amount of PETA (pentaerythritol triacrylate), which was necessary for the crosslinking of the produced mat. Blend solutions of chitosan and doped PANI (PANI/CH), at ratios 0:1 (control), 1:3, 3:5, 1:1 were produced and electrospun as described in Chapter 5. The TCD was fixed at 16cm and the humidity in the electrospinning chamber was set at 20% RH by a constant dry air flow and monitored using a temperature and humidity meter ST-321. The morphology of the electrospun membranes was then examined by using a Carl Zeiss (Leo) Scanning Electron Microscope (Model 1530VP) and the average diameter of the fibres was measured using the AxioVision software.

6.2.2 Stabilization of Electrospun Membranes

As both chitosan and PEO are soluble in water, the electrospun membranes will disintegrate when immersed in aqueous media for the cell culture. For that reason, a pre and/or post spinning process is required to render the membranes insoluble. In the present study, PETA (pentaerythritol triacrylate), which is suggested as both an initiator and crosslinker for photo-initiated cross-linking of PEO [234], [235] was added in the PANI-PEO solution prior to electrospinning at two different percentages

(10% and 30% in respect to PEO), and a post electrospinning treatment (40min under a UV light of 365nm wavelength and 4800μW/cm^2 intensity and wavelength of 365nm) [235] was used to cross-link the PANI/PEO mats. For the Chitosan – PANI mats, a neutralization process was used to deprotonate the chitosan molecule and render it insoluble in water. Three saturated salt solutions that are suggested in the literature [200], [204], [236], were compared as for their efficiency to maintain ("stabilize") the nanofibrous structure of the electrospun membranes containing chitosan and polyaniline in water. The electrospun membranes were not removed from the aluminium foil after electrospinning and dipped as such in saturated water solutions of Na_2CO_3 or NaOH for 3h or in a 90:10 methanol:water NaOH solution for 10min, as suggested in the above mentioned studies. Soon after treatment, they detached from the aluminium foil and could be easily handled. After that, they were thoroughly washed and immersed in phosphate buffered saline (PBS) of pH 7.4 (ThermoFisher Scientific Inc.), at 37°C for several days and their morphology was examined under a scanning electron microscope in specified time intervals, in order to monitor any changes on the nanofibrous structure such as fusion of fibres, increase in diameter size due to swelling, membrane disintegration in the aqueous media during the course of that time period.

6.2.3 Contact Angle Measurement

Cells are susceptible to changes of the hydrophobicity/hydrophilicity of the culture surface [237]; therefore the contact angle of the electrospun membranes was measured using the sessile drop method, with the relevant equipment (DataPhysics OCA) and using a droplet of water to calculate the contact angle.

6.2.4 Electrical Resistivity

Measurements of the membranes conductivity were performed, in order to confirm homogeneous and continuous distribution of the PANI in the nanofibrous membrane and to examine the effect of the PANI content in the membrane as well as changes occurring during the neutralization step. The electrical resistivity of the electrospun

membranes was measured using the four probe technique on rectangle specimens. A Keithley DC current source was used to generate a DC current I at the range of 100 mA to 10μA, and the voltage through the sample was measured in four different directions with a Keithley 2000 DMM voltameter. Each sample was measured three times and average values are reported.

6.2.5 Cell Culture

Two types of human cells were used for cell cultures to assess cell viability / behavior, osteoblasts (hOST-T85 cell line from eCACC) and fibroblasts (Neonatal foreskin human dermal fibroblast cells from Intercytex). Human osteoblast cells were grown in Minimum Essential Medium (MEM), supplemented with 10% v/v fetal bovine serum (Invitrogen), 1% v/v non-essential amino-acids (NEAA) and 2mM L-glutamine and incubated at 37°C/5% CO_2 in a humidity incubator. Human dermal fibroblasts were grown in Dulbecco's modified Eagle's medium (DMEM; Gibco), supplemented with 10% v/v fetal bovine serum (Invitrogen), and 2mM L-glutamine. Both cell types were thawed and grown for two days in T-175 tissue culture flasks before being seeded on the electrospun membranes. They were then trypsinized (0.25% trypsin-phenol red provided by Gibco™) for 5 min to detach from the flasks, centrifuged and resuspended in growth medium and finally counted with a nucleocounter NC-3000 using a viability and cell count assay Via1-Cassette™ by Cell Tech. For the cell culture, the electrospun samples were cut into small round pieces (d=2cm), were washed twice with sterile PBS solution and sterilized under UV light for 1h on each side. They were then placed in 6-well Ultra low attachment tissue culture well plates and secured at the bottom of each well with cell culture filters from which the bottom mesh has been previously removed. The electrospun membranes were soaked in cell growth medium overnight prior to seeding the cells previously grown in T-175 tissue culture flasks.

6.2.6 Cell Attachment and Viability Assay

In order to evaluate the cell viability, a LIVE/DEAD® Viability/Cytotoxicity Kit (ThermoFischer Scientific) was used 3 days after cell seeding. The growth medium was removed and the seeded membranes were given a gentle PBS wash. A PBS solution containing 0.2% of ethidium homodimer dye (dead staining) and 0.05% calcium dye (live staining) was then added in the wells and left to incubate for 40min. The samples were visualized using a Leica DMRX fluorescence microscope equipped with the appropriate fluorescence filters. Digital images were acquired using a DS-Qi1Mc Nikon digital camera.

6.2.6.1 Cell Proliferation Assay

Live human osteoblasts of passage number 52 and fibroblasts of passage number 5 were seeded at a density of $7x10^4$ per well, in duplicates on the electrospun membranes and on tissue culture plastic surface (as a positive control). Additional 3mL of the corresponding cell culture medium was added in each well. The seeded membranes were incubated at 37°C/5% CO_2. Cell attachment and proliferation were measured with a continual fluorescence assay, using AlamarBlue™ (AB Fisher Scientific). Resazurin, the active ingredient of alamarBlue® reagent, is a non-toxic, cell permeable compound that is blue in color and virtually non-fluorescent. Upon entering cells, resazurin is reduced to resorufin, a compound that is red in color and highly fluorescent. Viable cells continuously convert resazurin to resorufin, increasing the overall fluorescence and color of the media surrounding cells. After allowing some time for the cells to attach to the substrates (attachment time), in a tissue culture incubator, the supernatants were then removed and 3 mL fresh complete medium containing 10% (v/v) AB was added into each well. After another 5h of incubation, triplicate 200 mL aliquots of the AB containing medium was removed from each well and put in a black 96-well microtiter plate for fluorescence measurement. The fluorescence was read at emission and excitation wavelengths 530 nm and 590 nm, respectively, using a FLUOstar Omega Microplate Reader (BMG LabTech). Subsequently fresh medium without AB was replaced in the wells. For

continual assessment of cell proliferation, the AB assay was performed every other day on the same cell population for up to 6 days.

6.2.6.2 Morphological Assessment

For morphological assessment, samples in glass slides and tissue culture plastic were washed with PBS and then visualized on a Nikon eclipse Ti microscope. Digital images were acquired using a DSFi1 digital camera. As the morphology of the cells cultured on various membranes couldn't be assessed with normal contrast phase microscope (due to membrane opacity), the samples were prepared for scanning electron microscopy. They were fixed with 2.5% glutaraldehyde in PBS for 24 h at 4 °C, washed with PBS, and subsequently dehydrated in 15%, 30%, 50%, 70%, 85%, 95%, and 100% (twice) graded ethanol for 10 min each. They were left to dry in desiccator overnight and they were then sputter coated with Au/Pd for 60sec, and visualized with a scanning electron microscope (Carl Zeiss (Leo) - Model 1530VP).

6.2.7 Antibacterial Properties

The antibacterial activities of PANI/CH membranes were investigated by a zone inhibition method. Gram-negative *Escherichia coli* (*E. coli Strain K12*) and gram-positive *Bacillus Subtilis* (*B. subtilis*) cells were used as the model microorganisms. All electrospun mats with different contents of PANI were cut into 2 cm diameter discs, thoroughly washed with PBS and ethanol, and sterilized by UV light prior to bacterial viability test. Nutrient agar plates were inoculated with 1 mL of bacterial suspension containing around 1×10^5 colony forming units (CFUs)/mL bacteria. The composite nanofibres were gently placed on the inoculated plates and were incubated at 37 °C for 24 h for the incubation of *E. coli* and at 35°C for 24h for the *B. subtilis*. The inhibition zone around each sample was determined by measuring the diameter of inhibition area around each disk, with a ruler. Each experiment was performed in triplicate.

6.3 Results and Discussion

6.3.1 Production of PEO-Polyaniline and Chitosan-Polyaniline electrospun membranes

Based on the electrospinning studies analyzed in Chapters 4 and 5, the PANI-PEO-PETA and the PANI/CH blend solutions were electrospun using the parameters summarized in Tables 6.1 & 6.2 respectively. The resulting fibre diameters were measured (n=150 for each membrane) with the aid of the AxioVision software.

Table 6.1: Electrospinning parameters and resulting PANI/PEO nanofibre diameters at different PETA content

PANI:PEO:PETA ratio	Electrospinning Parameters				Nanofibre Diameter		
	Voltage (kV)	Flow Rate (mL/h)	TCD (cm)	RH (%)	Average (nm)	SD	Coefficient of Variation
1:1:0.1	9.5kV	2	12	20	907	210	0.23
1:1:0.3	14kV	2	12	20	327	289	0.88

The addition of 0.1% w/w PETA, didn't affect the electrospinning process or the diameter of the resulting fibres (Chapter 4.3.2). However, when 0.3% PETA was added to the electrospinning solution, a higher voltage had to be applied, in order to achieve continuous jet. This was anticipated since PETA has a surface tension of 41.5dyn/cm, higher than that of the solution before the PETA addition (30.2dyn/cm). As a result, fibres of a smaller average diameter are obtained but at the cost of very low uniformity as expressed by the coefficient of variation (Table 6.1). Many fused fibres were also observed on the electrospun mats, indicating slower solvent evaporation. This is not surprising since PETA, is a viscous liquid of quite high boiling point (205°C).

Table 6.2: Electrospinning parameters and resulting PANI/CH nanofibre diameters at different PANI content

PANI:CH ratio	Electrospinning Parameters				Nanofibre Diameter		
	Voltage (kV)	Flow Rate (mL/h)	TCD (cm)	RH (%)	Average (nm)	SD	Coefficient of Variation
0	26	1	13	35	111	64	0.53
1:3	26	1	16	35	116	44	0.38
3:5	28.5	0.3	16	20	130	123	0.95
1:1	29.5	0.3	16	20	160	126	0.78

Given that the concentration of chitosan was kept at 5% w/v to ensure electrospinnability of the solutions, by increasing the ratio of PANI in the blends, the total polymer concentration was increased as well so that at the blend with ratio 1:1, the total polymer concentration is 10% w/v. This made it impossible to keep the electrospinning parameters the same for all the electrospun blends. Therefore, at high PANI contents, the flow rate had to be lowered from 1mL/h to 0.3mL/h, and higher electric field needed to be applied in order to surpass the higher surface tension of the more concentrated solutions (Table 6.3).

Table 6.3: Measured Surface Tension for Chitosan and PANI/CH blend solutions

Solution Recipe	Surface Tension (mN/m)
PANI:CH 0:1	13.8
PANI:CH 1:3	14.9
PANI:CH 3:5	18.3
PANI:CH 1:1	23.6

Higher PANI content in the blend also increased the solution conductivity, requiring lower environmental humidity in order to make electrospinning possible. This is because higher charge mobility within the jet facilitates charge exchange between the surrounding water vapors and the jet, resulting in removal of charges from the jet and therefore requiring higher voltage to counteract this phenomenon. In a previous study the combined effect of humidity, applied voltage and flow rate on the electrospinning of conducting polymer solutions had been explained thoroughly [73]. Briefly, as the flow rate is being decreased, and higher voltages are used, the process becomes more unstable, resulting in higher charge mobility and charge density on the whipping jet, and thus causing it to split in smaller subjets. This jet splitting phenomenon is the cause of higher standard deviation values regarding the nanofibre diameter (Table 6.2). This can be visually observed in Figure 6.1 below, with the membranes with the higher PANI content (A & C), presenting a lot of thinner and short fibres, characteristic of the jet splitting [196].

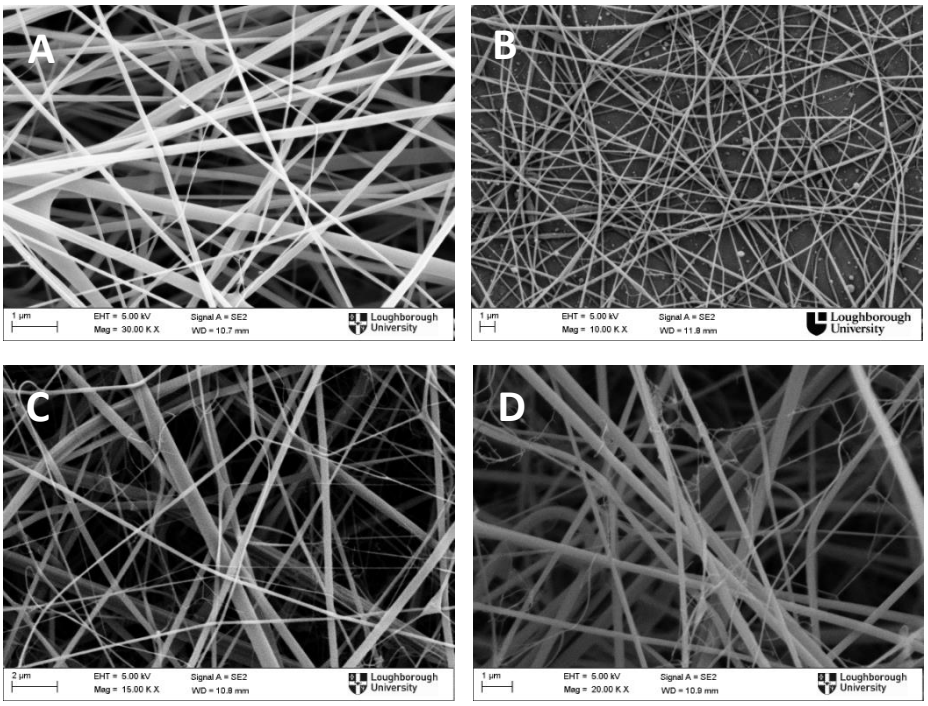


Figure 6.1: SEM images of A: Chitosan, B: PANI/CH 1:3, C: PANI/CH 3:5 D: PANI/CH 1:1 electrospun membranes – Images are representative of three membranes prepared for each condition

In Table 6.2, it is shown that decrease in flow rate results in nanofibres with larger diameter distribution range. Although the standard deviation is usually used as a

marker of membrane uniformity, the coefficient of variance was preferred over the standard deviation for this purpose, as a more appropriate statistical magnitude, given that it is independent of the measuring unit.

However, for the solutions which were electrospun at the same flow rate and applied voltage, 0:1 - 1:3 and 3:5 – 1:1, a decrease of coefficient of variance is observed from 0.53 to 0.38 and from 0.95 to 0.78 respectively which shows that the increasing PANI content has a positive effect in terms of membrane uniformity. Although jet splitting usually occurs in more concentrated and viscous solutions, and when higher electric field is used [196], here it seems that the higher concentration due to increased PANI content, as well as the increased charge per unit area due to the conducting PANI, have the opposite outcome. This can be explained by taking into consideration that the high mobility charges introduced by the dopant acid, offer higher charge mobility on the jet, balancing off the high charge density at the surface of the jet, which are generally the cause of the jet branching. The polarity of the chitosan itself must be also taken into account here. Chitosan is a positively charged molecule and it has been reported that when electrospun under positive high voltage (like in the present study) multiple jets are formed, instead of one, indicating process instability [215]. The addition of PANI here (Figures 6.1 B and 6.1 D), seems to be counteracting this phenomenon, probably due to the dopant acid, in this case CSA, as was explained in detail in Section 5.3.3. It also has to be noted here that when CSA and polyaniline base are dissolved in TFA, CSA is the main if not exclusive dopant of the polyaniline nitrogen atom, resulting in polyaniline salt with enhanced conductivity properties, despite the TFA being a stronger acid, as Niziol et al. had shown [207]. They also noted that in the absence of CSA, solubility of PANI in the TFA was poorer. The reason on why this is happening has not yet been investigated in depth by any study, however there is a general consensus in the literature based on the observation that sulfonated acids constitute in general the best dopants for polyaniline [123], [126], [197]. In the present study though, and as the solution system used is quite complex, further studies must be conducted in order to be able to draw robust conclusions regarding the interactions and bonds involved and on how these affect the electrospinning process.

6.3.2 Stabilization of the electrospun mats

The PANI-PEO mats were stabilized by crosslinking, using PETA, which acts both as cross linker and initiator when exposed to high intensity UV-light, according to protocols found in the literature [235].

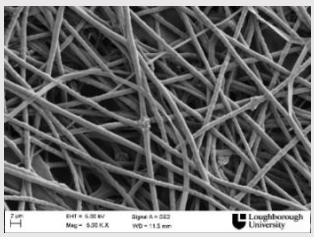
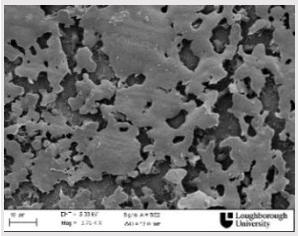
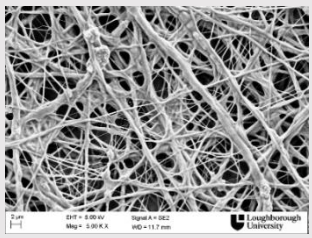
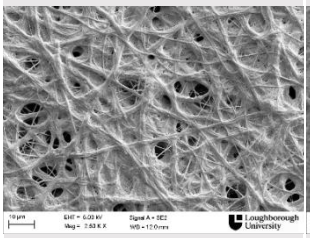
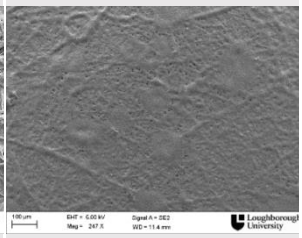
PANI:PEO:PETA ratio	DAY 0	DAY 7	DAY 14
1:1:0.1			
1:1:0.3			

Figure 6.2: Electrospun PEO containing membranes after crosslinking and immersion in PBS (7 and 14 days)

As shown in Figure 6.2, the crosslinking was unsuccessful in sustaining good nanofibrous structure after 2 weeks immersion in PBS solution, which was a necessary step in order to move forward with the cell cultures which often last in the order of days to weeks. Higher concentration of PETA in the electrospinning solution, would have been beneficial, but since PETA's biocompatibility is still ambiguous [238], [239], this would interfere and complicate the evaluation of the role of PANI in the mats to be examined for their biocompatibility. The discrepancy between this study and the literature regarding the optimum PETA concentration and UV irradiation parameters for PEO crosslinking, is probably due to firstly, oxygen quenching on the surface of the mats; here, no nitrogen flow was used during irradiation (Zhou et al. [235]), and secondly due to the presence of PANI in the mats. It is possible that the PANI molecules incorporated in the nanofibres interfere with the crosslinking of PEO. For

those reasons, the crosslinking of PANI-PEO mats was not brought forward for further study.

For the stabilization step of chitosan containing mats, three methods were tested as for their efficiency to neutralize the electrospun membranes. The PANI/CH membranes were dipped either in 5M NaOH water solution, 5M NaOH methanol/water solution (90:10) or in 5M $NaCO_3$ solution. The morphology of the nanofibrous membranes was examined after 0d, 7d and 15d of immersion in PBS. The results are summarized in Figure 6.3.

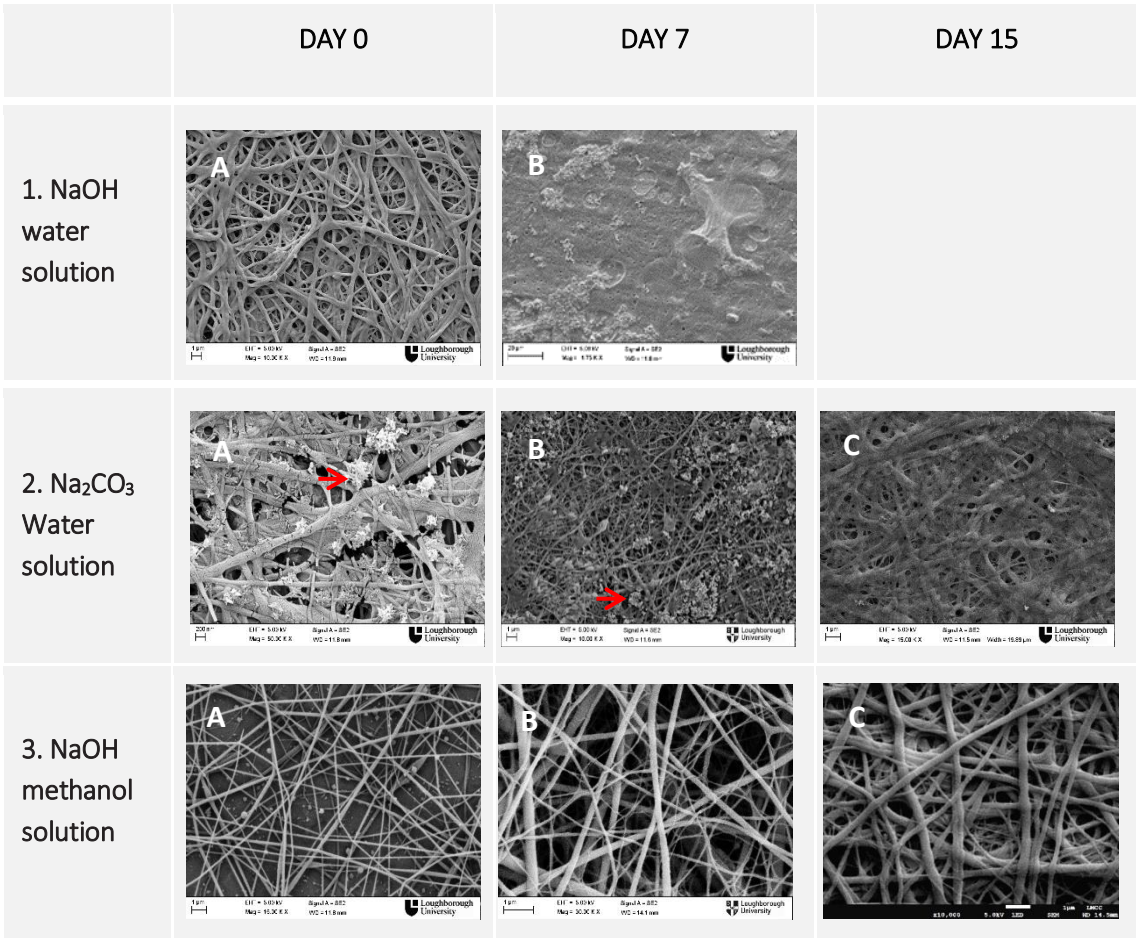


Figure 6.3: Electrospun chitosan containing membranes after neutralization and immersion in PBS (7 and 15 days)

A pH 7.4 PBS solution was judged suitable and convenient for testing the stability of the neutralized membranes; this PBS supports the osmotic balance of cells and is the same pH as cell culture medium. As the *in vitro* culture time of both osteoblasts and

fibroblasts usually does not exceed 14 days, the time frame of 15 days was also chosen on this basis. It is also in accordance with the time frame for a potential wound healing application [240]. Moreover, potential loss of structure is expected to happen because of the chitosan rather than the polyaniline since it is the more biodegradable of the two. The main mechanism of chitosan degradation in cell culture conditions would be by hydrolysis, which is mainly dependent on pH and temperature. Therefore, immersion of the neutralized membranes in PBS solution of pH 7.4, at 37°C over a period time of 15 days is expected to be sufficient to draw conclusions on membrane stability. The membranes were however kept even after that 15 day period to check on the long term degradation rate.

As shown in Figure 6.3, the NaOH aqueous solution, although initially it seemed successful in stabilizing the electrospun membrane, as the membrane retained its nanofibrous structure after immersion in the neutralizing water based solution (Figure 6.3, pic. 1A), when it was left one week in PBS solution, the nanofibrous structure was completely lost (pic. 1B). The neutralization with saturated Na_2CO_3 solution worked better, as the nanofibrous structure was retained even after 2 weeks in PBS (Figure 6.3 pic. 2B & 2C); however the excess salt precipitated (shown by arrows on Figure 6.3, pic. 2A and pic. 2B) on the nanofibres and although it was thoroughly washed, Na_2CO_3 remains were still present on the membrane after one week of immersion in PBS. Based on these results, the NaOH aqueous methanol solution, being the faster neutralization method (10min) seemed to maintain best the nanofibrous structure of the membranes, and when checked even after 30 days of immersion in PBS, the nanofibrous morphology was still intact. No change in nanofibre diameter was observed after the neutralization process. It has to be noted, that after immersion in alkaline NaOH methanol solution, partial dedoping of PANI occurs. This was observed visually as a gradual change of color of the electrospun membranes from deep green, to blue and it was further investigated with conductivity measurement of the membranes, which will be analysed in Section 6.3.5.

Different crosslinking methods of chitosan have been proposed in the literature, e.g. with glutaraldehyde [204] or with genipin [8], [241] which could by-pass this problem. However at this stage, where the investigation of potential toxicity is the main focus

point, cross-linking with glutaraldehyde would be compromising as it has been found to be toxic to biological tissues and genipin's cost was too high for this stage [242]. There is also the possibility that, different dopant acids for the polyaniline could be good candidates for sustaining the electrical conductivity of PANI at high pH values [243]. However, it is generally accepted that for biomedical applications, polyaniline will inevitably undergo partial dedoping under physiological conditions where the pH is around 7.4. For the purpose of wound healing applications though, this is not restrictive, given that skin exhibits acidic pH values (<5) [244], which renders polyaniline a very good candidate for this kind of applications. Here, cell culture was performed in normal pH conditions, mostly to prove the biocompatibility of the composite membranes as a first step rather than investigate the full potential of its conducting properties.

6.3.3 Characterization of neutralized electrospun membranes

The membranes were characterized in terms of hydrophilic properties and conductivity in order to confirm the successful and uniform incorporation of PANI in them and to evaluate the effect of PANI content on their biological properties.

6.3.4 Contact Angle

In order to confirm the incorporation of polyaniline in the membranes and in order to track changes in the membranes hydrophobicity, as it is an important factor affecting cell attachment, the electrospun membranes were measured for their contact angle after neutralization with NaOH methanol solution (Table 6.4). Contact angle of the electrospun membranes before neutralization couldn't be measured accurately, as they are too hydrophilic and the water droplet tends to get absorbed by the surface of the membrane, altering the nanofibrous structure and finally dissolving the material. The values reported in Table 6.4 represent the mean value of at least six repetitions performed at different regions of each of the triplicate membranes produced under the same conditions.

Table 6.4: Contact angle measurements for electrospun PANI/CH membranes after neutralization

PANI:CH ratio	Contact Angle (°)	
	Average	SD
0	41.3	6.72
1:3	46.67	6.47
3:5	53.09	8.17
1:1	70.34	6.35

The increase of the contact angle with increasing PANI content that can be clearly seen in Table 6.4, can be explained by the fact that polyaniline is inherently a highly hydrophobic material, especially at its emeraldine base state, which occurs after treatment with alkali, so it inevitably enhances the hydrophobic properties of the nanofibrous membranes. The monotonic increase of the contact angle with increasing PANI content also indicates that polyaniline is uniformly incorporated in the electrospun fibres. Lastly, all four electrospun membranes fall into the category of moderately hydrophilic surfaces as they all exhibit contact angles between 40° and 70°, which are also generally considered suitable for cell culture [237].

6.3.5 Electrical Conductivity

The electrical conductivity of the membranes was calculated from the measured resistances with the 4 point probe technique as was described in materials and methods. The sheet resistance R_S can be obtained from the characteristic resistances R_A and R_B by numerically solving the van der Pauw equation (Equation 7)

$$e^{-\pi R_A/R_S} + e^{-\pi R_B/R_S} = 1 \quad (7)$$

The characteristic resistances R_A and R_B are given from the measured voltage when a positive dc current I is injected into one contact and taken out from another contact. For example I_{12} = current injected into contact 1 and taken out of contact 2. Likewise for I_{23}, I_{34}, I_{41}, I_{21}, I_{14}, I_{43}, I_{32} (in amperes, A).

The respective measured voltages are V_{12}, V_{23}, V_{34}, V_{41}, V_{21}, V_{32}, V_{14}, V_{43}, (in volts, V) and from those the respective resistances are calculated:

$R_{21,34} = V_{34}/I_{21}$, $R_{12,43} = V_{43}/I_{12}$,

$R_{32,41} = V_{41}/I_{32}$, $R_{23,14} = V_{14}/I_{23}$,

$R_{43,12} = V_{12}/I_{43}$, $R_{34,21} = V_{21}/I_{34}$,

$R_{14,23} = V_{23}/I_{14}$, $R_{41,32} = V_{32}/I_{41}$

as well as the characteristic resistances:

$R_A = (R_{21,34} + R_{12,43} + R_{43,12} + R_{34,21})/4$ (8) and

$R_B = (R_{32,41} + R_{23,14} + R_{14,23} + R_{41,32})/4$ (9)

In this case: $R_A \sim R_B$, so equation (7) gives:

$$2e^{-\frac{\pi R_A}{R_S}} = 1$$

$$ln2 = \frac{\pi R_A}{R_S}$$

$$R_S = \frac{\pi R_A}{ln2}$$

The bulk resistivity (ρ) is then given by the equation:

$\rho = R_S d$ (10), where d is the measured thickness of the conducting layer.

The latter can then be converted to conductivity by simple inversion: $K = \frac{1}{\rho}$

Applying the above, the following conductivities are shown in Figure 6.4

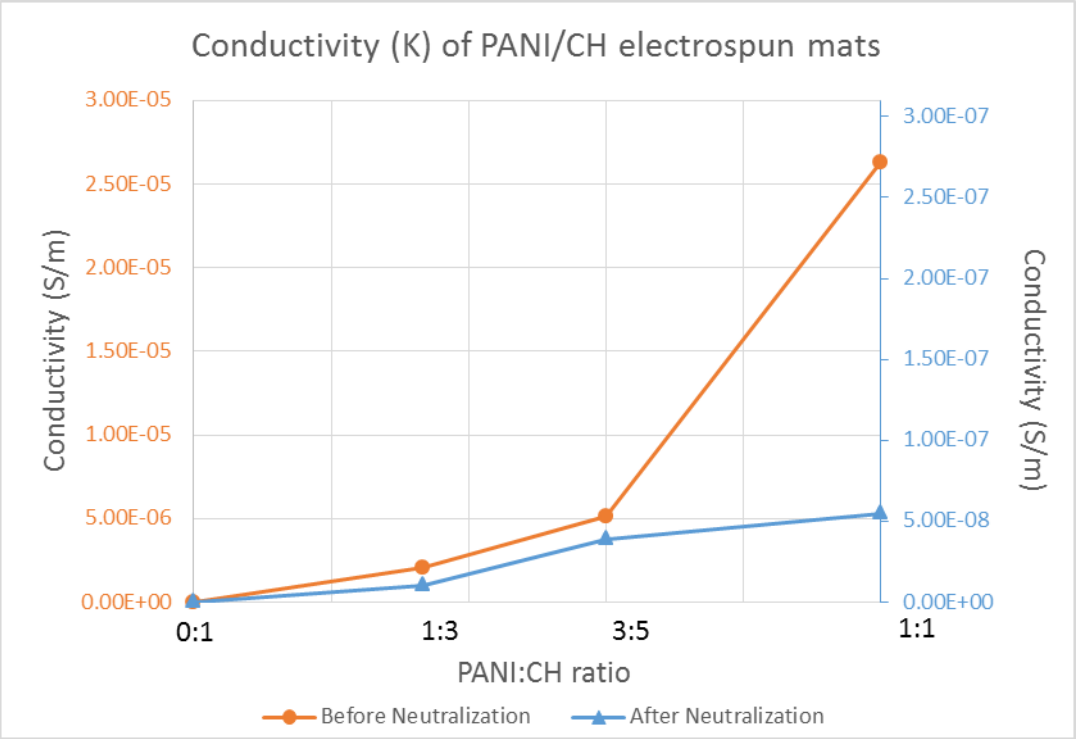


Figure 6.4: Comparison chart of membrane conductivity before and after neutralization (note the different order of magnitude for the two curves)

As can be seen from Figure 6.4, the dedoping that was observed visually during treatment with aqueous methanol NaOH solution, was confirmed by the conductivity measurements. A big decrease of at least 2 orders of magnitude is observed for all the samples containing polyaniline. The control pure chitosan sample did not change after the neutralization process and, as expected, it was not electrically conductive before or after the neutralization process. However, all the PANI/CH membranes, even after neutralization retained some conductivity, which was two orders of magnitude larger than the control chitosan. For tissue engineering purposes, as only very low currents need to be applied for cell excitation, usually at the range of μA [245], the membranes with the reported conductivities are considered worth to be investigated further for their effect on cell cultures. Generally, in order for a voltage to be considered safe for electrical excitation of cells it needs to be at the range of V/cm and the generated current at the range of μA [245], [246], therefore materials at the range of resistivity of semiconductors, are best candidates for this type of applications. It is also debated that even without electrical excitation, cells might be

able to communicate with electrical signals they produce which can be facilitated by an electrically conducting membrane [247].

It is also observed (Figure 6.4) that with higher PANI content, the membrane conductivity increases as well, as expected. There is more than one order of magnitude increase of conductivity between untreated PANI:CH 1:3 and 1:1 membrane, indicating good distribution of PANI in the membrane. When the membranes are treated with alkali, the increase in conductivity with increase of the PANI ratio is not as pronounced because the partial dedoping that occurs disrupts the charge mobility within the membrane, but still it is more than 3 orders of magnitude higher for the membrane with the highest amount of PANI.

6.3.6 Evaluation of Cell Attachment and Viability

To assess the cell viability, and to rule out possible and undesired acute cytotoxicity, the Live/Dead cell stain was used as a preliminary step. This test is a destructive method to assess cell viability, so it was performed on two of the human osteoblast cell seeded membranes (CH and PANI/CH 3:1).

Figure 6.5 shows the images obtained from the fluorescence microscope for the pure chitosan membrane and the PANI/CH 1:3 membrane respectively, after staining with calcium dye which is live cell stain (Figures 6.5 A, B & 6.5 E, F) and ethidium homodimer dye which stains the dead cells (Figures 6.5 C, D & 6.5 G, H). From Figures 6.5 A, B & 6.5 E, F it is shown that the cells have well attached and spread on the electrospun membranes after 3 days in culture. Calcein-AM is a non fluorescent, cell-permeant fluorescein derivative, which is converted into cell-impermeant, highly fluorescent calcein by cellular enzymes. Calcein accumulates inside live cells with intact membranes and causes them to fluorescent green. Ethidiumhomodimer-1 enters dead cells with damaged membranes and undergoes a 40-fold enhancement of fluorescence upon binding to their DNA causing the nuclei of the dead cells to fluoresce red. This double staining allows for simultaneous examination of both live and dead cells on the material surface [248]. It is evident from Figure 6.5, that while for green (live) fluorescence there is a high output, and a lot of cells can be seen on

the membrane surface, for the same region of the membranes, there are very few to none red fluorescent spots, indicating only one or two dead cells per image (comparing Figures 6.5 A to 6.5 C, 6.5 B to 6.5 D and so on). It has to be noted here that it was difficult to focus on the whole region of the membrane at this magnification as the membrane inevitably exhibited some wrinkles and folding in the medium.

Although this being a qualitative test, thus providing only a visual evaluation of viability, by comparing Figures 6.5 A & B to 6.5 E & F, it is obvious that more green fluorescence per image can be seen on the blend membrane, indicating that the membrane incorporating polyaniline supports better osteoblast attachment than the control chitosan; however no definitive conclusions should be reached yet, regarding which of the two membranes exhibits better cell compatibility. After cytotoxicity was ruled out, further quantitative tests were performed on all of the electrospun membranes containing different ratios of polyaniline and for both cell types (osteoblasts and fibroblasts).

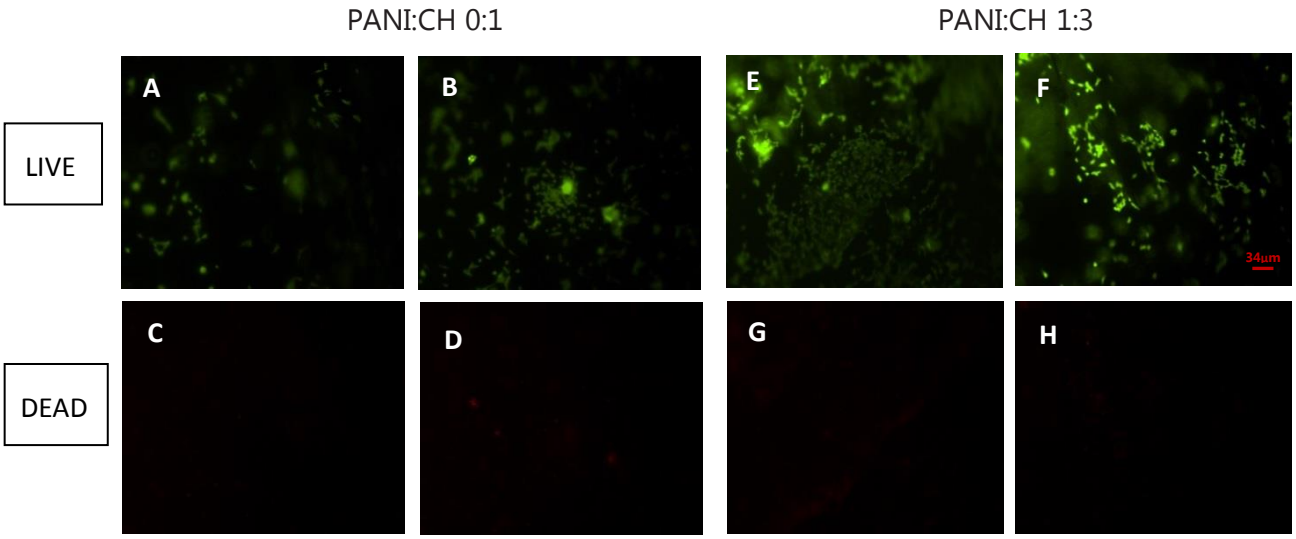


Figure 6.5: Fluorescence LIVE/DEAD stain for PANI:CH membranes (3d in culture): A & B, E & F: Live at two different membrane regions for each blend C & D, G & H Dead staining for the same two membrane regions of each blend

6.3.6.1 Cell proliferation

The cell proliferation studies were performed by using the fabricated electrospun membranes of different PANI/CH ratios, and tissue culture plastic and pure chitosan

as controls in order to evaluate how the added PANI affects cell growth as compared to the chitosan. In many studies it has been shown that electrospun chitosan membranes enhance osteoblast and fibroblast proliferation, offering a good substrate for tissue culture. The introduction of electrical properties to the electrospun membranes is expected to have an impact on how cells grow on those. The osteoblasts were allowed to proliferate for up to 9 days and the fibroblasts for up to 15 days. During preliminary experiments, it was observed that fibroblasts took longer to attach on the electrospun membranes; therefore time 0 was defined as the 3rd day after seeding. Over the testing period, relative cell numbers were assessed continually every other day using the Alamar Blue assay (AB). Figures 6.6 A, B & C show the AB fluorescence measurements of osteoblast and fibroblast cells, on electrospun chitosan and PANI/CH blend fibres with volume ratio of 3:1, 5:3, 1:1, pure CH as control and TCP as a reference. The same 3 days attachment period was applied on the osteoblast cell line too for reference.

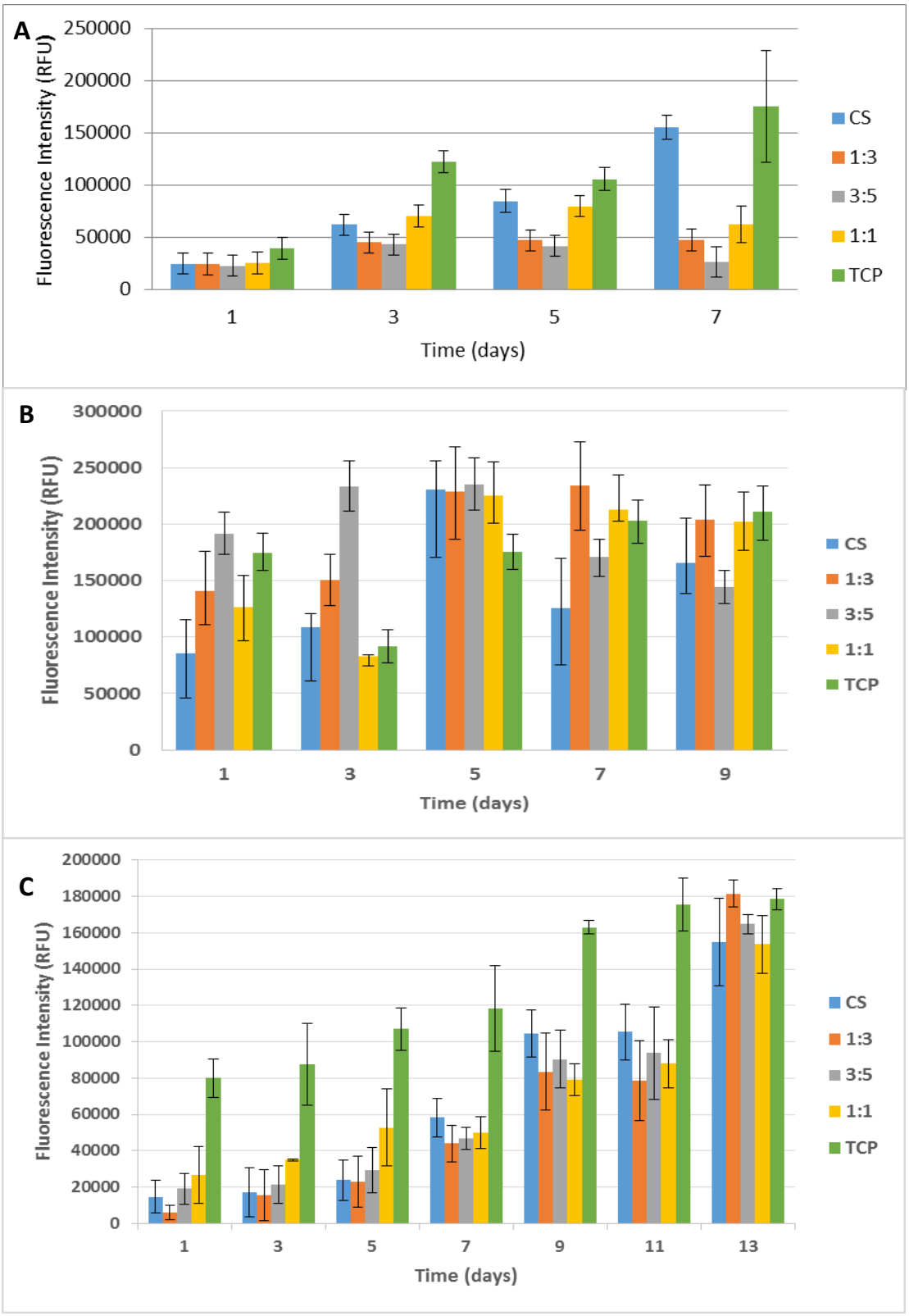


Figure 6.6: Proliferation rates of A: Osteoblasts – Attachment time 1 day. B: Osteoblasts - attachment time 3 days. C: Fibroblasts – Attachment time 3 days. All bars represent mean values from triplicate experiments and the error bars represent the ranges of the measured values.

Interestingly, when the osteoblasts were left to attach for longer period (3 days instead of 1) prior to the first medium change, which could cause loosely attached cells to become detached, the PANI/CH composite membranes, and especially the one with 3:5 PANI:CH ratio seem to promote a lot more cell proliferation, even more than the tissue culture plastic. It is worth to note here, that day 7, when 1 day was allowed for attachment, was expected to match the intensity measured on day 5, when 3 days were allowed for attachment. While this is true for the tissue culture plastic surface, when looking at the membrane data, a significant increase in intensity is noted: the pure chitosan shows an increase of around 75000 RFU which correspond to a 30% increase, the 1:3 membrane shows a an 80% increase, the 1:1 membrane presents a similar increase of around 75% and finally the 3:5 membrane presents a massive increase of almost one order of magnitude. The discrepancy of the results between 1 and 3 days of attachment, can be attributed to the nature of the assay that was used. The cell attachment mechanism can be described in three phases: A. Sedimentation of cells on the substrate which is guided by electrostatic interactions, B. Integrin mediated bonding of the exoskeleton on the substrate and flattening of the cell and C. Spreading of the cell on the cell on the substrate mediated by focal adhesions. Cell spreading seems to be accompanied by the organization of actin into microfilament bundles. The strength of adhesion becomes stronger with time [249].

In order to perform the Alamar Blue assay, the supernatant is removed and new medium containing AB reagent is added to the wells. After the set incubation time, the AB containing medium is removed again and fresh medium is added, till the next time that a measurement is performed, when it is removed again. If the cells didn't have enough time to reach the final phase of secure attachment on the membranes before the first measurement is taken, they may be aspirated with the culture medium. In this way, the cell density at day 1 is reduced and since the assay is continuous, the cells can't proliferate normally. This, verifies what was visually observed during the initial cytotoxicity test (Live/Dead cell stain) that was discussed in the previous section. By day 7, all membranes containing polyaniline seem to show higher cell numbers as compared to the control pure chitosan one and in some cases even more than the TCP. Rougher surfaces, such as nanofibres are usually known to

provide more sites for cell attachment due to the higher surface to volume ratio. However, at the initial stages of attachment, cells may require more time to securely attach on a rougher nanofibrous surface. The same pattern can be found in proliferation charts of other studies too, even though this phenomenon is many times overlooked and not explained in detail. In those studies, during the first days of cell culture, TCP initially seems to outperform nanofibrous membranes, by the end of the cell culture period nanofibrous mats exhibit higher number of cells attached to them, and this can be attributed to an initial lag of the cells to reach phase C of attachment [142], [161], [166], [250], [251].

As for fibroblast proliferation, as can be seen in Figure 6.6 C, the first 5 days in culture, the membrane with the higher polyaniline content (1:1 ratio) sustains cell growth better than the control pure chitosan and the rest of the composite membranes. After day 5 though, the rest of the membranes and especially the 1:3 PANI/CH one, seem to better promote cell growth, with the latter presenting a twofold increase of fluorescence intensity between days 11 and 13, exceeding the value for the tissue culture plastic. It is again evident here that the cells take longer to attach to the membranes as compared to the tissue culture plastic, but when they do, they proliferate well and can reach proliferation rates similar or higher than the standard tissue culture plastic. Looking at the characteristics of these membranes, it seems that although the difference in conductivity between PANI containing membranes and the pure chitosan one is not as vast, it is very possible that in terms of cell culture this offers enough conductivity for cells to attach and proliferate better. This may also be due to the different hydrophilicity of the 1:1 mat when compared to the pure chitosan one (Table 6.4), but when comparing the 1:3 mat which in general showed better cell proliferation, with the pure chitosan one, the contact angle doesn't differ as much. Further investigation as of why the incorporation of PANI maybe beneficial to cell proliferation should be conducted. These results agree with the cell proliferation results obtained by Gizdavic – Nikolaidis et al. [172], who showed an enhanced proliferation of fibroblasts on conductive nanofibrous HCl-doped 3ABAPANI – PLA mat, without any electrical stimulation. The mats with increased ABAPANI content exhibited higher contact angles (>85°), higher

conductivity (>6.9 10^{-5}S/m) and better cell attachment and proliferation, which was significantly higher than that of glass substrate or TCP. This was attributed to the nanofibrous structure of the mats, providing more sites for attachment, as opposed to the flat surfaces of glass and TCP, however no reason was given as of why more limited fibroblast proliferation was observed for pure PLA nanofibres and blends with lower ABAPANI content as well. Considering the fact that the mats with high ABAPANI content exhibit a rather hydrophobic surface (which should be hindering fibroblast attachment), it is surprising that they perform so much better in terms of cell proliferation. A more in depth investigation of this phenomenon has been conducted by Jeong et al. [134] who examined the adhesion of 3 different types of cells (mouse skeletal muscle cells (C2C12), human dermal fibroblasts and NIH-3T3 mouse embryo fibroblasts) on PLCL scaffolds enriched with polyaniline. They found a positive relationship between PANI concentration and cell mitochondria metabolic activity and they attributed this phenomenon to either the electroconductive properties of the scaffolds or to the modified surface chemistry however excluding the surface energy, as the hydrophobicity of the membranes defined by contact angle measurements, was not significantly affected by the PANI concentration.

6.3.6.2 Cell Morphology Assessment

Cell proliferation is important, but it has to be accompanied with visual examination of the cell morphology and attachment on the membranes in order to safely draw conclusions about biocompatibility of electrospun membranes. As the electrospun membranes are not transparent, normal phase contrast microscopy that is commonly used for evaluation of cell cultures could not be employed. Therefore, scanning electron microscopy was chosen as an appropriate method to assess the morphology of osteoblasts and fibroblasts on electrospun membranes. Initially, cells were cultured on glass slides where they exhibited similar characteristics with the ones cultured on tissue culture plastic when examined using optical microscopy (Figure 6.7). The glass slides were then coated with Au/Pd and examined under the scanning electron microscope, to be compared with the ones on the electrospun membranes (Figures 6.8 & 6.9).

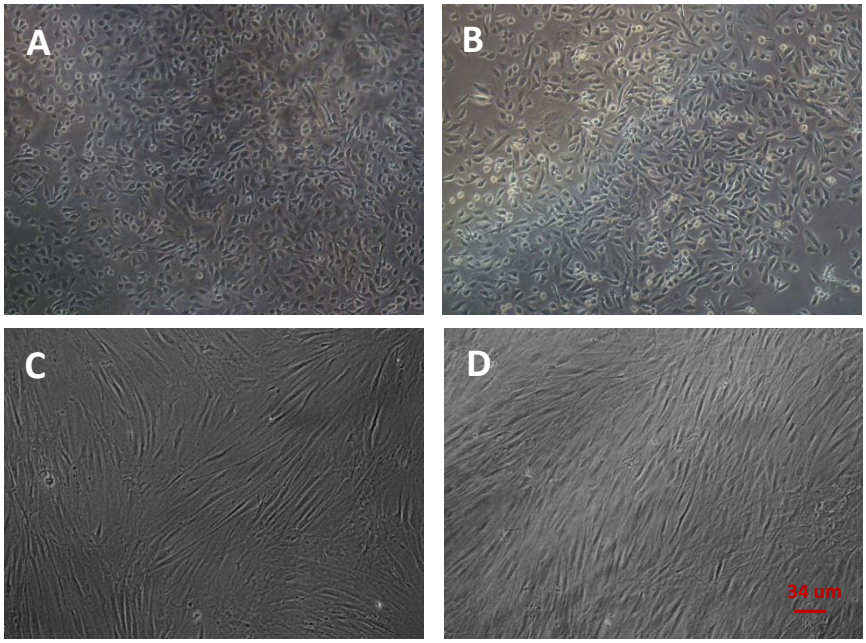


Figure 6.7: Microscope Images (10X) of A: osteoblasts on TCP B: osteoblasts on glass slides, C: fibroblasts on TCP, D: fibroblasts on glass slide

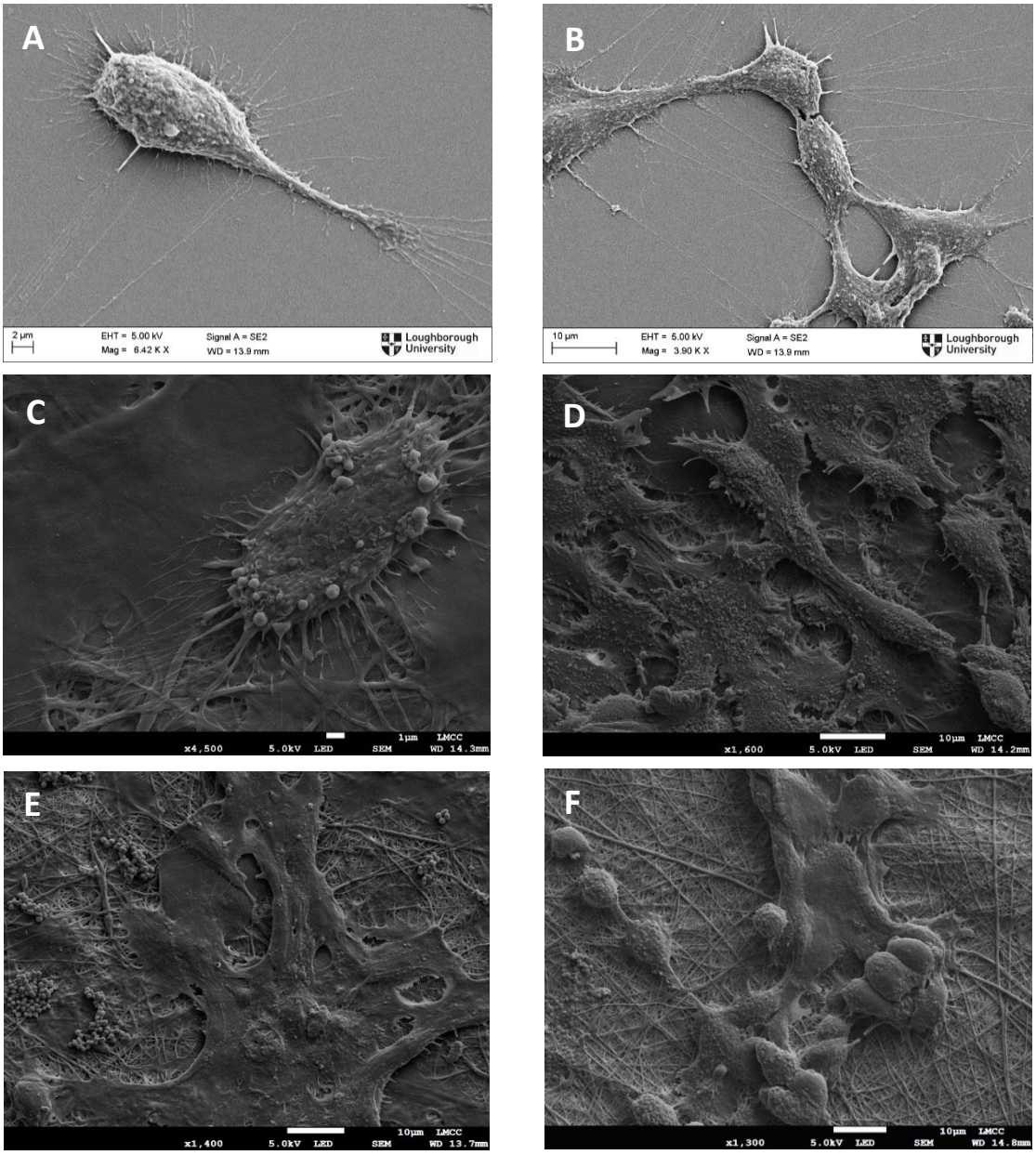


Figure 6.8: Scanning Electron Microscope Images of osteoblasts A&B: on glass slide, C&D: 1:3 PANI:CH membrane, E: 3:5 PANI:CH membrane F: 1:1 PANI:CH membrane

From Figure 6.8, it is evident that when comparing Figures 6.8 A & B to C, the shape and size of osteoblasts is very similar. They exhibit flattened shape with long pseudopodia, an indication of healthy attachment and a typical size of 15-20 µm and they seem to adhere to the nanofibrous surface in the same way as they do on glass slides and tissue culture plastic (Figure 6.7). The same is valid for the blend membranes too (Figures 6.8 D & E), with the exception of Figure 6.8 F, where more globular shapes are shown, indicating that the osteoblasts were unable to spread as

extensively on this membrane as on the others, possibly because of the higher hydrophobicity of this material.

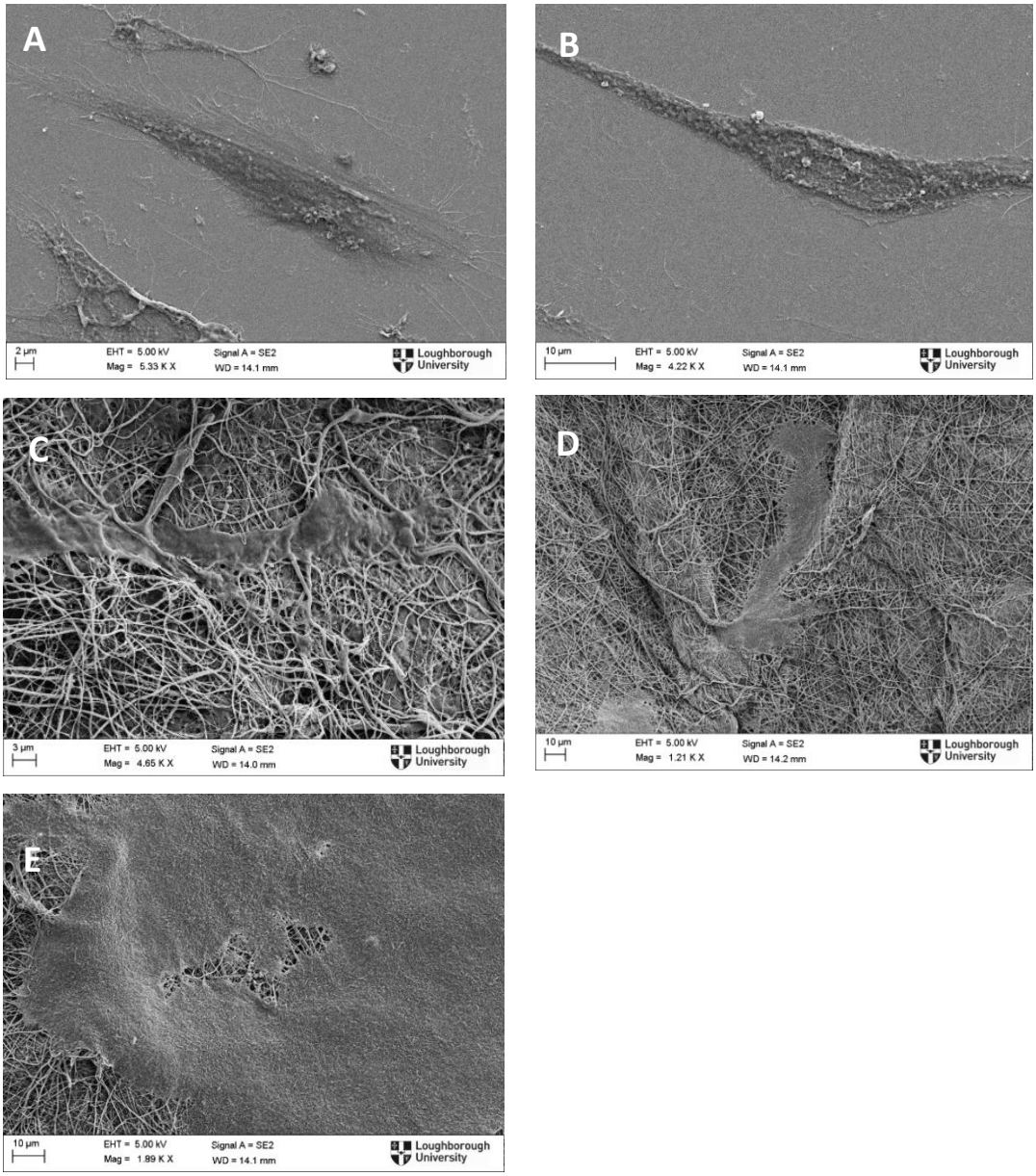


Figure 6.9: Scanning Electron Microscope Images of fibroblasts - A&B: on glass slide, C&D: 1:3 PANI:CH membrane, E: 1:1 PANI:CH membrane

Similar conclusions can be drawn from Figure 6.9 as well, where similar flattened and elongated shapes are observed on all the surfaces and especially on Figure 6.9 D which was taken after the end of the culture period (13 days), it is shown that cells have successfully attached and grown all along the nanofibrous surface, almost completely covering the nanofibres. Some lumps that appear on the surface are most

likely debris and pieces of dead cells which were not successfully washed away before the cell fixing treatment.

6.3.7 Investigation of Antibacterial Properties

Two methods were used to stabilize the PANI/CH mats: neutralization as described previously and cross-linking with glutaraldehyde vapors. The purpose of the latter was to stabilize the chitosan, while avoiding to deprotonate the amino groups both on the chitosan and the PANI molecule, in order to be able to make the comparison between non treated mats, crosslinked with glutaraldehyde and neutralized ones. It has to be noted here that the non treated mats, could not be thoroughly washed with PBS, as they would dissolve almost straight away. The results from the inhibition zone test against *E. coli* and *B. subtilis* for stabilized, cross linked with glutaraldehyde and non pretreated membranes are shown in Figures 6.10 A & B.

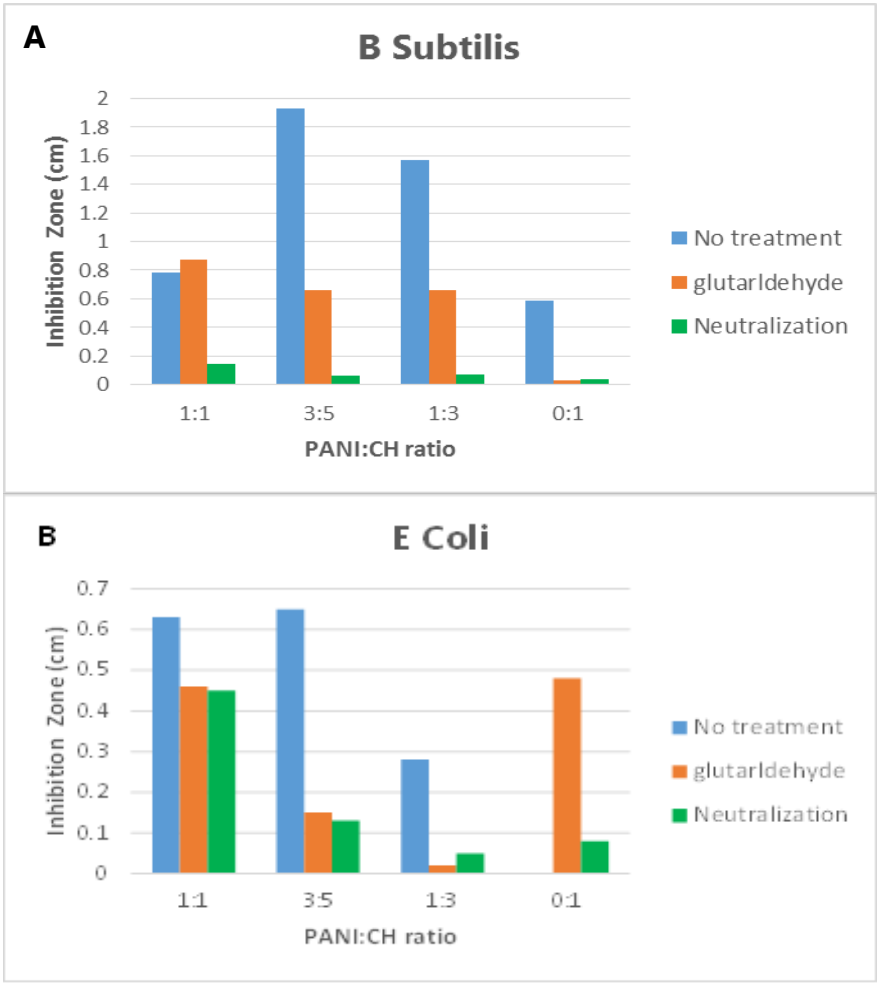


Figure 6.10: Antibacterial activity as evaluated by the inhibition zone (in cm) of blend mats against A: B. subtilis and B: E. coli. All bars represent mean values from triplicate experiments

A straight forward observation from Figure 6.10 is that for both model bacteria, the untreated mats exhibited higher inhibition zones than crosslinked and neutralized ones, which is a proof for the hypothesis articulated earlier, that apart from the electrostatic charge, the toxic agents used to process these materials may be contributing to the bactericidal activity of these materials. Moreover, it is shown that in general the crosslinked membranes, which maintain the protonated states of PANI and chitosan perform better than the neutralized ones. These results agree with the studies reporting that the cationic nature of the protonated state of chitosan, as well as the protonated state of PANI salt, must be affecting the bacteria's cell membrane [171], [230]. It is also shown that the antibacterial activity is stronger against *B. subtilis* which is gram positive than *E. coli* which is gram negative. Gram-negative bacteria are

generally considered more resistant to antibodies because of an extra outer cell membrane that they possess, which is most probably the reason why they seem to be less affected by the inhibitory effect of the mats tested here. It also seems that the mat with the higher PANI ratio, retains high antibacterial activity against *E. coli* even after neutralization, suggesting that the high PANI content contributes greatly to the inhibitory role, even when conductivity is partially lost. This can be directly compared with the zero content mat, where similar inhibitory effect is exhibited when glutaraldehyde is used as cross-linker, while this is almost lost when chitosan is deprotonated, indicating that the inhibitory effect is mainly due to the polyaniline. M. R. Gizdavic – Nikolaidis et al., have indeed shown that functionalized polyanilines seem to share the same bactericidal effect with particular cationic antimicrobial peptides (AMP), by interacting with and inserting into anionic bacterial membranes, thereby compromising membrane integrity and cell division, leading to cell lysis and death [170]. They also proved that exposure to a model functionalized PANI, led to significant changes in the expression levels of 218 (5.1%) genes which are amongst others involved in biofilm formation, energy metabolism and protection from oxidative stress.

Neutralized mats are not efficient against *B. subtilis*, but cross linked ones, and especially the one with high PANI content exhibit good bactericidal activity indicating that retention of the protonated state of PANI is absolutely necessary for interaction of the mat with the bacteria's cell membrane, in order to exhibit bactericidal effect.

6.4 Conclusions

The PANI/PEO nanofibrous membranes could not be assessed with respect to their biological properties, as no successful crosslinking was achieved, both because of the crosslinker affecting the electrospinning process and insufficient level of crosslinking when using low concentrations of crosslinker.

Novel nanofibrous membranes which combine the benefits of conducting polyaniline and biocompatible chitosan, were produced with the electrospinning method and were tested for their biocompatibility with human cell lines and their

antibacterial properties. The nanofibrous membranes incorporating different ratios of PANI to chitosan, exhibited higher contact angles, directly related to the polyaniline content in the blend, with higher polyaniline content resulting in more hydrophobic surface.

The effect of the neutralization that occurs upon the preparation for cell culture, on the properties of such composite membrane containing polyaniline, is studied for the first time. Although the neutralization process which was necessary to stabilize the chitosan in the aqueous medium and prepare the membranes for cell culture, inevitably dedoped the contained polyaniline to some extent, it is shown that the conductivity which was still retained was sufficient to have a positive impact on the attachment of human osteoblasts and fibroblasts as well as bactericidal activity. Especially regarding the mat containing 1:3 PANI:CH ratio, it seems that the retained conductivity due to PANI, together with the retained hydrophilicity due to high chitosan content showed a synergistic effect in promoting both osteoblast and fibroblast growth. None of the produced membranes showed any cytotoxicity; on the contrary cell attachment and proliferation was achieved and sustained during the culture period even when high amounts of PANI were incorporated in the mat, contradicting observations reported in the literature when different carrier polymers are used. This is attributed to the choice of materials, which seem to exhibit a combined beneficial effect on human osteoblasts and fibroblasts. Since the produced membranes are not cytotoxic, they are good candidates for wound dressing applications, where the nanofibrous membrane wouldn't be immersed in biological fluid and could retain fully its conducting properties. Based on these results, further research for determining how the fibroblast and osteoblast cell lines respond to electrical stimuli seems worthwhile and promising.

Another interesting finding emerging from the evaluation of cell proliferation on the substrates is that delayed adherence (1-2days) on the nanofibrous mats is observed, as opposed to the flat tissue culture surface. This is a finding in agreement with other proliferation assays in the literature which is rarely commented on, and despite the fact that the nanotopography that nanofibrous substrates offer are considered to be advantageous for cell attachment and proliferation, as it has been explained in

Section 2.2.2.2 From this study it is concluded that it should be taken into consideration when *in vitro* studies are performed, as it might lead to biased results regarding the biocompatibility of the tested material. However, when cells do attach, they proliferate rapidly, probably due to the facilitation of electrical signaling communication between them that the electroactive surface provides.

It has also been shown, that blend PANI/CH mats exhibit antibacterial activity, higher against gram positive *B. subtilis* and lower against gram negative *E. coli*. An alternative stabilizing method which consisted of crosslinking with the aid of glutaraldehyde vapors, proved to benefit the antibacterial action of these membranes. The conducting properties introduced by means of PANI incorporation, can also potentially offer a tool for controlled release of bioactive substances and/or electrical excitation of cells in biomedical applications.

This is the first time that a porous electroactive nanofibrous membrane is examined for its potential use in wound dressing applications, with promising results.

7| CONCLUSIONS & FUTURE WORK

7.1 Thesis Conclusions

The need for nanofibrous, electroactive scaffolds for use in medical applications has been highlighted in Chapter 2. In this study, some of the challenges related to meeting this need, have been identified and addressed. Firstly, in Chapters 3, 4, & 5, the key parameters affecting the electrospinnability of conducting polymers have been identified, with the use of experimental design, and a solution for overcoming some of the barriers involved has been proposed. Then, in Chapter 6, the applicability of the produced conducting nanofibrous scaffolds for tissue engineering purposes, has been investigated. Essential factors affecting the interaction of the mats with human cell lines are discussed. The current study was focused on PANI as a model conducting polymer, but the findings could be applied to other conducting polymers as well such as PPy or PEDOT, as they share similar conjugated structure and mechanisms with respect to conductivity.

PANI 60% doped with CSA and blended with carrier polymers PEO and chitosan was chosen for the experiments. The electrospinning windows of two PANI blends (PANI/PEO and PANI/CH) were determined. Humidity was shown to be the most important parameter affecting the electrospinning process and defining the electrospinning window for solutions containing high ratios of PANI. When the PANI content in the polymer blend was as high as 50%, electrospinning was feasible only at low relative humidity values (≤20%RH), indicating that for conducting polymers, the effect of humidity is significantly greater compared to that of non conducting polymers. Higher ambient humidity caused removal of charges from the conducting polymer jet, in a much more pronounced way than in a non conducting polymer jet, thus disrupting the process because of the higher charge mobility enhanced by the polymer's conductivity. This is the first systematic study examining the importance of environmental humidity on electrospinning of a conducting polymer. Humidity is an environmental parameter that can be easily controlled, with the introduction of a dry air flow, at a minor cost, even for industrial-scale operations.

Flow rate and strength of electric field also have an impact on the final nanofibre diameter. Higher values of applied voltage cause increased whipping instability, resulting in thinner nanofibres at all flow rates. However, when high voltage was combined with low flow rate, broader diameter distributions were obtained, as a result of the jet splitting phenomenon.

Regarding the flow rate, two competitive phenomena taking place simultaneously are causing its impact to be dependent on the applied voltage. Depending on the combination of the values of applied voltage and flow rate, different phenomenon prevails each time. Either the jet's solidification rate suppresses the extent of the jet stretching, leading to increase in diameter, or extensive jet stretching prevails, leading to thinner nanofibre diameters. The combined action of these phenomena being highlighted for the first time, sheds light to discrepancies that are encountered in the literature regarding the effect of voltage.

Finally, under prediction of the nanofibre diameters observed at low flow rates, when using Fridrikh's model was attributed to the more pronounced effect of solvent evaporation occurring at low flow rates and more importantly, at the higher rate of the discharge of the jet, since at low flow rate, the jet is in theory thinner.

These findings contribute significantly to the knowledge on how solutions of conducting polymers behave during electrospinning and it is anticipated that they will facilitate further the fabrication of conducting electrospun mats by increasing the productivity and eliminating disruptions.

Chitosan grafted PANI (CHgPANI) and blends of chitosan and PANI behave differently during electrospinning. The high rigidity of CHgPANI molecule due to the grafted PANI molecules on the chitosan backbone, didn't allow for repulsing PANI molecules to freely orientate, rendering it not electrospinnable. However, when PANI is in blend solution with chitosan, the chains of both polymers can freely move and orientate when high voltage is applied, thus formation of a continuous jet is rendered possible.

Regarding the second part of the study, the PANI/PEO nanofibrous membranes could not be assessed with respect to their biological properties, as no successful crosslinking was achieved.

The nanofibrous scaffolds incorporating different ratios of PANI to chitosan on the other hand, were successfully stabilized and further assessed as for their compatibility with human cell lines and their antibacterial properties. The mats containing higher amounts of PANI exhibited more hydrophobic surfaces. Although the neutralization process which was necessary for stabilizing the chitosan in the aqueous medium and preparing the mats for cell culture, inevitably dedoped the contained polyaniline to some extent, it is shown that some of the conductivity was still retained and according to the literature, it is sufficient to conduct the electricity needed for cell stimulation.

None of the produced membranes showed any cytotoxicity; on the contrary cell attachment and proliferation was achieved and sustained during the culture period. Especially regarding the mat containing 1:3 PANI:CH ratio, it seems that the retained conductivity due to PANI, together with the retained hydrophilicity due to high chitosan content showed a synergistic effect in promoting both osteoblast and fibroblast growth. Another interesting finding emerging from the evaluation of cell proliferation on the substrates is that delayed adherence (1-2days) on the nanofibrous mats is observed, as opposed to the flat tissue culture surface, but when cells do attach they proliferate very rapidly. This is something encountered in other studies in the literature too, but never commented on. It is highly possible, that during the attachment period there is a delay between phase B and phase C of attachment. As on phase B the cells have not yet developed focal adhesion on the surface, when in aqueous media they may move. When this happens, the roughness of the nanofibrous surface renders it more difficult for them to reattach and spread. From this study it is concluded that it should be taken into consideration when *in vitro* studies are performed, as it might lead to biased results regarding the biocompatibility of the tested material.

It has also been shown, that blend PANI/CH mats exhibit antibacterial activity, higher against Gram positive *B. subtilis* and lower against gram negative *E. coli*. An

alternative stabilizing method which consisted of crosslinking with the aid of glutaraldehyde vapors, during which no dedoping occurs, proved to benefit the antibacterial action of these membranes.

This is the first time that a composite electroactive nanofibrous membrane is examined for its potential use in wound dressing applications, with promising results. The conducting properties introduced by means of PANI incorporation, can also potentially offer a tool for controlled release of bioactive substances and/or electrical excitation of cells for applications in the broader field of biomedicine.

7.2 Future Work

Based on the results of the work conducted so far, further research regarding the electrospinnability of conducting polymers is proposed, and more specifically regarding to prediction of fibre morphology based on measurements of the current carried by the fibres to the collector. Usually, this tool is being overlooked, and rarely acquainted in the literature, but in this study it has been found very useful in terms of explaining phenomena relating to the morphology for produced fibres. It could therefore be used for prediction models and for deepening the understanding the behavior of charged jets.

Also, an alternative stabilization method, which wouldn't dedope the polyaniline could be used for future work (eg crosslinking with genipin) with cells, or the use of an alternative acid anion during polymerization of aniline, which would render it stable in the alkaline conditions needed for neutralization, would be worthwhile investigating not only for biomedical applications but for any other field where the conductivity of PANI in alkaline environments needs to be maintained at high levels.

Based on the fact that PANI/CH electrospun scaffolds are not cytotoxic, further research for determining whether the fibroblast and osteoblast cell lines respond positively to electrical stimuli seems worthwhile and promising.

Another way to enhance the biological performance of the produced scaffolds would be the increase of their porosity, which could be achieved by expansion of the

electrospun membranes. Recently, a big part of the research relating to electrospun scaffolds is focusing on finding ways to increase porosity for better cell infiltration and many techniques have emerged. A combination of high porosity with electroactivity is expected to be very beneficial for tissue engineering applications [252].

Lastly, with the use of PANI/CH nanofibrous scaffolds, a controlled pulsatile release of encapsulated drugs or growth factors upon electrical stimulation, is expected to be achieved, combining the benefits of nanotopography on cell growth, the possibility for electrical stimulation and the inherent antibacterial properties of the materials.

REFERENCES

[1] CKMNT Centre for Knowledge Management of Nanoscience & Technology, "Nanofibers for Biomedical and Healthcare Applications," 2013.

[2] P. A. Margareth Gagliardi, "Global Markets and technologies or Nanofibers," 2016.

[3] V. Leung and F. Ko, "Biomedical applications of nanofibers," *Polym. Adv. Technol.*, vol. 22, no. 3, pp. 350–365, Mar. 2011.

[4] D. Liang, B. S. Hsiao, and B. Chu, "Functional electrospun nanofibrous scaffolds for biomedical applications," *Adv. Drug Deliv. Rev.*, vol. 59, no. 14, pp. 1392–1412, Dec. 2007.

[5] C. P. Barnes, S. A. Sell, E. D. Boland, D. G. Simpson, and G. L. Bowlin, "Nanofiber technology: Designing the next generation of tissue engineering scaffolds," *Adv. Drug Deliv. Rev.*, vol. 59, no. 14, pp. 1413–1433, Dec. 2007.

[6] D. G. Yu, C. Branford-White, L. Li, X. M. Wu, and L. M. Zhu, "The compatibility of acyclovir with polyacrylonitrile in the electrospun drug-loaded nanofibers," *J. Appl. Polym. Sci.*, vol. 117, no. 3, pp. 1509–1515, 2010.

[7] P. Datta, J. Chatterjee, and S. Dhara, "Electrospun nanofibers of a phosphorylated polymer-A bioinspired approach for bone graft applications," *Colloids Surfaces B Biointerfaces*, vol. 94, pp. 177–183, Jun. 2012.

[8] M. E. Frohbergh *et al.*, "Electrospun hydroxyapatite-containing chitosan nanofibers crosslinked with genipin for bone tissue engineering," *Biomaterials*, vol. 33, no. 36, pp. 9167–9178, Dec. 2012.

[9] Z. Zhang, J. Hu, and P. X. Ma, "Nanofiber-based delivery of bioactive agents and stem cells to bone sites," *Adv. Drug Deliv. Rev.*, vol. 64, no. 12, pp. 1129–1141, Sep. 2012.

[10] N. Bölgen, I. Vargel, P. Korkusuz, Y. Z. Menceloğ lu, and E. Piş kin, "In vivo performance of antibiotic embedded electrospun PCL membranes for prevention of abdominal adhesions," *J. Biomed. Mater. Res. - Part B Appl. Biomater.*, vol. 81, no. 2, pp. 530–543, 2007.

[11] J. Xie, M. M. R. MacEwan, A. G. A. Schwartz, and Y. Xia, "Electrospun nanofibers for neural tissue engineering.," *Nanoscale*, vol. 2, no. 1, pp. 35–44, 2010.

[12] S. Sahoo, L. T. Ang, J. Cho-Hong Goh, and S. L. Toh, "Bioactive nanofibers for fibroblastic differentiation of mesenchymal precursor cells for ligament/tendon tissue engineering applications," *Differentiation*, vol. 79, no. 2, pp. 102–110, Feb. 2010.

[13] X. Zhang, D. Bogdanowicz, C. Erisken, N. M. Lee, and H. H. Lu, "Biomimetic scaffold design for functional and integrative tendon repair," *J. Shoulder Elb. Surg.*, vol. 21, no. 2, pp. 266–277, Mar. 2012.

[14] S. J. Kew *et al.*, "Regeneration and repair of tendon and ligament tissue using collagen fibre biomaterials," *Acta Biomater.*, vol. 7, no. 9, pp. 3237–3247, Sep.

2011.

[15] E. D. Boland, J. A. Matthews, K. J. Pawlowski, D. G. Simpson, G. E. Wnek, and G. L. Bowlin, "Electrospinning collagen and elastin: Preliminary vascular tissue engineering," *Front. Biosci.*, vol. 9, pp. 1422–1432, 2004.

[16] H. Wang, Y. Feng, Z. Fang, W. Yuan, and M. Khan, "Co-electrospun blends of PU and PEG as potential biocompatible scaffolds for small-diameter vascular tissue engineering," *Mater. Sci. Eng. C*, vol. 32, no. 8, pp. 2306–2315, Dec. 2012.

[17] Y. Orlova, N. Magome, L. Liu, Y. Chen, and K. Agladze, "Electrospun nanofibers as a tool for architecture control in engineered cardiac tissue," *Biomaterials*, vol. 32, no. 24, pp. 5615–5624, Aug. 2011.

[18] A. G. Guex *et al.*, "Fine-tuning of substrate architecture and surface chemistry promotes muscle tissue development," *Acta Biomater.*, vol. 8, no. 4, pp. 1481–1489, Apr. 2012.

[19] M. Tian *et al.*, "Bis-GMA/TEGDMA dental composites reinforced with electrospun nylon 6 nanocomposite nanofibers containing highly aligned fibrillar silicate single crystals," *Polymer (Guildf).*, vol. 48, no. 9, pp. 2720–2728, Apr. 2007.

[20] F. M. Chen, M. Zhang, and Z. F. Wu, "Toward delivery of multiple growth factors in tissue engineering," *Biomaterials*, vol. 31, no. 24, pp. 6279–6308, Aug. 2010.

[21] W. Li, R. M. Shanti, and R. S. Tuan, "Electrospinning Technology for Nanofibrous Scaffolds in Tissue Engineering," in *Nanotechnologies for the Life Sciences*, vol. 9, no. October 2015, K. CSSR, Ed. Wiley-VCH, 2006, pp. 135–187.

[22] S. Y. Chew, R. Mi, A. Hoke, and K. W. Leong, "Aligned Protein–Polymer Composite Fibers Enhance Nerve Regeneration: A Potential Tissue-Engineering Platform," *Adv. Funct. Mater.*, vol. 17, no. 8, pp. 1288–1296, 2007.

[23] H. Wang *et al.*, "The inhibition of tumor growth and metastasis by self-assembled nanofibers of taxol," *Biomaterials*, vol. 33, no. 24, pp. 5848–5853, 2012.

[24] S. T. Yohe, V. L. M. Herrera, Y. L. Colson, and M. W. Grinstaff, "3D superhydrophobic electrospun meshes as reinforcement materials for sustained local drug delivery against colorectal cancer cells," *J. Control. Release*, vol. 162, no. 1, pp. 92–101, Aug. 2012.

[25] R. Toshkova *et al.*, "Antitumor activity of quaternized chitosan-based electrospun implants against Graffi myeloid tumor," *Int. J. Pharm.*, vol. 400, no. 1–2, pp. 221–233, 2010.

[26] P. on Rujitanaroj, Y. C. Wang, J. Wang, and S. Y. Chew, "Nanofiber-mediated controlled release of siRNA complexes for long term gene-silencing applications," *Biomaterials*, vol. 32, no. 25, pp. 5915–5923, Sep. 2011.

[27] H. S. Kim and H. S. Yoo, "MMPs-responsive release of DNA from electrospun nanofibrous matrix for local gene therapy: In vitro and in vivo evaluation," *J. Control. Release*, vol. 145, no. 3, pp. 264–271, 2010.

[28] G. Buschle-Diller, J. Cooper, Z. Xie, Y. Wu, J. Waldrup, and X. Ren, "Release of antibiotics from electrospun bicomponent fibers," *Cellulose*, vol. 14, no. 6, pp. 553–562, Oct. 2007.

[29] H. S. Yoo, T. G. Kim, and T. G. Park, "Surface-functionalized electrospun nanofibers for tissue engineering and drug delivery," *Adv. Drug Deliv. Rev.*, vol. 61, no. 12, pp. 1033–1042, Oct. 2009.

[30] V. Holan *et al.*, "Cyclosporine A-loaded and stem cell-seeded electrospun nanofibers for cell-based therapy and local immunosuppression," *J. Control. Release*, vol. 156, no. 3, pp. 406–412, Dec. 2011.

[31] A. Formhals, "Process and apparatus for preparing artificial threads," 1975504, 1934.

[32] L. A. Bosworth, N. Alam, J. K. Wong, and S. Downes, "Investigation of 2D and 3D electrospun scaffolds intended for tendon repair," *J. Mater. Sci. Mater. Med.*, vol. 24, no. 6, pp. 1605–1614, 2013.

[33] M. F. Leong, H. F. Lu, T. C. Lim, C. Du, N. K. L. Ma, and A. C. A. Wan, "Electrospun polystyrene scaffolds as a synthetic substrate for xeno-free expansion and differentiation of human induced pluripotent stem cells," *Acta Biomater.*, vol. 46, pp. 266–277, 2016.

[34] G. R. Mitchell, K. Ahn, and F. J. Davis, "The potential of electrospinning in rapid manufacturing processes," *Virtual Phys. Prototyp.*, vol. 6, no. 2, pp. 63–77, 2011.

[35] L. Moroni, R. Schotel, D. Hamann, J. R. De Wijn, and C. A. Van Blitterswijk, "3D fiber-deposited electrospun integrated scaffolds enhance cartilage tissue formation," *Adv. Funct. Mater.*, vol. 18, no. 1, pp. 53–60, 2008.

[36] M. Kim, J. Son, H. Lee, H. Hwang, C. H. Choi, and G. Kim, "Highly porous 3D nanofibrous scaffolds processed with an electrospinning/laser process," *Curr. Appl. Phys.*, vol. 14, no. 1, pp. 1–7, 2014.

[37] V. Beachley and X. Wen, "Polymer nanofibrous structures: Fabrication, biofunctionalization, and cell interactions," *Prog. Polym. Sci.*, vol. 35, no. 7, pp. 868–892, Jul. 2010.

[38] P. Sadatmousavi, T. Mamo, and P. Chen, "Diethylene glycol functionalized self-assembling peptide nanofibers and their hydrophobic drug delivery potential," *Acta Biomater.*, vol. 8, no. 9, pp. 3241–3250, Sep. 2012.

[39] L. Feng *et al.*, "Super-hydrophobic surface of aligned polyacrylonitrile nanofibers," *Angew. Chemie - Int. Ed.*, vol. 41, no. 7, pp. 1221–1223, 2002.

[40] J. R. Porter, A. Henson, and K. C. Popat, "Biodegradable poly(e-caprolactone) nanowires for bone tissue engineering applications," *Biomaterials*, vol. 30, no. 5, pp. 780–788, Feb. 2009.

[41] S. Grimm *et al.*, "Nondestructive replication of self-ordered nanoporous alumina membranes via cross-linked polyacrylate nanofiber arrays," *Nano Lett.*, vol. 8, no. 7, pp. 1954–1959, Jul. 2008.

[42] Y. Z. Longa *et al.*, "Recent advances in synthesis, physical properties, and applications of conducting polymer nanotubes and nanofibers," *Prog. Polym.*

Sci., vol. 36, no. 10, pp. 1415–1442, Oct. 2011.

[43] J. Shao, C. Chen, Y. Wang, X. Chen, and C. Du, "Early stage structural evolution of PLLA porous scaffolds in thermally induced phase separation process and the corresponding biodegradability and biological property," *Polym. Degrad. Stab.*, vol. 97, no. 6, pp. 955–963, Jun. 2012.

[44] J. Bajakova, J. Chaloupek, M. Lacarin, and D. Lukáš, "'Drawing'- the Production of Individual Nanofibers By Experimental Method," in *Nanocon*, 2011, vol. 9, no. 1, pp. 21–23.

[45] A. S. Nain, J. C. Wong, C. Amon, and M. Sitti, "Drawing suspended polymer micro-/nanofibers using glass micropipettes," *Appl. Phys. Lett.*, vol. 89, no. 18, p. 183105, 2006.

[46] A. Chanthakulchan, P. Koomsap, and K. Auyson, "Development of an electrospinning-based rapid prototyping for scaffold fabrication," *Rapid Prototyp. J.*, vol. 21, no. 3, pp. 329–339, 2014.

[47] D. Li and Y. Xia, "Electrospinning of nanofibers: Reinventing the wheel?," *Adv. Mater.*, vol. 16, no. 14, pp. 1151–1170, Jul. 2004.

[48] B. Wang, Y. Wang, T. Yin, and Q. Yu, "Applications of Electrospinning Technique in Drug Delivery," *Chem. Eng. Commun.*, vol. 197, no. 10, pp. 1315–1338, Jun. 2010.

[49] C. J. Angammana and S. H. Jayaram, "A Theoretical Understanding of the Physical Mechanisms of Electrospinning," in *ESA Annual Meeting on Electrostatics*, 2011, pp. 1–9.

[50] D. H. Reneker, A. L. Yarin, H. Fong, and S. Koombhongse, "Bending instability of electrically charged liquid jets of polymer solutions in electrospinning," *J. Appl. Phys.*, vol. 87, no. 9, pp. 4531–4547, 2000.

[51] M. M. Hohman, M. Shin, G. Rutledge, and M. P. Brenner, "Electrospinning and electrically forced jets. I. Stability theory," *Phys. Fluids*, vol. 13, no. 8, pp. 2201–2220, 2001.

[52] S. V Fridrikh, J. H. Yu, M. P. Brenner, and G. C. Rutledge, "Controlling the Fiber Diameter During Electrospinning," *Phys. Rev. Lett.*, vol. 90, no. 14, p. 144502, Apr. 2003.

[53] M. M. Hohman, M. Shin, G. Rutledge, and M. P. Brenner, "Electrospinning and electrically forced jets. II. Applications," *Phys. Fluids*, vol. 13, no. 8, pp. 2221–2236, 2001.

[54] C. J. Angammana and S. H. Jayaram, "Analysis of the effects of solution conductivity on electrospinning process and fiber morphology," *IEEE Trans. Ind. Appl.*, vol. 47, no. 3, pp. 1109–1117, 2011.

[55] C. J. Thompson, G. G. Chase, A. L. Yarin, and D. H. Reneker, "Effects of parameters on nanofiber diameter determined from electrospinning model," *Polymer (Guildf).*, vol. 48, no. 23, pp. 6913–6922, Nov. 2007.

[56] S. Rafiei, S. Maghsoodloo, B. Noroozi, V. Mottaghitalab, and a K. Haghi, "Mathematical modeling in electrospinning process of nanofibers: a detailed

review," *Cellul. Chem. Technol.*, vol. 47, pp. 323–338, 2013.

[57] C. Sun, Y. Boluk, and C. Ayranci, "Investigation of nanofiber nonwoven meshes produced by electrospinning of cellulose nanocrystal suspensions in cellulose acetate solutions," *Cellulose*, vol. 22, no. 4, pp. 2457–2470, 2015.

[58] A. F. M. Barton, *CRC Handbook of Solubility Parameters and Other Cohesive Parameters*, 2 nd. CRC Press, 1991.

[59] K. A. G. Katsogiannis, G. T. Vladisavljević , and S. Georgiadou, "Porous electrospun polycaprolactone fibers: Effect of process parameters," *J. Polym. Sci. Part B Polym. Phys.*, vol. 54, no. 18, pp. 1878–1888, 2016.

[60] J. Lannutti, D. Reneker, T. Ma, D. Tomasko, and D. Farson, "Electrospinning for tissue engineering scaffolds," *Mater. Sci. Eng. C*, vol. 27, no. 3, pp. 504–509, Apr. 2007.

[61] V. Pillay *et al.*, "A review of the effect of processing variables on the fabrication of electrospun nanofibers for drug delivery applications," *J. Nanomater.*, vol. 2013, pp. 1–22, 2013.

[62] S. Megelski, J. S. Stephens, D. B. Chase, and J. F. Rabolt, "Micro- and Nanostructured Surface Morphology on Electrospun Polymer Fibers," pp. 8456–8466, 2002.

[63] F. Kayaci and T. Uyar, "Electrospun zein nanofibers incorporating cyclodextrins," *Carbohydr. Polym.*, vol. 90, no. 1, pp. 558–568, Sep. 2012.

[64] P. Bébin and R. E. Prud'Homme, "Effect of comp drif," *J. Polym. Sci. Part B Polym. Phys.*, vol. 39, no. 1, pp. 2363–2377, 2001.

[65] S. Torres-Giner, M. J. Ocio, and J. M. Lagaron, "Development of active antimicrobial fiber based chitosan polysaccharide nanostructures using electrospinning," *Eng. Life Sci.*, vol. 8, no. 3, pp. 303–314, Jun. 2008.

[66] D. Ben-yaakov, D. Andelman, R. Podgornik, D. Ben-yaakov, D. Andelman, and R. Podgornik, "Dielectric decrement as a source of ion-specific effects," vol. 74705, 2011.

[67] R. A. Stairs, "Calculation of surface tension of salt solutions: effective polarizability of solvated ions," vol. 787, pp. 781–787, 1995.

[68] S. Agarwal, A. Greiner, and J. H. Wendorff, "Progress in Polymer Science Functional materials by electrospinning of polymers," *Prog. Polym. Sci.*, vol. 38, no. 6, pp. 963–991, 2013.

[69] H. Dong, V. Nyame, A. G. Macdiarmid, and W. E. Jones, "Polyaniline/poly(methyl methacrylate) coaxial fibers: The fabrication and effects of the solution properties on the morphology of electrospun core fibers," *J. Polym. Sci. Part B Polym. Phys.*, vol. 42, no. 21, pp. 3934–3942, Nov. 2004.

[70] T. J. Sill and H. A. von Recum, "Electrospinning: Applications in drug delivery and tissue engineering," *Biomaterials*, vol. 29, no. 13, pp. 1989–2006, 2008.

[71] S. Izwan *et al.*, "A Review of Electrospun Conductive Polyaniline Based Nanofiber Composites and Blends : Processing Features , Applications , and

Future Directions," *Adv. MA*, vol. 2015, 2015.

[72] C. Wang, C. H. Hsu, and J. H. Lin, "Scaling laws in electrospinning of polystyrene solutions," *Macromolecules*, vol. 39, no. 22, pp. 7662–7672, 2006.

[73] P. Moutsatsou, K. Coopman, M. B. Smith, and S. Georgiadou, "Conductive PANI fibers and determining factors for the electrospinning window," *Polym. (United Kingdom)*, vol. 77, pp. 143–151, Oct. 2015.

[74] H. Fong, I. Chun, and D. H. Reneker, "Beaded Nanofibers Formed During Electrospinning," *Polymer (Guildf).*, vol. 3861, no. July 1999, pp. 4585–4592, 2016.

[75] J. H. Yu, S. V. Fridrikh, and G. C. Rutledge, "The role of elasticity in the formation of electrospun fibers," *Polymer*, vol. 47, no. 13. pp. 4789–4797, 2006.

[76] R. Rošic, J. Pelipenko, P. Kocbek, S. Baumgartner, M. Bešter-Rogač , and J. Kristl, "The role of rheology of polymer solutions in predicting nanofiber formation by electrospinning," *Eur. Polym. J.*, vol. 48, no. 8, pp. 1374–1384, Aug. 2012.

[77] R. M. Nezarati, M. B. Eifert, and E. Cosgriff-Hernandez, "Effects of humidity and solution viscosity on electrospun fiber morphology," *Tissue Eng. Part C Methods*, vol. 19, no. 10, pp. 810–819, 2013.

[78] M. G. Mckee, J. M. Layman, M. P. Cashion, and T. E. Long, "Phospholipid Nonwoven Electrospun Membranes," *Science (80-.).*, vol. 311, no. 5759, pp. 353–355, 2006.

[79] A. K. Haghi and M. Akbari, "Trends in electrospinning of natural nanofibers," *Phys. Status Solidi Appl. Mater. Sci.*, vol. 204, no. 6, pp. 1830–1834, 2007.

[80] Q. Yang *et al.*, "Influence of solvents on the formation of ultrathin uniform poly(vinyl pyrrolidone) nanofibers with electrospinning," *J. Polym. Sci. Part B Polym. Phys.*, vol. 42, no. 20, pp. 3721–3726, 2004.

[81] C. Zhang and X. Yuan, "Study on morphology of electrospun poly (vinyl alcohol) mats," *Eur. Polym. J.*, vol. 41, pp. 423–432, 2005.

[82] C. A. Bonino *et al.*, "Electrospinning alginate-based nanofibers: From blends to crosslinked low molecular weight alginate-only systems," *Carbohydr. Polym.*, vol. 85, no. 1, pp. 111–119, Apr. 2011.

[83] I. S. Chronakis, S. Grapenson, and A. Jakob, "Conductive polypyrrole nanofibers via electrospinning: Electrical and morphological properties," *Polymer (Guildf).*, vol. 47, no. 5, pp. 1597–1603, Feb. 2006.

[84] W. Tomaszewski, W. Swieszkowski, M. Szadkowski, M. Kudra, and D. Ciechanska, "Simple methods influencing on properties of electrospun fibrous mats," *J. Appl. Polym. Sci.*, vol. 125, no. 6, pp. 4261–4266, 2012.

[85] C. J. Angammana and S. H. Jayaram, "A Modified Electrospinning Method for Conductive and Insulating Materials," pp. 1–7, 2010.

[86] J. Fernández de la Mora, "The Fluid Dynamics of Taylor Cones," *Annu. Rev. Fluid Mech.*, vol. 39, no. 1, pp. 217–243, Jan. 2007.

[87] V. Beachley and X. Wen, "Effect of electrospinning parameters on the nanofiber diameter and length," *Mater. Sci. Eng. C*, vol. 29, no. 3, pp. 663–668, 2009.

[88] F. E. Ahmed, B. S. Lalia, and R. Hashaikeh, "A review on electrospinning for membrane fabrication: Challenges and applications," *Desalination*, vol. 356, pp. 15–30, Jan. 2015.

[89] J. . Deitzel, J. Kleinmeyer, D. Harris, and N. . Beck Tan, "The effect of processing variables on the morphology of electrospun nanofibers and textiles," *Polymer (Guildf).*, vol. 42, no. 1, pp. 261–272, 2001.

[90] G. Taylor, "Electrically driven jets," *Proc. R. Soc. London A*, vol. 313, no. 453–475, pp. 453–475, 1969.

[91] K. Garg and G. L. Bowlin, "Electrospinning jets and nanofibrous structures," *Biomicrofluidics*, vol. 5, no. 1, 2011.

[92] S. Li, G. Zheng, X. Wang, Y. Chen, D. Wu, and D. Sun, "Improved Electrical Conductivity of PANI / PEO Polymer via Electrospinning and its Application as NH 3 Gas Sensor," in *Nems2013*, 2013, vol. 1, pp. 891–894.

[93] Y. Yang, Z. Jia, Q. Li, and Z. Guan, "Experimental investigation of the governing parameters in the electrospinning of polyethylene oxide solution," *IEEE Trans. Dielectr. Electr. Insul.*, vol. 13, no. 3, pp. 580–584, 2006.

[94] W. Pan, X. W. He, and Y. Chen, "Preparation and Characterization of Polyacrylonitrile-Polyaniline Blend Nanofibers," *Appl. Mech. Mater.*, vol. 44–47, pp. 2195–2198, Dec. 2010.

[95] T. Mitarai, A. Shander, M. Tight, N. Fabrics, F. N. Martin, and J. T. English, "An Introduction to Electrospinning and Nanofibers," in *Journal of cardiothoracic and vascular anesthesia*, vol. 27, 2013, pp. 1–21.

[96] J. Sutasinpromprae, S. Jitjaicham, M. Nithitanakul, C. Meechaisue, and P. Supaphol, "Preparation and characterization of ultrafine electrospun polyacrylonitrile fibers and their subsequent pyrolysis to carbon fibers," *Polym. Int.*, vol. 55, no. 8, pp. 825–833, 2006.

[97] Z. Li and C. Wang, "Chapter 2 - Effects of Working Parameters on Electrospinning," in *One-Dimensional nanostructures Electrospinning Technique and Unique Nanofibers*, Berlin, Heidelberg: Springer Berlin Heidelberg, 2013, pp. 15–29.

[98] P. Gupta and G. L. Wilkes, "Some investigations on the fiber formation by utilizing a side-by-side bicomponent electrospinning approach," *Polymer (Guildf).*, vol. 44, no. 20, pp. 6353–6359, 2003.

[99] C. Wang, H. S. Chien, C. H. Hsu, Y. C. Wang, C. T. Wang, and H. A. Lu, "Electrospinning of polyacrylonitrile solutions at elevated temperatures," *Macromolecules*, vol. 40, no. 22, pp. 7973–7983, 2007.

[100] X. Yan and M. Gevelber, "Electrospinning of nanofibers: Characterization of jet dynamics and humidity effects," *Part. Sci. Technol.*, pp. 1–11, 2015.

[101] S. De Vrieze, T. Van Camp, A. Nelvig, B. Hagström, P. Westbroek, and K. De Clerck, "The effect of temperature and humidity on electrospinning," *J. Mater. Sci.*, vol. 44, no. 5, pp. 1357–1362, Oct. 2009.

[102] S. Tripatanasuwan, Z. Zhong, and D. H. Reneker, "Effect of evaporation and

solidification of the charged jet in electrospinning of poly(ethylene oxide) aqueous solution," *Polymer (Guildf).*, vol. 48, no. 19, pp. 5742–5746, Sep. 2007.

[103] C. L. Casper and J. S. Stephens, "Controlling Surface Morphology of Electrospun Polysterene Fibers: Effect of Humidity and Molecular Weight in Electrospinning Process," *Macromolecules*, vol. 37, pp. 573–578, 2004.

[104] C. Mit-uppatham, M. Nithitanakul, and P. Supaphol, "Ultrafine electrospun polyamide-6 fibers: Effect of solution conditions on morphology and average fiber diameter," *Macromol. Chem. Phys.*, vol. 205, no. 17, pp. 2327–2338, 2004.

[105] M. Lauricella, G. Pontrelli, I. Coluzza, D. Pisignano, and S. Succi, "JETSPIN: A specific-purpose open-source software for simulations of nanofiber electrospinning," *Comput. Phys. Commun.*, vol. 197, pp. 227–238, 2015.

[106] a. L. Yarin, S. Koombhongse, and D. H. Reneker, "Bending instability in electrospinning of nanofibers," *J. Appl. Phys.*, vol. 89, no. 5, pp. 3018–3026, 2001.

[107] B Ranby, "Conjugated Polymers and Related Materials: The Interconnection of Chemical and Electronic Structure," in *Proceedings of the 81st Nobel Symposium*, 1993, p. 502.

[108] A. J. Heeger, "Semiconducting and Metallic Polymers: The Fourth Generation of Polymeric Materials (Nobel Lecture)," *Angew. Chem. Int. Ed. Engl.*, vol. 40, no. 14, pp. 2591–2611, 2001.

[109] A. J. Heeger, "Semiconducting polymers: the Third Generation," *Chem. Soc. Rev.*, vol. 39, no. 7, p. 2354, Jul. 2010.

[110] D. Svirskis, J. Travas-Sejdic, A. Rodgers, and S. Garg, "Electrochemically controlled drug delivery based on intrinsically conducting polymers," *J. Control. Release*, vol. 146, no. 1, pp. 6–15, Aug. 2010.

[111] X. Liu, "Effective control of cell behavior on conducting polymers," University of Wollongong, 2009.

[112] B. Wessling, "New insight into Organic Metal Polyaniline Morphology and Structure," *Polymers (Basel).*, vol. 2, no. 4, pp. 786–798, Dec. 2010.

[113] L. Dai, "Chapter 2. Conducting Polymers," in *Intelligent Macromolecules for Smart Devices*, London: Spinger - Verlag London Limited, 2004, pp. 41–80.

[114] B. Wessling, "Conductive Polymers as Organic Nanometals," *Handb. Nanostructured Mater. Nanotechnol.*, no. January 2000, pp. 501–575, 2000.

[115] N. K. Guimard, N. Gomez, and C. E. Schmidt, "Conducting polymers in biomedical engineering," *Prog. Polym. Sci.*, vol. 32, no. 8–9, pp. 876–921, 2007.

[116] A. Ray, A. F. Richter, A. G. MacDiarmid, and A. J. Epstein, "Polyaniline: protonation/deprotonation of amine and imine sites," *Synth. Met.*, vol. 29, no. 1, pp. 151–156, 1989.

[117] A. G. MacDiarmid, S. K. Manohar, J. G. Masters, Y. Sun, and H. Weiss, "Polyaniline: Synthesis and Properties of Pernigraniline Base," *Synth. Met.*, vol. 41–43, no. 9, pp. 621–626, 1991.

[118] K. M. Molapo *et al.*, "Electronics of Conjugated Polymers (I): Polyaniline," *Int. J.*

Electrochem. Sci., vol. 7, pp. 11859–11875, 2012.

[119] C. Li *et al.*, "Electrospun Polyaniline/Poly(ethylene oxide) Composite Nanofibers Based Gas Sensor," *Electroanalysis*, vol. 26, no. 4, pp. 711–722, Apr. 2014.

[120] T. Thanpitcha, A. Sirivat, A. M. Jamieson, and R. Rujiravanit, "Preparation and characterization of polyaniline/chitosan blend film," *Carbohydr. Polym.*, vol. 64, no. 4, pp. 560–568, Jun. 2006.

[121] M. J. D. León, "Electrospinning Nanofibers of Polyaniline and Polyaniline / (Polystyrene and Polyethylene Oxide) Blends Abstract," in *Microscope*, 2001, vol. 1, pp. 1–5.

[122] T. H. Qazi, R. Rai, and A. R. Boccaccini, "Tissue engineering of electrically responsive tissues using polyaniline based polymers: A review," *Biomaterials*, vol. 35, no. 33, pp. 9068–9086, Aug. 2014.

[123] Y. Cao, P. Smith, and A. J. Heeger, "Counter-ion induced processibility of conducting polyaniline and of conducting polyblends of polyaniline in bulk polymers," *Synth. Met.*, vol. 48, no. 1, pp. 91–97, 1992.

[124] M. M. Ayad and E. A. Zaki, "Doping of polyaniline films with organic sulfonic acids in aqueous media and the effect of water on these doped films," *Eur. Polym. J.*, vol. 44, no. 11, pp. 3741–3747, 2008.

[125] J. Prokeš and J. Stejskal, "Polyaniline prepared in the presence of various acids: 2. Thermal stability of conductivity," *Polym. Degrad. Stab.*, vol. 86, no. 1, pp. 187–195, Oct. 2004.

[126] S. Bhadra, D. Khastgir, N. K. Singha, and J. H. Lee, "Progress in preparation, processing and applications of polyaniline," *Prog. Polym. Sci.*, vol. 34, no. 8, pp. 783–810, Aug. 2009.

[127] J. Jin, Q. Wang, and M. A. Haque, "Doping dependence of electrical and thermal conductivity of nanoscale polyaniline thin films," *J. Phys. D. Appl. Phys.*, vol. 43, no. 20, p. 205302, May 2010.

[128] T. Hodgkinson, X.-F. Yuan, and A. Bayat, "Electrospun silk fibroin fiber diameter influences in vitro dermal fibroblast behavior and promotes healing of ex vivo wound models," *J. Tissue Eng.*, vol. 5, p. 2041731414551661, 2014.

[129] A. Moayeri and A. Ajji, "Fabrication of polyaniline/poly (ethylene oxide)/non-covalently functionalized graphene nanofibers via electrospinning," *Synth. Met.*, vol. 200, pp. 7–15, 2015.

[130] A. Attout, S. Yunus, and P. Bertrand, "Electrospinning and alignment of polyaniline-based nanowires and nanotubes," in *Polymer Engineering and Science*, 2008, vol. 48, no. 9, pp. 1661–1666.

[131] A. Laforgue and L. Robitaille, "Fabrication of poly-3-hexylthiophene/polyethylene oxide nanofibers using electrospinning," *Synth. Met.*, vol. 158, no. 14, pp. 577–584, Aug. 2008.

[132] A. Subramanian, U. M. Krishnan, and S. Sethuraman, "Axially aligned electrically conducting biodegradable nanofibers for neural regeneration," *J. Mater. Sci. Mater. Med.*, vol. 23, no. 7, pp. 1797–1809, Jul. 2012.

[133] Y. Sharma *et al.*, "Fabrication of conducting electrospun nanofibers scaffold for three-dimensional cells culture," *Int. J. Biol. Macromol.*, vol. 51, no. 4, pp. 627–631, Nov. 2012.

[134] S. I. Jeong, I. D. Jun, M. J. Choi, Y. C. Nho, Y. M. Lee, and H. Shin, "Development of electroactive and elastic nanofibers that contain polyaniline and poly(L-lactide-co-ε -caprolactone) for the control of cell adhesion," *Macromol. Biosci.*, vol. 8, no. 7, pp. 627–637, Jul. 2008.

[135] A. G. MacDiarmid *et al.*, "Electrostatically-generated nanofibers of electronic polymers," *Synth. Met.*, vol. 119, no. 1–3, pp. 27–30, 2001.

[136] J. R. Cardenas, M. G. O. de Franca, E. A. de Vasconcelos, W. M. de Azevedo, and E. F. da Silva Jr., "Growth of sub-micron fibres of pure polyaniline using the electrospinning technique," *J. Phys. D. Appl. Phys.*, vol. 40, no. 4, pp. 1068–1071, Feb. 2007.

[137] Q. Z. Yu, M. M. Shi, M. Deng, M. Wang, and H. Z. Chen, "Morphology and conductivity of polyaniline sub-micron fibers prepared by electrospinning," *Mater. Sci. Eng. B Solid-State Mater. Adv. Technol.*, vol. 150, no. 1, pp. 70–76, Apr. 2008.

[138] J. Xie *et al.*, "Conductive Core-Sheath Nanofibers and Their Potential Application in Neural Tissue Engineering," *Adv. Funct. Mater.*, vol. 19, no. 14, pp. 2312–2318, Jul. 2009.

[139] J. Y. Lee, C. a Bashur, A. S. Goldstein, and C. E. Schmidt, "Polypyrrole-coated electrospun PLGA nanofibers for neural tissue applications," *Biomaterials*, vol. 30, no. 26, pp. 4325–35, Sep. 2009.

[140] H. Dong and W. E. Jones, "Preparation of submicron polypyrrole/poly(methyl methacrylate) coaxial fibers and conversion to polypyrrole tubes and carbon tubes," *Langmuir*, vol. 22, no. 26, pp. 11384–11387, Dec. 2006.

[141] S. Ji, Y. Li, and M. Yang, "Gas sensing properties of a composite composed of electrospun poly(methyl methacrylate) nanofibers and in situ polymerized polyaniline," *Sensors Actuators, B Chem.*, vol. 133, no. 2, pp. 644–649, Aug. 2008.

[142] Y. Xia, X. Lu, and H. Zhu, "Natural silk fibroin/polyaniline (core/shell) coaxial fiber: Fabrication and application for cell proliferation," *Compos. Sci. Technol.*, vol. 77, pp. 37–41, Mar. 2013.

[143] Y. Zhang, Z.-M. Huang, X. Xu, C. T. Lim, and S. Ramakrishna, "Preparation of Core-Shell Structured PCL-r-Gelatin Bi-Component Nanofibers by Coaxial Electrospinning," *Chem. Mater.*, vol. 16, no. 20, pp. 3406–3409, 2004.

[144] I. Moreno, V. González-González, and J. Romero-García, "Control release of lactate dehydrogenase encapsulated in poly (vinyl alcohol) nanofibers via electrospinning," *Eur. Polym. J.*, vol. 47, no. 6, pp. 1264–1272, Jun. 2011.

[145] D. Li and Y. Xia, "Direct fabrication of composite and ceramic hollow nanofibers by electrospinning," *Nano Lett.*, vol. 4, no. 5, pp. 933–938, May 2004.

[146] D. Chen, Y. E. Miao, and T. Liu, "Electrically conductive polyaniline/polyimide nanofiber membranes prepared via a combination of electrospinning and

subsequent in situ polymerization growth," *ACS Appl. Mater. Interfaces*, vol. 5, no. 4, pp. 1206–1212, 2013.

[147] M. R. Abidian, D. H. Kim, and D. C. Martin, "Conducting-polymer nanotubes for controlled drug release," *Adv. Mater.*, vol. 18, no. 4, pp. 405–409, Mar. 2006.

[148] A. A. Pud, "Stability and degradation of conducting polymers in electrochemical systems," *Synth. Met.*, vol. 66, no. 1, pp. 1–18, 1994.

[149] T. S. Tsai *et al.*, "A polyvinyl alcohol-polyaniline based electro-conductive hydrogel for controlled stimuli-actuable release of indomethacin," *Polymers (Basel).*, vol. 3, no. 1, pp. 150–172, Jan. 2011.

[150] A. P. Andrezej Franek, Roman Kostur, Jakub Taradaj, Edward Blaszczak, Zbigniew Dolibog, "Effect of High Voltage Monophasic Stimulation on Pressure Ulcer Healing: Results From a Randomized Controlled Trial," *Wounds*, vol. 23, no. 1, pp. 15–23, 2011.

[151] E. T. Ahmad, "High-voltage pulsed galvanic stimulation: effect of treatment duration on healing of chronic pressure ulcers.," *Ann. Burns Fire Disasters*, vol. 21, no. 3, pp. 124–8, 2008.

[152] R. Balint, N. J. Cassidy, and S. H. Cartmell, "Electrical Stimulation: A Novel Tool for Tissue Engineering," *Tissue Eng. Part B-Reviews*, vol. 19, no. 1, pp. 48–57, 2013.

[153] T. J. Rivers, T. W. Hudson, and C. E. Schmidt, "Synthesis of a novel, biodegradable electrically conducting polymer for biomedical applications," *Adv. Funct. Mater.*, vol. 12, no. 1, pp. 33–37, Jan. 2002.

[154] A. Kotwal and C. E. Schmidt, "Electrical stimulation alters protein adsorption and nerve cell interactions with electrically conducting biomaterials," *Biomaterials*, vol. 22, no. 10, pp. 1055–1064, May 2001.

[155] M. E. Mycielska and M. B. a Djamgoz, "Cellular mechanisms of direct-current electric field effects: galvanotaxis and metastatic disease," *J. Cell Sci.*, vol. 117, no. Pt 9, pp. 1631–1639, Apr. 2004.

[156] M. Rouabhia, H. Park, S. Meng, H. Derbali, and Z. Zhang, "Electrical stimulation promotes wound healing by enhancing dermal fibroblast activity and promoting myofibroblast transdifferentiation.," *PLoS One*, vol. 8, no. 8, p. e71660, Jan. 2013.

[157] T. Lindfors, H. Aarnio, and A. Ivaska, "Potassium-selective electrodes with stable and geometrically well-defined internal solid contact based on nanoparticles of polyaniline and plasticized poly(vinyl chloride)," *Anal. Chem.*, vol. 79, no. 22, pp. 8571–8577, 2007.

[158] M. Li, Y. Guo, Y. Wei, A. G. MacDiarmid, and P. I. Lelkes, "Electrospinning polyaniline-contained gelatin nanofibers for tissue engineering applications," *Biomaterials*, vol. 27, no. 13, pp. 2705–2715, May 2006.

[159] V. Guarino, M. A. Alvarez-perez, A. Borriello, T. Napolitano, and L. Ambrosio, "Conductive PANi / PEGDA Macroporous Hydrogels For Nerve Regeneration," *Adv. Healthc. Mater.*, vol. 2, pp. 218–227, 2013.

[160] H.-S. Kim, H. L. Hobbs, L. Wang, M. J. Rutten, and C. C. Wamser, "Biocompatible composites of polyaniline nanofibers and collagen," *Synth. Met.*, vol. 159, no. 13, pp. 1313–1318, Jul. 2009.

[161] J. C. C. Wu *et al.*, "Nanostructured bioactive material based on polycaprolactone and polyaniline fiber-scaffolds," *Synth. Met.*, vol. 198, pp. 41–50, 2014.

[162] M. Chen, Y. Sun, and Y. Chen, "Electrically conductive nanofibers with highly oriented structures and their potential application in skeletal muscle tissue engineering SN," *Acta Biomater.*, vol. 9, pp. 5562–5572, 2013.

[163] M. P. Prabhakaran, L. Ghasemi-Mobarakeh, G. Jin, and S. Ramakrishna, "Electrospun conducting polymer nanofibers and electrical stimulation of nerve stem cells," *J. Biosci. Bioeng.*, vol. 112, no. 5, pp. 501–507, Nov. 2011.

[164] H. Baniasadi, A. Ramazani S.A., and S. Mashayekhan, "Fabrication and characterization of conductive chitosan/gelatin-based scaffolds for nerve tissue engineering," *Int. J. Biol. Macromol.*, vol. 74, pp. 360–366, 2015.

[165] T. G. Kim and T. G. Park, "Biodegradable polymer nanocylinders fabricated by transverse fragmentation of electrospun nanofibers through aminolysis," *Macromol. Rapid Commun.*, vol. 29, no. 14, pp. 1231–1236, Jul. 2008.

[166] P. R. Bidez, S. Li, A. G. Macdiarmid, E. C. Venancio, Y. Wei, and P. I. Lelkes, "Polyaniline, an electroactive polymer, supports adhesion and proliferation of cardiac myoblasts," *J. Biomater. Sci. Polym. Ed.*, vol. 17, no. January 2014, pp. 199–212, Jan. 2006.

[167] P. Humpolicek, V. Kasparkova, P. Saha, and J. Stejskal, "Biocompatibility of polyaniline," *Synth. Met.*, vol. 162, no. 7–8, pp. 722–727, May 2012.

[168] E. Llorens, E. Armelin, M. del M. Pérez-Madrigal, L. J. del Valle, C. Alemán, and J. Puiggalí, "Nanomembranes and nanofibers from biodegradable conducting polymers," *Polymers (Basel).*, vol. 5, no. 3, pp. 1115–1157, Sep. 2013.

[169] X. Ma, J. Ge, Y. Li, B. Guo, and P. X. Ma, "Nanofibrous electroactive scaffolds from a chitosan-grafted-aniline tetramer by electrospinning for tissue engineering," *RSC Adv.*, vol. 4, no. 26, pp. 13652–13661, 2014.

[170] M. R. Gizdavic-Nikolaidis, J. R. Bennett, S. Swift, A. J. Easteal, and M. Ambrose, "Broad spectrum antimicrobial activity of functionalized polyanilines," *Acta Biomater.*, vol. 7, no. 12, pp. 4204–4209, Dec. 2011.

[171] Z. Kucekova, V. Kasparkova, P. Humpolicek, P. Sevcikova, and J. Stejskal, "Antibacterial properties of polyaniline-silver films," *Chem. Pap.*, vol. 67, no. 8, pp. 1103–1108, Jan. 2013.

[172] M. Gizdavic-Nikolaidis, S. Ray, J. R. Bennett, A. J. Easteal, and R. P. Cooney, "Electrospun Functionalized Polyaniline Copolymer-Based Nanofibers with Potential Application in Tissue Engineering," *Macromol. Biosci.*, vol. 10, no. 12, pp. 1424–1431, Dec. 2010.

[173] C. Dhivya, S. A. A. Vandarkuzhali, and N. Radha, "Antimicrobial activities of nanostructured polyanilines doped with aromatic nitro compounds," *Arab. J. Chem.*, Dec. 2014.

[174] S. Kamalesh, P. Tan, J. Wang, T. Lee, E. T. Kang, and C. H. Wang, "Biocompatibility of electroactive polymers in tissues," *J. Biomed. Mater. Res.*, vol. 52, no. 3, pp. 467–478, 2000.

[175] C. H. Wang, Y. Q. Dong, K. Sengothi, K. L. Tan, and E. T. Kang, "In-vivo tissue response to polyaniline," *Synth. Met.*, vol. 102, no. 1–3, pp. 1313–1314, 1999.

[176] M. Mattioli-Belmonte *et al.*, "Tailoring biomaterial compatibility: In vivo tissue response versus in vitro cell behavior," *Int. J. Artif. Organs*, vol. 26, no. 12, pp. 1077–1085, 2003.

[177] Y. Zhang and G. C. Rutledge, "Electrical conductivity of electrospun polyaniline and polyaniline-blend fibers and mats," *Macromolecules*, vol. 45, no. 10, pp. 4238–4246, 2012.

[178] C. Merlini, A. Pegoretti, T. M. Araujo, S. D. A. S. Ramoa, W. H. Schreiner, and G. M. De Oliveira Barra, "Electrospinning of doped and undoped-polyaniline/poly(vinylidene fluoride) blends," *Synth. Met.*, vol. 213, pp. 34–41, Mar. 2016.

[179] R. Castagna *et al.*, "Ultrathin electrospun PANI nanofibers for neuronal tissue engineering," *J. Appl. Polym. Sci.*, vol. 133, no. 35, pp. 1–10, 2016.

[180] W. Serrano, A. Meléndez, I. Ramos, and N. J. Pinto, "Electrospun composite poly(lactic acid)/polyaniline nanofibers from low concentrations in CHCl3: Making a biocompatible polyester electro-active," *Polym. (United Kingdom)*, vol. 55, no. 22, pp. 5727–5733, 2014.

[181] M. Shahi, A. Moghimi, B. Naderizadeh, and B. Maddah, "Electrospun PVA–PANI and PVA–PANI– composite nanofibers," *Sci. Iran.*, vol. 18, no. 6, pp. 1327–1331, 2011.

[182] M. R. Karim, "Fabrication of electrospun aligned nanofibers from conducting polyaniline copolymer/polyvinyl alcohol/chitosan oligossacaride in aqueous solutions," *Synth. Met.*, vol. 178, pp. 34–37, 2013.

[183] M. K. Shin *et al.*, "Enhanced conductivity of aligned PANi/PEO/MWNT nanofibers by electrospinning," *Sensors Actuators, B Chem.*, vol. 134, no. 1, pp. 122–126, Aug. 2008.

[184] J. Stejskal and R. G. Gilbert, "Polyaniline - Preparation of a Conducting Polymer (IUPAC Technical Report)," *Pure Appl. Chem.*, vol. 74, no. 5, pp. 857–867, 2002.

[185] S. David, Y. F. Nicolau, F. Melis, and A. Revillon, "Molecular weight of polyaniline synthesized by oxidation of aniline with ammonium persulfate and with ferric chloride," *Synth. Met.*, vol. 69, no. 1–3, pp. 125–126, 1995.

[186] Z. Huang, Y. Zhang, M. Kotaki, and S. Ramakrishna, "A review on polymer nanofibers by electrospinning and their applications in nanocomposites," vol. 63, pp. 2223–2253, 2003.

[187] M. Pakravan, M. C. Heuzey, and A. Ajji, "A fundamental study of chitosan/PEO electrospinning," *Polymer (Guildf).*, vol. 52, no. 21, pp. 4813–4824, Sep. 2011.

[188] X. Geng, O. H. Kwon, and J. Jang, "Electrospinning of chitosan dissolved in concentrated acetic acid solution," *Biomaterials*, vol. 26, no. 27, pp. 5427–5432,

Sep. 2005.

[189] G. Ciric-Marjanovic, "Recent advances in polyaniline research: Polymerization mechanisms, structural aspects, properties and applications," *Synth. Met.*, vol. 177, no. 3, pp. 1–47, Aug. 2013.

[190] G. M. O. Barra, M. E. Leyva, B. G. Soares, L. H. Mattoso, and M. Sens, "Electrically conductive, melt-processed polyaniline/EVA blends," *J. Appl. Polym. Sci.*, vol. 82, no. 1, pp. 114–123, Oct. 2001.

[191] W. Rob, E. Victoria, K. B. Park, D. Walker, M. Hankin, and P. Taupin, *PEG and PEG conjugates toxicity: towards an understanding of the toxicity of PEG and its relevance to PEGylated biologicals*, no. February. Birkhäuser Basel, 2009.

[192] X. Y. Liu, J.-M. Nothias, A. Scavone, M. Garfinkel, and J. M. Millis, "Biocompatibility investigation of polyethylene glycol and alginate-poly-L-lysine for islet encapsulation," *ASAIO J. (American Soc. Artif. Intern. Organs)*, vol. 56, no. 3, pp. 241–245, 2010.

[193] J. Pelipenko, J. Kristl, B. Janković , S. Baumgartner, and P. Kocbek, "The impact of relative humidity during electrospinning on the morphology and mechanical properties of nanofibers," *Int. J. Pharm.*, vol. 456, no. 1, pp. 125–34, Nov. 2013.

[194] L. Huang, N. N. Bui, S. S. Manickam, and J. R. McCutcheon, "Controlling electrospun nanofiber morphology and mechanical properties using humidity," *J. Polym. Sci. Part B Polym. Phys.*, vol. 49, no. 24, pp. 1734–1744, 2011.

[195] J. A. Knopf, "Investigation of Linear Electrospinning Jets," University of Delaware, 2009.

[196] D. H. Reneker and A. L. Yarin, "Electrospinning jets and polymer nanofibers," *Polymer (Guildf).*, vol. 49, no. 10, pp. 2387–2425, May 2008.

[197] S. Saravanan, C. Joseph Mathai, M. R. Anantharaman, S. Venkatachalam, and P. V. Prabhakaran, "Investigations on the electrical and structural properties of polyaniline doped with camphor sulphonic acid," *J. Phys. Chem. Solids*, vol. 67, no. 7, pp. 1496–1501, Jul. 2006.

[198] M. Magnuson, J. Guo, and S. Butorin, "The electronic structure of polyaniline and doped phases studied by soft x-ray absorption and emission spectroscopies," *J. Chem. …*, vol. 4756, no. 111, pp. 4756–4761, 1999.

[199] E. R. S. Circular, N B S, Arthur A. Maryott, *Table of Dielectric Constants of Pure Liquids*. Washington D.C.: National Bureau of Standards Circular 514, 1951.

[200] B. K. Gu, S. J. Park, M. S. Kim, C. M. Kang, J. Il Kim, and C. H. Kim, "Fabrication of sonicated chitosan nanofiber mat with enlarged porosity for use as hemostatic materials," *Carbohydr. Polym.*, vol. 97, no. 1, pp. 65–73, Aug. 2013.

[201] F. Croisier and C. Jérôme, "Chitosan-based biomaterials for tissue engineering," *Eur. Polym. J.*, vol. 49, no. 4, pp. 780–792, 2013.

[202] P. Marcasuzaa, S. Reynaud, F. Ehrenfeld, A. Khoukh, and J. Desbrieres, "Chitosan-graft-polyaniline-based hydrogels: Elaboration and properties," *Biomacromolecules*, vol. 11, no. 6, pp. 1684–1691, 2010.

[203] R. Jayakumar, M. Prabaharan, R. L. Reis, and J. F. Mano, "Graft copolymerized

chitosan - Present status and applications," *Carbohydr. Polym.*, vol. 62, no. 2, pp. 142–158, Nov. 2005.

[204] K. Sun and Z. H. Li, "Preparations, properties and applications of chitosan based nanofibers fabricated by electrospinning," *Express Polym. Lett.*, vol. 5, no. 4, pp. 342–361, Feb. 2011.

[205] M. Hasegawa, A. Isogai, F. Onabe, and M. Usuda, "Dissolving states of cellulose and chitosan in trifluoroacetic acid," *J. Appl. Polym. Sci.*, vol. 45, no. 10, pp. 1857–1863, 1992.

[206] K. Ohkawa, D. Cha, H. Kim, A. Nishida, and H. Yamamoto, "Electrospinning of Chitosan," *Macromol. Rapid Commun.*, vol. 25, no. 18, pp. 1600–1605, 2004.

[207] J. Nizioł, E. Gondek, and K. J. Plucinski, "Characterization of solution and solid state properties of polyaniline processed from trifluoroacetic acid," *J. Mater. Sci. Mater. Electron.*, vol. 23, no. 12, pp. 2194–2201, 2012.

[208] N. M. Alves and J. F. Mano, "Chitosan derivatives obtained by chemical modifications for biomedical and environmental applications," *Int. J. Biol. Macromol.*, vol. 43, no. 5, pp. 401–414, Dec. 2008.

[209] S. Yang, S. A. Tirmizi, A. Burns, A. A. Barney, and W. M. Risen, "Chitaline materials: Soluble Chitosan-polyaniline copolymers and their conductive doped forms," *Synth. Met.*, vol. 32, no. 2, pp. 191–200, Oct. 1989.

[210] S. R. Khairkar and A. R. Raut, "Synthesis of Chitosan-graft-Polyaniline-Based Composites," vol. 2, no. 4, pp. 62–67, 2014.

[211] A. Tiwari and V. Singh, "Synthesis and characterization of electrical conducting chitosan-graft-polyaniline," *Express Polym. Lett.*, vol. 1, no. 5, pp. 308–317, May 2007.

[212] W. A. Yee, M. Kotaki, Y. Liu, and X. Lu, "Morphology, polymorphism behavior and molecular orientation of electrospun poly(vinylidene fluoride) fibers," *Polymer (Guildf).*, vol. 48, no. 2, pp. 512–521, Jan. 2007.

[213] X. Zhao, P. Li, B. Guo, and P. X. Ma, "Antibacterial and conductive injectable hydrogels based on quaternized chitosan-graft-polyaniline/oxidized dextran for tissue engineering," *Acta Biomater.*, vol. 26, pp. 236–248, 2015.

[214] C. Meechaisue, R. Dubin, P. Supaphol, V. P. Hoven, and J. Kohn, "Electrospun mat of tyrosine-derived polycarbonate fibers for potential use as tissue scaffolding material.," *J. Biomater. Sci. Polym. Ed.*, vol. 17, no. 9, pp. 1039–56, 2006.

[215] D. Terada, H. Kobayashi, K. Zhang, A. Tiwari, C. Yoshikawa, and N. Hanagata, "Transient charge-masking effect of applied voltage on electrospinning of pure chitosan nanofibers from aqueous solutions," *Sci. Technol. Adv. Mater.*, vol. 13, no. 1, p. 15003, Jan. 2012.

[216] J. P. Foreman and A. P. Monkman, "Theoretical investigations into the structural and electronic influences on the hydrogen bonding in doped polyaniline," *Synth. Met.*, vol. 135–136, pp. 375–376, 2003.

[217] W. Łuzny and K. Piwowarczyk, "Hydrogen bonds in camphorsulfonic acid

doped polyaniline," *Polimery/Polymers*, vol. 56, no. 9, pp. 652–656, 2011.

[218] G. Ma *et al.*, "Hyaluronic acid/chitosan polyelectrolyte complexes nanofibers prepared by electrospinning," *Mater. Lett.*, vol. 74, pp. 78–80, May 2012.

[219] S. Meng, M. Rouabhia, and Z. Zhang, "Electrical stimulation modulates osteoblast proliferation and bone protein production through heparin-bioactivated conductive scaffolds," *Bioelectromagnetics*, vol. 34, no. 3, pp. 189–199, 2013.

[220] R. Mishra, D. B. Raina, M. Pelkonen, L. Lidgren, M. Tgil, and A. Kumar, "Study of in vitro and in vivo bone formation in composite cryogels and the influence of electrical stimulation," *Int. J. Biol. Sci.*, vol. 11, no. 11, pp. 1325–1336, Jan. 2015.

[221] M. Rouabhia, H. J. Park, and Z. Zhang, "Electrically Activated Primary Human Fibroblasts Improve In Vitro and In Vivo Skin Regeneration," *J. Cell. Physiol.*, vol. 231, no. 8, pp. 1814–1821, 2016.

[222] B. Myers, *Wound Management: Principles and Practice*, 2nd ed. Tulsa, OK: Pearson, 2008.

[223] I. Savina, R. Shevchenko, I. Allan, M. Illsley, and M. Sergey, "Cryogels as a component of topical wound dressings," in *Supermacroporous Cryogels: Biomedical and Biotechnological Applications*, A. Kumar, Ed. Francis, CRC Press Taylor& Francis, pp. 1–20.

[224] E. Caló and V. V. Khutoryanskiy, "Biomedical applications of hydrogels: A review of patents and commercial products," *Eur. Polym. J.*, vol. 65, pp. 252–267, 2015.

[225] H. Suhaimi, S. Wang, T. Thornton, and D. B. Das, "On glucose diffusivity of tissue engineering membranes and scaffolds," *Chem. Eng. Sci.*, vol. 126, pp. 244–256, 2015.

[226] M. Abrigo, S. L. McArthur, and P. Kingshott, "Electrospun nanofibers as dressings for chronic wound care: Advances, challenges, and future prospects," *Macromol. Biosci.*, vol. 14, no. 6, pp. 772–792, 2014.

[227] X. Zhang *et al.*, "Cellular responses of aniline oligomers: a preliminary study," *Toxicol. Res. (Camb).*, vol. 1, p. 201, 2012.

[228] E. I. Rabea, M. E. T. Badawy, C. V. Stevens, G. Smagghe, and W. Steurbaut, "Chitosan as antimicrobial agent: Applications and mode of action," *Biomacromolecules*, vol. 4, no. 6, pp. 1457–1465, 2003.

[229] A. El Hadrami, L. R. Adam, I. El Hadrami, and F. Daayf, "Chitosan in plant protection," *Mar. Drugs*, vol. 8, no. 4, pp. 968–987, 2010.

[230] I. M. Helander, E. L. Nurmiaho-Lassila, R. Ahvenainen, J. Rhoades, and S. Roller, "Chitosan disrupts the barrier properties of the outer membrane of Gram-negative bacteria," *Int. J. Food Microbiol.*, vol. 71, no. 2–3, pp. 235–244, 2001.

[231] Y. Andres, L. Giraud, C. Gerente, and P. Le Cloirec, "Antibacterial effects of chitosan powder: mechanisms of action.," *Environ. Technol.*, vol. 28, no. 12, pp. 1357–1363, 2007.

[232] N. M. Barkoula, B. Alcock, N. O. Cabrera, and T. Peijs, "Fatigue properties of

highly oriented polypropylene tapes and all-polypropylene composites," *Polym. Polym. Compos.*, vol. 16, no. 2, pp. 101–113, 2008.

[233] N. Shiy, X. Guo, Hemin Jing, J. Gong Yang, and C. Sun, "Antibacterial Effect of the Conducting Polyaniline," *J. Mater. Sci. Technol.*, vol. 22, no. 3, pp. 289–290, 2006.

[234] M. Doytcheva, D. Dotcheva, R. Stamenova, and C. Tsvetanov, "UV-Initiated Crosslinking of Poly(ethylene oxide) with Pentaerythritol Triacrylate in Solid State," *Macromol. Mater. Eng.*, vol. 286, no. 1, pp. 30–33, 2001.

[235] C. Zhou, Q. Wang, and Q. Wu, "UV-initiated crosslinking of electrospun poly(ethylene oxide) nanofibers with pentaerythritol triacrylate: Effect of irradiation time and incorporated cellulose nanocrystals," *Carbohydr. Polym.*, vol. 87, no. 2, pp. 1779–1786, 2012.

[236] P. Sangsanoh and P. Supaphol, "Stability improvement of electrospun chitosan nanofibrous membranes in neutral or weak basic aqueous solutions," *Biomacromolecules*, vol. 7, no. 10, pp. 2710–2714, Oct. 2006.

[237] Y. Arima and H. Iwata, "Effect of wettability and surface functional groups on protein adsorption and cell adhesion using well-defined mixed self-assembled monolayers," *Biomaterials*, vol. 28, no. 20, pp. 3074–3082, 2007.

[238] "NTP repor on the toxicology studies of pentaerythritol triacrylate_GMM4.pdf," 2005.

[239] C. Chen *et al.*, "In Vitro and In Vivo Characterization of Pentaerythritol Triacrylate-co-Trimethylolpropane Nanocomposite Scaffolds as Potential Bone Augments and Grafts," *Tissue Eng. Part A*, vol. 21, no. 1–2, pp. 320–331, 2015.

[240] N. Ninan *et al.*, "Wound healing analysis of pectin/carboxymethyl cellulose/microfibrillated cellulose based composite scaffolds," *Mater. Lett.*, vol. 132, pp. 34–37, 2014.

[241] A. Hadjizadeh and C. J. Doillon, "Directional migration of endothelial cells towards angiogenesis using polymer fibres in a 3D co-culture system.," *J. Tissue Eng. Regen. Med.*, vol. 4, no. 7, pp. 524–531, 2010.

[242] A. J. Bavariya *et al.*, "Evaluation of biocompatibility and degradation of chitosan nanofiber membrane crosslinked with genipin," *J. Biomed. Mater. Res. - Part B Appl. Biomater.*, vol. 102, no. 5, pp. 1084–1092, 2014.

[243] P. Bober, P. Humpolíč ek, J. Pacherník, J. Stejskal, and T. Lindfors, "Conducting polyaniline based cell culture substrate for embryonic stem cells and embryoid bodies," *RSC Adv.*, vol. 5, no. 62, pp. 50328–50335, 2015.

[244] H. Lambers, S. Piessens, A. Bloem, H. Pronk, and P. Finkel, "Natural skin surface pH is on average below 5, which is beneficial for its resident flora," *Int. J. Cosmet. Sci.*, vol. 28, no. 5, pp. 359–370, 2006.

[245] S. Meng, M. Rouabhia, Z. Zhang, D. De, F. De, and U. Laval, "Electrical stimulation in tissue regeneration," *Appl. Biomed. Eng.*, pp. 37–62, 2011.

[246] P. Zhang, Z. T. Liu, G. X. He, J. P. Liu, and J. Feng, "Low-Voltage Direct-Current Stimulation is Safe and Promotes Angiogenesis in Rabbits with Myocardial

Infarction," *Cell Biochem. Biophys.*, vol. 59, no. 1, pp. 19–27, 2011.

[247] P. Kohl and R. G. Gourdie, "Fibroblast-myocyte electrotonic coupling: Does it occur in native cardiac tissue?," *J. Mol. Cell. Cardiol.*, vol. 70, pp. 37–46, 2014.

[248] N. Bhattarai, D. Edmondson, O. Veiseh, F. A. Matsen, and M. Zhang, "Electrospun chitosan-based nanofibers and their cellular compatibility," *Biomaterials*, vol. 26, no. 31, pp. 6176–6184, Nov. 2005.

[249] A. A. Khalili and M. R. Ahmad, "A Review of cell adhesion studies for biomedical and biological applications," *Int. J. Mol. Sci.*, vol. 16, no. 8, pp. 18149–18184, 2015.

[250] M. Gümüşderelioglu, S. Dalkiranoğlu, R. S. T. Aydin, and S. Çakmak, "A novel dermal substitute based on biofunctionalized electrospun PCL nanofibrous matrix," *J. Biomed. Mater. Res. - Part A*, vol. 98 A, no. 3, pp. 461–472, Sep. 2011.

[251] J. Pelipenko, P. Kocbek, B. Govedarica, R. Rošic, S. Baumgartner, and J. Kristl, "The topography of electrospun nanofibers and its impact on the growth and mobility of keratinocytes," *Eur. J. Pharm. Biopharm.*, vol. 84, no. 2, pp. 401–411, Oct. 2013.

[252] J. Wu and Y. Hong, "Enhancing cell infiltration of electrospun fibrous scaffolds in tissue regeneration," *Bioact. Mater.*, vol. 1, no. 1, pp. 56–64, 2016.